

Old Dominion University

ODU Digital Commons

Civil & Environmental Engineering Theses &
Dissertations

Civil & Environmental Engineering

Spring 1992

Inelastic Stability of Nonproportionally Loaded Steel Sway Beam-Columns and Space Frames

Saleh Ali Eidan
Old Dominion University

Follow this and additional works at: https://digitalcommons.odu.edu/cee_etds



Part of the [Civil Engineering Commons](#)

Recommended Citation

Eidan, Saleh A.. "Inelastic Stability of Nonproportionally Loaded Steel Sway Beam-Columns and Space Frames" (1992). Doctor of Philosophy (PhD), Dissertation, Civil & Environmental Engineering, Old Dominion University, DOI: 10.25777/27st-xr86
https://digitalcommons.odu.edu/cee_etds/90

This Dissertation is brought to you for free and open access by the Civil & Environmental Engineering at ODU Digital Commons. It has been accepted for inclusion in Civil & Environmental Engineering Theses & Dissertations by an authorized administrator of ODU Digital Commons. For more information, please contact digitalcommons@odu.edu.

**INELASTIC STABILITY OF NONPROPORTIONALLY LOADED STEEL SWAY
BEAM-COLUMNS AND SPACE FRAMES**

By

SALEH ALI EIDAN

B. S., January 1981, California State University, Sacramento, USA

M. S., July 1983, California State University, Sacramento, USA

A Dissertation Submitted to the Faculty of
Old Dominion University in Partial Fulfillment of the
Requirements for the Degree of

DOCTOR OF PHILOSOPHY

CIVIL ENGINEERING

OLD DOMINION UNIVERSITY

MAY 1992

Approved by:

Dr. Zia Razzaq, Chairman

Dr. Francois Cheong-Siat-Moy

Dr. Duc T. Nguyen

Dr. Nahil Sobh

Dr. Gene J.-W. Hou

INELASTIC STABILITY OF NONPROPORTIONALLY LOADED STEEL SWAY BEAM-COLUMNS AND SPACE FRAMES

Saleh Ali Eidan
Old Dominion University, 1992
Advisor: Dr. Zia Razzaq

Abstract

A comprehensive study of the inelastic stability of steel beam-columns and frames subjected to nonproportional loads is conducted. A set of materially nonlinear differential equations of equilibrium for planar and biaxially loaded beam-columns are first formulated including sidesway. The analysis includes the effect of flexible connections, and initial imperfections in the form of member crookedness and residual stresses. Also, hollow rectangular sections are adopted for the study. First, an iterative numerical solution procedure is formulated for sway beam-columns utilizing central finite-differences with second-order truncation errors. Next, using the beam-column analysis, an inelastic frame analysis procedure is formulated by a conversion of the governing equations to a system of three-dimensional inelastic slope-deflection equations. The three-dimensional frame analysis is verified experimentally by conducting a rigorous test on a 15-foot high three-story single-bay structural steel space frame. The experimental results are in good agreement with the theoretical predictions. The strength of beam-columns, and plane and space frames with flexible connections is found to be load path dependent.

**To: My wife
Adeeba S. Eidan
and Daughters
Rolla, Rana, Raneem, and Raniah Saleh Eidan**

Acknowledgement

Sincere appreciation is due to Dr. Zia Razzaq for his advice, comments, and criticism. His guidance throughout the course of this research helped in the ultimate completion of the work.

Also, the author would like to thank Dr. F. Cheong-Siat-Moy of California State University at Sacramento, for his recommendation to work with Dr. Zia Razzaq, and for his participation in the dissertation committee. My thanks and respect are also extended to Dr. Nabil Sobh, Dr. Duc T. Nguyen, Dr. Gene J.-W. Hou, and Dr. Osman A. Akan for their participation.

A special appreciation is also due to Dr. Saleh Al-Athel, Chairman of King Abdulaziz City for Science and Technology, KACST, Saudi Arabia, for his valuable advice and guidance regarding where and how to pursue a doctoral degree program. Also, the support provided by the government of Saudi Arabia, through KACST, is sincerely appreciated. Special thanks are also due to Dr. Tarun K. Agarwal and Dr. Majdi A. Baddoura for their help in the laboratory, and for making the academic life at ODU more interesting and enjoyable. The help provided by Mr. W. J. Owens and Mr. J. B. Robertson in the test frame fabrication is also appreciated.

Of utmost value was the moral and spiritual support provided by the author's parents Ali Abdullah Eidan and Muneera Ibrabim Al-Rubaishi who served as constant lights not only throughout this research but also in other spheres of life.

TABLE OF CONTENTS

1. INTRODUCTION	1
1.1 Background	1
1.2 Literature Review	3
1.2.1 Columns and Beam-Columns	3
1.2.2 Frames	6
1.3 The Problems	9
1.4 Objective and Scope	10
1.5 Assumptions and Conditions	10
2. PARTIALLY RESTRAINED IMPERFECT SWAY BEAM-COLUMNS ...	12
2.1 Cross-Sectional Analysis	12
2.2 Governing Equations for Space Sway Beam-Columns	15
2.3 Boundary Conditions	18
2.4 Finite-Difference Formulation	19
2.5 Load Paths	22
2.5.1 Load Paths for Uniaxially Loaded Sway Beam-Columns .	22
2.5.2 Load Paths for Biaxially Loaded Sway Beam-Columns ..	24
2.6 Solution Procedure for Sway Beam-Columns	25
2.7 Analysis and Behavior of Sway Beam-Columns	26
2.7.1 Comparison to Published Results for Special Cases	27

2.7.2	Behavior of Uniaxially Loaded Sway Beam-Columns	30
2.7.3	Behavior of Biaxially Loaded Sway Beam-Columns	33
2.8	Inelastic Slope-Deflection Equations for Sway Planar Beam- Column	40
2.9	Inelastic Slope-Deflection Equations for Sway Space Beam- Column	45
3.	FLEXIBLY CONNECTED IMPERFECT SWAY FRAMES	49
3.1	Portal Frame	49
3.1.1	Analysis	50
3.1.2	Load Paths	52
3.1.3	Solution Procedure	52
3.1.4	Load Combinations	54
3.1.5	Types of Frames Studied	54
3.1.6	Frame Behavior	55
3.2	Orthogonal Space Frame	58
3.2.1	Analysis	58
3.2.2	Load Path	65
3.2.3	Solution Procedure	66
3.2.4	Frames Studied	68
3.2.5	Frame Behavior	69
4.	EXPERIMENTAL INVESTIGATION	73
4.1	Three-Story Single-Bay Space Frame	73
4.1.1	Frame Material Properties	74
4.1.2	Instrumentation	74

4.1.3	Rotational Stiffness Measurement Procedure	76
4.1.4	Residual Stresses	77
4.1.5	Initial Crookedness	79
4.2	Frame Test	80
4.2.1	Load Apparatus	80
4.2.2	Nonproportional Experimental Loads	82
4.2.3	Test Procedure	82
4.3	Theory versus Experiment	84
5.	CONCLUSIONS AND FUTURE RESEARCH	87
5.1	Conclusions	87
5.2	Future Research	88
	REFERENCES	89
	TABLES	93
	FIGURES	125
	APPENDIX A Cross-Sectional Inelastic Rate Equation	293
	APPENDIX B Inelastic Parameters	296
	APPENDIX C Portal Frame Shear Equilibrium Equation	299
	APPENDIX D Computer Programs	301
D.1	Biaxial Sway Beam-Column	305
D.2	Sway Portal Frame (SPF)	318
D.3	Sway Space Frame (SSF)	326
	VITA	341

LIST OF TABLES

<u>TABLE</u>	<u>PAGE</u>
1. Comparison of dimensionless maximum axial loads for columns crooked uniaxially or biaxially (7x7x0.375 in. cross section)	93
2. Comparison of dimensionless maximum axial loads for columns crooked uniaxially or biaxially (6x8x0.375 in. cross section)	93
3. Comparison of dimensionless maximum axial loads p , for nonsway pinned-end members with lateral load W (W8x31 cross section)	94
4. Comparison of dimensionless maximum loads for biaxially loaded nonsway beam-columns, with equal biaxial rotational springs of stiffness K_3 (6x8x0.375 in. cross section)	95
5. Comparison of dimensionless maximum loads for biaxially loaded nonsway beam-columns, with equal biaxial end rotational restraints of stiffness K_2 ; (W8x31 cross section)	96
6. Maximum dimensionless external loads for uniaxially loaded sway beam-columns, with equal end rotational restraints of stiffness K_2	97
7. Maximum dimensionless external loads for uniaxially loaded sway beam-columns, with equal end rotational restraints of stiffness K_2	98
8. Effect of imperfection on the strength of sway beam-columns loaded uniaxially, with lateral spring stiffness $K_y = 0.0$ and with equal end rotational restraints of stiffness K_2	99
9. Effect of imperfection on the strength of sway beam-columns loaded uniaxially, with lateral spring stiffness $K_y = 0.10$ kip/in. and equal end rotational restraints of stiffness K_2	100
10. Effect of imperfection on the strength of sway beam-columns loaded uniaxially, with lateral spring stiffness $K_y = 2.0$ kip/in. and equal end rotational restraints of stiffness K_2	101

11.	Effect of imperfection on the strength of sway beam-columns loaded uniaxially, with lateral spring stiffness $K_y = 1.0E+15$ kip/in. and equal end rotational restraints of stiffness K_2	102
12.	Maximum dimensionless external loads for uniaxially loaded sway beam-columns, with bilinear lateral restraints and equal end rotational restraints	103
13.	Maximum dimensionless external loads for biaxially loaded sway beam-columns, with equal end rotational restraints of stiffness K_3	104
14.	Maximum dimensionless external loads for biaxially loaded imperfect sway beam-columns with unequal partial end rotational restraints with stiffnesses K_3 and K_2 values at bottom and top, respectively	105
15.	Maximum dimensionless external loads for biaxially loaded sway beam-columns with equal partial end rotational restraints of stiffness K_2 value and with lateral restraints of various stiffnesses	106
16.	Maximum dimensionless external axial loads, with load path LP3, for biaxially loaded imperfect sway beam-columns with equal partial end rotational restraints and with lateral restraints of various stiffnesses; $M_x = M_y = 0.5M_Y$	107
17.	Maximum dimensionless external axial loads for sway beam-columns with biaxial imperfections, with equal partial end rotational restraints and with lateral restraints of various stiffnesses	108
18.	Effect of crookedness and residual stresses on the peak loads of biaxially loaded sway beam-columns with end rotational restraints ..	109
19.	Comparison of externally applied dimensionless maximum loads to published results for imperfect nonsway portal frame	110
20.	Maximum dimensionless external loads for sway portal frames with rigid beam-to-column connections, and with partial rotational restraints at the bases of stiffness K_2	111
21.	Maximum dimensionless external loads for imperfect sway portal frame FR5	112
22.	Effect of crookedness and residual stresses on the strength of sway portal frames with rigid beam-to-column connections, and with partial rotational restraints at bases of stiffness K_3	113
23.	Comparison of dimensionless maximum loads for sway portal frames with different residual stress distributions	114

24.	Maximum dimensionless applied loads for single-story single-bay sway space frames with rigid joints	115
25.	Maximum dimensionless applied loads for single-story single-bay sway space frames with flexible joints	116
26.	Effect of crookedness and residual stresses on dimensionless maximum loads of single-story single-bay sway space frames with flexible joints	117
27.	Comparison of dimensionless maximum loads for sway single-story single-bay space frames with different residual stress distributions . . .	118
28.	Experimental method of sectioning results for residual stress determination for 2x3x0.1875 in. section, with an initial length of 8.187 in.	119
29.	Experimental method of sectioning results for residual stress determination for 2x2x0.1875 in. section, with an initial length of 7.986 in.	120
30.	Initial crookedness in test frame columns measured before test at five equidistant points along each column with base of frame as reference point	121
31.	Test frame deflections at joints 29 and 32 in x-direction	122
32.	Test frame deflections at joints 29 and 32 in y-direction	123
33.	Experimental deflection and angle of twist of Column 20	124

LIST OF FIGURES

<u>FIGURE</u>	<u>PAGE</u>
1. Discretized hollow rectangular section subjected to axial load and biaxial bending moments	125
2. Stress-strain relationship with elastic unloading	126
3. Cross section and residual stress distribution (Ref. 21)	127
4. Square section ($B = D$) with idealized residual stress distribution . . .	128
5. Rectangular section with idealized residual stress distribution	129
6. Imperfect sway beam-column with biaxial restraints	130
7. Moment-rotation relationship	131
8. Loading paths for nonproportional loading	132
9. Axial load versus top deflection of elastically loaded Sway beam-column of Ref. 9	133
10. Laterally loaded pinned column	134
11. Residual stress strain pattern for an I-section	135
12. Dimensionless axial load versus top deflection of imperfect column with $K_{By} = K_b$, and $K_{Ty} = K_d$	136
13. Dimensionless axial load versus top deflection of imperfect column with $K_{By} = K_c$, and $K_{Ty} = K_d$	137
14. Dimensionless axial load versus top deflection of imperfect column with $K_{By} = K_d$, and $K_{Ty} = K_d$	138
15. Stiffness degradation curves for uniaxially loaded sway beam-columns BC1, BC3, BC4, BC5, and BC6, with $K_{Bx} = K_{Tx} = K_2$	139

16.	Stiffness degradation curves for uniaxially loaded sway beam-columns BC7, BC8, and BC10, with $K_{Bx} = K_{Tx} = K_3$	140
17.	Stiffness degradation curves ($\bar{D}-p$) for uniaxially loaded sway beam-column BC5, for load paths NP1 and NP2, with $K_{Bx} = K_{Tx} = K_2$...	141
18.	Stiffness degradation curves ($\bar{D}-m_x$) for uniaxially loaded sway beam-column BC5, for load paths NP1 and NP2, with $K_{Bx} = K_{Tx} = K_2$...	142
19.	Interaction curve for uniaxially loaded sway beam-column BC10 for load paths NP3 and NP4, with $K_{Bx} = K_{Tx} = K_3$	143
20.	Stiffness degradation curves ($\bar{D}-p$) for uniaxially loaded sway beam-columns BC12, BC13, BC14, and BC15	144
21.	Stiffness degradation curves ($\bar{D}-m_x$) for uniaxially loaded sway beam-columns BC12, BC13, BC14, and BC15	145
22.	Stiffness degradation curve ($\bar{D} - p$) for uniaxially loaded sway beam-column BC30, with bilinear rotational restraints and load path NP3 .	146
23.	Stiffness degradation curve ($\bar{D} - m_x$) for uniaxially loaded sway beam-column BC30, with bilinear rotational restraints and load path NP3 .	147
24.	Stiffness degradation versus spring moment versus for uniaxially loaded sway beam-column BC30, with bilinear rotational restraints and load path NP3	148
25.	Effect of the type of residual stress distribution (RSD) on stiffness degradation ($\bar{D} - p$) of uniaxially loaded sway beam-column	149
26.	Effect of the type of residual stress distribution (RSD) on stiffness degradation ($\bar{D} - m_x$) of uniaxially loaded sway beam-column	150
27.	Dimensionless bending moment versus top deflection for uniaxially loaded sway beam-columns with two different residual stress distributions (RSD)	151
28.	Stiffness degradation curve ($\bar{D}-p$) for biaxially loaded sway beam-columns BC32 through BC36	152
29.	Stiffness degradation curve ($\bar{D}-p$) for biaxially sway loaded sway beam-column BC35 with LP1 load path	153

30.	Stiffness degradation curve ($\bar{D}-m_x$) for biaxially loaded sway beam-column BC35 with LP1 and LP2 load paths	154
31.	Stiffness degradation curve ($\bar{D}-m_y$) for biaxially loaded sway beam-column BC35 with load paths LP1 and LP2	155
32.	Axial load versus top deflection for biaxially loaded sway beam-column BC39 with equal end restraints and with load paths LP5 and LP6 ...	156
33.	Stiffness degradation curve ($\bar{D}-p$) for biaxially loaded sway beam-columns BC42 and BC43	157
34.	Stiffness degradation curve for member BC42 with load path LP3, $m_x = 1.38$ and $m_y = 1.12$	158
35.	Stiffness degradation curve ($\bar{D}-m_x$) for member BC42 with load paths LP3 and LP4	159
36.	Stiffness degradation curve ($\bar{D}-m_y$) for member BC42 with load path LP4	160
37.	Moment versus midspan deflection for biaxially loaded sway beam-column BC42 with equal end restraints and with load paths LP1 and LP2	161
38.	Interaction diagrams for biaxially loaded sway beam-column BC43 with equal end restraints and with load paths LP3 and LP4	162
39.	Interaction curves for biaxially loaded sway beam-column BC43 with equal end restraints and with load paths LP3 and LP4	163
40.	Stiffness degradation curve ($\bar{D}-P$) for biaxially loaded imperfect sway beam-column with end rotational restraints of type K_2 and with load path LP7	164
41.	Stiffness degradation curve ($\bar{D}-m_x$) for biaxially loaded imperfect sway beam-column with end rotational restraints of type K_2 and with load path LP7	165
42.	Stiffness degradation curve ($\bar{D}-m_y$) for biaxially loaded sway beam-column with rotational spring of K_2 type and with load path LP7 ...	166

43.	Dimensionless axial load versus lateral spring stiffness for biaxially loaded sway beam-column with various rotational end restraints, with $m_x = 0.5$, and load path NP2	167
44.	Dimensionless axial load versus lateral spring stiffness for biaxially loaded sway column with various rotational end restraints	168
45.	Stiffness degradation curve (\bar{D} -P) for biaxially loaded sway beam-column with load path LP7	169
46.	Stiffness degradation curve (\bar{D} - m_x) for biaxially loaded sway beam-column with load path LP7	170
47.	Stiffness degradation curve (\bar{D} - m_y) for biaxially loaded sway beam-column with load path LP7	171
48.	Spread of plasticity in the cross sections before axial load is incremented (corresponding to point A in Figures 47 - 49)	172
49.	Spread of plasticity in the cross sections after axial load is incremented (corresponding to point B in Figures 47 - 49)	173
50.	Unloaded elements in the section (dashed) and newly plastified elements (dotted)	174
51.	Dimensionless bending moment versus midspan deflection in yz plane for a biaxially loaded sway beam-column	175
52.	Dimensionless bending moment versus top deflection in yz plane for a biaxially loaded sway beam-column	176
53.	Interaction curves for biaxially loaded sway beam-column based on tangent modulus approach, and including elastic unloading	177
54.	Effect of residual stresses and crookedness on the stiffness degradation of biaxially loaded sway beam-columns with load path LP5	178
55.	Dimensionless axial load versus top deflection of biaxially loaded sway beam-column with residual stresses and/or crookedness and with load path LP5	179
56.	Stiffness degradation ($\bar{D} - m_x$) for biaxially loaded sway beam-column with residual stresses and/or crookedness and with load path LP6 ..	180

57.	Effect of the type of residual stress distribution (RSD) on stiffness degradation ($\bar{D} - p$) of biaxially loaded sway beam-column	181
58.	Effect of type residual stress distribution (RSD) on stiffness degradation ($\bar{D} - m_x$) of biaxially loaded sway beam-column	182
59.	Dimensionless axial load versus midspan deflection of biaxially loaded sway beam-column with different residual stress distributions (RSD) .	183
60.	Dimensionless axial load versus top deflection of biaxially loaded sway beam-column with different residual stress distributions (RSD)	184
61.	Sway beam-column subjected to uniaxial loading	185
62.	Sway beam-column subjected to biaxial loading	186
63.	Imperfect unbraced portal frame with loading	187
64.	Stiffness degradation ($\bar{D}-p$) for sway plane frame PF9 with load paths LPF2 and LPF3	188
65.	Stiffness degradation ($\bar{D} - m_x$) for sway plane frame PF9 with load paths LPF2 and LPF3	189
66.	Dimensionless vertical load versus top deflection curves for sway portal frame PF9 with load paths LPF2 and LPF3	190
67.	Stiffness degradation ($\bar{D}-p$) for sway plane frame PF10 with load path LPF2	191
68.	Dimensionless stiffness degradation ($\bar{D} - m_x$) for sway plane frame PF10 with load path LPF2	192
69.	Dimensionless vertical load versus top deflection of plane frame PF10 with load path LPF2	193
70.	Effect of residual stresses and/or crookedness on stiffness degradation of sway portal frames under load path LPF1	194
71.	Stiffness degradation ($\bar{D} - m_x$) of sway portal frames with residual stresses and/or crookedness with load path LPF1	195
72.	Dimensionless vertical load versus top deflection of plane frames with residual stresses and/or crookedness and with load path LPF1	196

73.	Dimensionless bending moment versus rotation at Joint 1 of plane frames with residual stresses and/or crookedness and with load path LPF1	197
74.	Stiffness degradation ($\bar{D} - p$) of sway portal frames with residual stresses and/or crookedness and with load path LPF2	198
75.	Stiffness degradation ($\bar{D} - m_x$) for sway portal frames with residual stresses and/or crookedness and with load path LPF2	199
76.	Dimensionless vertical load versus top deflection of plane frames with residual stresses and/or crookedness and with load path LPF2	200
77.	Stiffness degradation ($\bar{D} - p$) of sway portal frames with residual stresses and/or crookedness and with load path LPF3	201
78.	Stiffness degradation ($\bar{D} - m_x$) for sway portal frames with residual stresses and/or crookedness and with load path LPF3	202
79.	Dimensionless vertical load versus top deflection of plane frames with residual stresses and/or crookedness and with load path LPF3	203
80.	Dimensionless vertical load versus rotation at Joint 1 of sway plane frames with residual stresses and/or crookedness and with load path LPF3	204
81.	Dimensionless bending moment versus rotation at Joint 1 of sway plane frames with residual stresses and/or crookedness and with load path LPF3	205
82.	Stiffness degradation of sway portal frame with different residual stress distributions (RSDs) and load path LPF1	206
83.	Stiffness degradation of sway portal frame with different residual stress distribution and load path LPF1	207
84.	Dimensionless vertical load versus top deflection of sway portal frame with load path LPF1 and different residual stress distributions (RSDs)	208
85.	Stiffness degradation ($\bar{D} - p$) of sway portal frame with load path LPF2 and different residual stress distributions (RSDs)	209

86.	Stiffness degradation ($\bar{D} - m_x$) of sway portal frame with load path LPF2 and different residual stress distributions (RSDs)	210
87.	Dimensionless vertical load versus top deflection of sway portal frame with load path LPF2 and different residual stress distributions (RSDs)	211
88.	Stiffness degradation ($\bar{D} - p$) of sway portal frame with load path LPF3 and different residual stress distributions (RSDs)	212
89.	Stiffness degradation ($\bar{D} - m_x$) of sway portal frame with load path LPF3 and different residual stress distributions (RSDs)	213
90.	Dimensionless vertical load versus top deflection of sway portal frame with load path LPF3 and different residual stress distributions (RSDs)	214
91.	Flexibly-connected single-story single-bay unbraced sway space frame	215
92.	Typical space frame Joint	216
93.	Space frame joint moments used in slope-deflection formulation	217
94.	Stiffness degradation ($\bar{D} - p$) of single-story single-bay sway space frames SF2 and SF4	218
95.	Stiffness degradation ($\bar{D} - m_y$) of single-story single-bay sway space frames SF2 and SF4	219
96.	Dimensionless vertical load versus top deflection ($p - \Delta_x$) of single-story single-bay sway space frames SF2 and SF4	220
97.	Stiffness degradation ($\bar{D} - p$) of single-story single-bay sway space frame SF24	221
98.	Stiffness degradation ($\bar{D} - m_x$) of single-story single-bay sway space frame SF24	222
99.	Dimensionless vertical load versus top deflection ($p - \Delta_x$) of single-bay single-story sway space frame SF24	223

100.	Stiffness degradation ($\bar{D} - p$) for single-story single-bay sway space frames with various combinations of residual stresses and crookedness, with load path SL1	224
101.	Stiffness degradation ($\bar{D} - m_y$) for single-story single-bay sway space frames with various combinations of residual stresses and crookedness, with load path SL1	225
102.	Dimensionless vertical load versus top deflection ($p - \Delta_x$) for single-story single-bay sway space frames with various combinations of residual stresses and crookedness; with load path SL1	226
103.	Dimensionless vertical load versus top deflection ($p - \Delta_x$) relationships of Figure 102 with horizontal scale magnification	227
104.	Dimensionless bending moment versus top deflection ($m_y - \Delta_x$) for single-story single-bay sway space frames with various combinations of residual stresses and crookedness, with load path SL1	228
105.	Stiffness degradation ($\bar{D} - p$) for a single-bay single-story space frames with different combination of residual stresses and crookedness, with load path SL2	229
106.	Stiffness degradation ($\bar{D} - m_x$) for single-story single-bay sway space frames with various combinations of residual stresses and crookedness, with load path SL2	230
107.	Bending moment versus top deflection ($m_y - \Delta_x$) for single-story single-bay sway space frames with various combinations of residual stresses and crookedness, with load path SL2	231
108.	Dimensionless vertical load versus top deflection ($p - \Delta_x$) for single-story single-bay sway space frames with various combinations of residual stresses and crookedness, with load path SL2	232
109.	Stiffness degradation ($\bar{D} - p$) for single-story single-bay sway space frames with various combinations of residual stresses and crookedness, with load path SL3	233
110.	Stiffness degradation ($\bar{D} - m_y$) for single-story single-bay sway space frames with various combinations of residual stresses and crookedness, with load path SL3	234

111.	Dimensionless vertical load versus top deflection ($p - \Delta_x$) for single-story single-bay sway space frames with various combinations of residual stresses and crookedness, with load path SL3	235
112.	Bending moment versus top deflection ($m_y - \Delta_x$) for single-story single-bay sway space frames with various combinations of residual stresses and crookedness, with load path SL3	236
113.	Stiffness degradation ($\bar{D} - p$) for single-story single-bay sway space frame with various combinations of residual stresses and crookedness, with load path SL4	237
114.	Stiffness degradation ($\bar{D} - m_x$) for single-story single-bay space sway frames with various combinations of residual stresses and crookedness, with load path SL4	238
115.	Dimensionless vertical load versus top deflection ($p - \Delta_x$) for single-story single-bay sway space frames with various combinations of residual stresses and crookedness, with load path SL4	239
116.	Bending moment versus top deflection ($m_y - \Delta_x$) for single-story single-bay sway space frames with various combinations of residual stresses and crookedness, with load path SL4	240
117.	Dimensionless bending moment versus top deflection ($m_y - \Delta_x$) for single-story single-bay sway space frames with various residual stress distributions and load path SL1	241
118.	Stiffness degradation ($\bar{D} - m_x$) for single-story single-bay sway space frames with various residual stress distributions and with load path SL2	242
119.	Stiffness degradation ($\bar{D} - m_x$) for single-story single-bay sway space frames with various residual stress distributions and load path SL4 ..	243
120.	Bending moment versus top deflection ($m_y - \Delta_x$) for single-story single-bay sway space frames with various residual stress distributions and load path SL4	244
121.	Test frame	245
122.	Three-story single-bay space frame	246

123.	Stub column with center strain gages	247
124.	Stub column with corner strain gages	248
125.	Stress-strain curve the stub column with strain gages at member corners	249
126.	Setup for LVDTs	250
127.	Schematic diagram for LVDTs setup	251
128.	Jack, load cell and looped cable	252
129.	Schematic diagram showing the jack and cable	253
130.	NEFF hardware and the personal computer used	254
131.	Bases connection detail	255
132.	Schematic diagram showing setup for base joint rotation measurement	256
133.	Base moment-rotation relationship	257
134.	Strips numbering for the square section	258
135.	Strips numbering for the rectangular section	258
136.	Distribution of residual stresses across wall thickness for square section (Vertical scale: 1 in = 100 ksi)	259
137.	Distribution of residual stresses across wall thickness for rectangular section (Vertical scale: 1 in = 100 ksi)	260
138.	Loading jack (27) and cable arrangement for frame horizontal load application	261
139.	Schematic diagram of setup for lateral force application	262
140.	Loading beam assembly at frame top	263
141.	Schematic diagram of loading beam assembly at frame top	264
142.	Loading jacks in frame test	265
143.	Start of plastification in Beam 23 at $P_2 = 19.5$ kips	266

144.	Nearly complete plastification of Beam 23 at $P_2 = 23.0$ kips	267
145.	Plastification of Beam 23, Beam 24, and Column 20	268
146.	Dial gages attached to Column 20 for measuring torsional angle	269
147.	Schematic diagram for dial gages on Column 20 for measuring torsional angle	270
148.	Experimental vertical load P_1 versus angle of twist of the test frame	271
149.	Experimental vertical load P_2 versus angle of twist of the test frame	272
150.	Experimental vertical load P_1 versus angle of twist of Column 20	273
151.	Experimental vertical load P_1 versus horizontal deflection at midspan of Column 20 in the y-direction	274
152.	Lateral load versus frame top deflection Δ_x	275
153.	Vertical load P_1 versus frame top deflection Δ_x	276
154.	Vertical load P_2 versus frame top deflection Δ_x	277
155.	Lateral load H versus frame top deflection Δ_y	278
156.	Vertical load P_1 versus frame top deflection Δ_y	279
157.	Vertical load P_2 versus frame top deflection Δ_y	280
158.	Lateral load H versus normal strain in column 18 at location S1	281
159.	Lateral load H versus normal strain in column 18 at location S2	282
160.	Vertical load P_1 versus normal strain in column 18 at location S1	283
161.	Vertical load P_1 versus normal strain in column 18 at location S2	284
162.	Lateral load H versus normal strain in column 20 at location S3	285
163.	Lateral load H versus normal strain in column 20 at location S4	286
164.	Vertical load P_2 versus normal strain in column 20 at location S3	287
165.	Vertical load P_2 versus normal strain in column 20 at location S4	288

166.	Locations of strain gages on Columns 18 and 20	289
167.	Stiffness degradation curve ($\bar{D}-H$) for three-story single-bay sway space frame with the load path used in experiment	290
168.	Stiffness degradation curve ($\bar{D}-P_1$) for three-story single-bay sway space frame with the load path used in experiment	291
169.	Stiffness degradation curve ($\bar{D}-P_2$) for three-story single-bay sway space frame with the load path used in experiment	292

NOMENCLATURE

A	Area
A_e, A_p	Elastic and plastic areas
A_{ij}, a_{ij}	Inelastic cross-sectional properties
B	Section width
D	Section depth
E	Young's modulus
$\{F\}$	Load vector
$\{F\}_p$	Load vector due to plastification
I	Moment of inertia
$[K]$	Member global tangent stiffness matrix
K_{Bx}, K_{Tx}	Rotational stiffnesses about x axis
K_{By}, K_{Ty}	Rotational stiffnesses about y axis
K_{sa}, K_{sb}	Spring rotational stiffness
$[K_t]$	Cross-sectional tangent stiffness matrix
K_x, K_y	Lateral spring stiffness in xz and yz planes
L	Member length
$\{M\}$	Moment vector
$\{M\}_a$	Applied moment vector

M_{Bx}, M_{Tx}	Applied moments about x axis
M_{By}, M_{Ty}	Applied moments about y axis
$\{M_{cg}\}$	Moment vector associated with member crookedness
$\{M_{pg}\}$	Moment vector containing plastic forces
M_{xp}, M_{yp}	Moments due to plastified elements in the member
M_{xre}, M_{yre}	Moments due to residual stresses
P	Applied axial load
P_p	Axial load due to plastified elements in the member
P_r	Axial load due to residual stresses
$R_{(i,j)}$	Stability coefficient for the elastic portion
$R_{p(i,j)}$	Stability coefficient for the plastic portion
$R_{c(i,j)}$	Stability coefficient associated with member crookedness
R_x, R_y	Reaction at bottom of a single member
U	Total deflection in x-direction
V	Total deflection in y-direction
W	Applied lateral load
c	Distance between end B and W
dA	Elemental area
$\{f\}$	Cross-sectional dimensionless load vector
$\{\dot{f}\}$	Cross-sectional load rate vector
g	Global
h	Distance between nodes
m_{Bx}, m_{Tx}	Spring moments at bottom and top about x axis

m_{By}, m_{Ty}	Spring moments at bottom and top about y axis
m_x, m_y	Dimensionless moments
\bar{m}_x, \bar{m}_y	Cross-sectional dimensionless moments
m_s	Spring moment
m_{sa}	Spring plastic moment
n	Total nodes
u	Deflection due to load in x-direction
v	Deflection due to load in y-direction
u_0	Initial member crookedness in x-direction
v_0	Initial member crookedness in y-direction
u_{0i}	Midspan initial crookedness amplitude in x-direction
v_{0i}	Midspan initial crookedness amplitude in y-direction
u_n	Top deflection in x-direction
v_n	Top deflection in y-direction
x, y, z	Global coordinates
z_i	Nodal distance from end B
α_c	Angle of twist of Column 20
α_f	Angle of twist of test frame
β	Coefficient matrix for plane frame
β_x	Coefficient matrix for space frame
$\{ \delta \}$	Cross-sectional deformation vector
$\{ \dot{\delta} \}$	Cross-sectional deformation rate vector

ε	Normal strain
$\dot{\varepsilon}$	Strain rate
ε_0	Average axial strain
$\bar{\varepsilon}_0$	Dimensionless average axial strain
ε_r	Residual strain
θ_B, θ_T	Bottom and top member rotations
$\dot{\sigma}$	Stress rate
σ_e	Elastic stress
σ_Y	Yield stress
Φ_x, Φ_y	Bending curvatures
$\bar{\varphi}_x, \bar{\varphi}_y$	Dimensionless bending curvatures
$\{\Delta\}$	Frame deformation vector
\int_A	Cross-sectional integration

1. INTRODUCTION

1.1 Background

The current methods of inelastic frame analysis are based on the contention that the applied loads are proportional in nature. The actual structures, on the contrary, are subjected to nonproportional loads. One example is that of relatively constant gravity loads with variable horizontal loading. This research is primarily aimed at studying the influence of nonproportional loads on the theoretical and experimental behavior of sway space frames. Furthermore, before such an investigation is conducted, it is necessary to formulate accurate theoretical analysis of the individual members which form a structure. Thus, a rigorous theoretical study is also conducted for plane and space beam-columns with practical boundary conditions and initial imperfections. Consequently, a substantial part of this research is oriented toward a comprehensive study at the member level. The member equations are then used to analyze sway plane frames before generalizing for the space frames.

The member analysis is conducted using an equilibrium approach coupled with an iterative finite-difference formulation in order to predicted the load-deformation behavior. A set of materially nonlinear ordinary differential equations are formulated which govern the member load-deformation behavior for gradually increasing nonproportional static loads. Using a difference- type formulation, the

sway beam-column equations for both two- and three-dimensional problems are also exploited to arrive at equations that contain the member deformations at the boundaries. These equations are then utilized for the plane and the space frame analysis.

Due to the complexity of the coupled nonlinear differential equations for the problems described herein, a validation of the theoretical models becomes one of the key issues. To include every conceivable nonlinear term is both impractical and unnecessary. Furthermore, nonlinear equations have multiple roots and there is always a danger of converging to an inapplicable root. An effective way to verify theoretical predictions is to conduct laboratory experiments. The test results can provide a meaningful means of checking the validity of the assumptions made in the theoretical formulations. Consequently, a comprehensive test on a real three-story single-bay orthogonal framed structure is also conducted.

The main thrust of the research is to study members and frames with rectangular tubular cross section. Such sections are quite stiff torsionally, therefore, twisting deformations are ignored. Even for some open section members studied by some past investigators, the twisting deformations for members subjected to combined axial load and biaxial bending did not prove to have a very substantial effect on the load-carrying capacity. Torsional effects must, however, be accounted for in space frames with external torques or for those constructed from thin-walled open section members.

In this dissertation, theoretical procedures are presented to predict the behavior of nonproportionally loaded inelastic members and frames in the presence

of sway. In addition, the theoretical results are compared to those from a large scale frame test also conducted as a part of this research.

1.2 Literature Review

Presented in this section is a summarized literature survey of the relevant publications for both members and frames.

1.2.1 Columns and Beam-Columns

Ellis, Jury, and Kirk (1) determined theoretically the ultimate capacity of steel columns loaded biaxially. The section is a hollow square and no imperfections are considered. Also, the tangent modulus approach is used. The length of the column is divided into small elements and an iterative method of analysis is formulated. The cross section is also divided into a number of small elements. A comparison of the results for uniaxial loading cases is made to the existing theoretical results. The results for an annular cross section are compared to other theoretical and experimental results. The comparison is found to be favorable.

Ellis and Marshall (4) conducted a theoretical investigation of the ultimate capacity of steel columns loaded biaxially. The cross section used is a thin-walled square, the material is assumed to be perfectly elastic-plastic mild steel, and no material unloading is included. The theoretical predictions are compared to the existing results for certain cases and the agreement is found to be good.

Harstead and Birnstiel (8), and Birnstiel (9) conducted a theoretical and experimental study on H-columns under biaxial bending. Sixteen columns are tested and the results are compared with those obtained theoretically. The theoretical study

is based on the tangent modulus approach. The experimental results are also compared with the CRC interaction equations. The theoretical study shows the influence of residual stresses on the deformational response and the ultimate capacity of the columns under biaxial bending.

Tebedge and Chen (13) formulated design criteria for H-columns under biaxial loading. The column out-of-straightness and residual stresses are taken into consideration. Various I-sections are used in the study, and the tangent modulus approach is followed. Several load-moment interaction diagrams are developed for various slenderness ratios. The results are compared to CRC (Column Research Council) interaction formulas. It is found that the CRC procedure is over-conservative for short columns, conservative for intermediate columns, and less conservative for long columns.

Vinnakota and Aysto (15) studied the inelastic spatial stability of restrained beam-columns. Although the residual stresses are accounted for, the crookedness of the columns is not included. The method presented is based on the tangent modulus approach. The predicted ultimate load and the load-deformation response shows a satisfactory agreement with the available tests and analytical results.

Chen and Atsuta (18,19) published a comprehensive literature review and summary of beam-column research conducted up to 1976. Reference 18 presents the work done on planar beam-columns while Reference 19 covers beam-columns in a three-dimensional space. A limited amount of results are also described in Reference 18 for nonproportionally loaded cross sections and members. An algorithm and some numerical results are given for nonsway I-section beam-columns. A summary of tests conducted by Gent and Milner (11) on nonsway I-section beam-

columns subjected to nonproportional biaxial loading are also presented. It is found that if torsion is included in the analysis, the collapse load is reduced by less than 2 percent.

Razzaq and McVinnie (23,27) conducted theoretical and experimental studies on hollow rectangular section nonsway beam-columns subjected to nonproportional loading. Material unloading is not included in the theory, however, good correlation is obtained with the test results since pinned-end conditions are used.

Razzaq (24) investigated the effects of linear and nonlinear partial rotational end restraints on steel planar column strength. The study is performed for a W8x31 section with residual stresses and initial crookedness. Both equal and unequal end restraints are considered. It is concluded that the nonlinear moment-rotation relationships should be approximated by simple elastic-plastic or bilinear relationships as opposed to trilinear or curve-fitted nonlinear ones. The effects of partial restraints and initial imperfections on the column strength are found to be quite important.

Razzaq and Calash (26) conducted a rigorous inelastic analysis of imperfect columns with linear or nonlinear biaxial partial restraints. The study is conducted for a thin-walled hollow rectangular section. A central finite-difference procedure is used and the effect of imperfections on the column strength explained. It is found that the residual stresses are less detrimental to the column strength than the crookedness. Also, for a number of cases, it is found that the strength of nearly-perfect columns does not depend upon the slenderness or the degree of rotational end restraint stiffness. For crooked columns with or without residual stresses,

however, an increase in the degree of end fixity is found to increase the column strength.

Razzaq and Darbhamulla (28, 29, 30), Darbhamulla and Razzaq (31), and Darbhamulla (37) studied imperfect rectangular tubular nonsway beam-columns with nonproportional biaxial loads. Two types of sections are considered, namely an I-section and a hollow rectangular section. Elastic unloading in the plastic range is included. The effect of nonproportional loading on the beam-column strength is found to be quite significant.

A review of the published research shows that no research has been conducted on sway beam-columns under the influence of nonproportional loading.

1.2.2 Frames

Yura and Galambos (2) conducted research on the strength of single-story steel frames. The structures are unbraced, symmetric, and with rigid joints. The study is based on the tangent modulus approach. The structures are subjected to various concentrated vertical and lateral loads. Inelastic and residual stresses are taken into consideration. The interaction curves are established and the results are compared to the interaction equations used in building design. It is found that the frame strength can be predicted by a plastic analysis of the deformed structure up to the buckling load, and that the P-delta effect is important for frames permitted to sway. Also, the AISC interaction equations are found to give unconservative results by as much as 30% when sway is permitted.

Lu (3) studied the inelastic buckling of steel frames. The procedure is explained with reference to a portal frame subjected to concentrated loads at the

beam-column connections and a distributed load over the beam. A laboratory test is also conducted and the results compared to the theory. The test results are in good agreement with the predicted frame behavior.

Korn and Galambos (5) studied the behavior of elastic-plastic frames. The stress-strain relationship is assumed to be ideal elastic-plastic and the loading is static, proportional, and monotonically increasing up to failure. The first- and second-order analysis for unbraced plane frames is included. For frames having a reasonably linear behavior at working loads, it is found that at least 86% of the predicted first-order load-carrying capacity is obtained. Load-deformation curves are also presented to show the deviations between the first- and the second-order analysis.

Wright and Gaylord (6) presented the analysis of unbraced multistory steel frames. It is assumed in the elastic-plastic analysis that plastic hinges form at discrete points while the remainder of the structure remains elastic. The theoretical results compared well with those found experimentally.

McVinnie and Gaylord (7) investigated the inelastic buckling of unbraced space frames. The study was for single-story single-bay orthogonal space frames. It is assumed that the structure deforms symmetrically when the load is less than the critical load. Also, unloading of the inelastic material is not accounted for. It is found that it is unlikely that a single-story frame with biaxially loaded columns and with slenderness ratios of less than 100 will become unstable at a load less than 90% of the mechanism load. Also, the authors found that the AISC provision for columns in plastically designed unbraced frames was conservative when applied to the biaxially loaded columns.

McNamee and Lu (12) analyzed theoretically the inelastic multistory frame buckling problem, and verified the results with a laboratory experiment on a three-story sway plane frame. Concentrated loads are applied to the beams with two point loads per beam. The tests are conducted, and the results are found to be in excellent agreement with the theory.

Wood, Beaulieu, and Adams (16) presented an approximate technique in which the $P-\Delta$ effect is included in the analysis by modifying the first-order results. The theoretical results are also compared to some available experimental ones. The technique presented does not converge for very flexible frames with high axial loads.

Cheong-Siat-Moy (17) presented a design procedure for braced and unbraced multistory frames. It is found that the complexity of unbraced multistory steel frame design can be significantly reduced by breaking it down into smaller story units.

Razzaq and Naim (20) conducted a study of elastic instability of unbraced space frames. Single-story single-bay space frames are studied with various column orientations and concentrated joint load patterns. The results are compared with those obtained using the well-known, though approximate, effective length approach. It is found that the effective length approach is very approximate and may underestimate drastically the instability loads of some frames since it does not account for the three-dimensional interaction such as that due to different cross-sectional orientations of the columns. Furthermore, it is found that a dramatic increase in the instability load of space frames may be achieved by orienting the cross-sectional major principal axis of alternate columns at right angles to each other.

Wen and Rahimzadeh (25) presented a nonlinear finite element analysis for elastic frames. Both plane and space frames are considered. The stiffness matrix elements are presented and include the axial loads to account for the P-delta effect. The study also accounts for large displacements. A comparison of the numerical results with fixed coordinate procedure and beam-column methods along with other methods mentioned in the paper indicates that the method presented is competitive.

Darbhamulla and Razzaq (34) presented a solution procedure for flexibly-connected nonsway plane frames subjected to nonproportional loading. In the study, the strength of the frames loaded nonproportionally is found to be substantially less than that of the frames loaded proportionally. Also, it is found that a dramatic difference exists between the behavior of nonproportionally and proportionally loaded frames.

Chandra, Krishna, and Trikha (35,36) presented a nonlinear analysis of steel space structures. In the study, it is found that an instantaneous secant stiffness procedure converges more rapidly than the Newton-Raphson technique.

A review of the existing literature shows that no study has been conducted in the past on unbraced plane or space frames subjected to nonproportional loads.

1.3 The Problems

To study the inelastic instability behavior of members and frames with sway and subjected to nonproportional loads, solution procedures are developed for the following types of structures:

1. Planar beam-columns.
2. Space beam-columns.

3. Portal frames.
4. Space frames.

The theoretical analysis includes both linear and bilinear rotational end restraints. The member analysis also includes partial lateral restraints. An experimental study of a three-story single-bay space frame is also conducted under nonproportional loads in order to verify the inelastic theoretical procedures presented.

1.4 Objective and Scope

The main objective of this research is to study the effect of nonproportional loading on the stability and behavior of sway beam-columns, and plane and space frames with flexible connections. Based on materially nonlinear differential equations of equilibrium, a procedure for analyzing plane and space frames is formulated through member-level inelastic slope-deflection equations. Only orthogonal frames are considered, that is, no inclined members are included. Furthermore, hollow square and rectangular members are adopted. These members are considered torsionally stiff and consequently torsional deformations are neglected.

To verify the theoretical results, a laboratory experiment is conducted on a three-story single-bay space steel frame and the results are compared to the theory.

1.5 Assumptions and Conditions

The following assumptions and conditions are adopted in this dissertation:

1. The deflections are small in accordance with the small deflection theory.

2. The material is elastic-plastic and unloads elastically in the inelastic range.
3. Torsional effects are negligible.
4. Plate local buckling does not occur in the members.
5. Member shear deformation and axial shortening are negligible.

The external loads are nonproportional in nature and are applied gradually, that is, no dynamic effects are included.

2. PARTIALLY RESTRAINED IMPERFECT SWAY BEAM-COLUMNS

The governing nonlinear differential equations of equilibrium for a partially restrained imperfect sway beam-column are presented in this chapter. An iterative algorithm based on a finite-difference scheme is formulated. The imperfections include cross-sectional residual stresses and initial member crookedness. The approach presented by Razzaq (24) for inelastic columns has been previously modified by Razzaq and Darbhamulla (28, 29, 30, 31) for biaxially restrained *nonsway* columns and beam-columns. This analysis is extended herein to include biaxial *sway* in the presence of biaxial lateral translational restraints. First, several special nonsway and sway cases are analyzed and compared to known results for a verification of the analysis. Next, the behavior of both uniaxially and biaxially loaded sway beam-columns is studied under the influence of nonproportional loads. Lastly, the beam-column equations are exploited to generate inelastic slope-deflection equations for use in frame analysis presented latter in this dissertation.

2.1 Cross-Sectional Analysis

Figure 1 shows a discretized hollow rectangular section with a width B , depth D , and a wall thickness t . Each wall of the cross section is divided into finite elemental areas. In this figure, ΔA represents a typical elemental area. Figure 2 shows an elastic-plastic stress-strain relationship for the material including elastic

unloading. In this figure, E is the Young's modulus, σ_Y is the yield stress, and ϵ_Y is the yield strain. The compression and tension stress-strain relationships are assumed to be identical. The cross section has initial residual stresses. The residual stress distribution shown in Figure 3 is by Ballio and Campanini (21), with the maximum tensile and compressive residual stresses equal to $\sigma_{rt} = 0.5\sigma_Y$ and $\sigma_{rc} = -0.2\sigma_Y$, respectively. Figures 4 and 5 show the idealized versions of the residual stresses found experimentally for the square and rectangular sections used, respectively, in the space frame test described in Chapter 4. The experiments showed that compressive residual stresses exist at the corners while tensile residual stresses exist at the center of each wall of the cross sections. These residual stresses are opposite in nature to those shown in Figure 3. In Figure 4, $\sigma_{rt} = 0.21\sigma_Y$ and $\sigma_{rc} = -0.17\sigma_Y$. In Figure 5, $\sigma_{rt} = 0.12\sigma_Y$ and $\sigma_{rc} = -0.18\sigma_Y$.

The loading on the cross section consists of an axial load P applied perpendicular to the xy -plane, and bending moments M_x and M_y about the x and y axes, respectively. The normal strain, ϵ , at a point (x,y) of the cross section is expressed as:

$$\epsilon = \epsilon_0 + \Phi_x y - \Phi_y x + \epsilon_r \quad (1)$$

in which ϵ_0 is the average axial strain; Φ_x and Φ_y are the bending curvatures about the x and y axes, respectively; ϵ_r is the residual strain. The stress-strain rate relationship is given by:

$$\dot{\sigma} = E_t \dot{\epsilon} \quad (2)$$

in which E_t equals E if the material is elastic; it equals zero if the material is plastic. The axial and the biaxial moment equilibrium equations for the cross section can be written as:

$$P = -\int_{A_e} \sigma_e dA - \int_{A_p} \sigma_Y dA \quad (3)$$

$$M_x = \int_{A_e} \sigma_e y dA + \int_{A_p} \sigma_Y y dA \quad (4)$$

$$M_y = -\int_{A_e} \sigma_e x dA - \int_{A_p} \sigma_Y x dA \quad (5)$$

in which Da is an elemental area of the cross section, and σ is the normal stress on that area. The subscripts e and p refer to the elastic and plastic parts, respectively, of a partially plastified section; \int_A denotes cross-sectional integration. Thus, given an axial load, and a pair of bending moments, the strain distribution is found while following Equation 2. In other words, compatible ε_0 , Φ_x and Φ_y are obtained which satisfy equilibrium for P , M_x and M_y . The cross-sectional dimensionless load and deformation vectors, $\{f\}$ and $\{\delta\}$, can be expressed as follows:

$$\{f\} = \{p \quad \bar{m}_x \quad \bar{m}_y\}^T \quad (6)$$

$$\{\delta\} = \{\bar{\varepsilon}_0 \quad \bar{\varphi}_x \quad \bar{\varphi}_y\}^T \quad (7)$$

where the various terms are defined in Appendix A. The solution procedure (Reference 19) involves starting at a known state and incrementally converging to the next state for which only $\{f\}$ is known. The deformation vector $\{\delta\}$ is determined

by iteratively adjusting a cross-sectional tangent stiffness matrix, $[K_t]$, relating the increments in $\{f\}$ to the increments in $\{\delta\}$ through the following rate equation:

$$\{\dot{f}\} = [K_t] \{\dot{\delta}\} \quad (8)$$

The various components of this equation are defined in Appendix A. The process is repeated until the imbalance between the external loads and the internal forces becomes zero or is within a tolerance. Once the strain distribution, ϵ , is found, the internal resisting forces are evaluated by numerical summation over the discretized cross section shown in Figure 1. This is readily done by replacing the integrals in Equations 3, 4, and 5 by summations.

2.2 Governing Equations for Space Sway Beam-Columns

Figure 6 shows a partially restrained imperfect sway beam-column BT of length L in the three-dimensional space x, y, z . The origin of the longitudinal coordinate z is at B. The member is provided with end rotational springs having an initial set of stiffnesses K_{Tx} , K_{Bx} , K_{Ty} , and K_{By} . The translational springs provided at the top end have stiffnesses K_x and K_y . The member is subjected to a lateral load W in the yz plane, and an axial load P and biaxial end moments M_{Bx} , M_{By} , M_{Tx} , and M_{Ty} applied at the boundaries.

The total deflections U and V including member initial crookedness are given by:

$$U = u + u_{oi} \quad (9)$$

$$\mathbf{V} = \mathbf{v} + \mathbf{v}_{0i} \quad (10)$$

where u and v are the deflections due to the applied loads, and u_{0i} and v_{0i} represent the crookedness in the xz and yz planes, respectively, and given by:

$$u_{0i} = u_0 \sin \frac{\pi z}{L} \quad (11)$$

$$v_{0i} = v_0 \sin \frac{\pi z}{L} \quad (12)$$

In Equations 11 and 12, u_0 and v_0 are the midspan initial amplitudes taken as $L/1000$ for a crooked member and as $L/100,000$ for a nearly straight one.

If the spring moments at the member ends B and T are represented, respectively, by (m_{Bx}, m_{By}) and (m_{Tx}, m_{Ty}) , the total external moments M_x and M_y at any location z can be expressed as follows:

$$M_x = PV - m_{Bx} - M_{Bx} - zR_y \quad (0 \leq z \leq c) \quad (13a)$$

$$M_x = PV - W(z-c) - m_{Bx} - M_{Bx} - zR_y \quad (z \geq c) \quad (13b)$$

$$M_y = -PU + m_{By} - M_{By} + zR_x \quad (14)$$

where c is the distance of the load W from B, and the reactions are given by:

$$R_x = \frac{1}{L} \{ PU_n + m_{Ty} - m_{By} + M_{By} + M_{Ty} \} \quad (15)$$

$$R_y = \frac{1}{L} \{ PV_n + W(L-c) - m_{Bx} + m_{Tx} - M_{Bx} - M_{Tx} \} \quad (16)$$

In these equations, U_n and V_n are the member top end deflections in the x and y directions, respectively.

Substituting Equation 1 into the first term on the right hand side of each of Equations 3, 4, and 5, noting that $\Phi_x = -v''$, and $\Phi_y = u''$, and utilizing Equations 13 and 14, the following materially nonlinear ordinary differential equations are obtained:

$$a_{11}\varepsilon_0 + a_{12}v'' + a_{13}u'' = -P - P_r - P_p \quad (17)$$

$$a_{21}\varepsilon_0 + a_{22}v'' + a_{23}u'' = M_x - M_{xre} - M_{xp} \quad (18)$$

$$a_{31}\varepsilon_0 + a_{32}v'' + a_{33}u'' = M_y + M_{yre} + M_{yp} \quad (19)$$

in which the primes designate differentiation relative to z; a_{ij} are the inelastic cross-sectional coefficients described in Appendix B. The terms P_r , P_p , M_{xre} , M_{yre} , M_{xp} , and M_{yp} are the inelastic load and moment parameters defined in Reference 25 and also summarized in Appendix B.

At the global level, Equation 17 is enforced by first solving it for ε_0 explicitly and then substituting it into Equations 18 and 19. This results into the following two materially nonlinear ordinary differential equations:

$$A_{xx}v'' + A_{xy}u'' = a_{21}P_t + M_x - M_{xx} \quad (20)$$

$$A_{yx}v'' + A_{yy}u'' = a_{31}P_t + M_y - M_{yy} \quad (21)$$

where:

$$A_{xx} = (a_{11}a_{22} - a_{12}a_{21})/a_{11} \quad (22)$$

$$A_{xy} = (a_{11}a_{23} - a_{21}a_{13})/a_{11} \quad (23)$$

$$A_{yx} = (a_{11}a_{32} - a_{12}a_{31})/a_{11} \quad (24)$$

$$A_{yy} = (a_{11}a_{33} - a_{13}a_{31})/a_{11} \quad (25)$$

$$P_t = (P + P_r + P_p)/a_{11} \quad (26)$$

$$M_{xx} = M_{xre} + M_{xp} \quad (27)$$

$$M_{yy} = M_{yre} + M_{yp} \quad (28)$$

In the elastic range, the terms defined in Equations 22 through 28 are constant for each load level. In the inelastic range, however, these terms must be calculated iteratively since they become dependent upon u and v .

2.3 Boundary Conditions

The restraining springs at the boundaries are assumed to behave elastically or bilinearly during the loading process following Figure 7. The resisting spring moments for a space sway beam-column appearing in Equations 13 through 16 are m_{Bx} , m_{By} , m_{Tx} and m_{Ty} and are dependent upon the moment-rotation (m - θ) relationships of the end connections. For a linear m - θ relationship, the spring moment, m_s , follows the line OA in Figure 7 and is given by:

$$m_s = K_{sa} \theta; \quad |\theta| \leq |\theta_a| \quad (29)$$

For a bilinear relationship, the spring moment follows the path OAB shown in Figure 7. The portion OA is represented by Equation 29, while the portion AB is represented by:

$$m_s = (K_{sa} - K_{sb}) \theta_a + K_{sb} \theta; \quad |\theta| \geq |\theta_a| \quad (30)$$

where K_{sa} , and K_{sb} are the spring rotational stiffnesses. For $\theta = \theta_a$, the spring "plastic" moment m_{sa} is also shown in Figure 7.

The deflection at end B is zero. Thus:

$$u(0) = v(0) = 0 \quad (31)$$

The top end reactions in both planes are given by:

$$R_x(L) = - K_x u(L) \quad (32)$$

$$R_y(L) = - K_y v(L) \quad (33)$$

where K_x and K_y are the translational spring stiffnesses.

2.4 Finite-Difference Formulation

The numerical procedure is based on a second-order central finite-difference scheme applied to Equations 20 and 21 at n equidistant nodes over $(0, L)$, and by invoking the appropriate boundary conditions. Using the finite-difference expression for a second-order derivative (21), Equations 20 and 21 become:

$$A_{xxi}(v_{i-1} - 2v_i + v_{i+1}) + A_{xyi}(u_{i-1} - 2u_i + u_{i+1}) = (a_{2li}P_{\bar{u}} + M_{xi} - M_{xxi})h^2 \quad (34)$$

$$A_{yxi}(v_{i-1} - 2v_i + v_{i+1}) + A_{yyi}(u_{i-1} - 2u_i + u_{i+1}) = (a_{3ii}P_{ii} + M_{yi} - M_{yyi})h^2 \quad (35)$$

where h is the distance between two consecutive nodes along the member length. Applying Equations 34 and 35 at nodes $i = 1, 2, 3, \dots, n$ along the member length, and using the boundary conditions given in Section 2.3, the following nonlinear matrix equation is obtained:

$$[K]\{\Delta\} = \{M\} \quad (36)$$

In this equation, $[K]$ is the global tangent stiffness matrix of order $2(n+2)$. The vector $\{\Delta\}$ contains the member deflections defined as follows:

$$\{\Delta\} = \{u_1 \ v_1 \ u_2 \ v_2 \ \dots \ u_{n-1} \ v_{n-1} \ u_n \ v_n \ \theta_{Bx} \ \theta_{By} \ \theta_{Tx} \ \theta_{Ty}\}^T \quad (37)$$

in which θ_{Bx} , θ_{By} , θ_{Tx} and θ_{Ty} are the rotations at the ends B and T. The load vector $\{M\}$ is given by:

$$\{M\} = \{F\} + \{F\}_p + \{M\}_a \quad (38)$$

in which $\{F\}$ is the external load vector associated with member crookedness, $\{F\}_p$ is the load vector containing the plastic forces, and $\{M\}_a$ is the applied nodal moment vector.

In order to clearly visualize the various vectors in Equation 38, consider a member loaded uniaxially about the major axis. For this problem, only Equation 34 is applicable with all v terms set equal to zero. The vectors $\{F\}$ and $\{F\}_p$ are expanded as follows:

$$\{F\} = h^2 P \begin{Bmatrix} (a_{21})_1 + v_{01} \\ (a_{21})_2 + v_{02} \\ \vdots \\ (a_{21})_{n-1} + v_{0(n-1)} \\ (a_{21})_1 + v_{01} \\ (a_{21})_n + v_{0n} \\ (a_{21})_n + v_{0n} \end{Bmatrix} \quad (38a)$$

$$\{F\}_p = h^2 \begin{Bmatrix} (a_{21})_1(P_r + P_p)_1 - (M_{xx})_1 \\ (a_{21})_2(P_r + P_p)_2 - (M_{xx})_2 \\ \vdots \\ (a_{21})_{n-1}(P_r + P_p)_{n-1} - (M_{xx})_{n-1} \\ (a_{21})_1(P_r + P_p)_1 - (M_{xx})_1 \\ (a_{21})_n(P_r + P_p)_n - (M_{xx})_n \\ (a_{21})_n(P_r - P_p)_n - (M_{xx})_n \end{Bmatrix} \quad (38b)$$

The right hand side terms are generated for nodes $i = 1, 2, 3, \dots, n$. For generating $\{M_a\}$, note that the moments at any node i are given by Equations 13a and 13b and correspond to the second term on the right hand side of Equation 34. The nodal moments M_{xi} include unknown deflection terms which must be transferred to the left hand side of Equation 34. The vector $\{M_a\}$ is then isolated and written as follows:

$$\{M_a\} = h^2 \begin{Bmatrix} \frac{z_1-L}{L} & \frac{z_1}{L} \\ \frac{z_2-L}{L} & \frac{z_2}{L} \\ \vdots & \vdots \\ \frac{z_{n-1}-L}{L} & \frac{z_{n-1}}{L} \\ \frac{z_1-L}{L} & \frac{z_1}{L} \\ \frac{z_n-L}{L} & \frac{z_n}{L} \\ \frac{z_n-L}{L} & \frac{z_n}{L} \end{Bmatrix} \begin{Bmatrix} M_{Tx} \\ M_{Bx} \end{Bmatrix} \quad (38c)$$

Equation 36 is nonlinear since $[K]$ and $\{F\}_p$ are dependent on $\{\Delta\}$. If the initial member crookedness is included in the lateral displacement terms, the deflection vector can be written as:

$$\{\bar{\Delta}\} = \{U_1 \quad V_1 \quad U_2 \quad V_2 \quad \dots \quad U_{n-1} \quad V_{n-1} \quad U_n \quad V_n \quad \theta_{Bx} \quad \theta_{By} \quad \theta_{Tx} \quad \theta_{Ty}\}^T \quad (39)$$

In this expression, the slope terms are the same as those in Equation 37.

2.5 Load Paths

Two different sets of load paths are adopted, one for the uniaxially loaded sway beam-columns and the other for the biaxially loaded sway beam-columns. These are described in this section.

2.5.1 Load Paths for Uniaxially Loaded Sway Beam-Columns

Five load paths designated as NP1 through NP5 are used for the uniaxial loading case. With reference to Figure 8, these are defined as follows:

NP1: The axial load P is first applied incrementally and then held constant, followed by gradually increasing equal end moments until the load-carrying capacity of the member is reached. This corresponds to the path OAB.

NP2: The equal end moments corresponding to the load-carrying capacity obtained in NP1 are first applied incrementally and then held constant, followed by a gradually increasing axial load P until the member collapse occurs. The load path NP2 corresponds to the path OCB.

NP3: The equal end moments are first applied and then held constant, followed by gradually increasing axial load P until the member collapses. This loading path is the reverse of NP1. The load path NP3 corresponds to the path OCB.

NP4: The axial load corresponding to the load-carrying capacity obtained in NP3 is applied first incrementally and then held constant, followed by gradually increasing equal end moments until the collapse occurs. This load path is the reverse of NP2 and corresponds to the path OAB.

NP5: The equal end moments are first applied incrementally, followed by gradually increasing both the axial load P and the equal end moments M_x simultaneously until collapse occurs. This corresponds to the path OJB.

The following four specific load paths are from Reference 37, and are designated herein as LC1 through LC4:

LC1: A relatively large axial load is first applied incrementally and then held constant, followed by gradually increasing the equal end moments until collapse occurs.

LC2: The maximum end moments corresponding to LC1 are first applied incrementally and then held constant, followed by a gradually increasing axial load until collapse occurs.

LC3: Relatively large equal end moments are first applied incrementally and then held constant, followed by a gradually increasing axial load until collapse occurs.

LC4: The maximum axial load corresponding to LC3 is first applied incrementally and then held constant, followed by gradually increasing equal end moments until collapse occurs.

The load paths LC1 through LC4 correspond, respectively, to the load paths NP1 through NP4 except for the magnitudes of the axial load and the moments.

2.5.2 Load Paths for Biaxially Loaded Sway Beam-Columns

Seven different load paths designated as **LP1** through **LP7** are used for biaxially loaded sway beam-columns and are defined below with reference to Figure 8:

LP1: The axial load P is first applied incrementally and then held constant, followed by M_x and M_y simultaneously until collapse occurs. This corresponds to the path OAE.

LP2: The moments M_x and M_y are first applied proportionally until the peak values obtained in **LP1** are attained, followed by the axial load P until collapse occurs. The load path **LP2** corresponds to the path OFE.

LP3: The axial load P of the same magnitude as in **LP1** is first applied incrementally and then held constant. Next, the M_x value achieved in **LP1** is applied and held constant, followed by M_y until collapse occurs. The load path **LP3** corresponds to the path OABE.

LP4: This load path is the reverse of **LP3**, that is, M_y achieved in **LP1** is first applied followed by M_x achieved in **LP1**, and then followed by load P until collapse occurs. This corresponds to the path OGFE.

LP5: The moments M_x and M_y are first applied proportionally, followed by the axial load P until collapse occurs. The load path **LP5** corresponds to the path OFE.

LP6: The axial load P of the same magnitude as that reached in **LP5** is first applied incrementally and then held constant, followed by M_x and M_y simultaneously until collapse occurs. This corresponds to the path OAE.

LP7: The moments M_x and M_y are first applied incrementally in a proportional manner and held constant, followed by a gradual increase in both the axial load P and the end moments until collapse occurs. The load path **LP7** corresponds to the path OHE.

Numerical results based on these load paths are presented latter in this dissertation.

2.6 Solution Procedure for Sway Beam-Columns

The inelastic beam-column solution procedure used in the present study is basically the same as that given by Razzaq (23) with modifications to account for biaxial loading and sway. The solution steps are as follows:

1. Evaluate the initial cross-sectional properties at n nodes along the member length and assemble the initial global sway beam-column stiffness matrix $[K]$ in Equation 36.
2. Specify small external loads and formulate $\{M\}_1$ using Equation 38.
3. Solve for the deformation vector $\{\Delta\}$ in Equation 36.
4. Compute the external nodal forces $\{f\}_1$ and deformations $\{\delta\}_1$ defined in Equations 6 and 7, respectively, in the elastic range corresponding to $\{M\}_1$.
5. Increase $\{M\}$ to $\{M\}_2 = \{M\}_1 + \{\delta M\}$, in which $\{\delta M\}$ is the resultant load increment vector. Solve Equation 36 for $\{\Delta\}$, and compute the external force vector $\{f\}_2$ corresponding to $\{M\}_2$.

6. Using $\{f\}_2$ and the tangent stiffness procedure (Reference 18), determine $[K_t]$ in Equation 8 for all n cross sections.
7. Solve for an updated $\{\Delta\}$ after assembling $[K]$, $\{F\}$ and $\{F\}_p$ while utilizing the cross-sectional coefficients obtained in Step 6.
8. Using $\{\Delta\}$ from Step 7, formulate the load vector $\{M\}_3$.
9. If $|\{M\}_3 - \{M\}_2| \leq \alpha$, where α is the tolerance taken as 0.01% of the member yield-load capacity, go to Step 11.
10. Set $\{M\}_1 = \{M\}_2$, $\{f\}_1 = \{f\}_2$ and $\{M\}_2 = \{M\}_3$, go to Step 6.
11. Set $\{M\}_1 = \{M\}_3$; $\{f\}_1 = \{f\}_3$, and repeat Steps 5-10 until the maximum load carrying capacity of the beam-column is reached.

The procedure is carried out using constant load increments throughout the elastic range. In the inelastic range, these load increments are successively reduced to avoid severe imbalance between the external and the internal forces. The member maximum load is obtained within a tolerance of 0.0002 times the cross-sectional yield capacity.

2.7 Analysis and Behavior of Sway Beam-Columns

In Figure 1, the side with the dimension B is divided into 48 elements (4 layers with 12 elements per layer), and the side with the dimension $(D - 2t)$ is divided into 56 elements (4 layers with 14 elements per layer). This provides a total of 208 elements per cross section. This discretization is found to be suitable for convergence purposes. Also, for the finite-difference scheme, a total of 11 nodes over the member length $[0, L]$ is found to be sufficient.

2.7.1 Comparison to Published Results for Special Cases

To assess the accuracy of the computational procedure, a comparison is made to some published results for columns and beam-columns with or without sway.

Galambos (10) investigated the elastic instability of planar beam-columns subjected to axial load and end moments. Equations 4.77 and 4.78 in Reference 10 are the elastic slope-deflection equations modified for axial load. For a comparison, a 7x7x0.375 in. hollow square cross section is adopted. A 12 ft long steel member with fixed base, free top, and subjected to an axial load and a moment at the top is analyzed using the procedure in Reference 10. Figure 9 shows the dimensionless axial load p versus the top deflection for this member including the P- Δ effect, in which $p = P/P_Y$. The curve shown in the figure is for both the predicted and reference values indicating that the results are identical.

Razzaq and Calash (26) studied the behavior of imperfect columns with biaxial partial restraints. The columns were initially crooked in one or both principal directions, and possessed initial residual stresses. Elastic unloading of plastic material was not included. The following four rotational end restraint stiffnesses were used in the study:

$$K_a = 0.0 \text{ kip-in/rad}$$

$$K_b = 5397.22 \text{ kip-in/rad}$$

$$K_c = 15506.94 \text{ kip-in/rad}$$

$$K_d = 1.0E+15 \text{ kip-in/rad}$$

Two types of cross sections were considered, a 7 x 7 x 0.375 in. hollow square section and a 6 x 8 x 0.375 in. hollow rectangular section. The material properties,

E and σ_Y were taken as 29,000 ksi and 46.0 ksi, respectively. For a 12 ft long column, Tables 1 and 2 summarize the results for 16 cases, eight with the hollow square section and eight with the hollow rectangular section. The midspan crookedness is taken as $L/1000$. For nearly straight members, it is taken as $L/100,000$. The columns are either uniaxially crooked (Columns 1 to 4, and 9 to 12), or biaxially crooked (Columns 5 to 8, and 13 to 16). The column peak loads found by the present study are in good agreement with those presented in Reference 26. Similarly an excellent comparison of the results is obtained as shown in Table 2 for hollow rectangular section (Columns 9 through 16).

Figure 10 shows a pinned-end nonsway beam-column subjected to an axial load P , and a concentrated lateral point load W applied at midspan. Moy (14) conducted a theoretical study of this type of beam-column. A W8x31 section was used with L/r_x taken as 20, 40, and 60, where r_x is the radius of gyration about the x axis. Table 3 shows 9 beam-columns of A36 steel numbered 17 through 25. The lateral load is applied and held constant at the W value given in the table while the axial load P is incremented until the collapse occurs. The predicted loads are in good agreement with the loads from Reference 14.

Razzaq and Darbhamulla (29 and 30) studied the behavior of biaxially loaded imperfect nonsway beam-columns with a hollow rectangular section and an I-section. The following four rotational spring stiffnesses were considered:

$$K_1 = 0.0 \text{ kip-in/rad}$$

$$K_2 = 13,333 \text{ kip-in/rad}$$

$$K_3 = 24,000 \text{ kip-in/rad}$$

$$K_4 = 1.0E+15 \text{ kip-in/rad}$$

Tables 4 and 5 summarize the predicted and previously obtained (References 29 and 30) maximum dimensionless external loads for load paths LP1 through LP4. The members used in Table 4 have a 6x8x0.375 in. hollow rectangular section with $L = 12$ ft, $E = 29,000$ ksi, $\sigma_Y = 46$ ksi, and residual stresses as shown in Figure 3. The beam-columns are biaxially crooked, and have equal rotational end restraints of stiffness K_3 . The beam-column results in Table 5 are for a W8x31 section of A36 steel. The beam-column length is 12 ft and it is crooked in both planes. The W section beam-columns possess a residual stress distribution as shown in Figure 11. The beam-columns are partially restrained with equal end rotational springs of stiffness K_2 . The results in Tables 4 and 5 show that the predicted results are in good agreement with those in References 29 and 30.

Finally, the results for uniaxially loaded imperfect and inelastic sway columns with unequal end restraints are compared to those given by Lord (32). Lord conducted a study with a W8x31 section of A36 steel relative to the minor axis. The length of each column was taken as 12 ft. The columns were initially crooked and possessed residual stresses as shown in Figure 11. Figures 12 through 14 show the load versus the top deflection curves for the columns with rotational end restraint stiffnesses equal to K_a at T, and equal to K_b , K_c , and K_d , respectively, at end B. Elastic unloading of plastic material was neglected. The curves in the figures show that the predicted results are in excellent agreement with those given in Reference 32.

2.7.2 Behavior of Uniaxially Loaded Sway Beam-Columns

Considering the deflections in the yz plane only, a sway beam-column is obtained as a special case of the one shown in Figure 6. The member is imperfect and has a 7x7x0.375 in. hollow square section. It is crooked in the yz plane and has residual stresses defined by $\sigma_{rc} = -0.2 \sigma_Y$ and $\sigma_{rt} = 0.5 \sigma_Y$ as shown in Figure 3 unless otherwise mentioned. Tables 6 and 7 give the results for a total of 11 members designated as BC1 through BC11. The beam-columns are subjected to an axial load and external equal end moments ($M_{Bx} = M_{Tx} = M_x$) applied nonproportionally. The members under study are partially restrained at both ends by rotational springs corresponding to the moment-rotation relationship shown in Figure 7. The tables summarize the dimensionless external loads $p = P/P_Y$ and $m_x = M_x/M_{xY}$. The results in Table 6 are obtained for the load paths NP1 and NP2. The rotational end restraints used for this table are of stiffness K_2 . Table 7 presents the results based on load paths NP3 and NP4, and the restraints used have a stiffness K_3 . The effect of lateral spring stiffness, K_y , on the maximum axial load, p_{max} , is shown in the last column of Tables 6 and 7. The results show the dramatic influence of nonproportional loading on the load-carrying-capacity of the sway beam-columns. The results in Tables 6 and 7 are only the maximum external loads, and the loading history for any path is shown graphically in Figures 15 through 19. Figures 15 and 16 show stiffness degradation curves in the form of the relationships between the dimensionless determinant, \bar{D} , of the member tangent stiffness matrix, with the initial tangent stiffness determinant used as a normalizing factor, and the dimensionless axial load p , for various lateral springs stiffnesses. From the figures, it is clear that

the member stiffness and strength decrease with a decrease in the lateral spring stiffness. Figures 17 and 18 show $\bar{D}-p$ and $\bar{D}-m_x$ curves for BC5 subjected to load paths NP1 and NP2. The very significant effect of the load paths on the beam-column response is quite clear here. In Figure 17, the dashed curve is for the member following the load path NP1. For the load path NP1, the determinant decreases rapidly until the point Q_1 is reached. The moment is then incremented while holding p constant. The solid curve in the same figure shows the $\bar{D}-p$ curve for the load path NP2. This curve starts at $\bar{D} = 0.12$. The initial rising part of this curve is due to the member experiencing elastic unloading of portions of the member. When p reaches a higher value, the member starts to lose its stiffness again and ultimately drops down to zero at point Q_2 . Similar behavior is observed in $\bar{D}-m_x$ curves shown in Figure 18.

Figure 19 shows $p-m_x$ interaction relationships for the sway beam-column BC10. The curves are constructed from the results in Table 7, in which p or m_x are held constant at different values and attain the member collapse loads for a given load path. As seen from Figure 19, the member peak loads are load-path dependent. The results in Table 8 show the effect of imperfections on the strength of sway beam-columns, with lateral spring stiffness $K_y = 0.0$, and with equal rotational end restraints of stiffness K_2 . The results for beam-columns BC12 through BC15 in this table are obtained for various residual stress and crookedness values. The member has a 6x8x0.375 in. hollow rectangular section, and the load paths NP3 and NP4 are used. Figures 20 and 21 show the $\bar{D}-p$ and $\bar{D}-m_x$ curves for the members. These

figures show that the members with residual stresses and crookedness are weaker in strength. In addition, the residual stresses affect the strength of members more than the crookedness. Tables 9 through 11 present similar results with $K_y = 0.10, 2.0,$ and $1.0E+15,$ respectively.

Table 12 summarizes the maximum dimensionless external loads for sway beam-columns with the hollow rectangular section, bilinear lateral restraints and equal end rotational restraints. Figure 7 shows the bilinear spring moment-rotation relationship. Here K_{sa} is taken as K_2 , and K_{sb} as K_b . The spring yield moment, m_{sa} , is taken as 97.0 kip-in/rad. Also a 6x8x0.375 in. hollow rectangular section is used. Figures 22 and 23 show the stiffness degradation \bar{D} versus p and m_x , respectively, for member BC30 with the load path NP3. Figure 22 shows an increase in the member stiffness in the initial part of the \bar{D} - p curve. This type of member stiffening occurs due to material unloading. The unloading occurs since the axial load is applied last. This increase in the stiffness is observed for \bar{D} in the range from 0.05 to 0.45 whereafter a decrease in \bar{D} is experienced. Also, since the end moments are first applied, \bar{D} remains constant initially in the elastic range whereafter it decreases almost suddenly due to the yielding of the rotational springs while the member is still elastic. The member stiffness remains constant after the spring stiffness is reduced. Subsequently, it begins to decrease as the member itself develops plastic action. At a dimensionless moment equal to 0.93, the axial load is incremented and some member unloading occurs. This causes a jump in the \bar{D} - m_x

curve as shown by the vertical line at $m_x = 0.93$. Figure 24 shows the stiffness degradation \bar{D} versus the spring moment m_s relationship and having the same type of characteristics as the \bar{D} - m_x curve.

As mentioned earlier, it was found that there is a difference between the measured residual stress distributions (RSD) shown in Figures 4 or 5 and that given in Reference 20 shown in Figure 3. To study the effect of the type of RSD distribution on the behavior of hollow rectangular section sway member, a member of length 5 ft. with $\sigma_Y = 46$ ksi is considered. The rotational restraint stiffness is taken as zero at the top and as infinite at the bottom end of the member. The translational stiffness K_x is taken as 1.0 kip/in., and the load path NP5 is used. With the RSD given in Figure 3, the maximum dimensionless loads obtained are $p = 0.204$ and $m_x = 1.062$. With the RSD in Figure 5, $p = 0.196$ and $m_x = 1.056$. In both cases, $m_x = 0.891$ is first applied. A slight increase in the peak loads is found if RSD shown in Figure 3 is used. Figures 25, 26, and 27 show a comparison of the \bar{D} - p , \bar{D} - m_x , and m_x - Δ_{cx} relationships based on the two RSD distributions. The member with the RSD given in Figure 5 is stiffer.

2.7.3 Behavior of Biaxially Loaded Sway Beam-Columns

The behavior of 12 ft. long biaxially loaded imperfect sway beam-columns is investigated with equal and unequal end rotational restraints, with various load paths. A 6x8x0.375 in. hollow rectangular section is used with $E = 29,000$ ksi, and $\sigma_Y = 46$ ksi. Figure 6 shows the member which is crooked in both the xz and the yz planes

and has a residual stress distribution of the type shown in Figure 3 unless otherwise mentioned.

Table 13 presents the maximum dimensionless external loads for sway beam-columns numbered BC32 through BC36 with equal end rotational restraints of stiffness K_3 , for load paths LP1 and LP2. The first column of results under dimensionless external load in the table shows no axial load in either load path, that is, only biaxial moments are applied. These cases do not represent a stability problem. Nevertheless, the results show that an increase in the lateral spring stiffness results in an increase in the moment capacity. In the second column of the results, the axial load is seen to range from 0.20 to 0.33. These results show that the effect of load path dependence exists for some cases when a small to moderate axial load is introduced into the problem. As an example, the maximum axial load for BC33 is increased by 21% (p is increased from 0.24 to 0.29) when the load path is reversed from LP1 to LP2. Similarly, the maximum axial load for BC34 is increased by 32%, from 0.22 to 0.29. When the axial load is about 50% of the axial yield load, a reversal of the load path has no effect. This is seen from the last three columns presented in the table. Also, the maximum dimensionless axial load which the member can carry is given in the last column of the table for various lateral stiffnesses. If this axial load is reduced by a small amount, a member may be able to sustain significant bending moments. This is observed for the beam-column BC34. As the axial load is reduced from 0.79 to 0.75, it can carry m_x and m_y of 0.27 and 0.29, respectively.

The effect of the lateral restraint stiffness on the beam-column strength is also observed from Table 13. When a moderate axial load is applied using the load path

LP1, a significant increase in the moment is obtained by introducing a partial lateral restraint. For example, the moment-carrying capacity of member BC33 is much greater than that of member BC32. For a dimensionless axial load of 0.50, the moments for BC33 increase by 83% and 89% for m_x and m_y , respectively, relative to the moments for BC32. The members subjected to a low to moderate axial load as an initial loading for LP1 show a noticeable change in the peak axial load when the load path is reversed from LP1 to LP2. For example, for the beam-column BC36, when the load path LP1 is used with an axial load of 0.27, the biaxial moments m_x and m_y of 1.62 and 1.77, respectively, are achieved at collapse. However, when the load path LP2 is used with the corresponding moments from LP1, the maximum axial load is found to be 22% higher than that from LP1. Figures 28 through 31 show the stiffness degradation curves for some representative cases. Figure 28 shows the effect of lateral restraint stiffness on the stiffness degradation $\bar{D}-p$ for the beam-columns BC32 through BC36. Figures 29, 30, and 31 show the stiffness degradation \bar{D} versus p , m_x , and m_y , respectively, for the beam-column BC35.

Table 14 summarizes the maximum dimensionless external loads for imperfect sway beam-columns with unequal partial end rotational restraints and with stiffnesses K_3 and K_2 at the bottom and top, respectively. The load paths LP5 and LP6 are adopted in this table with various lateral restraints. Five cases are studied here, namely, BC37 through BC41. The first column under the dimensionless external loads is for bending problems since no axial load is introduced. The effect of the load paths LP5 and LP6 is observed here only when a high value of the external moments is applied using LP5. The second and the third columns show the effect

of the nonproportional loads for various lateral restraint stiffnesses. It is seen that when the load path LP6 is used corresponding to the axial load achieved by the load path LP5, a reduction in the moment-carrying capacity occurs. This is true for all lateral restraints stiffnesses except when $K_x = K_y = 1.0$ kip/in. for which a small change in the maximum moments is observed when the load path is reversed. For example, consider the beam-columns BC37 and BC39 with lateral restraint stiffnesses of 0.0 and 1.0 kip/in., respectively. For the beam-column BC37, with load path LP5, the m_x and m_y moments are incremented to the maximum values of 1.71 and 1.43, respectively, whereafter a peak axial load of 0.16 is attained. However, when the load path LP6 is used and the axial load of 0.16 is first applied, the peak m_x and m_y moments attained are 1.40 and 1.17, respectively, that is, a reduction of 22% on each moment. For the beam-column BC39, a substantial change in the peak moments is observed when the load path is reversed in the presence of a lateral restraint stiffness of 1.0 kip/in. Figure 32 shows a comparison of the axial load versus the top deflection curves obtained with LP5 and LP6 for the beam-column BC39.

Table 15 summarizes the maximum dimensionless loads for the sway beam-columns with equal partial end rotational restraints of stiffness K_2 and with load paths LP1 through LP4. The first and the last columns, under the maximum external load in the table, are for bending and axial load problems, respectively. The second and the third columns are for moderate axial load, and it is seen from the results that only the load paths LP2 and LP4 exhibit the load path effect. Applying the load path LP2 with the moments obtained in LP1, the maximum axial load obtained is 0.25. This represents a 25% increase in the member axial strength compared to that with load path LP1. With load path LP4, the maximum axial load obtained is 0.13. This

load is 53% less than the load obtained with LP1. Figure 33 shows the stiffness degradation curves $\bar{D}-p$ for the beam-columns BC42 and BC43. The figure shows the effect of the lateral spring stiffness on the stiffness degradation of the beam-columns. Figures 34 through 36 show the stiffness degradation \bar{D} versus p , m_x and m_y for BC42 with the load paths LP3 and LP4. The \bar{D} value with the load path LP4 is close to zero when the axial load is applied. Similarly, \bar{D} nearly equals to zero with the load path LP3 when even a small m_y moment is applied. Figure 37 shows the moment versus the midspan deflection for the beam-column BC42 with load paths LP1 and LP2. The flat top portion of the curve for LP2 indicates that the axial load is held constant. Figures 38 and 39 show the interaction relationship, $p - m_x$ and $p - m_y$, respectively, for the beam-column BC43 with LP3 and LP4. The figures clearly show that the beam-column strength is load-path dependent.

Figures 40, 41, and 42 show \bar{D} versus p , m_x and m_y for a beam-column with no lateral restraint, with end rotational restraints of stiffness K_2 and with the load path LP7. Figure 40 shows that at the start of the axial load application, the determinant was 0.36 due to a previously applied biaxial moment. A rapid increase in the stiffness occurs when the axial load is incremented. The quantity Q in these figures represents the final axial load or the moments reached at collapse. The rapid increase in the \bar{D} value in these curves is due to the elastic unloading of the plastic material.

Tables 16 and 17 show the maximum dimensionless external axial loads for the beam-columns with equal partial end rotational restraints and with various lateral spring stiffnesses. The results in Table 16 are obtained with the load path LP3 with $m_x = m_y = 0.50$ applied first. Table 17 is strictly for the axial load only, that is, with $m_x = m_y = 0$. The effect of the lateral restraints as well as of the rotational restraints on the beam-column strength is observed from the results given in these tables. For a given rotational restraint, the maximum axial load obtained increases as the lateral restraint stiffness increases. Also, for a given lateral restraint stiffness, an increase in the load is observed as the rotational stiffness increases. Figures 43 and 44 show the effect of various lateral restraint stiffnesses on the axial load for given end rotational restraint stiffnesses.

To demonstrate the phenomenon of the material unloading, Figures 45, 46, and 47 for biaxially loaded imperfect beam-column are used with the load path LP7. The beam-column possesses partial end rotational restraints at B and T with stiffnesses K_4 and K_2 , respectively. In the figures, the point A corresponds to the results after the final moment increment but before the axial load is applied. At this stage, some elements of the beam-column are plastified. When the axial load is applied, some of the plastified elements unload elastically thereby resulting in an increase in the beam-column stiffness. This is observed in the figures as the increase in the stiffness from point A to point B. Corresponding to the state A in these figures, Figure 48 shows the cross-sectional plastification at nodes 1, 4, 7, 10, and 13 along the beam-column length. The plastified elements are shaded dark. Figure 49 shows the plastified elements corresponding to the state B. Figure 50 which shows A "combination" of Figures 48 and 49 leads to the unloaded elements as shaded, and

the newly plastified elements by x marks. Figures 51 and 52 present the corresponding m_x versus the midspan and the top deflections, respectively.

Figure 53 shows a comparison of the m_x - m_y interaction curves for a 6x8x0.375 in. hollow rectangular section beam based on the tangent modulus approach and the analysis including elastic unloading. For these curves, the translational spring stiffness along the x and the y axes are taken as 1.0 kip/in. and 2.0 kip/in, respectively. The end rotational restraints at the beam ends are all identical in both planes and possess a stiffness of 15,000 kip-in/rad. The load path consisted of first applying m_x and holding it constant, and then incrementing m_y until its collapse value is attained. The inclusion of elastic unloading clearly results in higher moment capacities for the beam.

Table 18 shows the effect of crookedness and residual stresses on the peak loads of beam-columns subjected to the load paths LP5 and LP6. A total of four cases are studied with or without crookedness and residual stresses. The beam-columns are restrained at end B with a rotational restraint of stiffness K_4 about both the x and the y axes. At the top end T, the x and the y axes rotational restraints have a stiffness K_c . The translational stiffnesses K_x and K_y are taken as 1.0 kip/in. The dimensionless external loads show only small differences for various imperfections. Figures 54, 55, and 56 clearly show the effect of imperfections on the beam-column behavior.

A biaxially loaded imperfect sway beam-column with 2x3x0.1875 in. section is studied under the influence of the load path LP7, for two different types of residual stress distributions (RSDs). The RSDs are shown in Figures 3 and 5. The bottom end rotational restraints have infinite stiffness while those at the top have zero

stiffness about the x and the y axes. The top end translational restraint has a stiffness equal to 1.0 kip/in. along each of the x and the y axes. Figures 57 and 58 compare the $\bar{D} - p$ and $\bar{D} - m_x$ curves for the two types of RSDs. The beam-columns are first loaded by equal end moments gradually until $m_x = 0.572$ and $m_y = 0.696$ are reached. Next, the axial load is incremented together with the moments. The maximum loads attained at collapse are $p = 0.068$, $m_x = 0.716$, and $m_y = 0.881$ for the beam-column with RSD given in Figure 3; $p = 0.067$, $m_x = 0.712$, and $m_y = 0.877$ for the beam-column with RSD given in Figure 5. The curves show that while the beam-column stiffness degradation depends on the type of RSD, the ultimate strengths are not much affected. Figures 59 and 60 are the corresponding axial load versus the midspan and the top deflections.

2.8 Inelastic Slope-Deflection Equations for Sway Planar Beam-Column

For use in a plane frame analysis problem, the beam-column slope-deflection equations including inelastic action and sway are derived herein. The inelastic slope-deflection equations for a nonsway beam-column are presented by Darbhamulla (36). A modified version of these equations including the sway are derived herein for the type of beam-column shown in Figure 61.

Equation 36 is the global stiffness matrix equation for an imperfect sway beam-column in space and is derived using finite-differences. Setting K_y equal to zero, dropping the out-of-plane equations, and using partitioning technique to separate the boundary deflections from the internal ones leads to a matrix equation of the following type:

$$\begin{bmatrix} K_{x11} & K_{x12} \\ K_{x21} & K_{x22} \end{bmatrix} \begin{Bmatrix} \Delta_{x1} \\ \Delta_{x2} \end{Bmatrix} = \begin{Bmatrix} F_{x1} \\ F_{x2} \end{Bmatrix} + \begin{Bmatrix} F_{xp1} \\ F_{xp2} \end{Bmatrix} + \begin{Bmatrix} M_{x1} \\ M_{x2} \end{Bmatrix} \quad (40)$$

in which K_{xij} are the partitioned element stiffnesses; $\{F_{x1}\}$ and $\{F_{x2}\}$ are the vectors associated with the member crookedness; $\{F_{xp1}\}$ and $\{F_{xp2}\}$ are the vector containing the moments due to the plastified elements and residual stresses; $\{M_{x1}\}$ and $\{M_{x2}\}$ include the applied external moments. The vectors $\{\Delta_{x1}\}$ and $\{\Delta_{x2}\}$ contain the deflections defined below:

$$\{\Delta_{x1}\} = \{v_1 \quad v_2 \quad \dots \quad v_{n-1}\} \quad (41)$$

$$\{\Delta_{x2}\} = \{\theta_{Bx} \quad \theta_{Tx} \quad v_n\} \quad (42)$$

Expanding Equation 40 results in:

$$[K_{x11}] \{\Delta_{x1}\} + [K_{x12}] \{\Delta_{x2}\} = \{F_{x1}\} + \{F_{xp1}\} + \{M_{x1}\} \quad (43)$$

$$[K_{x21}] \{\Delta_{x1}\} + [K_{x22}] \{\Delta_{x2}\} = \{F_{x2}\} + \{F_{xp2}\} + \{M_{x2}\} \quad (44)$$

Solving Equation 43 for $\{\Delta_{x1}\}$ and substituting the result into Equation 44, the following condensed equation is obtained:

$$[K_{xr}] \{\Delta_{x2}\} = \{F_{xr}\} + \{F_{xpr}\} + \{M_{xr}\} \quad (45)$$

where:

$$[K_{xr}] = [K_{x12}] [K_{x11}]^{-1} [K_{x21}] + [K_{x22}] \quad (46)$$

$$\{F_{xr}\} = \{F_{x2}\} - [K_{x21}] [K_{x11}]^{-1} \{F_{x1}\} \quad (47)$$

$$\{ F_{xpr} \} = \{ F_{xp2} \} - [K_{x21}] [K_{x11}]^{-1} \{ F_{xp1} \} \quad (48)$$

$$\{ M_{x1} \} = \{ M_{x2} \} - [K_{x21}] [K_{x11}]^{-1} \{ M_{x1} \} \quad (49)$$

From Equation 45:

$$\{ \Delta_{x2} \} = [K_{xx}]^{-1} (\{ F_{xx} \} + \{ F_{xpr} \} + \{ M_{xx} \}) \quad (50)$$

Before a formal set of inelastic slope-equations is obtained, the vector $\{ M_{xx} \}$ must be expressed in terms of a coefficient matrix $[\beta_x]$ and a vector containing the applied member end moments M_{Bx} and M_{Tx} as follow:

$$\{ M_{xx} \} = [\beta_x] \{ M_{xa} \} \quad (51)$$

in which:

$$\{ M_{xa} \} = \{ M_{xB} \quad M_{xT} \} \quad (52)$$

The moment vectors $\{ M_{x1} \}$ and $\{ M_{x2} \}$ in Equation 49 are obtained by splitting Equation 38c into two parts as follows:

$$\{ M_{x1} \} = h^2 \begin{Bmatrix} \frac{z_1 - L}{L} & \frac{z_1}{L} \\ \frac{z_2 - L}{L} & \frac{z_2}{L} \\ \cdot & \cdot \\ \cdot & \cdot \\ \frac{z_{n-1} - L}{L} & \frac{z_{n-1}}{L} \end{Bmatrix} \begin{Bmatrix} M_{Bx} \\ M_{Tx} \end{Bmatrix} \quad (53)$$

$$\{M_{x2}\} = h^2 \begin{pmatrix} \frac{z_1 - L}{L} & \frac{z_1}{L} \\ \frac{z_n - L}{L} & \frac{z_n}{L} \end{pmatrix} \begin{Bmatrix} M_{Bx} \\ M_{Tx} \end{Bmatrix} \quad (54)$$

These equations can also be written in the following condensed form:

$$\{M_{x1}\} = [Q_{x1}] \{M_{xa}\} \quad (55)$$

$$\{M_{x2}\} = [Q_{x2}] \{M_{xa}\} \quad (56)$$

Substituting Equations 55 and 56 into Equation 49 and factorizing the load vector $\{M_{xa}\}$, the following equation is obtained:

$$\{M_{xr}\} = [[Q_{x1}] - [K_{x21}] [K_{x11}]^{-1} [Q_{x2}]] \{M_{xa}\} \quad (57)$$

Comparing Equation 57 to Equation 51, it is seen that the first major bracketed term in the in right hand side of Equation 57 represents the matrix $[\beta_x]$, and substituting Equation 51 into Equation 50, the following equation is obtained:

$$\{\Delta_{x2}\} = [K_{xr}]^{-1} [\{F_{xr}\} + \{F_{xpr}\} + [\beta_x] \{M_{xa}\}] \quad (58)$$

which may be rewritten as:

$$\{\Delta_{x2}\} = [G_x] \{M_{xa}\} + \{S_{xr}\} + \{S_{xpr}\} \quad (59)$$

where:

$$[G_x] = [K_{xr}]^{-1} [\beta_x] \quad (60)$$

$$\{ S_{xr} \} = [K_{xr}]^{-1} \{ F_{xr} \} \quad (61)$$

$$\{ S_{xpr} \} = [K_{xr}]^{-1} \{ F_{xpr} \} \quad (62)$$

The end moments of the sway beam-column shown in Figure 61 can be obtained from Equation 59 in terms of the member end deflections in the matrix form as follow:

$$\{ M_{xa} \} = [R_x] \{ \Delta_{x2} \} - \{ R_{xc} \} - \{ R_{xp} \} \quad (63)$$

in which,

$$[R_x] = [G_x]^{-1} \quad (64)$$

$$\{ R_{xc} \} = [G_x]^{-1} \{ S_{xr} \} \quad (65)$$

$$\{ R_{xp} \} = [G_x]^{-1} \{ S_{xpr} \} \quad (66)$$

Here, $[R_x]$ is the stiffness matrix for the sway beam-column bent about its major axis and depends on the axial load and the cross-sectional properties; $\{R_{xc}\}$ is the load vector associated with the member crookedness, and $\{R_{xp}\}$ is the load vector containing the forces produced due to the plastification and residual stresses in the member. The end moments are obtained from Equation 63 as follows:

$$(M_{xa})_{Bi} = R_{x(11,i)} \theta_{Bx} + R_{x(12,i)} \theta_{Tx} + R_{x(13,i)} v_n - R_{xc(1,i)} - R_{xp(1,i)} \quad (67)$$

$$(M_{xa})_{Ti} = R_{x(21,i)} \theta_{Bx} + R_{x(22,i)} \theta_{Tx} + R_{x(23,i)} v_n - R_{xc(2,i)} - R_{xp(2,i)} \quad (68)$$

where B and T refer to the top and the bottom ends of the beam-column, respectively; i refers to the beam-column number under consideration; $R_{x(j,i)}$ are the beam-column elemental stiffness terms. Equations 67 and 68 are the inelastic slope-

deflection equations for sway beam-column bent about the major axis. These equations will be used later for evaluating the global stiffness matrix of the sway portal frame.

2.9 Inelastic Slope-Deflection Equations for Sway Space Beam-Column

A set of inelastic slope-deflection equations are derived in the previous section for the sway planar beam-column. For a beam-column loaded biaxially as shown in Figure 62, a complete set of global inelastic slope-deflection equations are needed for use in space frame analysis. Equation 36 is a global tangent stiffness equation for a sway beam-column in space. It contains all of the elastic and inelastic properties in both planes of bending. In order to separate the boundary terms from the internal ones, Equation 36 is partitioned in the following form:

$$\begin{bmatrix} \mathbf{K}_{11} & \mathbf{K}_{12} \\ \mathbf{K}_{21} & \mathbf{K}_{22} \end{bmatrix} \begin{Bmatrix} \Delta_1 \\ \Delta_2 \end{Bmatrix} = \begin{Bmatrix} \mathbf{F}_1 \\ \mathbf{F}_2 \end{Bmatrix} + \begin{Bmatrix} \mathbf{F}_{p1} \\ \mathbf{F}_{p2} \end{Bmatrix} + \begin{Bmatrix} \mathbf{M}_1 \\ \mathbf{M}_2 \end{Bmatrix} \quad (69)$$

where \mathbf{K}_{ij} refer to the partitioned elemental stiffnesses; $\{\mathbf{F}_1\}$ and $\{\mathbf{F}_2\}$ are the vectors associated with the member crookedness; $\{\mathbf{F}_{p1}\}$ and $\{\mathbf{F}_{p2}\}$ are the load vectors containing the plastification and residual stress effects; $\{\mathbf{M}_1\}$ and $\{\mathbf{M}_2\}$ include the applied external moments in both the xz and yz planes. The deflection vectors $\{\Delta_1\}$ and $\{\Delta_2\}$ are defined as follows:

$$\{\Delta_1\} = \{v_1 \quad u_1 \quad v_2 \quad u_2 \quad \dots \quad v_{n-2} \quad u_{n-2} \quad v_{n-1} \quad u_{n-1}\} \quad (70)$$

$$\{\Delta_2\} = \{\theta_{Bx} \ \theta_{By} \ \theta_{Tx} \ \theta_{Ty} \ v_n \ u_n\} \quad (71)$$

Expanding Equation 69 results into the following two equations:

$$[K_{11}]\{\Delta_1\} + [K_{12}]\{\Delta_2\} = \{F_1\} + \{F_{p1}\} + \{M_1\} \quad (72)$$

$$[K_{21}]\{\Delta_1\} + [K_{22}]\{\Delta_2\} = \{F_2\} + \{F_{p2}\} + \{M_2\} \quad (73)$$

Solving Equation 72 for $\{\Delta_1\}$ and substituting it into Equation 73 leads to the following equation:

$$[K_r]\{\Delta_2\} = \{F_r\} + \{F_{pr}\} + \{M_r\} \quad (74)$$

where:

$$[K_r] = [K_{12}][K_{11}]^{-1}[K_{21}] + [K_{22}] \quad (75)$$

$$\{F_r\} = \{F_2\} - [K_{21}][K_{11}]^{-1}\{F_1\} \quad (76)$$

$$\{F_{pr}\} = \{F_{p2}\} - [K_{21}][K_{11}]^{-1}\{F_{p1}\} \quad (77)$$

$$\{M_r\} = \{M_2\} - [K_{21}][K_{11}]^{-1}\{M_1\} \quad (78)$$

The vector $\{M_r\}$ in Equation 74 can be written in terms of a coefficient matrix $[\beta]$ and beam-column end moments M_{Bx} , M_{By} , M_{Tx} and M_{Ty} as follow:

$$\{M_r\} = [\beta]\{M_a\} \quad (79)$$

where:

$$\{M_a\} = \{M_{Bx} \ M_{By} \ M_{Tx} \ M_{Ty}\}^T \quad (80)$$

The matrix $[\beta]$ is obtained in a manner similar to that for the planar beam-column except that all of terms in both the xz and the yz planes must be included. Of course, M_{Bx} , M_{By} , M_{Tx} and M_{Ty} are the moments at the ends B and T. Using Equation 79, Equation 74 can be written as follows:

$$\{\Delta_2\} = [G]\{M_a\} + \{S_r\} + \{S_{pr}\} \quad (81)$$

where:

$$[G] = [K_r]^{-1} [\beta] \quad (82)$$

$$\{S_r\} = [K_r]^{-1} \{F_r\} \quad (83)$$

$$\{S_{pr}\} = [K_r]^{-1} \{F_{pr}\} \quad (84)$$

The end moments for the sway space beam-column are obtained by solving Equation 81 for $\{M_a\}$:

$$\{M_a\} = [R]\{\Delta_2\} - \{R_c\} - \{R_p\} \quad (85)$$

where:

$$[R] = [G]^{-1} \quad (86)$$

$$\{R_c\} = [G]^{-1} \{S_r\} \quad (87)$$

$$\{R_p\} = [G]^{-1} \{S_{pr}\} \quad (88)$$

in which $[R]$ is the tangent stiffness matrix for the sway space beam-column; $\{\Delta_2\}$ is the boundary deflection vector; $\{R_s\}$ is the load vector containing the P-delta effects;

$\{R_p\}$ is the load vector containing the plastification and residual stress effects. The end moments for the member i are obtained from Equation 85 as follows:

$$(M_{xa})_{Bi} = R_{x(11,i)}\theta_{Bx} + R_{x(12,i)}\theta_{Tx} + R_{x(13,i)}v_n - R_{xc(1,i)} - R_{xp(1,i)} \quad (89)$$

$$(M_{xa})_{Ti} = R_{x(21,i)}\theta_{Bx} + R_{x(22,i)}\theta_{Tx} + R_{x(23,i)}v_n - R_{xc(2,i)} - R_{xp(2,i)} \quad (90)$$

$$(M_{ya})_{Bi} = R_{y(11,i)}\theta_{By} + R_{y(12,i)}\theta_{Ty} + R_{y(13,i)}u_n - R_{yc(1,i)} - R_{yp(1,i)} \quad (91)$$

$$(M_{ya})_{Ti} = R_{y(21,i)}\theta_{By} + R_{y(22,i)}\theta_{Ty} + R_{y(23,i)}u_n - R_{yc(2,i)} - R_{yp(2,i)} \quad (92)$$

Equations 89 through 92 are used for space frame analysis presented in Chapter 3.

3. FLEXIBLY CONNECTED IMPERFECT SWAY FRAMES

An inelastic slope-deflection solution procedure for flexibly connected sway plane and space frames is presented in this chapter. The examples of a portal frame and a single-story single-bay orthogonal space frame are studied in depth. The solution procedure is also applied to the three-story test frame in Chapter 4.

3.1 Portal Frame

Figure 63 shows schematically an imperfect unbraced portal frame with flexible joints at B and C, and flexible base connections at A and D. All three members are loaded about their major axes. The initial member crookedness in the plane of the loading is given by Equation 12. Also, the member cross section is assumed to have an initial residual stress of the type shown in Figure 3 unless otherwise mentioned. As seen from Figure 63, the frame has six joints. Springs exist between joints 2 and 3, and joints 4 and 5 as well as at the supports. The distances between joints 2 and 3 as well as between joints 4 and 5 are taken as zero. The structure is subjected to nonproportional loading which includes a horizontal load H applied at B, vertical loads P_1 and P_2 , and bending moments M_1 and M_2 at B and C, as shown in Figure 63.

3.1.1 Analysis

The analysis is conducted by using the inelastic slope-deflection expressions in Equations 67 and 68. Using the joint numbers in Figure 63, and applying the inelastic slope-deflection equations to the three members of the frame in Figure 63 leads to:

$$M_{x(1,2)} = R_{x(11,1)} \theta_{x1} + R_{x(12,1)} \theta_{x2} + R_{x(13,1)} v_c - R_{xc(1,1)} - R_{xp(1,1)} \quad (94)$$

$$M_{x(2,1)} = R_{x(21,1)} \theta_{x1} + R_{x(22,1)} \theta_{x2} + R_{x(23,1)} v_c - R_{xc(2,1)} - R_{xp(2,1)} \quad (95)$$

$$M_{x(3,4)} = R_{x(11,2)} \theta_{x3} + R_{x(12,2)} \theta_{x4} - R_{xc(1,2)} - R_{xp(1,2)} \quad (96)$$

$$M_{x(4,3)} = R_{x(21,2)} \theta_{x3} + R_{x(22,2)} \theta_{x4} - R_{xc(2,2)} - R_{xp(2,2)} \quad (97)$$

$$M_{x(5,6)} = R_{x(11,3)} \theta_{x5} + R_{x(12,3)} \theta_{x6} + R_{x(13,3)} v_c - R_{xc(1,3)} - R_{xp(1,3)} \quad (98)$$

$$M_{x(6,5)} = R_{x(21,3)} \theta_{x5} + R_{x(22,3)} \theta_{x6} + R_{x(23,3)} v_c - R_{xc(2,3)} - R_{xp(2,3)} \quad (99)$$

Here, the first subscript refers to the member stiffness of one end with respect to the other end. The second subscript refers to the member number. Next, an enforcement of the joint moment equilibrium at A, B, C, and D leads to:

$$M_{x(1,2)} + K_A \theta_{x1} = 0 \quad (100)$$

$$M_{x(2,1)} + K_B (\theta_{x2} - \theta_{x3}) + M_1 = 0 \quad (101)$$

$$M_{x(3,4)} + K_B (\theta_{x3} - \theta_{x2}) = 0 \quad (102)$$

$$M_{x(4,3)} + K_C (\theta_{x4} - \theta_{x5}) = 0 \quad (103)$$

$$M_{x(5,6)} + K_C(\theta_{x5} - \theta_{x4}) + M_2 = 0 \quad (104)$$

$$M_{x(6,5)} + K_D \theta_{x6} = 0 \quad (105)$$

Substituting Equations 94 through 99 into Equations 100 through 105, a total of six equations containing seven unknowns are obtained. Therefore, one more equation is required to solve for the unknowns. This is obtained by using the shear condition at the base of the structure:

$$H_1 + H_2 = H \quad (106)$$

where H_1 and H_2 are the shear forces at the frame bases obtained by considering the moment equilibrium of each column. The resulting form of Equation 106 is:

$$M_{x(1,2)} + M_{x(2,1)} + P v_n + M_{x(5,6)} + M_{x(6,5)} + P v_n = H L_c \quad (107)$$

Substituting for the moments $M_{x(i,j)}$ in the above equation from Equations 94, 95, 98, and 99, the following equation is obtained:

$$\Psi_{x1} \theta_{x1} + \Psi_{x2} \theta_{x2} + \Psi_{x3} \theta_{x5} + \Psi_{x4} \theta_{x6} + \Psi_{x5} v_n = H L_c + \Psi_{x6} \quad (108)$$

in which the Ψ_{xk} terms for $k = 1, 2, \dots, 6$, are defined in Appendix C.

Substituting Equations 94 through 99 into Equations 100 through 105, and including Equation 108 results in a nonlinear global matrix equation as follows:

$$[K_{xg}] \{ \delta_{xg} \} = \{ M_{xcg} \} + \{ M_{xpg} \} + \{ M_{xg} \} \quad (109)$$

in which $[K_{xg}]$ is the global tangent stiffness matrix of the order 7×7 , $\{ \delta_{xg} \}$ is the deflection vector containing 6 rotations (θ_{x1} through θ_{x6}) and one frame horizontal translation, v_n , at B or C; $\{ M_{xcg} \}$ is associated with the member crookedness; $\{ M_{xg} \}$

contains the applied moments; $\{M_{xpg}\}$ is the plastic force vector generated beyond the elastic range. To determine $\{\delta_{xg}\}$, Equation 109 must be solved iteratively for each external load level. The various load paths considered herein are defined in Section 3.1.2 and the procedure for solving Equation 109 is defined in Section 3.1.3.

3.1.2 Load Paths

The load paths used earlier by Darbhamulla (36) are adopted here for comparison purpose and numerical study. Figure 8 shows a variety of load paths for a three-dimensional problem, however, it can also be used for a two-dimensional problem by adopting various load paths in one plane. Referring to the m_x - p plane in this figure, the following load paths are adopted herein:

- LPF1:** Both p and m are applied simultaneously in a proportional manner. This corresponds to the path OB.
- LPF2:** An axial load p is first applied, followed by both p and m_x applied simultaneously. This corresponds to the path ODB.
- LPF3:** Both p and m_x are applied simultaneously in a proportional manner until m_x reaches the ultimate value obtained in LPF2, followed by an increase in the axial load p while holding the moment constant. This corresponds to the path OKB.

3.1.3 Solution Procedure

The algorithm by Darbhamulla (36) for a nonsway portal frame is modified here for the sway case. Equation 109 is materially and geometrically nonlinear since

the tangent stiffness matrix $[K_{xg}]$ and the load vectors on the right hand side are dependent upon the deformation vector $\{\delta_{xg}\}$. To predict the load-deformation behavior of the frame, the following iterative scheme is devised:

1. Evaluate the initial elastic properties and deduce Equation 63 for each member.
2. Assemble global stiffness matrix $[K_{xg}]$ in Equation 109.
3. Prescribe small load increments and formulate the load vectors $\{M_{xcg}\}$ and $\{M_{xpg}\}$ in Equation 109.
4. Solve Equation 109 for $\{\delta_{xg}\}$.
5. Compute the member end forces vector $\{M_{xa}\}$ using Equation 63. Next, determine the member end actions using static equilibrium, and formulate the load vector $\{M\} = \{M_i\}$ in Equation 31. Here, i refers to the iteration number.
6. Analyze the members with $\{M_i\}$ individually using the procedure given in Chapter 2, and compute the converged member stiffness matrices $[K]$ in Equation 31 of Chapter 2 .
7. Update the inelastic slope-deflection Equation 63 for each member, re-assemble $[K_{xg}]$, $\{M_{xcg}\}$ and $\{M_{xpg}\}$, and update $\{\delta_{xg}\}$ using Equation 109.
8. Recompute the member end force vectors $\{M_{xa}\}$ using Equation 63, and update $\{M\} = \{M\}_{i+1}$ in Equation 31.
9. If $|\{M\}_{i+1} - \{M\}_i| \leq \alpha$, where α is the tolerance taken as 0.01%, go to Step 11.
10. Set $\{M\}_i = \{M\}_{i+1}$, and go to Step 6.

11. If $|[K]| \Rightarrow 0.0$, go to Step 13.
12. Increase (or change) the external loads, that is, P and/or M, update the load vectors $\{M_{xcg}\}$ and $\{M_{xpg}\}$ in Equation 109, and go to Step 4.
13. Stop

The solution procedure described herein is programmed in FORTRAN on a sequential IBM 3090 computer using the vectorization facilities provided. The program is named SPF (Sway Portal Frame) and a listing is included in Appendix D.

3.1.4 Load Combinations

The following load combinations are considered for the portal frame study:

FL1: An axial load P_1 , and a counterclockwise bending moment M_1 are used while keeping $P_2 = M_2 = 0.0$

FL2: Same loading as FL1 except that the bending moment M_2 is applied clockwise.

FL3: In addition to the loads in FL1, P_2 and M_3 are also applied.

3.1.5 Types of Frames Studied

The numerical study of the portal frame is based on many frame configurations. Frame crookedness is one of the important aspects, therefore, with reference to Figure 38, the following frame types are considered:

FR1: The members AB, BC, and CD are nearly perfect with v_{0i} in Equation 12 and with $v_0 = L/100,000$. The v_{0i} for the members AB and CD is as shown in Figure 63 while for member BC it is opposite to that shown in the figure.

FR2: The members AB and CD are initially crooked as shown in Figure 63 with v_{0i} given in Equation 12 and with $v_0 = L/1000$. Member BC is crooked opposite to the direction shown in the figure.

FR3: The member AB is nearly perfect as in FR1, and the members BC and CD are initially crooked as in FR2.

FR4: The members AB and BC are initially crooked as in FR2, and the member CD is nearly perfect as in FR1.

FR5: The member AB is initially crooked as shown in the figure, and the members BC and CD are initially crooked opposite to those in the figure.

3.1.6 Frame Behavior

Figure 63 shows schematically an imperfect sway portal frame. It is assembled from members of 7x7x0.375 in. hollow square section for the columns, and 6x8x0.375 in. hollow rectangular section for the beam. The material used for the frame is steel with a modulus of elasticity $E=29,000$ ksi, and a yield stress $\sigma_Y = 46$ ksi. The length of each member is taken as 12 ft, and each member is divided by means of 17 equidistant nodes along its length. Also, each member has initial crookedness defined by Equation 12.

Darbhamulla (36) studied the effects of nonproportional loads on nonsway portal frames with partial rotational restraints. Table 19 shows a comparison of the externally applied dimensionless maximum loads to those given in Reference 36 for imperfect nonsway portal frames. A W8x31 section is used for the columns and a S12x31.8 section is used for the beam. Each member is 15 ft. long. The beam-

column joints are connected by partial rotational restraints of stiffness K_2 and the joints at the foundations are taken as rigid. The columns are bent about their minor axes and the beam about its major axis. The results in the table show excellent agreement with Reference 36.

A total of 19 frames, PF1 through PF19, are studied in order to investigate the effect of nonproportional loads on the frame behavior and strength. Table 20 presents the maximum dimensionless external loads for sway portal frames FR1, FR2, FR3, and FR5 with rigid beam-to-column connections, and with partial rotational restraints at the bases of stiffness K_2 , and subjected to FL3 and FL4 loading. The results show that there are major differences between the strength of frames subjected to the proportional loading LPF1 and those with nonproportional loading LPF2 or LPF3. However, no significant differences are observed between the collapse loads based on LPF2 and LPF3.

Table 21 shows the maximum dimensionless external loads obtained for the imperfect sway portal frame FR5. The beam-to-column connections are rigid and the bases are connected to the foundations by rotational restraints of stiffness K_2 . Frame loading types FL1 through FL4 are considered. It is seen that when the frame is loaded at only one joint (loading FL1 or FL2), the maximum vertical load is increased by 38% to 44% of the column squash load. When nonproportional load paths LPF2 or LPF3 are used, a reduction in the applied moment m_x is noticed as compared with that for the proportional load path LPF1. Figures 64, 65, and 66 present the behavior of the frame PF9 for the load paths LPF2 and LPF3. These figures show the stiffness degradation curves $(\bar{D} - p)$ and $(\bar{D} - m_x)$, and the

dimensionless vertical load versus top (horizontal) deflection of the joint C shown in Figure 63. From these figures, it is clear that the frame loses its stiffness faster under the load path LPF2. Figures 67, 68, and 69 show the behavior of the frame PF10 with the load path LPF2.

Table 22 presents the effect of member crookedness and residual stresses on the strength of the sway portal frames with rigid beam-to-column connections and with partial rotational restraints at the bases of stiffness K_3 . The frame type used is FR5 with FL4 loading. The results show that the perfect frame is stronger than the crooked one. Figures 70 through 81 depict the behavior of frames PF13 through PF16. In each figure, four curves are plotted, one for each frame. Figures 70, 71, 72, and 73 show the $(\bar{D} - p)$, $(\bar{D} - m_x)$, $(p - \Delta)$, and $(m_x - \theta_{x1})$ curves, respectively, where θ_{x1} is the joint 1 rotation, for the frames with the load path LPF1. From the figures, it is clear that the frame with crookedness and residual stresses loses its stiffness faster than others, and the perfect frame has the highest stiffness. Similarly, Figures 74, 75, and 76 present the $(\bar{D} - p)$, $(\bar{D} - m_x)$, and $(\bar{D} - \Delta)$ curves, respectively, for the same frames subjected to the load path LPF2. Also, Figures 77 through 81 present similar curves for the frames with the load path LPF3.

Table 23 summarizes the dimensionless maximum loads for the sway portal frames PF17, PF18, and PF19 with different residual stress distributions (RSD). The behavior of frames is studied with different RSDs depicted in Figures 3, 4, and 5. The frames under consideration are of the type FR5 with frame loading FL3 and are

subjected to load paths LPF1, LPF2, and LPF3. The columns are constructed from 2x2x0.1875 in. hollow square sections, and the beam is a 2x3x0.1875 in. hollow rectangular section loaded about the major axis. All joints are rigid. No significant difference is noticed between the frame strength with RSD of Figure 3 and that of the frame with RSD of Figures 4 and 5 when the load path LPF1 or LPF2 is used. The load path LP3 gives a 13% increase in the vertical load when the RSDs of Figures 4 and 5 are used. The results also illustrated graphically in Figures 82 through 90. The figures show that the stiffness of the frames also depends on the residual stress distribution and that they are weaker when RSD given by Figure 3 is used.

3.2 Orthogonal Space Frame

Figure 91 shows an unbraced single-story single-bay space frame with flexible connections and foundation attachments. The joints are numbered from 1 through 15. Following the same format as for the portal frame of section 3.1, the joints are numbered in such a way that each rotational spring connects two joints with a zero distance between them. The space frame is imperfect with member initial crookedness given by Equations 11 and 12. The cross section of the members is assumed to have initial residual stresses of the type shown in Figure 3 unless otherwise mentioned.

3.2.1 Analysis

The inelastic slope-deflection equations for sway beam-column in space have been derived in the previous chapter. A set of global tangent stiffness equations are

needed to obtain the solution of the unknown rotations and translations of the frame. Equilibrium and compatibility conditions are enforced at each joint. Figure 92a shows one such joint with subscript i denoting the joint between two columns and subscripts j and k denoting the nodes connecting the beam end to the rotational springs. Figure 92b shows typical joint loads which include two horizontal loads P_{ix} and P_{iy} , a vertical load P_{iz} , and a pair of moments M_{ix} and M_{iy} .

Figure 93 shows a typical joint i with the members and the springs connected to it. Joint i is connected to the top column CT, the bottom column CB, and the rotational springs about the x and the y axes with stiffnesses K_{xi} and K_{yi} , respectively. The members B1, B2, CB, and CT are connected at their ends by the joints $l-k$, $m-j$, $h-i$, and $i-n$, respectively. Applying Equations 89 and 90 to beams B1 and B2, the following internal moment equations are obtained:

$$M_{xj(B1)} = R_{x(21,B1)} \theta_{xm} + R_{x(22,B1)} \theta_{xj} - R_{xc(2,B1)} - R_{xp(2,B1)} \quad (110)$$

$$M_{yj(B2)} = R_{x(21,B2)} \theta_{yl} + R_{x(22,B2)} \theta_{yk} - R_{xc(2,B2)} - R_{xp(2,B2)} \quad (111)$$

In generating Equations 110 and 111, the displacements v_n and u_n in Equations 89 and 90 are set equal zero. For columns CB and CT, Equations 89 through 92 become:

$$M_{xi(CT)} = R_{x(11,CT)} \theta_{xi} + R_{x(12,CT)} \theta_{xm} + R_{x(13,CT)} (\Delta_{ym} - \Delta_{yi}) - R_{xc(1,CT)} - R_{xp(1,CT)} \quad (112)$$

$$M_{yi(CT)} = R_{y(11,CT)} \theta_{xi} + R_{y(12,CT)} \theta_{ym} + R_{y(13,CT)} (\Delta_{xm} - \Delta_{xi}) - R_{yc(1,CT)} - R_{yp(1,CT)} \quad (113)$$

$$M_{xi(CB)} = R_{x(21,CB)} \theta_{xh} + R_{x(22,CB)} \theta_{xi} + R_{x(23,CB)} \Delta_{yi} - R_{xc(2,CB)} - R_{xp(2,CB)} \quad (114)$$

$$M_{yi(CB)} = R_{y(21,CB)} \theta_{yh} + R_{y(22,CB)} \theta_{yi} + R_{y(23,CB)} \Delta_{xi} - R_{yc(2,CB)} - R_{yp(2,CB)} \quad (115)$$

The resisting moments at joints i, j, and k are expressed as follows:

$$M_{xi(R)} = K_{xi} (\theta_{xi} - \theta_{xj}) + M_{xi} \quad (116)$$

$$M_{yi(R)} = K_{yi} (\theta_{yi} - \theta_{yj}) + M_{yi} \quad (117)$$

$$M_{xj(R)} = K_{xj} (\theta_{xj} - \theta_{xi}) \quad (118)$$

$$M_{yk(R)} = K_{yk} (\theta_{yk} - \theta_{yi}) \quad (119)$$

in which the subscript R refers to the appropriate "resisting" moments. The moment equilibrium conditions at joints i,j, and k are as follow:

$$M_{xi(CT)} + M_{xi(CB)} + M_{xi(R)} = 0 \quad (120)$$

$$M_{yi(CT)} + M_{yi(CB)} + M_{yi(R)} = 0 \quad (121)$$

$$M_{xj(R)} + M_{xj(B1)} = 0 \quad (122)$$

$$M_{yk(R)} + M_{yk(B2)} = 0 \quad (123)$$

Applying Equations 89 through 92 to column 1 of the single-story single-bay space frame shown in Figure 91 leads to the following equations:

$$M_{x(1,5)} = R_{x(11,1)} \theta_{x1} + R_{x(12,1)} \theta_{x5} + R_{x(13,1)} \Delta_y - R_{xc(1,1)} - R_{xp(1,1)} \quad (124)$$

$$M_{y(1,5)} = R_{y(11,1)} \theta_{y1} + R_{y(12,1)} \theta_{y5} + R_{y(13,1)} \Delta_x - R_{yc(1,1)} - R_{yp(1,1)} \quad (125)$$

$$M_{x(5,1)} = R_{x(21,1)} \theta_{x1} + R_{x(22,1)} \theta_{x5} + R_{x(23,1)} \Delta_y - R_{xc(2,1)} - R_{xp(2,1)} \quad (126)$$

$$M_{y(5,1)} = R_{y(21,1)} \theta_{y1} + R_{y(22,1)} \theta_{y5} + R_{y(23,1)} \Delta_x - R_{yc(2,1)} - R_{yp(2,1)} \quad (127)$$

For Column 2, the equation are:

$$M_{x(2,6)} = R_{x(11,2)} \theta_{x2} + R_{x(12,2)} \theta_{x6} + R_{x(13,2)} \Delta_y - R_{xc(1,2)} - R_{xp(1,2)} \quad (128)$$

$$M_{y(2,6)} = R_{y(11,2)} \theta_{y2} + R_{y(12,2)} \theta_{y6} + R_{y(13,2)} \Delta_x - R_{yc(1,2)} - R_{yp(1,2)} \quad (129)$$

$$M_{x(6,2)} = R_{x(21,2)} \theta_{x2} + R_{x(22,2)} \theta_{x6} + R_{x(23,2)} \Delta_y - R_{xc(2,2)} - R_{xp(2,2)} \quad (130)$$

$$M_{y(6,2)} = R_{y(21,2)} \theta_{y2} + R_{y(22,2)} \theta_{y6} + R_{y(23,2)} \Delta_x - R_{yc(2,2)} - R_{yp(2,2)} \quad (131)$$

For Column 3, the equations are:

$$M_{x(3,7)} = R_{x(11,3)} \theta_{x3} + R_{x(12,3)} \theta_{x7} + R_{x(13,3)} \Delta_y - R_{xc(1,3)} - R_{xp(1,3)} \quad (132)$$

$$M_{y(3,7)} = R_{y(11,3)} \theta_{y3} + R_{y(12,3)} \theta_{y7} + R_{y(13,3)} \Delta_x - R_{yc(1,3)} - R_{yp(1,3)} \quad (133)$$

$$M_{x(7,3)} = R_{x(21,3)} \theta_{x3} + R_{x(22,3)} \theta_{x7} + R_{x(23,3)} \Delta_y - R_{xc(2,3)} - R_{xp(2,3)} \quad (134)$$

$$M_{y(7,3)} = R_{y(21,3)} \theta_{y3} + R_{y(22,3)} \theta_{y7} + R_{y(23,3)} \Delta_x - R_{yc(2,3)} - R_{yp(2,3)} \quad (135)$$

For Column 4, the equations are:

$$M_{x(4,8)} = R_{x(11,4)} \theta_{x4} + R_{x(12,4)} \theta_{x8} + R_{x(13,4)} \Delta_y - R_{xc(1,4)} - R_{xp(1,4)} \quad (136)$$

$$M_{y(4,8)} = R_{y(11,4)} \theta_{y4} + R_{y(12,4)} \theta_{y8} + R_{y(13,4)} \Delta_x - R_{yc(1,4)} - R_{yp(1,4)} \quad (137)$$

$$M_{x(8,4)} = R_{x(21,4)} \theta_{x4} + R_{x(22,4)} \theta_{x8} + R_{x(23,4)} \Delta_y - R_{xc(2,4)} - R_{xp(2,4)} \quad (138)$$

$$M_{y(8,4)} = R_{y(21,4)} \theta_{y4} + R_{y(22,4)} \theta_{y8} + R_{y(23,4)} \Delta_x - R_{yc(2,4)} - R_{yp(2,4)} \quad (139)$$

For Beam 5, the equations are:

$$M_{y(9,10)} = R_{x(11,5)} \theta_{y9} + R_{x(12,5)} \theta_{y10} - R_{xc(1,5)} - R_{xp(1,5)} \quad (140)$$

$$M_{y(10,9)} = R_{x(21,5)} \theta_{y9} + R_{x(22,5)} \theta_{y10} - R_{xc(2,5)} - R_{xp(2,5)} \quad (141)$$

For Beam 6, the equations are:

$$M_{x(11,12)} = R_{x(11,6)} \theta_{x11} + R_{x(12,6)} \theta_{x12} - R_{xc(1,6)} - R_{xp(1,6)} \quad (142)$$

$$M_{x(12,11)} = R_{x(21,6)} \theta_{x11} + R_{x(22,6)} \theta_{x12} - R_{xc(2,6)} - R_{xp(2,6)} \quad (143)$$

For Beam 7, the equations are:

$$M_{y(13,14)} = R_{x(11,7)} \theta_{y13} + R_{x(12,7)} \theta_{y14} - R_{xc(1,7)} - R_{xp(1,7)} \quad (144)$$

$$M_{y(14,13)} = R_{x(21,7)} \theta_{y13} + R_{x(22,7)} \theta_{y14} - R_{xc(2,7)} - R_{xp(2,7)} \quad (145)$$

Lastly, for Beam 8, the equations are:

$$M_{x(15,16)} = R_{x(11,8)} \theta_{x15} + R_{x(12,8)} \theta_{x16} - R_{xc(1,8)} - R_{xp(1,8)} \quad (146)$$

$$M_{x(16,15)} = R_{x(21,8)} \theta_{x15} + R_{x(22,8)} \theta_{x16} - R_{xc(2,8)} - R_{xp(2,8)} \quad (147)$$

Enforcing the compatibility and equilibrium conditions at each joint leads to:

$$M_{x(1,5)} + K_{x1} \theta_{x1} = 0 \quad (148)$$

$$M_{y(1,5)} + K_{y1} \theta_{y1} = 0 \quad (149)$$

$$M_{x(2,6)} + K_{x2} \theta_{x2} = 0 \quad (150)$$

$$M_{y(2,6)} + K_{y2} \theta_{y2} = 0 \quad (151)$$

$$M_{x(3,7)} + K_{x3} \theta_{x3} = 0 \quad (152)$$

$$M_{y(3,7)} + K_{y3} \theta_{y3} = 0 \quad (153)$$

$$M_{x(4,8)} + K_{x4} \theta_{x4} = 0 \quad (154)$$

$$M_{y(4,8)} + K_{y4} \theta_{y4} = 0 \quad (155)$$

$$M_{x(5,1)} + K_{x5} (\theta_{x5} - \theta_{x15}) + M_{x5} = 0 \quad (156)$$

$$M_{y(5,1)} + K_{y5} (\theta_{y5} - \theta_{y9}) + M_{y5} = 0 \quad (157)$$

$$M_{x(6,2)} + K_{x6} (\theta_{x6} - \theta_{x11}) + M_{x6} = 0 \quad (158)$$

$$M_{y(6,2)} + K_{y6} (\theta_{y6} - \theta_{y10}) + M_{y6} = 0 \quad (159)$$

$$M_{x(7,3)} + K_{x7} (\theta_{x7} - \theta_{x12}) + M_{x7} = 0 \quad (160)$$

$$M_{y(7,3)} + K_{y7} (\theta_{y7} - \theta_{y14}) + M_{y7} = 0 \quad (161)$$

$$M_{x(8,4)} + K_{x8} (\theta_{x8} - \theta_{x13}) + M_{x8} = 0 \quad (162)$$

$$M_{y(8,4)} + K_{y8} (\theta_{y8} - \theta_{y16}) + M_{y8} = 0 \quad (163)$$

$$M_{y(9,10)} + K_{y5} (\theta_{y9} - \theta_{y5}) = 0 \quad (164)$$

$$M_{y(10,9)} + K_{y6} (\theta_{y10} - \theta_{y6}) = 0 \quad (165)$$

$$M_{x(11,12)} + K_{x6} (\theta_{x11} - \theta_{x6}) = 0 \quad (166)$$

$$M_{x(12,11)} + K_{x7}(\theta_{x12} - \theta_{x7}) = 0 \quad (167)$$

$$M_{y(13,14)} + K_{y8}(\theta_{y13} - \theta_{y8}) = 0 \quad (168)$$

$$M_{y(14,13)} + K_{y7}(\theta_{y14} - \theta_{y7}) = 0 \quad (169)$$

$$M_{x(15,16)} + K_{x5}(\theta_{x15} - \theta_{x5}) = 0 \quad (170)$$

$$8M_{x(16,15)} + K_{x8}(\theta_{x16} - \theta_{x8}) = 0 \quad (171)$$

Equations 148 through 171 form a set of 16 equations with 18 unknown deflection quantities. In order to complete the required minimum equations to solve for the unknown deformations in the space frame, two additional equations are needed. These are obtained by using the following shear equilibrium equations at the base of the frame in the x and in the y directions:

$$H_{x1} + H_{x2} + H_{x3} + H_{x4} = 2H_x \quad (172)$$

$$H_{y1} + H_{y2} + H_{y3} + H_{y4} = 2H_y \quad (173)$$

where H_{xi} and H_{yi} are the horizontal reactions in the x and the y directions, respectively, at the frame base at nodes 1 through 4 shown in Figure 91, and H_x and H_y are the external horizontal loads applied at the top of the frame in the x and the y directions, respectively. The horizontal reactions can be expressed in terms of the end moments for each column. The column moments are expressed by Equations 124 through 139. Thus, Equations 172 and 173 are converted to a useful form.

Substituting Equations 124 through 147 into Equations 148 through 171, together with Equations 172 and 173, finally leads to the following global tangent stiffness matrix equation:

$$[K_g] \{ \delta_g \} = \{ M_{cg} \} + \{ M_{pg} \} + \{ M_g \} \quad (174)$$

where $[K_g]$ is the global tangent stiffness matrix, $\{ \delta_g \}$ is the deflection vector, $\{ M_{cg} \}$ is the load vector associated with the initial crookedness of the members, $\{ M_{pg} \}$ is the plastic load vector, and $\{ M_g \}$ is the externally applied load vector. Equations 174 is solved for the global deflections iteratively using the solution procedure described in Section 3.2.3.

3.2.2 Load Paths

A study of the behavior of the single-story single-bay space frame shown in Figure 91 is presented in Section 3.2.5. The loading consists of the vertical loads P , λP , and λP at the joints 5 through 8, respectively, and the bending moments M_x and M_y applied in the directions as shown in Figure 91. Referring to Figure 8, the following load paths are considered herein:

SL1: The vertical load P is first applied at each of the joints 5 through 8 with $\lambda = 1.0$, then held constant, and then followed by the bending moments M_x and M_y applied proportionally at all of the nodes as shown in Figure 91 until the frame collapse occurs. This corresponds to the load path OAE.

SL2: The bending moments M_x and M_y corresponding to SL1 are first applied proportionally to the same joints as in SL1, held constant, and then followed

by the vertical load P , and with $\lambda = 1.0$, at the same joints until collapse occurs. This follows the load path OFE.

SL3: The vertical load P reached in SL1 is first applied at the same joint, followed by a further increase in the vertical load P , with $\lambda = 1.0$, and the bending moments M_x and M_y simultaneously until collapse occurs. This load path corresponds to the load path ODE.

SL4: The bending moments M_x and M_y reached in SL1 are first applied, followed by the vertical load P at the same joints, with $\lambda = 1.0$, and the bending moments M_x and M_y simultaneously until collapse occurs. This corresponds to the load path OHE.

SL5: T vertical load P applied at joints 5 and 6, that is, $\lambda = 0.0$, with until collapse occurs. This corresponds to the load path OA.

3.2.3 Solution Procedure

The algorithm used for the sway portal frame is modified here to handle the inelastic stability analysis of the sway space frames. In the elastic range, Equation 174 is solved non-iteratively for a given set of external loads. In the inelastic range, this equation becomes nonlinear since the tangent stiffness matrix $[K_g]$ and the load vectors on the right hand side become dependent upon the extent of plastification. To predict the load-deformation behavior of the frame, the following iterative scheme is devised:

1. Evaluate the initial elastic properties of the frame members and formulate Equation 85 for each member in the elastic range.

2. Prescribe a set of external loads $[K_g]$, $\{M_{cg}\}$, $\{M_{pg}\}$, and $\{M_g\}$ in Equation 174. Note that in the elastic range, $\{M_{pg}\} = \{0\}$.
3. Solve Equation 174 for $\{\delta_g\}$.
4. Using $\{\delta_g\}$ from Step 3, compute the end moment vector $\{M_a\}$ for each member, using Equation 85. Next, determine the end actions using static equilibrium, and formulate the load vector $\{M\} = \{M\}_i$ in Equation 38 for each member. Here, i refers to the iteration number.
5. Analyze the members with $\{M\}_i$ individually using the procedure given in Chapter 2, and compute the locally converged member stiffness matrices $[K]$ in Equation 36.
6. Update the inelastic slope-deflection Equation 85 for each member, reassemble $[K_g]$, $\{M_{cg}\}$ and $\{M_{pg}\}$, and solve for $\{\delta_g\}$ using Equation 174.
7. Recompute the member end moment vectors $\{M_a\}$ using Equation 85, and update $\{M\} = \{M\}_{i+1}$ in Equation 38.
8. If $|\{M\}_{i+1} - \{M\}_i| \leq \alpha$, where α is the tolerance taken as 0.01%, go to step 10.
9. Set $\{M\}_i = \{M\}_{i+1}$, and go to step 5.
10. If $[K] \Rightarrow 0.0$, go to step 12.
11. Specify the next set of load levels, update the load vectors $\{M_{cg}\}$ and $\{M_{pg}\}$ in Equation 174, and go to step 3.
12. Stop

The solution procedure described herein is programmed in the FORTRAN language on a sequential IBM 3090 computer using the vectorization facilities. The program is named SSF (Sway Space Frame) and its listing is presented in Appendix D.

3.2.4 Frames Studied

Three types of frame crookedness configurations are chosen here to study the behavior of the single-story single-bay space frame shown in Figure 91, under the influence of nonproportional loading. For the numerical study presented herein, the applied moments about the x and the y axes are taken equal to each other, that is, $m_x = m_y = m$. Also, each of the four columns is subjected to an axial load p except for the frame subjected to the load path SL5. For the frames studied, the crookedness is considered to be present only in the columns in the specified directions. Beams 5 through 8 are taken as nearly straight in all of the frames considered below, that is, with a midspan crookedness of $L/100,000$ measured downward (negative z direction). Referring to Figure 91 and the frame global coordinates, the following types of framed are studied:

SFR1: Columns 1 and 4 are crooked in the negative x direction and Columns 2 and 3 are crooked in the positive x direction. Also, Columns 1 and 2 are crooked in the positive y direction and Columns 3 and 4 are crooked in the negative y direction.

SFR2: All of the columns in the frame are crooked in the directions opposite to those for the frame SFR1.

SFR3: All of the columns in the frame are crooked in the negative x and the negative y directions.

3.2.5 Frame Behavior

Unless otherwise mentioned, the beam and column sizes, and the material properties adopted for the space frames are the same as those used for studying the behavior of the portal frame, and are outlined in Section 3.1.6.

Table 24 summarizes the maximum dimensionless applied loads for single-story single-bay sway space frames SFR1, SFR2, and SFR3 with rigid joints. The load paths used here are SL1 through SL5. The results clearly show the influence of the nonproportional loads on the frame maximum loads. For example, when the load path SL1 is utilized for the frame type SFR1, the maximum loads obtained are $p = 0.70$ and $m = 1.23$. However, when the load path is reversed, that is, when the load path SL2 is used, the frame maximum loads become $p = 1.24$ and $m = 1.23$. This type of behavior is also observed for all other cases presented in the table for the load paths SL1 through SL4.

An interesting result is also obtained for the space frame SFp1 which is subjected to the load path SL5. For $\lambda = 0.0$, that is, the external loading consists of only two vertical loads applied at the joints 5 and 6 shown in Figure 91. As given in Table 24, p is found to be 3.76. This means that the total frame load, $2p$, equal 7.52 times the squash load for one column. This is attributed to the combined effect of material unloading and the interaction of the various members of the frame in the presence of unsymmetric loading of this type.

The behavior of the frames SF2 and SF4, referred to in table 24, is depicted by the curves in Figure 94 through 96. These figures show the stiffness degradations curves $\bar{D}-p$ and $\bar{D}-m_y$, and the load-deflection curve $P-\Delta_x$.

Table 25 shows the maximum dimensionless applied loads for the sway frames SF13 through SF24. The joints and the foundation connections for these frames are partially fixed and possess equal rotational restraint stiffness of K_c ($=15506.94$ kip-in/rad). The effect of the load path dependence on maximum loads of these frames is seen from the results in this table. For example, when the load path SL1 is used for the frame SF13, p and m are found to be 0.79 and 0.21, respectively. However, with the load path SL2 p and m results become 0.30 and 0.21, respectively. This means that the frame vertical load with the load path SL1 is about 2.6 times that with the load path SL2. Also, the strength of the frame types SFR1 and SFR2 is found to be practically identical for each given load path. However, the frame type SFR3 exhibits substantially different maximum loads compared to those obtained for the frame types SFR1 and SFR2, for a given load path. Figures 97, 98, and 99 show the $\bar{D}-p$, $\bar{D}-m_y$, and $p-\Delta_x$ curves for the frame SF24 under the influence of the load path SL4.

Table 26 presents the effect of crookedness and residual stress distributions (RSDs) on the dimensionless maximum loads of the space frames with flexible joints. The beam-to-column connections as well as the bases have a rotational restraint stiffness of K_3 ($=24,000$ kip-in/rad). The frame is type SFR3 is adopted. The results for a total of 16 frames, SF25 through SF40, are presented in this table. The results show that the nearly perfect frames are stronger than the imperfect ones. Figures

100 through 104 show the behavior of the frames subjected to the load path SL1. Figure 101 shows $\bar{D}-m_y$ relationships for the frames SF25 through SF28 with the load path SL1. These curves are generated only after a specific value of p is applied. Therefore, at $m_y = 0$, the \bar{D} value is already relatively small. As the moment is increased, the influence of nonproportional loading is exhibited by the reductions and successive increases in the frame stiffness. Figures 102 and 103 present the $p - \Delta$ curves for these frames. In Figure 102, the deflection due to the vertical loads is small as indicated by the apparently "vertical" part of the curve. The horizontal part of the curve indicates that the vertical load is held constant while the deflection continued to increase under the influence of increasing external moments. Figure 103 shows the magnified version of the vertical line presented in Figure 102. In Figure 103, only the horizontal is shown magnified. Figures 105 through 108 show the behavior curves for frames SF25 through SF28 with the load path SL2. Figures 109 through 112 show the curves for these frames with the load path SL3. Figures 113 through 116 show the curves for these frames with the load path SL4. The frames with both the residual stresses and the crookedness are found to have the least stiffness.

A comparison of the space frame behavior for the various types of residual stress distributions (RSDs) given in Figures 3, 4, and 5 is also conducted. The space frame studied is of the type SFR3. The frame consists of columns with 2x2x0.1875 in. hollow square section, and beams with 2x3x0.1875 in. hollow rectangular section. Each member is 5 ft long. For the frames for which the (RSDs) given by Figures 4 and 5, the RSD of Figures 4 is assigned to the columns and the RSD of Figure 5

is assigned to the beams. For the frames with RSD given by Figure 3, all members are assumed to have the same RSD pattern. Table 27 shows a comparison of the maximum dimensionless external loads for the sway frames with different residual stress distributions. A total of four frames, SF41 through SF44, are investigated with the load paths SL1 through SL4. The partial rotational restraint of stiffness for each connection is taken as 5,961.1 kip-in/rad. With the load path SL1, the maximum moment obtained with the RSD of Figures 4 and 5 is slightly higher than the moment achieved with the RSD of Figure 3. With the load path SL3, identical maximum loads are obtained. The results for the load paths SL2 and SL3 depend on the outcome of the load path SL1 and hence cannot be compared. Figures 117 through 120 present sample behavior curves for the space frames with different RSDs. These figures show that although the frames with the RSDs given in Figures 4 and 5 are stiffer than those with the RSD in Figure 3, their load-carrying capacities are practically the same.

4. EXPERIMENTAL INVESTIGATION

4.1 Three-Story Single-Bay Space Frame

To verify the accuracy of the theoretical solution procedure presented in Chapter 3 for orthogonal space frames, a three-story single-bay structural steel frame is tested in the laboratory under three-dimensional nonproportional loading conditions. Hot-rolled hollow square and rectangular structural steel tubing is used for the test frame columns and beams, respectively. This chapter presents the details of the experiment, and a comparison of the experimental and theoretical behavior of the frame.

Figure 121 shows the major portion of the unbraced three-story single-bay orthogonal space frame tested. Figure 122 shows the test frame schematically. The total frame height is 15 feet with each story having a height of 5 feet. Also, the bay width is 5 feet in both principal directions. Each column has a 2 x 2 x 0.1875 in. hollow square section, and each of the beams has a 2 x 3 x 0.1875 in. hollow rectangular section. The beams are oriented in the usual fashion, that is, with their major axis oriented horizontally. Square plates with dimensions 6 x 6 x 0.5 in. are welded to the four columns at the frame base which in turn are bolted to the flanges of I-section foundation beams. The I-section beams are anchored to the ground by 1/2 in. diameter bolts with 36-inch spacing. No stiffeners are used to reinforce the web of the foundation beams, therefore, the column bases at nodes 1 through 4 in

Figure 122 are capable of developing partially restrained rotations about the global x axis.

4.1.1 Frame Material Properties

To determine the material Young's modulus and the yield stress, two stub column compression tests were conducted on 8-inch long specimens of the hollow square section. The test procedure followed is given in Reference 29. Four strain gages were mounted to the mid-height of one stub column. Each gage was mounted at the center of each side of the specimen as shown in Figure 123. Four additional strain gages were mounted at the corners of another identical stub column specimen at mid-height as shown in Figure 124. The stub columns were loaded in compression, and the output from strain gages was recorded. Figure 125 shows the experimental stress-strain relationship as the solid curve based on the stub column test with corner gages. The dashed line is the idealized relationship used for defining the Young's modulus and the material yield stress. The average E and σ_y values from the two specimens are found to be 29,000 ksi and 75 ksi, respectively.

4.1.2 Instrumentation

The frame deflections are measured at the beam-to-column connections in both the x and the y directions. Figure 126 shows an overall view of the deflection measurement setup including deflection transducers called LVDTs (Linear Variable Differential Transformers), and string and pulley. Figure 127 is the corresponding schematic diagram. As shown in the diagram, a small hook (1) is welded to the test

frame (2) at the joint level. A string (3) tied to the hook stretches horizontally toward a frictionless pulley (4) mounted on an isolated and rigid support. Beyond the pulley, the string drops vertically downward and passes through the LVDT (5). The end of the string is lightly loaded by a dead weight (6) to eliminate any string slack and for maintaining a small uniform tension during the experiment. Any motion of the frame at the joint level moves the rod inside the LVDT by equal magnitude. The LVDT's (manufactured by Schaevits Engineering) are hollow cylindrical inductance devices and develop linear output differential voltage between two inductance coils for any movement of core rod along the central axis. The devices are calibrated earlier for the gage factor and for the maximum range of the linear output. The maximum linear range of the LVDT is ± 4.0 inches. Figures 128 and 129 show a photograph and a corresponding schematic diagram, respectively, of a part of the vertical loading the apparatus. As shown in Figure 129, a load cell (7) is mounted at the top of a jack (8). The jack is attached to the flanges of a girder (9). The applied loads are transferred through a 0.5-inch diameter steel loading cable (10). Above the load cell and below the girder, a channel (11) is mounted with three rollers (12) which freely rotate inside the channel. The applied loads are measured by a load cell (manufactured by MTS System Corporation).

The measurement of the strains in the frame members is conducted by using a total of 68 strain gages. Four gages, with one on each face are placed at the midspan of each column. A single strain gage is located at the bottom face of each beam at its midspan. In addition, two strain gages are located near each of the four column bases. The recording of the output from the LVDTs, the load cells, and the

strain gages is carried out by an on-line computer. All of the devices except the strain gages are connected to a multichannel strain gage conditioner and amplifier. Figure 130 shows the data acquisition system for recording the analog output signals which are fed into a converter called the NEFF System 470. The NEFF system is shown as item (13) for digitizing the output. The strain gage signals are directly fed into another converter. An IBM-PC compatible computer (14) is used for the digital data acquisition and reduction. The test output is stored in the raw data form on the computer hard disk and later converted and stored as text data. This is done by the data acquisition software by playing back the raw output.

4.1.3 Rotational Stiffness Measurement Procedure

The frame is anchored to a pair of I-section foundation beams which run along the x-axis as indicated in Figure 122. A pilot test was first conducted to measure any possible rotations of the frame bases. The rotation about the y-axis was found to be practically nonexistent and thus giving an infinite rotational stiffness about that axis. However, the column bases rotated due to the flexibility of the unstiffened upper flanges of the foundation I-section beams. Figures 131 and 132 show a typical setup for the measurement of the rotation. In Figure 132, a stiff steel strip (15) of 8 inches length is welded to the column base plate (16). The steel strip cantilevers horizontally outward along the y-axis. A single LVDT (17) is mounted on an isolated external support to record the vertical movement of the end of the steel strip. The distance between the base plate center and the LVDT is used to calculate the base rotation. The outer fiber normal strain near the base of the column is obtained by using a linear extrapolation of the output from two strain

gages (19) in Figure 132. The distance between the base plate and the lower strain gage is 1.0 in., and the other strain gage is right above the first one at a distance of 1.50 in. from the first gage. These strains are used to calculate the internal bending moment at the column base induced by the external loading on the frame. The bending moment versus the base rotation are plotted in Figure 133. The initial offset θ_0 is due to the fact that the result used for this plot are based on the load pair P_2, P_2 shown in Figure 122, after the load pair P_1, P_1 is applied. The slope of the line in Figure 133 provide the rotational restraint stiffness at the column base about the x axis, and is found to be 7,023 kip-in/rad.

4.1.4 Residual Stresses

In order to predict the frame behavior theoretically, it is necessary to know the distribution of the residual stresses in the hollow square and rectangular members. For this purpose, the method of sectioning is used on two specimens, namely a 2 x 3 x 0.1875 in. hollow rectangular section and a 2 x 2 x 0.1875 in. hollow square section, with lengths of 8.175 in. and 7.986 in., respectively. The initial lengths are precisely obtained after milling the ends to a tolerance of ± 0.0001 in. The square section is divided into 16 longitudinal strips; four corner strips and twelve strips from the four sides. The rectangular section is divided into 20 longitudinal strips; four corner strips, six from the two short sides, and ten from the two long sides. Figures 134 and 135 show the strip locations in the two sections. After the strips were carefully cut, they were straightened out for the final length measurements. All of the strips exhibited an outward bend (compression on the

outside) before they were straightened out. The midspan flexural deflection of each of the strips was measured and recorded. The residual stresses obtained from the residual strains in the strips for the two sections are given in the fifth column of Tables 28 and 29. The last column in these tables presents the average residual stress in the strips. The average values are obtained by using the stresses in the strips that are located at the same distance from the center of gravity of the section. Figures 4 and 5 show the resulting idealized residual stress distributions for the two sections, and are employed in the theory.

The cross-sectional residual stresses were also found for the hollow square section using an alternate experimental approach as follows. A total of 16 strain gages were first mounted on the outside of an 8-inch long stub column with the 2 x 2 x 0.1875 in. section. The strain gages were mounted at the center of each strip, and then initialized. Next, the section was sliced parallel to the plane of the section, resulting in a 1.5 in. long ring type short column including the 16 strain gages. The ring was then sliced longitudinally between the gages and the final gage readings were recorded. The strain in all of the strips was found to be compressive. Furthermore all of the strips exhibited an outward bend (compression on the outside). The outward bend indicated that the residual stresses also varied across the thickness of the section walls. Knowing the average axial strain from the method of sectioning and the strip midspan deflections, a numerical computation was performed to find the inner and the outer fiber residual strains in the section. Figures 135 and 136 show the calculated distribution of stresses across the thickness of the wall for each strip. The strips in the figures are numbered according to their locations as indicated in Figures 133 and 134. The inner and outer faces of the strips are also

identified in these figures. The dashed lines in Figure 135 represent the strain distribution across the thickness found by using the output from the strain gages as well as the residual axial strains reported in Table 28. As seen from Figure 136, the two test procedures for finding average residual stresses are in good agreement. The elements with no apparent dashed lines in Figure 135 indicate that identical results are obtained using the two procedures.

4.1.5 Initial Crookedness

To measure the initial crookedness of the frame columns, a theodolite is used. The initial crookedness is measured for each column in both the x and the y directions. The initial crookedness is a measurement of the horizontal shift of the central axis of the column from a vertical axis which passes through the center of the base of the first story column. Readings are taken at the member ends and at three other equidistant internal points. The interpolated crookedness values for the columns numbered 1 through 12 in Figure 122 are tabulated in Table 30. In this table, the crookedness of the base of the frame is shown to be zero. The measured crookedness values are used as a part of the input to the computer program for conducting the analysis of the three-story test frame. To adapt to the finite difference scheme, interpolated values of the crookedness were used at the node points.

4.2 Frame Test

4.2.1 Loading Apparatus

The loading system designed for two equal horizontal loads (H , H) along the x axis is shown in Figures 138 and 139. A channel (20) running horizontally is attached to the second story level at the beam-column joints. The central point of the channel is pulled by a looped around horizontal cable (21) of 0.25-inch diameter which wraps around a pulley (22) mounted on an isolated support system. The cable is further looped around a jack (23) mounted upside down on an isolated support system as shown in Figure 138. For the load measurement, a load cell (24) is placed behind the channel.

As shown in Figures 140 and 141, a short I-beam (25) is placed at the top of the frame across two adjoining beams. The support points on the beams are located close to the column center such that there is a sufficient space between the I-beam and the column for the loading cables to be able to pass through. With reference to Figures 140 and 141, the loading cable (10) wraps around the I-beam (25) and runs along the full length of the 15-ft column toward the foundation. For stabilizing the short loading I-beams, 2-inch diameter bearing balls (26) are placed in between the I-beam and the frame beams (27). The bearing ball sits and projects above a pair of from two square steel blocks (28) which are been separately welded to the I-beam and the frame beams. The blocks are grooved to form a ball-and-socket joint. This arrangement allows for the vertical loading of the beams without any twisting moments.

For pulling the vertical load cables, the setup used at the frame bottom is shown in Figures 128 and 129. First, a pair of long girders running along the y axis

are placed on top of the foundation beams and bolted in place. These girders project outside of the test frame base dimensions. Next, a pair of cross girders (9) running parallel to the two top loading I-beams (25) are placed near the two frame corners to be loaded. The cross girders are bolted to the foundation beams. A loading jack (8) is mounted on the top of the cross girder (9) at a point which is right under the center of the top loading I-beams (25). A channel (11) and a three-roller system (12) is mounted under the girder (9) for the loading cables to pass around and move smoothly. Two additional but similar roller systems are also mounted, one at the top of the I-beam (25) and another at the top of the jack (8). Subsequently, a single cable (10) of 0.50-inch diameter is run starting from the bottom of the frame to the top, going over the top I-beam, running vertically down, going around the bottom roller system, going toward the jack, going around the jack, going down again and appearing on the same side of the starting point. This cable is taken through one more similar route before it is tied to the starting point of the cable by "eyes and clips". The cables are initially stretched to remove any slack. When the jack is opened, it stretches the cables and provides a self-reacting frame compression system with little or no load-transfer to the foundation. Figure 141 shows a photograph of the first story with the loading jacks marked as Jack-1 for P_1 , Jack-2 for P_2 , and Jack-H for the horizontal load.

The beam-to-column connections at joints 30 and 32 were reinforced by welding 2x2x0.25 in. angles. The angles were welded at four locations, namely, two at the connections of beams 21 and 22 to column 18, and two at the connections of beams 23 and 24 to column 20.

4.2.2 Nonproportional Experimental Loads

With reference to Figure 122, the steps given below are followed to apply the set of nonproportional load pairs (H, H) ; (P_1, P_1) ; (P_2, P_2) , to the three-story test frame:

1. Apply a horizontal load pair (H, H) at joints 17 and 20 in gradual increments until $H = H_a$.
2. With $H = H_a$ held constant, apply a vertical load pair P_1, P_1 on beams 21 and 22 in gradual increments until $P_1 = (P_1)_a$.
3. Holding H and P_1 constant at H_a and $(P_1)_a$, respectively, apply another vertical load pair (P_2, P_2) on beams 23 and 24 in gradual increments until $P_2 = (P_2)_a$.
4. Holding H and P_2 constant at H_a and $(P_2)_a$, respectively, increase P_1 gradually beyond $(P_1)_a$ to a new value $(P_1)_b$.
5. Holding H and P_1 constant at H_a and $(P_1)_b$, respectively, increase P_2 gradually beyond $(P_2)_a$ until the frame load-carrying capacity is reached at $P = (P_2)_b$.

For the frame tested, $H_a = 1.0$ kip; $(P_1)_a = 16.50$ kips; $(P_1)_b = 21.50$ kips; $(P_2)_a = 18.50$ kips; $(P_2)_b = 24.50$ kips.

4.2.3 Test Procedure

A number of elastic pilot tests were conducted on the test frame to ensure that all of the instruments were functioning properly before loading into the inelastic range. As shown in Figure 122, the horizontal load pair (H, H) was applied to the frame through the beam-to-column connections at joints 17 and 20, in the positive x direction. The vertical load pairs (P_1, P_1) and (P_2, P_2) were applied by means of

the loading beams described previously. At every load increment, the jacks were locked completely and left for approximately two to three minutes to allow the hydraulic system to stabilize before the test output was recorded. The output consists of readings from 66 strain gages, 16 deflection transducers (LVDTs), and three load cells. One day before the test, the frame was lightly coated by a water-proof cement paint to observe the initiation of yielding exhibited by the flaking of the paint induced by the cracking of the mill-scale. This provided a visual check on the condition of the members. The test procedure is summarized as follows:

1. The strain gages, the LVDTs, and the load cells are initialized.
2. The horizontal load pair (H, H) is first applied incrementally until $H = H_a$.
3. With H held constant at H_a , the vertical load pair (P_1, P_1) is incremented gradually until $P_1 = (P_1)_a$.
4. With the P_1 held constant at $(P_1)_a$, the vertical load pair (P_2, P_2) is incremented gradually until $P_2 = (P_2)_a$.
5. With $H = H_a$ and $P_2 = (P_2)_a$ held constant, the vertical load pair (P_1, P_1) is incremented again until P_1 reaches a new higher load level $(P_1)_b$.
6. With $H = H_a$ and $P_1 = (P_1)_a$ held constant, the vertical load pair (P_2, P_2) is incremented again until P_2 reaches the peak load $(P_2)_b$.
7. Lastly, the frame is gradually unloaded by removing the load pairs one by one in a sequence opposite to that used for the loading process. Thus the loads are removed in the following manner: Reduce $(P_2)_b$ to $(P_2)_a$; $(P_1)_b$ to $(P_1)_a$; $(P_2)_a$ to zero; $(P_1)_a$ to zero, and finally H_a to zero.

The loads and deformations are recorded at each load increment described in Steps 2 through 8. The test results are stored in a hard disk of an IBM-PC.

4.3 Theory versus Experiment

A twisting of the frame was observed during the test. This twisting affected all of the joint deflections. Tables 31 presents the frame deflections at joints 29 and 32 in the x direction. Since the frame developed twisting, the average of the joints 29 and 32 displacements is calculated and entered in the table for a comparison to the theoretical predictions. The angle of twist at the frame top is measured by using the deflections of the two top frame joints and is entered in the last column of the table. Table 32 summarizes the displacements at joints 31 and 32 and their average. Figures 148 and 149 present, respectively, the vertical loads P_1 and P_2 versus the frame angle of twist. The maximum angle of twist which the frame experienced during the test is $\alpha_f = 0.0183$ rad. In addition to the frame twisting, the mid-height twisting of column 20 was also measured by means of two dial gages mounted at 5 in. and 9 in., respectively. Table 33 presents the experimental deflections and the calculated angle of twist of column 20. Figures 150 and 151 show the vertical load P_1 versus the angle of twist and the midspan deflection, respectively.

Figures 152 through 154 show a comparison of the theory and the experiment in the form of curves relating the applied loads to the frame horizontal deflection along the x axis. Figure 152 shows the lateral load, H, versus the frame top deflection in the x direction. The experimental deflection is in good agreement with the theory. At $H = 1.0$ kip, the "humps" in the experimental curve are in part due to the fluctuations in the NEFF system. The other source of the fluctuation is the

variation in H due to the application of P_1 and P_2 . During the test, H was adjusted periodically to maintain the 1.0 kip value. Figure 153 shows the vertical load P_1 versus the lateral deflection at the frame top. The figure shows the start of the vertical load P_1 at a horizontal deflection (point A) of about 1.7 in. Next, the load P_1 is held constant at 16.5 kips (Point B) while the load P_2 is incremented. During the application of P_2 , the P_1 - Δ_x relationship in Figure 153 goes from point B to point C. The horizontal displacement from the Point B to the point C is not clear in the experimental curve due to the average of the displacements considered. The load P_1 is incremented again starting at the Point C until the point D is reached at about 20.5 kips. Holding P_1 constant at its new value, P_2 is incremented to collapse. During this phase of loading, the curves in Figure 153 move from D to E. Figure 154 shows the vertical load P_2 versus the frame top deflection in the x direction. The load P_2 starts near point B with a prior deflection due to the vertical load P_1 . Next, P_2 is increased gradually to 19.5 kips (point C). The P_2 - Δ_x relationship moves from the point C to the point D while P_1 is incremented from 16.5 kips to 20.5 kips. Next, P_2 is incremented to 24.5 kips which corresponds to the frame collapse. The results in Figures 153 and 154 show that the peak loads and the deflections from the theory and the experiment are in good agreement.

Figures 155 through 157 show the lateral load H, the vertical load P_1 , and the vertical load P_2 versus the frame top deflection Δ_y , respectively. Figures 158 and 159 show the relationships between the lateral load H and the normal strains at locations S1 and S2 for column 18. Figure 160 shows the relationships between the applied load P_1 and the normal strain at location S1. Figure 161 shows the

relationships between P_2 and the normal strain at S1. Figures 162 to 165 are similar curves for column 20. The locations for the normal strain measurement gages for these columns are identified in Figure 166. The experimental curves are seen to be in good agreement with the theory. The maximum strength P_2 obtained by the theory is 25.44 kip, that is, 3.8% higher than that reached by the experiment.

Figures 167 through 169 show the total stiffness degradation curves for the three-story test frame. In Figure 167, \bar{D} is constant during the application of the lateral load H , that is, from point A to point B. The sudden drop in the curve from B to C is due to the application of the vertical load pairs (P_1, P_1) and (P_2, P_2) . Figure 168 shows the decrease in \bar{D} as (P_1, P_1) increases from $(0,0)$ at D to $[(P_1)_a, (P_1)_a]$ at E. A sudden drop in \bar{D} from E to F is due to the first application of (P_2, P_2) as it increases from $(0,0)$ at E to $[(P_2)_a, (P_2)_a]$ at F. The vertical load pair (P_1, P_1) is increased again from $[(P_1)_a, (P_1)_a]$ at F to $[(P_1)_b, (P_1)_b]$ at G. Figure 169 shows the decrease in \bar{D} as (P_2, P_2) increases from $(0, 0)$ at Q to $[(P_2)_a, (P_2)_a]$ at I. A sudden drop in \bar{D} from I to J is due to the second application of (P_1, P_1) as it increases from $[(P_1)_a, (P_1)_a]$ at I to $[(P_1)_b, (P_1)_b]$ at J. Finally, (P_2, P_2) is increased from $[(P_2)_a, (P_2)_a]$ at J to $[(P_2)_b, (P_2)_b]$ at K. The effect of the vertical load pairs on the frame stiffness degradation is seen clearly from these figures.

5. CONCLUSIONS AND FUTURE RESEARCH

5.1 Conclusions

Within the range of the parameters considered, the following conclusions are drawn from this research:

1. The load-deformation behavior of the space frame tested is in good agreement with the theory.
2. The inelastic slope-deflection procedure for plane and space sway frames presented herein is computationally stable and converges rapidly.
3. The strength of the beam-columns, and plane and space frames with flexible connections is load path dependent.
4. An increase in the lateral restraint stiffness results in an increase in the member strength. However, there exists a threshold restraint stiffness beyond which no further increase in the member strength is achieved.
5. When only one joint of a portal frame is subjected to a concentrated vertical load, the frame can carry more load than the squash load of the column.
6. When only two joints of a single-story single-bay space frame are subjected to concentrated vertical loads, each load at collapse may be larger than the column squash load.

7. Unbraced frames subjected to vertical loads exhibit very small lateral deflections.
8. Residual stresses show a significantly larger effect on the member stiffness than the initial crookedness.
9. The torsional deformations do not have a noticeable effect on the load-carrying capacity of a space frame.

5.2 Future Research

The next significant step in research in this field is the inclusion of torsional effects for thin-walled sections. The analysis procedure should also be modified to account for axial member shortening. Parallel and supercomputing procedures should be developed for very rapid practical solutions to load path dependent inelastic frame analysis and design problems.

REFERENCES

1. Ellis, J. S., Jury, E. J., and Kirk, D. W., "Ultimate Capacity of Steel Column Loaded Biaxially," *Transaction, Engineering Institute of Canada*, Vol. 7, No. A-2, pp. 3-11, February, 1964.
2. Yura, J. A., and Galambos, T. V., "Strength of Single-Story Steel Frames," *Journal of the Structural Division*, ASCE, Vol. 91, No. 5, October, 1965, pp. 81-101.
3. Lu, Le-Wu, "Inelastic Buckling of Steel Frames," *Journal of the Structural Division*, ASCE, Vol. 91, No. 6, December, 1965, pp. 185-213.
4. Ellis, J. S., and Marshall, P. J., "The ultimate Capacity of Steel Columns Loaded Biaxially," *Supplement to Column Research Council*, Annual Meeting, April, 1967, pp. 1-8.
5. Korn, A., and Galambos, T. V., "Behavior of Elastic-Plastic Frames," *Journal of the Structural Division*, ASCE, Vol. 98, No. 5, May, 1968, pp. 1119-1141.
6. Wright, E. W., and Gaylord, E. H., "Analysis of Unbraced Multistory Steel Rigid Frames," *Journal of the Structural Division*, ASCE, Vol. 95, No. 5, May, 1968, pp. 1143-1163.
7. McVinnie, W. W., and Gaylord, E. H., "Inelastic Buckling of Unbraced Space Frames," *Journal of the Structural Division*, ASCE, Vol. 94, No. 8, August, 1968, pp. 1863-1885.
8. Harstead, G., Birnstiel, C., and Leu, K., "Inelastic H-Columns Under Biaxial Bending," *Journal of Structural Engineering*, ASCE, Vol. 94, No. 10, October, 1968, pp. 2371-2398.
9. Birnstiel, C., "Experiments on H-Columns Under Biaxial Bending," *Journal of Structural Engineering*, ASCE, Vol. 94, No. 10, October, 1968, pp. 2429-2449.
10. Galambos, T. V., *Structural Members and Frames*, Printice Hall, Inc., Englewood Cliffs, New Jersey, 1968.

11. Gent, A.R., and Milner, H.R., "The Ultimate Load Capacity of Elastically Restrained H-Columns Under Biaxial Bending," *Proceedings of the Institution of Civil Engineers*, Vol. 41, London, England, December, 1968, pp. 685-704.
12. McNamee, B. M., and Lu, Le-Wu, "Inelastic Multistory Frame Buckling," *Journal of the Structural Division*, ASCE, Vol. 98, No. 7, July, 1972, pp. 1613-1631.
13. Tebedge N., and Chen, W., "Design Criteria For H-Columns Under Biaxial Loading," *Journal of the Structural Division*, ASCE, Vol. 100, No. 3, March, 1974, pp. 579-598.
14. Cheong-Siat-Moy, F., "General Analysis of Laterally Loaded Beam-Column," *Journal of the Structural Division*, ASCE, Vol. 100, No. 6, June, 1974, pp. 1263-1278.
15. Vinnakota, S., and Aysto, P., "Elastic Spatial Stability of Restrained Beam-Column," *Journal of the Structural Division*, ASCE, Vol. 100, No. 11, November, 1974, pp. 2235-2254.
16. Wood, B. R., Beaulieu, D., and Adams, P. F., "Column Design By P-Delta Method," *Journal of the Structural Division*, ASCE, Vol. 102, No. 2, February, 1976, pp. 411-420.
17. Cheong-Siat-Moy, F., "Multistory Frame Design Using Story Stiffness Concept," *Journal of the Structural Division*, ASCE, Vol. 102, No. 6, June, 1976, pp. 1197-1212.
18. Chen, W. F., and Atsuta, T., *Theory of Beam-Columns*, Vol. 1, McGraw-Hill, Inc., New York, 1976.
19. Chen, W. F., and Atsuta, T., *Theory of Beam-Columns*, Vol. 2, McGraw-Hill, Inc., New York, 1977.
20. Razzaq, Z., and Naim, M., "Elastic Instability of Unbraced Space Frames," *Journal of the Structural Division*, ASCE, Vol. 106. No. ST7, July, 1980, pp. 1389-1400.
21. Balio, G., and Companini, G., "Equivalent Bending Moments for Beam-Columns," *Journal of Constructional Steel Research*, Vol. 1, No. 3, May, 1981.
22. Burden, R. L., Faires, J. D., and Reynolds, A. C., *Numerical Analysis*, Second Edition, Prindle, Weber and Schmidt, Massachusetts, 1981.
23. Razzaq, Z., and McVinnie, W. W., "Rectangular Tubular Steel Columns Loaded Biaxially," *Journal of Structural Mechanics*, Vol. X, No. 4, 1982.

24. Razzaq, Z., "Restraint Effect on Steel Column Strength," *Journal of Structural Engineering*, ASCE, Vol. 109, No. 2, February, 1983, pp. 314-334.
25. Wen, R., and Rahimzadeh, J., "Nonlinear Elastic Frame Analysis By Finite Element," *Journal of Structural Engineering*, ASCE, Vol. 109, No. 8, August, 1983, pp. 1952-1971.
26. Razzaq, Z., and Calash, A. Y., "Imperfect Columns With Biaxial Partial Restraints," *Journal of Structural Engineering*, ASCE, Vol. 111, No. 4, April, 1985, pp. 758-776.
27. Razzaq, Z., and McVinnie, W. W., "Theoretical and Experimental Behavior of Biaxially Loaded Inelastic Columns," *Journal of Structural Mechanics*, Vol. 14, No. 3, March, 1986.
28. Razzaq, Z., and Darbhamulla, S. P., "Restraint Modelling Effect on Beam-Column Strength," *SSRC Proceedings*, Annual Technical Session, April, 1986, pp. 233-243.
29. Razzaq, Z., and Darbhamulla, S. P., "Nonproportionally Loaded Elasto-Plastic Steel Beam-Column," *SSRC Proceeding*, Annual Technical Session, 1987, pp. 1-7.
30. Razzaq, Z., and Darbhamulla, S. P., "Behavior and Strength of Non-proportionally Loaded Imperfect Beam-Columns Restrained Partially," *SSRC Proceedings*, Annual Technical Session, March, 1987, pp 1-9.
31. Darbhamulla, S. P., and Razzaq, Z., "Imperfect Rectangular Tubular Beam-Columns With Nonproportional Biaxial Loads," *SSRC Proceedings*, Annual Technical Session, 1988, pp. 15-29.
32. Lord, A., "Inelastic Minor-Axis Analysis of Partially Restrained Imperfect Steel Column with Sway," *Structures Research Report No. 7*, Old Dominion University, May, 1988.
33. Galambos, T. V., *Guide to Stability Design Criteria for Metal Structures*, Fourth Edition, John Wiley and Sons, Inc., New York, N. Y., 1988.
34. Darbhamulla, S. P., and Razzaq, Z., "Portal Frame Stability With Non-proportional Loads," *Proceeding, Seventh Structures Congress*, ASCE, San Francisco, May, 1989.
35. Chandra, R., Trikha, D. N., and Krishna, P., "Nonlinear Analysis of Steel Space Structures," *Journal of Structural Engineering*, ASCE, Vol. 116, No. 4, April, 1990, pp. 899-909.

36. Chandra, R., Krishna, P., and Trikha, D. N., "Elastic-Plastic Analysis of Steel Space Structures," *Journal of Structural Engineering*, ASCE, Vol. 116, No. 4, April, 1990, pp. 939-955.
37. Darbhamulla, S. P., "Nonproportionally Loaded Steel Beam-Columns and Flexibly-Connected Nonsway Frames," *Ph.D. Dissertation*, Old Dominion University, May, 1990.

Table 1. Comparison of dimensionless maximum axial loads for columns crooked uniaxially or biaxially (7x7x0.375 in. cross section)

Rest- raint	Case No.	Uniaxially Crooked		Case No.	Biaxially Crooked	
		Predicted	Reference 26		Predicted	Reference 26
K_a	1	0.86	0.86	5	0.82	0.81
K_b	2	0.89	0.89	6	0.86	0.86
K_c	3	0.93	0.93	7	0.91	0.91
K_d	4	0.96	0.96	8	0.96	0.95

Table 2. Comparison of dimensionless maximum axial loads for columns crooked uniaxially or biaxially (6x8x0.375 in. cross section)

Rest- raint	Case No.	Uniaxially Crooked		Case No.	Biaxially Crooked	
		Predicted	Reference 26		Predicted	Reference 26
K_a	9	0.85	0.87	13	0.80	0.80
K_b	10	0.92	0.91	14	0.84	0.84
K_c	11	0.94	0.94	15	0.89	0.89
K_d	12	0.97	0.97	16	0.94	0.94

Table 3. Comparison of dimensionless maximum axial loads p , for nonsway pinned-end members with lateral load W (W8x31 cross section)

Case No.	L/r_x	W (kips)	$p = P/P_Y$	
			Predicted	Reference 14
17	20.0	5.0	0.92	0.92
18	20.0	10.0	0.85	0.85
19	20.0	15.0	0.77	0.77
20	40.0	5.0	0.82	0.79
21	40.0	10.0	0.65	0.67
22	40.0	15.0	0.50	0.52
23	60.0	5.0	0.66	0.67
24	60.0	10.0	0.44	0.45
25	60.0	15.0	0.25	0.26

Table 4. Comparison of dimensionless maximum loads for biaxially loaded nonsway beam-columns, with equal biaxial rotational springs of stiffness K_3 (6x8x0.375 in. cross section)

Case No.	Load Path	Load	Dimensionless External Load	
			Predict	Reference 37
26	LP1	p	0.25	0.25
		m_x	1.43	1.43
		m_y	1.52	1.52
27	LP2	m_x	1.43	1.43
		m_y	1.52	1.52
		p	0.35	0.34
28	LP3	p	0.25	0.25
		m_x	1.43	1.43
		m_y	1.84	1.84
29	LP1	p	0.75	0.75
		m_x	0.33	0.35
		m_y	0.35	0.37
30	LP2	m_x	0.35	0.35
		m_y	0.37	0.37
		p	0.74	0.75
31	LP3	p	0.75	0.75
		m_x	0.35	0.35
		m_y	0.47	0.47

Table 5. Comparison of dimensionless maximum loads for biaxially loaded nonsway beam-columns, with equal biaxial end rotational restraints of stiffness K_2 ; (W8x31 cross section)

Case No.	Load Path	Load	Dimensionless External Load	
			Predicted	Reference 37
32	LP3	p	0.25	0.25
		m_x	0.86	0.86
		m_y	0.51	0.51
33	LP4	p	0.25	0.25
		m_x	0.86	0.86
		m_y	0.51	0.51
34	LP3	p	0.53	0.53
		m_x	0.41	0.41
		m_y	0.24	0.24
35	LP4	p	0.50	0.50
		m_x	0.41	0.41
		m_y	0.24	0.24

Table 6. Maximum dimensionless external loads for uniaxially loaded sway beam-columns, with equal end rotational restraints of stiffness K_2

Case No.	K_y kip/in	Load Path	Load	Dimensionless External Load				
BC1	1.0E-9	NP1	p	0.00	0.20	0.28	0.35	-
			m_x	1.70	1.69	1.34	0.00	-
		NP2	p	0.00	0.21	0.29	0.35	-
			m_x	1.70	1.69	1.34	0.00	-
BC2	0.25	NP1	p	0.00	0.22	0.31	0.43	-
			m_x	1.70	1.68	1.40	0.00	-
		NP2	p	0.00	0.21	0.30	0.43	-
			m_x	1.70	1.68	1.40	0.00	-
BC3	0.5	NP1	p	0.00	0.24	0.49	0.51	-
			m_x	1.70	1.62	0.70	0.00	-
		NP2	p	0.00	0.23	0.49	0.51	-
			m_x	1.70	1.62	0.69	0.00	-
BC4	1.0	NP1	p	0.00	0.24	0.35	0.46	0.66
			m_x	1.70	1.65	1.25	0.91	0.00
		NP2	p	0.00	0.22	0.35	0.46	0.66
			m_x	1.70	1.65	1.25	0.91	0.00
BC5	1.5	NP1	p	0.00	0.22	0.47	0.57	0.74
			m_x	1.70	1.68	0.88	0.63	0.00
		NP2	p	0.00	0.21	0.39	0.45	0.74
			m_x	1.70	1.68	0.88	0.63	0.00
BC6	2.0	NP1	p	0.00	0.20	0.43	0.63	0.90
			m_x	1.70	1.66	1.00	0.51	0.00
		NP2	p	0.00	0.22	0.43	0.63	0.90
			m_x	1.70	1.66	1.00	0.51	0.00

Table 7. Maximum dimensionless external loads for uniaxially loaded sway beam-columns, with equal end rotational restraints of stiffness K_2

Case No.	K_2 kip/in	Load Path	Load	Dimensionless External Load				
BC7	1.0E-9	NP3	p m	0.00	0.27	0.36	0.48	0.57
				3.01	2.51	2.04	1.61	0.00
		NP4	p m	0.00	0.27	0.36	0.48	0.57
				3.01	2.40	1.83	1.19	0.00
BC8	0.5	NP3	p m	0.00	0.26	0.31	0.49	0.72
				3.37	2.63	2.24	1.51	0.00
		NP4	p m	0.00	0.26	0.31	0.49	0.72
				3.37	2.07	2.02	1.49	0.00
BC9	1.0	NP3	p m	0.00	0.22	0.35	0.48	0.82
				3.37	2.83	2.30	1.58	0.00
		NP4	p m	0.00	0.20	0.35	0.48	0.83
				3.37	2.74	2.02	1.44	0.19
BC10	1.5	NP3	p m	0.00	0.24	0.30	0.46	0.90
				4.37	3.21	2.41	1.58	0.00
		NP4	p m	0.00	0.24	0.30	0.46	0.90
				4.37	2.28	1.95	1.63	0.09
BC11	2.0	NP3	p m	0.00	0.24	0.28	0.43	0.94
				5.47	3.01	2.50	1.69	0.00
		NP4	p m	0.00	0.24	0.28	0.43	0.94
				5.47	2.26	2.05	1.62	0.00

Table 8. Effect of imperfection on the strength of sway beam-columns loaded uniaxially, with lateral spring stiffness $K_y = 0.0$ and with equal end rotational restraints of stiffness K_2

Case No.	Initial Crookedness	Residual Stress, $\bar{\sigma}_{rc}$	Load Path	Load	Peak Loads
BC12	L/100,000	-0.2	NP3	p m_x	0.30 1.13
			NP4	p m_x	0.30 1.14
BC13	L/100,000	0.0	NP3	p m_x	0.30 1.13
			NP4	p m_x	0.30 1.14
BC14	L/1000	-0.2	NP3	p m_x	0.30 1.13
			NP4	p m_x	0.30 1.18
BC15	L/1000	0.0	NP3	p m_x	0.30 1.13
			NP4	p m_x	0.30 1.13

Table 9. Effect of imperfection on the strength of sway beam-columns loaded uniaxially, with lateral spring stiffness $K_y = 0.10$ kip/in. and equal end rotational restraints of stiffness K_2

Case No.	Initial Crookedness	Residual Stress, $\bar{\sigma}_r$	Load Path	Load	Peak Loads
BC16	L/100,000	-0.2	NP3	p m_x	0.32 1.13
			NP4	p m_x	0.32 1.13
BC17	L/100,000	0.0	NP3	p m_x	0.33 1.13
			NP4	p m_x	0.33 1.13
BC18	L/1000	-0.2	NP3	p m_x	0.32 1.13
			NP4	p m_x	0.32 1.19
BC19	L/1000	0.0	NP3	p m_x	0.34 1.13
			NP4	p m_x	0.34 0.97

Table 10. Effect of imperfection on the strength of sway beam-columns loaded uniaxially, with lateral spring stiffness $K_y = 2.0$ kip/in. and equal end rotational restraints of stiffness K_2

Case No.	Initial Crookedness	Residual Stress, $\bar{\sigma}_{rc}$	Load Path	Load	Peak Loads
BC20	L/100,000	-0.2	NP3	p m_x	0.39 1.13
			NP4	p m_x	0.39 1.13
BC21	L/100,000	0.0	NP3	p m_x	0.39 1.13
			NP4	p m_x	0.39 1.13
BC22	L/1000	-0.2	NP3	p m_x	0.38 1.13
			NP4	p m_x	0.38 1.06
BC23	L/1000	0.0	NP3	p m_x	0.38 1.13
			NP4	p m_x	0.38 1.13

Table 11. Effect of imperfection on the strength of sway beam-columns loaded uniaxially, with lateral spring stiffness $K_y = 1.0E+15$ kip/in. and equal end rotational restraints of stiffness K_2

Case No.	Initial Crookedness	Residual Stress, $\bar{\sigma}_{rc}$	Load Path	Load	Peak Loads
BC24	L/100,000	-0.2	NP3	p m_x	0.39 1.13
			NP4	p m_x	0.39 1.13
BC25	L/100,000	0.0	NP3	p m_x	0.39 1.13
			NP4	p m_x	0.39 1.13
BC26	L/1000	-0.2	NP3	p m_x	0.38 1.13
			NP4	p m_x	0.38 1.06
BC27	L/1000	0.0	NP3	p m_x	0.38 1.13
			NP4	p m_x	0.38 1.13

Table 12. Maximum dimensionless external loads for uniaxially loaded sway beam-columns, with bilinear lateral restraints and equal end rotational restraints

Case No.	K_y	Load Path	Load	Maximum External Load					
BC28	0.00	NP3	p	0.00	0.00	0.00	0.00	0.34	0.34
			m_x	1.79	1.21	0.93	0.32	0.12	0.00
		NP4	p	0.00	0.00	0.00	0.00	0.34	0.34
			m_x	1.79	1.21	0.93	0.32	0.24	0.24
BC29	0.10	NP3	p	0.00	0.03	0.03	0.03	0.37	0.37
			m_x	1.79	1.21	0.93	0.32	0.12	0.00
		NP4	p	0.00	0.03	0.03	0.03	0.37	0.37
			m_x	1.79	1.87	1.87	1.87	0.24	0.24
BC30	2.00	NP3	p	0.00	0.23	0.33	0.63	0.77	0.89
			m_x	1.79	1.21	0.93	0.32	0.12	0.00
		NP4	p	0.00	0.23	0.33	0.63	0.77	0.89
			m_x	1.79	1.21	0.93	0.37	0.12	0.02
BC31	∞	NP3	p	0.00	0.23	0.33	0.66	0.81	0.90
			m_x	1.79	1.21	0.93	0.32	0.12	0.00
		NP4	p	0.00	0.14	0.33	0.66	0.81	0.90
			m_x	1.79	2.07	0.93	0.32	0.12	0.02

Table 13. Maximum dimensionless external loads for biaxially loaded sway beam-columns, with equal end rotational restraints of stiffness K_3

Case No.	$K_x = K_y$ (kip/in)	Load Path	Load	Dimensionless External Load				
BC32	1.E-9	LP1	p	0.00	0.20	0.50	0.53	-
			m_x	2.82	1.90	0.53	0.00	-
			m_y	3.09	2.06	0.56	0.00	-
		LP2	p	0.00	0.29	0.50	0.53	-
			m_x	2.82	1.90	0.53	0.00	-
			m_y	3.09	2.06	0.56	0.00	-
BC33	0.5	LP1	p	0.00	0.24	0.50	0.69	-
			m_x	2.93	1.77	0.97	0.00	-
			m_y	3.17	1.92	1.06	0.00	-
		LP2	p	0.00	0.29	0.50	0.69	-
			m_x	2.93	1.77	0.97	0.00	-
			m_y	3.17	1.92	1.06	0.00	-
BC34	1.0	LP1	p	0.00	0.22	0.49	0.75	0.79
			m_x	2.93	1.89	0.99	0.27	0.00
			m_y	3.17	2.00	1.05	0.29	0.00
		LP2	p	0.00	0.29	0.50	0.75	0.79
			m_x	2.93	1.89	0.99	0.27	0.00
			m_y	3.17	2.00	1.05	0.29	0.00
BC35	1.5	LP1	p	0.00	0.27	0.56	0.75	0.91
			m_x	2.93	1.62	0.76	0.33	0.00
			m_y	3.42	1.77	0.83	0.36	0.00
		LP2	p	0.00	0.33	0.56	0.75	0.91
			m_x	2.93	1.62	0.76	0.33	0.00
			m_y	3.42	1.77	0.83	0.36	0.00
BC36	2.0	LP1	p	0.00	0.27	0.56	0.75	0.91
			m_x	2.93	1.62	0.76	0.33	0.00
			m_y	3.42	1.77	0.83	0.36	0.00
		LP2	p	0.00	0.33	0.56	0.75	0.91
			m_x	2.93	1.62	0.76	0.33	0.00
			m_y	3.42	1.77	0.83	0.36	0.00

Table 14. Maximum dimensionless external loads for biaxially loaded imperfect sway beam-columns with unequal partial end rotational restrains with stiffnesses K_3 and K_2 values at bottom and top, respectively

Case No.	$K_x = K_y$ (kip/in)	Load Path	Load	Dimensionless External Load				
BC37	0.0	LP5	m_x	2.27	1.71	1.30	0.91	0.00
			m_y	1.89	1.43	1.07	0.76	0.00
			p	0.00	0.16	0.19	0.25	0.42
		LP6	p	0.00	0.16	0.19	0.25	0.42
			m_x	2.27	1.40	1.18	0.89	0.04
			m_y	1.89	1.17	0.99	0.74	0.02
BC38	0.5	LP5	m_x	2.46	1.60	1.21	0.61	0.00
			m_y	2.05	1.33	1.01	0.51	0.00
			p	0.00	0.27	0.33	0.44	0.57
		LP6	p	0.00	0.27	0.33	0.44	0.57
			m_x	2.46	1.36	1.10	0.59	0.00
			m_y	2.05	1.14	0.92	0.49	0.00
BC39	1.0	LP5	m_x	2.38	1.90	1.21	0.50	0.00
			m_y	1.98	1.58	1.01	0.42	0.00
			p	0.00	0.17	0.34	0.57	0.71
		LP6	p	0.00	0.17	0.34	0.57	0.71
			m_x	2.38	1.98	1.22	0.49	0.02
			m_y	1.98	1.65	1.02	0.41	0.02
BC40	1.5	LP5	m_x	2.35	1.70	1.21	0.50	0.00
			m_y	1.96	1.42	1.01	0.42	0.00
			p	0.00	0.26	0.34	0.62	0.82
		LP6	p	0.00	0.26	0.34	0.62	0.82
			m_x	2.35	1.63	1.25	0.51	0.00
			m_y	1.96	1.36	1.04	0.42	0.00
BC41	2.0	LP5	m_x	2.33	1.90	1.30	0.50	0.00
			m_y	1.94	1.58	1.09	0.42	0.00
			p	0.00	0.22	0.35	0.63	0.88
		LP6	p	0.00	0.22	0.35	0.63	0.88
			m_x	2.33	1.58	1.16	0.50	0.01
			m_y	1.94	1.32	0.97	0.42	0.01

Table 15. Maximum dimensionless external loads for biaxially loaded sway beam-columns with equal partial end rotational restraints of stiffness K_2 value and with lateral restraints of various stiffnesses

Case No.	$K_x = K_y$ (kip/in)	Load Path	load	Maximum External Load			
BC42	0.0	LP1	p	0.00	0.20	0.33	0.34
			m_x	2.10	1.43	0.64	0.00
			m_y	1.66	1.12	0.51	0.00
		LP2	p	0.12	0.25	0.33	0.34
			m_x	2.10	1.43	0.64	0.00
			m_y	1.66	1.12	0.52	0.00
		LP3	p	0.00	0.20	0.33	0.34
			m_x	2.10	1.43	0.64	0.00
BC43	0.5	LP1	m_y	3.10	1.11	0.52	0.00
			p	0.10	0.13	0.33	0.34
			m_x	2.10	1.43	0.64	0.00
		m_y	1.66	1.12	0.51	0.00	
BC43	0.5	LP1	p	0.00	0.21	0.38	0.49
			m_x	2.78	1.38	0.90	0.00
			m_y	2.20	1.08	0.70	0.00
		LP2	p	0.00	0.26	0.39	0.49
			m_x	2.78	1.38	0.90	0.00
			m_y	2.74	1.08	0.70	0.00
		LP3	p	0.00	0.21	0.38	0.49
			m_x	2.78	1.38	0.90	0.00
BC43	0.5	LP3	m_y	2.83	1.12	0.74	0.00
			p	0.00	0.29	0.33	0.49
			m_x	2.78	1.38	0.90	0.00
		m_y	2.20	1.08	0.70	0.00	

Table 16. Maximum dimensionless external axial loads, with load path LP3, for biaxially loaded imperfect sway beam-columns with equal partial end rotational restraints and with lateral restraints of various stiffnesses; $M_x = M_y = 0.5M_y$

$K_{Bx} = K_{Tx}$ (kip-in/rad) →	13,333	24,000	1.0E+15
$K_x = K_y$ ↓ (kip/in)	Maximum External Axial Load		
0.0	0.33	0.53	0.86
0.2	0.39	0.55	0.87
0.4	0.44	0.65	0.88
0.6	0.49	0.71	0.90
0.8	0.54	0.75	0.91
1.0	0.55	0.79	0.92
1.2	0.55	0.82	0.93
1.4	0.53	0.86	0.94
1.6	0.53	0.87	0.94
1.8	0.53	0.87	0.94
2.0	0.53	0.87	0.94
2.2	0.53	0.87	0.94
2.4	0.53	0.87	0.94
2.6	0.53	0.87	0.94
2.8	0.53	0.87	0.94

Table 17. Maximum dimensionless external axial loads for sway beam-columns with biaxial imperfections, with equal partial end rotational restraints and with lateral restraints of various stiffnesses

$K_{Bx} = K_{Tx}$ (kip-in/rad) -	13,333	24,000	1.0E+15
$K_x = K_y$ † (kip/in)	Maximum External Axial Load		
0.0	0.34	0.53	0.86
0.2	0.40	0.59	0.87
0.4	0.46	0.65	0.88
0.6	0.52	0.72	0.90
0.8	0.59	0.77	0.91
1.0	0.65	0.80	0.95
1.2	0.72	0.82	0.95
1.4	0.77	0.85	0.95
1.6	0.81	0.88	0.95
1.8	0.85	0.91	0.95
2.0	0.89	0.91	0.95
2.2	0.89	0.91	0.95
2.4	0.89	0.91	0.95
2.6	0.89	0.91	0.95
2.8	0.89	0.91	0.95

Table 18. Effect of crookedness and residual stresses on the peak loads of biaxially loaded sway beam-columns with end rotational restraints

Case No.	Initial Imperfection	Residual stress, $\bar{\sigma}_{rc}$	Load	Dimensionless External Load	
				LP5	LP6
BC44	L/1000	-0.2	p	0.50	0.50
			m_x	0.45	0.44
			m_y	0.51	0.52
BC45	L/1000	0.0	p	0.50	0.50
			m_x	0.45	0.44
			m_y	0.51	0.53
BC46	L/100,000	-0.2	p	0.51	0.51
			m_x	0.45	0.44
			m_y	0.51	0.52
BC47	L/100,000	0.0	p	0.51	0.51
			m_x	0.45	0.44
			m_y	0.51	0.53

Table 19. Comparison of externally applied dimensionless maximum loads to published results for imperfect nonsway portal frame

Frame Type	Loaded Frame	Load	Maximum Dimensionless Load					
			LPF1		LPF2		LPF3	
			Pred.	Ref. 37	Pred.	Ref. 37	Pred.	Ref. 37
FR1	FL1	p	0.67	0.67	0.75	0.75	0.75	0.75
		m_v	0.67	0.67	0.24	0.25	0.25	0.25
FR1	FL2	p	0.72	0.72	0.76	0.76	0.	0.
		m_v	0.72	0.72	0.25	0.26	0.26	0.26
FR2	FL1	p	0.64	0.64	0.71	0.71	0.71	0.71
		m_v	0.64	0.64	0.20	0.21	0.21	0.21
FR2	FL2	p	0.71	0.71	0.80	0.82	0.84	0.84
		m_v	0.71	0.71	0.29	0.32	0.32	0.32
FR3	FL1	p	0.67	0.67	0.75	0.75	0.75	0.75
		m_v	0.67	0.67	0.25	0.25	0.21	0.21
FR3	FL2	p	0.72	0.72	0.76	0.76	0.76	0.76
		m_v	0.72	0.72	0.25	0.26	0.26	0.26
FR4	FL1	p	0.64	0.64	0.71	0.71	0.71	0.71
		m_v	0.64	0.64	0.20	0.21	0.21	0.21
FR4	FL2	p	0.72	0.72	0.82	0.82	0.83	0.84
		m_v	0.72	0.72	0.31	0.32	0.32	0.32

Table 20. Maximum dimensionless external loads for sway portal frames with rigid beam-to-column connections, and with partial rotational restraints at the bases of stiffness K_2

Frame No.	Frame Type	Frame Load	Load	Maximum Dimensionless External Load		
				LPF1	LPF2	LPF3
PF1	FR1	FL3	p m_x	0.71	0.71	0.71
				0.71	0.10	0.10
PF2	FR2	FL4	p m_x	0.68	0.71	0.71
				0.68	0.10	0.10
PF3	FR3	FL3	p m_x	0.71	0.67	0.70
				0.71	0.08	0.08
PF4	FR5	FL4	p m_x	0.68	0.71	0.71
				0.68	0.10	0.10
PF5	FR5	FL3	p m_x	0.65	0.71	0.71
				0.65	0.10	0.10
PF6	FR5	FL4	p m_x	0.68	0.73	0.70
				0.68	0.11	0.11
PF7	FR5	FL3	p m_x	0.67	0.70	0.70
				0.67	0.10	0.10
PF8	FR5	FL4	p m_x	0.68	0.70	0.70
				0.68	0.10	0.10

Table 21. Maximum dimensionless external loads for imperfect sway portal frame FR5

Frame No.	Frame Load	Load	Maximum Dimensionless External Load		
			LPF1	LPF2	LPF3
PF9	FL1	p	1.40	1.38	1.44
		m_x	0.67	0.42	0.42
PF10	FL2	p	1.44	1.45	1.45
		m_x	0.69	0.45	0.45
PF11	FL3	p	0.58	0.60	0.60
		m_x	0.28	0.05	0.05
PF12	FL4	p	0.58	0.68	0.70
		m_x	0.28	0.08	0.08

Table 22. Effect of crookedness and residual stresses on the strength of sway portal frames with rigid beam-to-column connections, and with partial rotational restraints at bases of stiffness K_3

Frame No.	Initial Crookedness	Residual Stress, $\bar{\sigma}_r$	Load	Maximum Dimensionless External Load		
				LPF1	LPF2	LPF3
PF13	L/1000	-0.2	p	0.67	0.72	0.68
			m_x	0.48	0.10	0.10
PF14	L/1000	0.0	p	0.67	0.73	0.73
			m_x	0.48	0.11	0.11
PF15	L/100,000	-0.2	p	0.67	0.76	0.68
			m_x	0.48	0.12	0.12
PF16	L/100,000	0.0	p	0.68	0.78	0.77
			m_x	0.49	0.13	0.13

Table 23. Comparison of dimensionless maximum loads for sway portal frames with different residual stress distributions

Frame No.	Load Paths	Load	Dimensionless External Load with	
			RSD from Figures 4 & 5	RSD from Figure 3
PF17	LPF1	p	0.79	0.81
		m_x	2.15	2.20
PF18	LPF2	p	0.77	0.78
		m_x	0.46	0.47
PF19	LPF3	p	0.81	0.72
		m_x	0.46	0.47

Table 24. Maximum dimensionless applied loads for single-story single-bay sway space frames with rigid joints

Frame Type	Frame No.	Load Path	Load	Maximum Load
SFR1	SF1	SL1	p m	0.70 1.23
	SF2	SL2	p m	1.24 1.23
	SF3	SL3	p m	0.79 0.04
	SF4	SL4	p m	0.78 1.61
	SFP1	SL5	p m	3.76 0.00
SFR2	SF5	SL1	p m	0.70 1.20
	SF6	SL2	p m	1.11 1.20
	SF7	SL3	p m	0.79 0.04
	SF8	SL4	p m	1.25 1.79
	SFP2	SL5	p m	3.76 0.00
SFR3	SF9	SL1	p m	0.70 1.12
	SF10	SL2	p m	0.75 1.12
	SF11	SL3	p m	0.79 0.04
	SF12	SL4	p m	0.81 1.50
	SFP3	SL5	p m	3.76 0.00

Table 25. Maximum dimensionless applied loads for single-story single-bay sway space frames with flexible joints

Frame Type	Frame No.	Load Path	Load	Maximum Load
SFR1	SF13	SL1	p m	0.79 0.21
	SF14	SL2	p m	0.30 0.21
	SF15	SL3	p m	0.83 0.02
	SF16	SL4	p m	0.32 0.36
SFR2	SF17	SL1	p m	0.79 0.21
	SF18	SL2	p m	0.30 0.21
	SF19	SL3	p m	0.83 0.02
	SF20	SL4	p m	0.32 0.36
SFR3	SF21	SL1	p m	0.79 0.04
	SF22	SL2	p m	0.35 0.04
	SF23	SL3	p m	0.83 0.02
	SF24	SL4	p m	0.34 0.21

Table 26. Effect of crookedness and residual stresses on dimensionless maximum loads of single-story single-bay sway space frames with flexible joints

Load Path	Frame No.	Initial Crookedness	Residual Stress, $\bar{\sigma}_{rc}$	Load	Maximum Load
SL1	SF25	L/1000	-0.2	p m	0.40 0.65
	SF26	L/1000	0.0	p m	0.40 0.67
	SF27	L/100,000	-0.2	p m	0.40 0.66
	SF28	L/100,000	0.0	p m	0.40 0.70
SL2	SF29	L/1000	-0.2	p m	0.36 0.65
	SF30	L/1000	0.0	p m	0.47 0.67
	SF31	L/100,000	-0.2	p m	0.40 0.66
	SF32	L/100,000	0.0	p m	0.39 0.70
SL3	SF33	L/1000	-0.2	p m	0.31 0.04
	SF34	L/1000	0.0	p m	0.50 0.05
	SF35	L/100,000	-0.2	p m	0.50 0.05
	SF36	L/100,000	0.0	p m	0.50 0.05
SL4	SF37	L/1000	-0.2	p m	0.38 0.83
	SF38	L/1000	0.0	p m	0.37 0.84
	SF39	L/100,000	-0.2	p m	0.38 0.84
	SF40	L/100,000	0.0	p m	0.37 0.97

Table 27. Comparison of dimensionless maximum loads for sway single-story single-bay space frames with different residual stress distributions

Frame No.	Load Paths	Load	Dimensionless External Load with	
			RSD from Figures 4 & 5	RSD from Figure 3
SF41	SL1	p	0.56	0.56
		m	1.78	1.73
SF42	SL2	p	0.49	0.52
		m	1.78	1.73
SF43	SL3	p	0.64	0.64
		m	0.15	0.15
SF44	SL4	p	0.45	0.48
		m	2.59	2.60

Table 28. Experimental method of sectioning results for residual stress determination for 2x3x0.1875 in. section, with an initial length of 8.187 in.

Element No.	Final Length (in.)	Change in Length (in.)	Residual Strain (10^{-6}) in/in.	Residual Stress (ksi)	Average Residual Stress (ksi)
1	8.179	+0.004	-489.30	-14.19	-13.30
2	8.177	+0.002	-244.65	-7.10	-5.33
3	8.174	-0.001	+122.32	+3.55	+4.44
4	8.172	-0.003	+366.97	+10.64	+8.87
5	8.174	-0.001	+122.32	+3.55	+4.44
6	8.176	+0.001	-122.32	-3.55	-5.33
7	8.179	+0.004	-489.30	-14.19	-13.30
8	8.176	+0.001	-122.32	-3.55	-1.78
9	8.173	-0.002	+244.65	+7.10	+7.10
10	8.174	-0.001	+122.32	+3.55	-1.78
11	8.178	+0.003	-366.97	-10.64	-13.30
12	8.176	+0.001	-122.32	-3.55	-5.33
13	8.173	-0.002	+244.32	+7.10	+4.44
14	8.173	-0.002	+244.65	+7.10	+8.87
15	8.174	-0.001	+122.32	+3.55	+4.44
16	8.178	+0.002	-244.65	-7.10	-5.33
17	8.179	+0.004	-489.30	-4.19	-13.30
18	8.176	+0.001	-122.32	-3.55	-1.78
19	8.173	-0.002	+244.65	+7.10	+7.10
20	8.175	+0.000	0.00	0.00	-1.78

Table 29. Experimental method of sectioning results for residual stress determination for 2x2x0.1875 in. section, with an initial length of 7.986 in.

Element No.	Final Length (in.)	Change in Length (in.)	Residual Strain (10^{-6})in/in.	Residual Stress (ksi)	Average Residual Stress (ksi)
1	7.989	+0.003	-357.66	-10.89	-12.71
2	7.984	-0.002	+250.44	+7.26	+4.10
3	7.982	-0.004	+500.88	+14.52	+15.67
4	7.985	-0.001	+125.22	+3.63	+4.10
5	7.989	+0.003	-375.66	-10.89	-12.71
6	7.986	0.000	0.00	0.00	+4.10
7	7.981	-0.005	+625.10	+18.13	+15.67
8	7.985	-0.001	+125.22	+3.63	+4.10
9	7.990	+0.004	-500.88	-14.52	-12.71
10	7.985	-0.001	+125.22	+3.63	+4.10
11	7.982	-0.004	+500.88	+14.52	+15.67
12	7.985	-0.001	+125.22	+3.63	+4.10
13	7.990	+0.004	-500.88	-14.52	-12.71
14	7.985	-0.001	+125.22	+3.63	+4.10
15	7.982	-0.004	+500.88	+14.52	+15.67
16	7.984	-0.002	+250.44	+7.26	+4.10

Table 30. Initial crookedness in test frame columns measured before test at five equidistant points along each column with base of frame as reference point

Columns	Directions	Crookedness of the Columns at Location (in.)				
		1	2	3	4	5
1	x	0.000	-0.132	-0.328	-0.589	-0.785
	y	0.000	-0.101	-0.189	-0.311	-0.471
2	x	0.000	-0.203	-0.347	-0.534	-0.732
	y	0.000	-0.023	-0.032	-0.097	-0.172
3	x	0.000	-0.037	-0.140	-0.259	-0.386
	y	0.000	-0.035	-0.008	-0.043	-0.121
4	x	0.000	-0.161	-0.314	-0.440	-0.553
	y	0.000	0.053	0.104	0.155	0.208
9	x	-0.785	-0.984	-1.164	-1.326	-1.455
	y	-0.471	-0.521	-0.572	-0.571	-0.595
10	x	-0.732	-0.993	-1.176	-1.377	-1.514
	y	-0.172	-0.256	-0.316	-0.381	-0.450
11	x	-0.386	-0.500	-0.647	-0.903	-1.055
	y	-0.121	-0.121	-0.228	-0.289	-0.393
12	x	-0.553	-0.682	-0.822	-1.066	-1.296
	y	-0.208	-0.354	-0.407	-0.465	-0.535
17	x	-1.455	-1.579	-1.812	-1.961	-2.184
	y	-0.595	-0.632	-0.720	-0.768	-0.836
18	x	-1.514	-1.610	-1.704	-1.798	-1.830
	y	-0.450	-0.534	-0.594	-0.659	-0.728
19	x	-1.055	-1.216	-1.382	-1.522	-1.637
	y	-0.393	-0.393	-0.500	-0.562	-0.665
20	x	-1.296	-1.418	-1.624	-1.839	-2.069
	y	-0.535	-0.681	-0.734	-0.792	-0.862

Table 31. Test frame deflections at joints 29 and 32 in x direction

Applied Loads (kips)			Displacement in x Direction (in.)			Angle of Twist (rad.)
H	P ₁	P ₂	Joint 29	Joint 32	Average	
0	0	0	0	0	0	0
0.226	0	0	0.347	0.347	0.347	0
0.446	0	0	0.704	0.704	0.704	0
0.999	0	0	1.757	1.963	1.725	-0.0011
0.991	.205	0	1.759	1.689	1.724	-0.001
1.006	5.011	0	1.712	1.685	1.698	-.0004
1.025	9.951	0	1.659	1.666	1.663	.00012
1.047	15.963	0	1.585	1.630	1.607	.00076
1.050	16.813	0	1.580	1.629	1.604	.00082
1.047	16.726	0.293	1.571	1.631	1.601	.001
1.002	16.626	7.189	1.498	1.634	1.566	.0023
0.961	16.460	16.979	1.395	1.808	1.601	.0069
0.921	16.514	19.473	1.335	1.843	1.589	.0085
.991	16.755	19.519	1.365	1.925	1.645	.0093
0.986	17.844	19.503	1.313	1.901	1.607	.0098
0.985	18.735	19.257	1.255	1.881	1.568	0.0104
.998	20.674	19.411	1.148	1.870	1.509	0.012
0.977	20.658	20.350	1.127	1.870	1.498	0.0124
1.044	20.210	22.551	1.295	2.233	1.764	0.0156
1.044	20.749	23.414	1.278	2.245	1.761	0.0161
1.025	20.641	24.137	1.281	2.308	1.794	0.0171
1.018	20.637	24.352	1.283	2.328	1.805	0.0174
1.010	20.633	24.768	1.282	2.377	1.830	0.0183

Table 32. Test frame deflections at joints 29 and 32 in y direction

Applied Loads (kips)			Displacement in y Direction (in.)		
H	P ₁	P ₂	Joint 31	Joint 32	Average
0	0	0	0	0	0
0.226	0	0	0.0045	-0.0094	-0.0025
0.446	0	0	0.0076	-0.0287	-0.0106
0.999	0	0	-0.0045	-0.097	-0.0508
0.991	.205	0	-0.0047	-0.0962	-0.0505
1.006	5.011	0	0.003	-0.1164	-0.0567
1.025	9.951	0	0.0003	-0.1495	-0.0746
1.047	15.963	0	-0.0206	-0.1992	-0.1099
1.050	16.813	0	-0.0206	-0.2027	-0.1117
1.047	16.726	0.293	-0.0197	-0.2037	-0.1117
1.002	16.626	7.189	-0.0527	-0.3001	-0.1764
0.961	16.460	16.979	-0.0763	-0.3604	-0.2184
0.921	16.514	19.473	-0.0774	-0.3354	-0.2064
.991	16.755	19.519	-0.1347	-0.4125	-0.2736
0.986	17.844	19.503	-0.1735	-0.4388	-0.3062
0.985	18.735	19.257	-0.2040	-0.4537	-0.3289
.998	20.674	19.411	-0.2634	-0.4555	-0.3595
0.977	20.658	20.350	-0.2707	-0.4557	-0.3632
1.044	20.210	22.551	-0.2666	-0.3413	-0.3040
1.044	20.749	23.414	-0.2518	-0.3102	-0.2810
1.025	20.641	24.137	-0.2287	-0.2158	-0.2223
1.018	20.637	24.352	-0.2278	-0.1926	-0.2102
1.010	20.633	24.768	-0.2214	-0.1377	-0.1796

Table 33. Experimental deflection and angle of twist of Column 20

Applied load P_1 , (kips)	Displacement for Dial gage 1, (in.)	Displacement for Dial gage 2, (in.)	Displacement at Midspan of Column 20, (in.)	Angle of Twist, (rad.)
0.000	0.0000	0.0000	0.00000	0.0000
0.210	0.0090	0.0110	-0.00650	0.0005
0.800	0.0065	0.0110	-0.01662	0.0011
1.170	0.0050	0.0100	0.00125	0.0013
2.200	-0.0010	0.004	0.00725	0.0013
3.55	-0.0090	-0.005	0.01400	0.0010
5.0	-0.018	-0.0130	0.02425	0.0013
7.5	-0.033	-0.0300	0.03675	0.0008
19.5	-0.0480	-0.0450	0.05175	0.0008
16.5	-0.1170	-0.1150	0.11950	0.0005

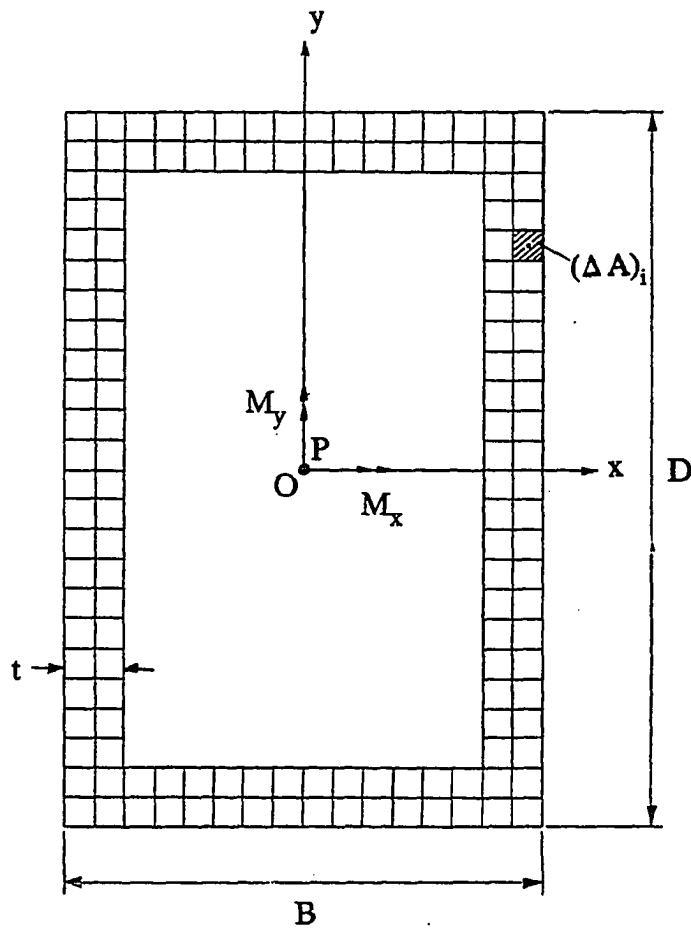


Figure 1. Discretized hollow rectangular section subjected to axial load and biaxial bending moments

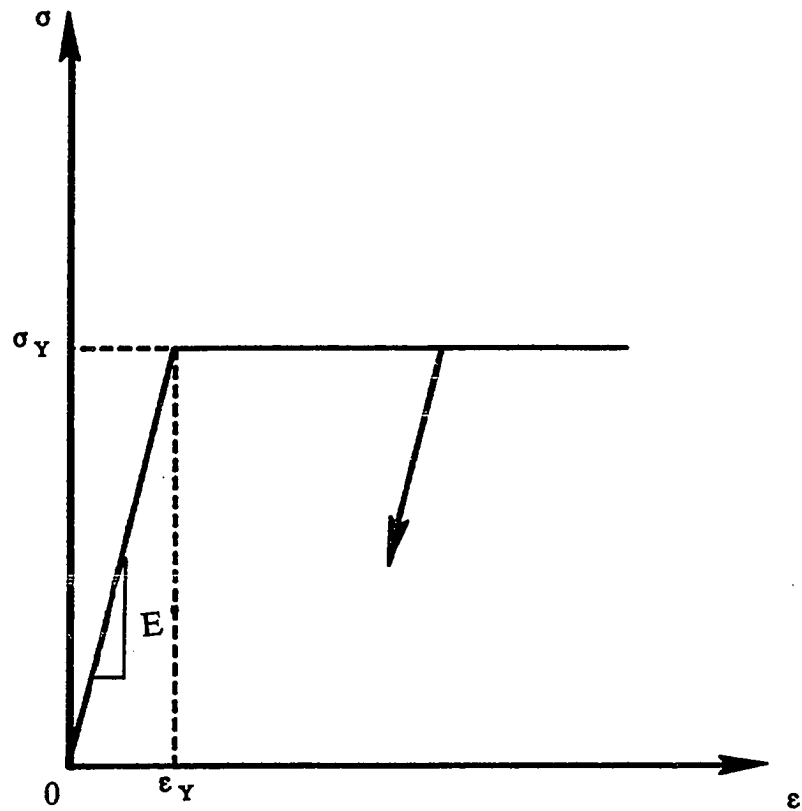


Figure 2. Stress-strain relationship with elastic unloading

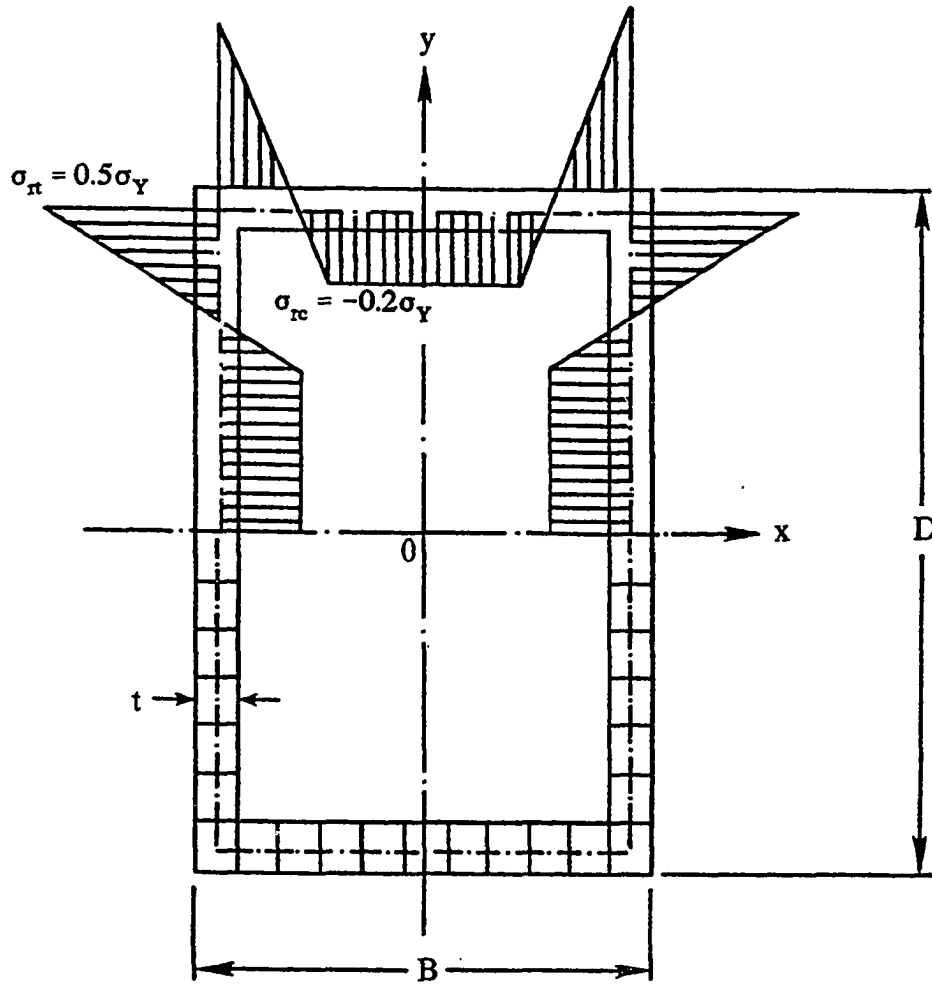


Figure 3. Cross section and residual stress distribution (Ref. 21)

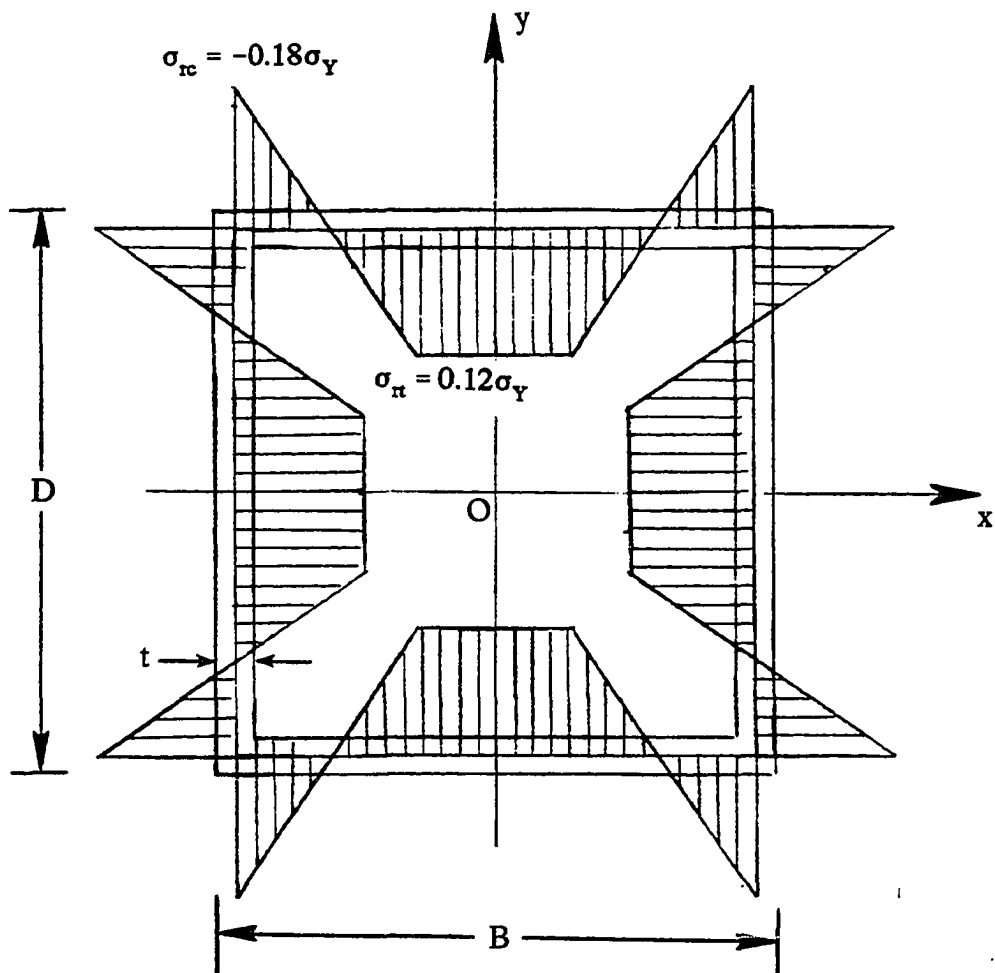


Figure 4. Square section ($B = D$) with idealized residual stress distribution

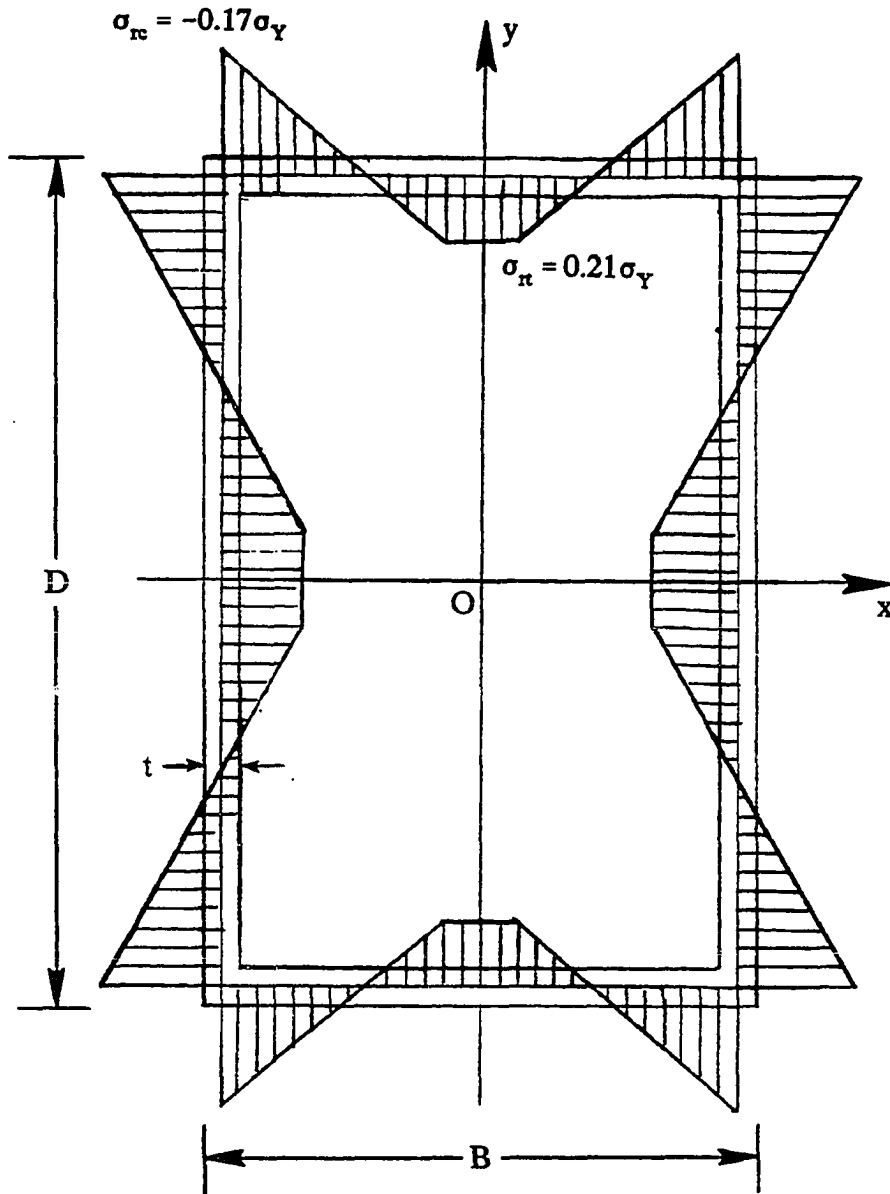


Figure 5. Rectangular section with idealized residual stress distribution

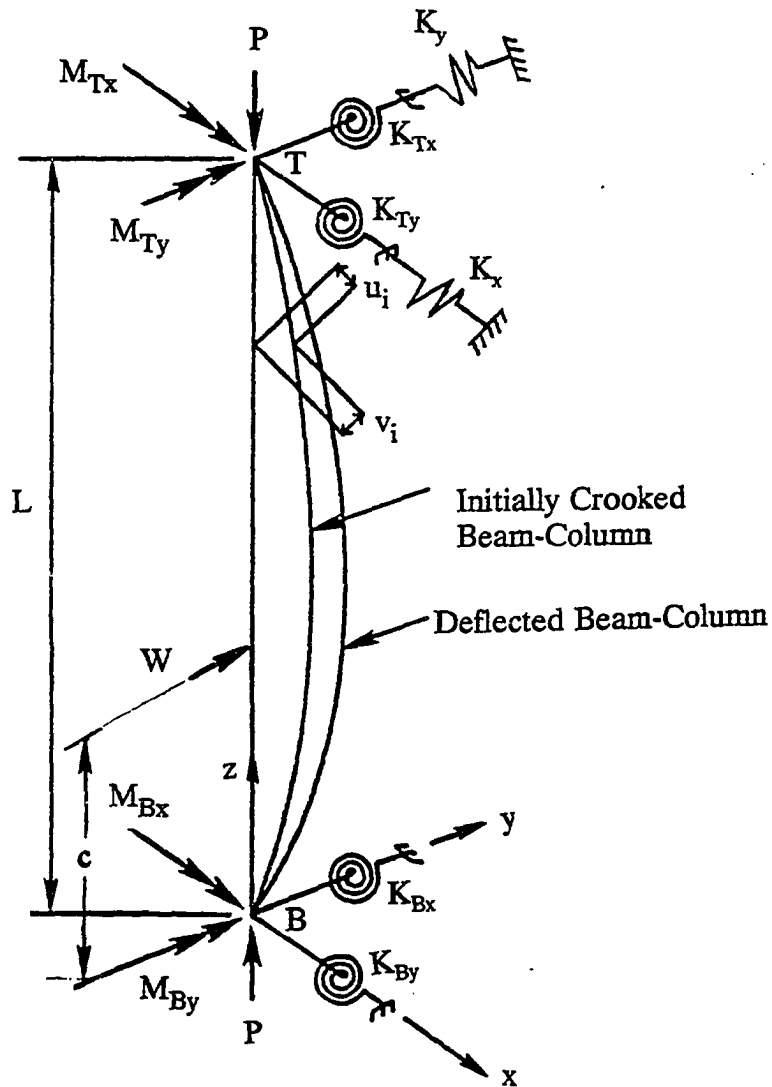


Figure 6. Imperfect sway beam-column with biaxial restraints

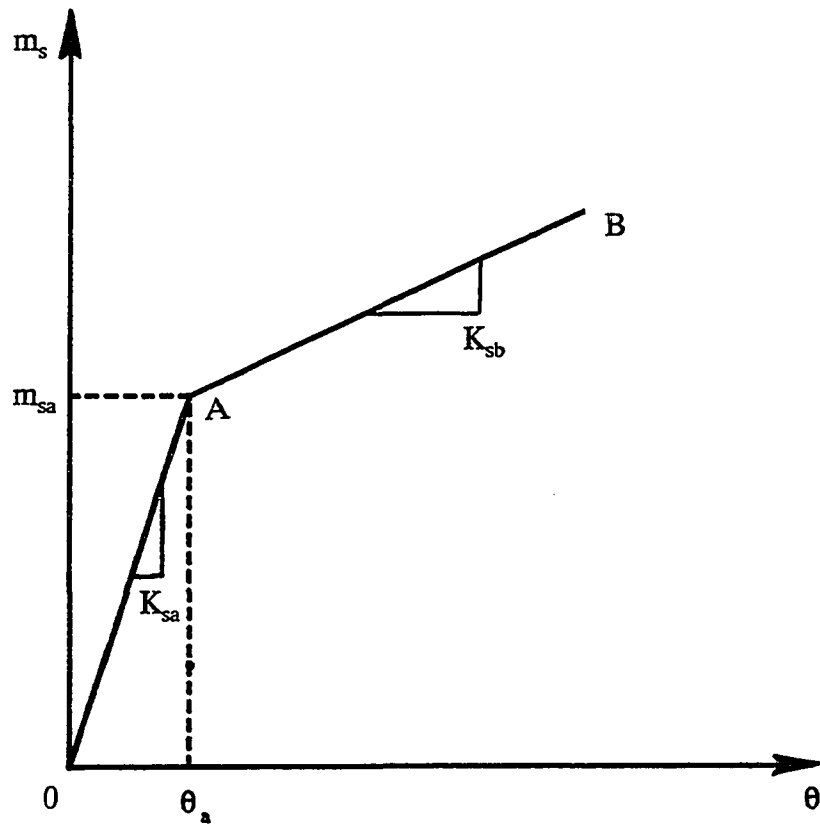


Figure 7. Moment-rotation relationship

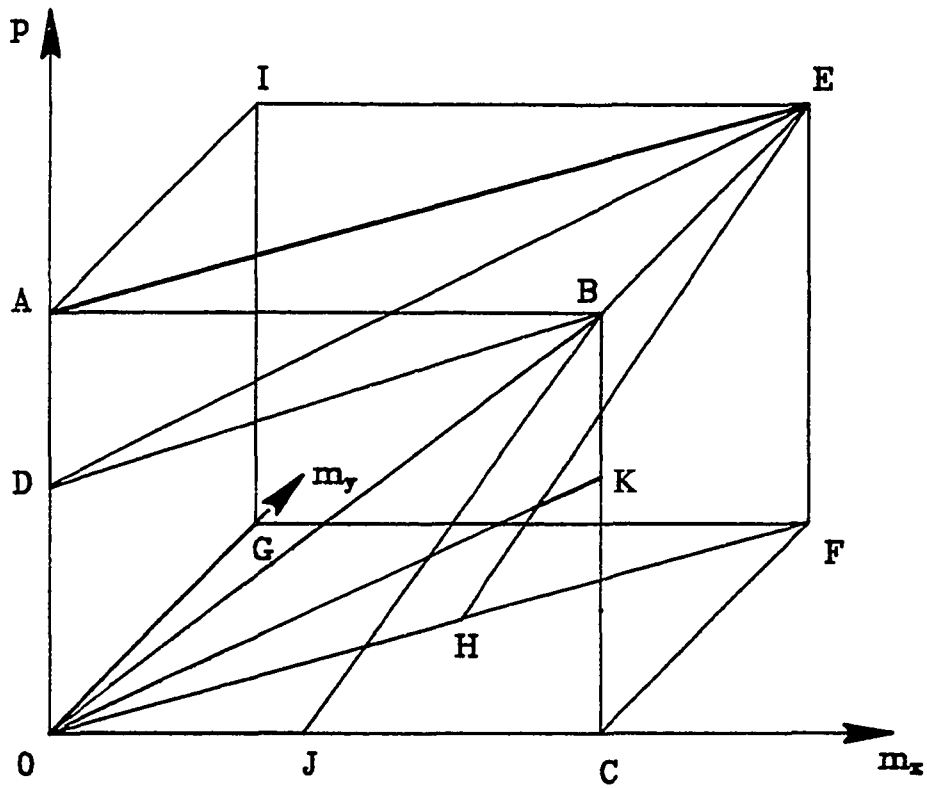


Figure 8. Loading paths for nonproportional loading

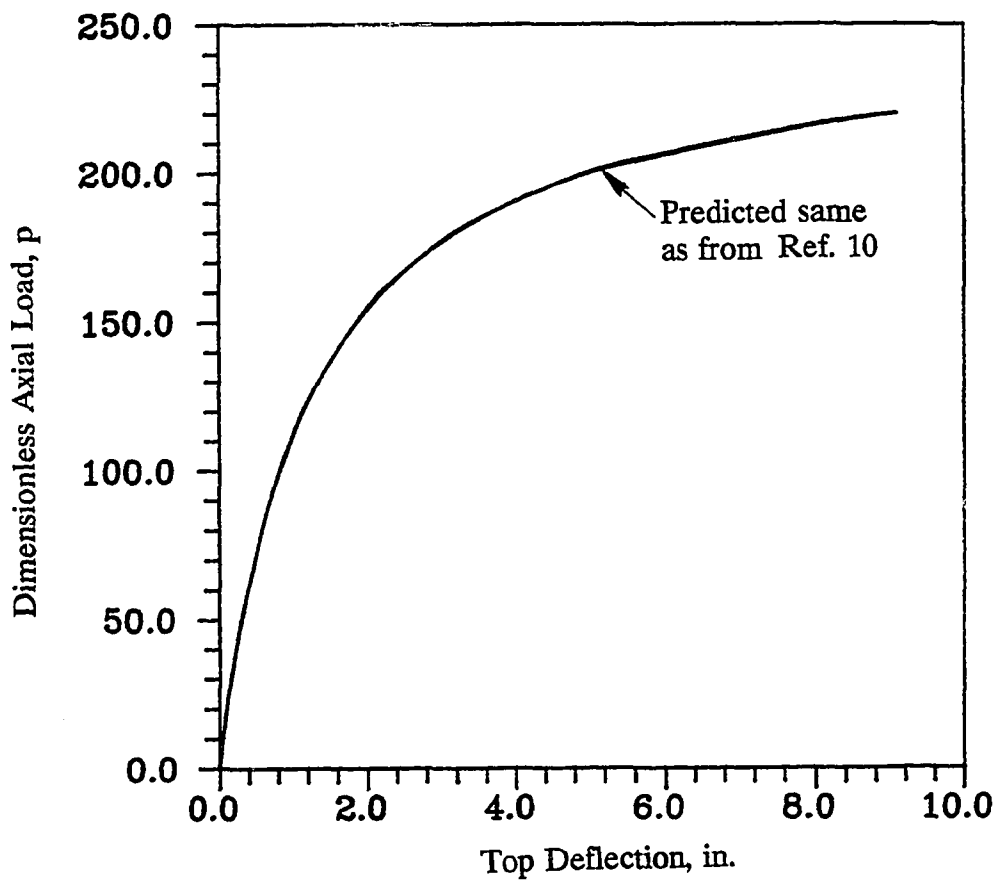


Figure 9. Axial load versus top deflection of elastically loaded sway beam-column of Ref. 9

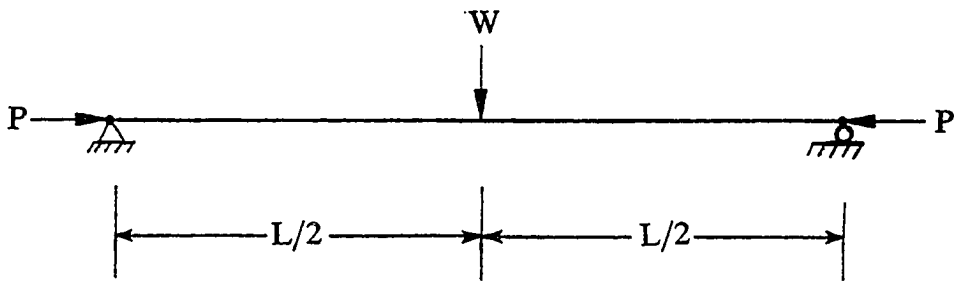


Figure 10. Laterally loaded pinned column

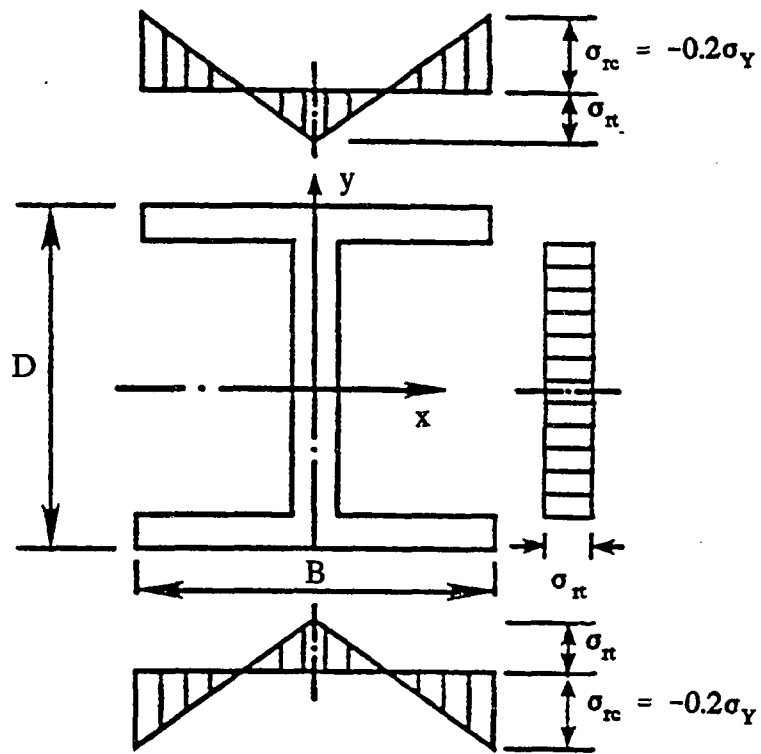


Figure 11. Residual stress strain pattern for an I-section

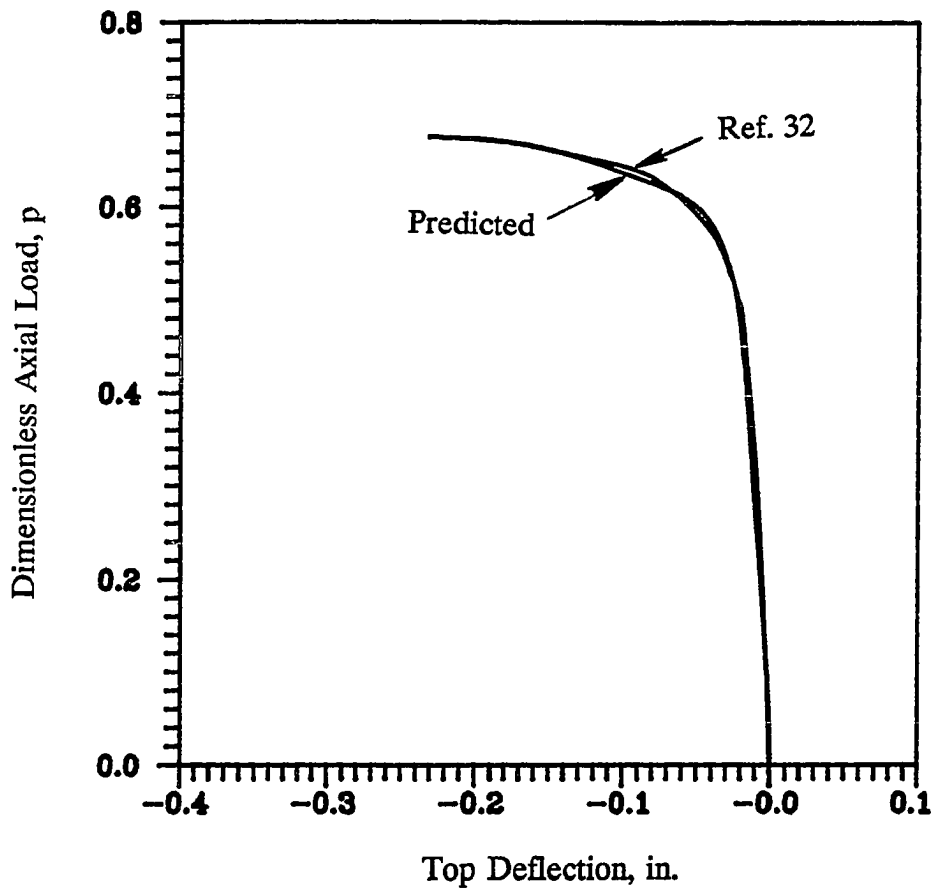


Figure 12. Dimensionless axial load versus top deflection of imperfect column with $K_{By} = K_b$, and $K_{Ty} = K_d$

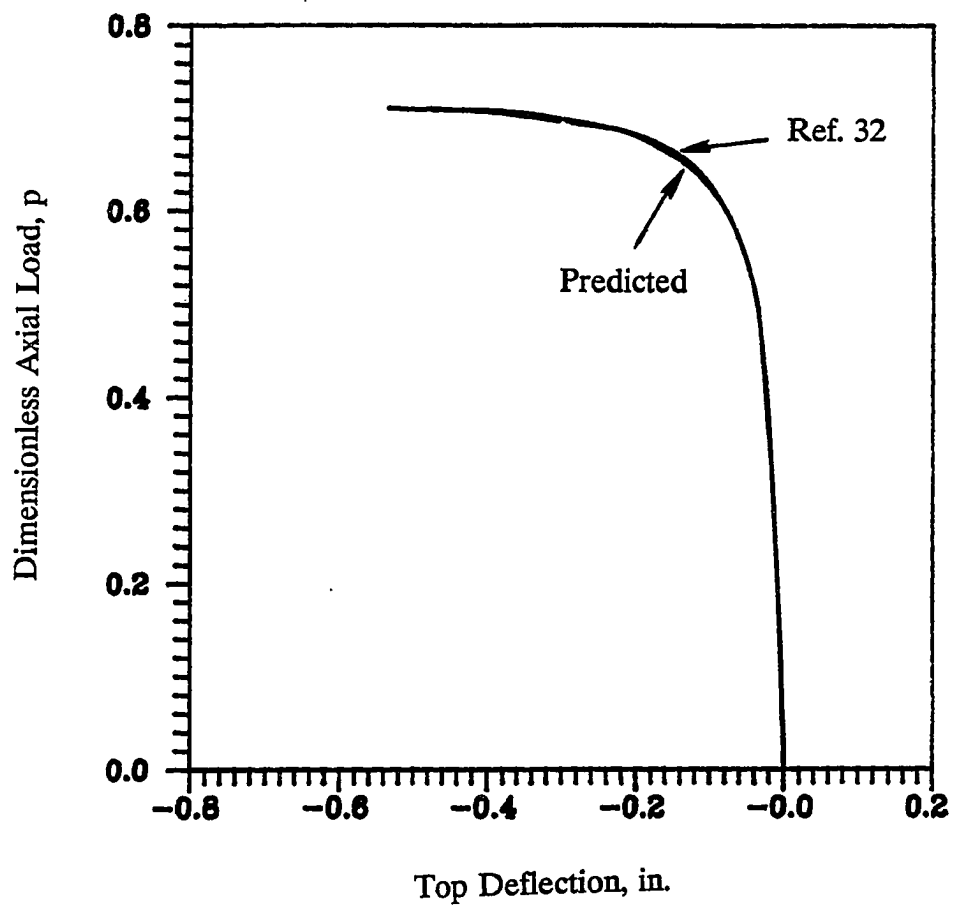


Figure 13. Dimensionless axial load versus top deflection of imperfect column with $K_{By} = K_c$ and $K_{Ty} = K_d$

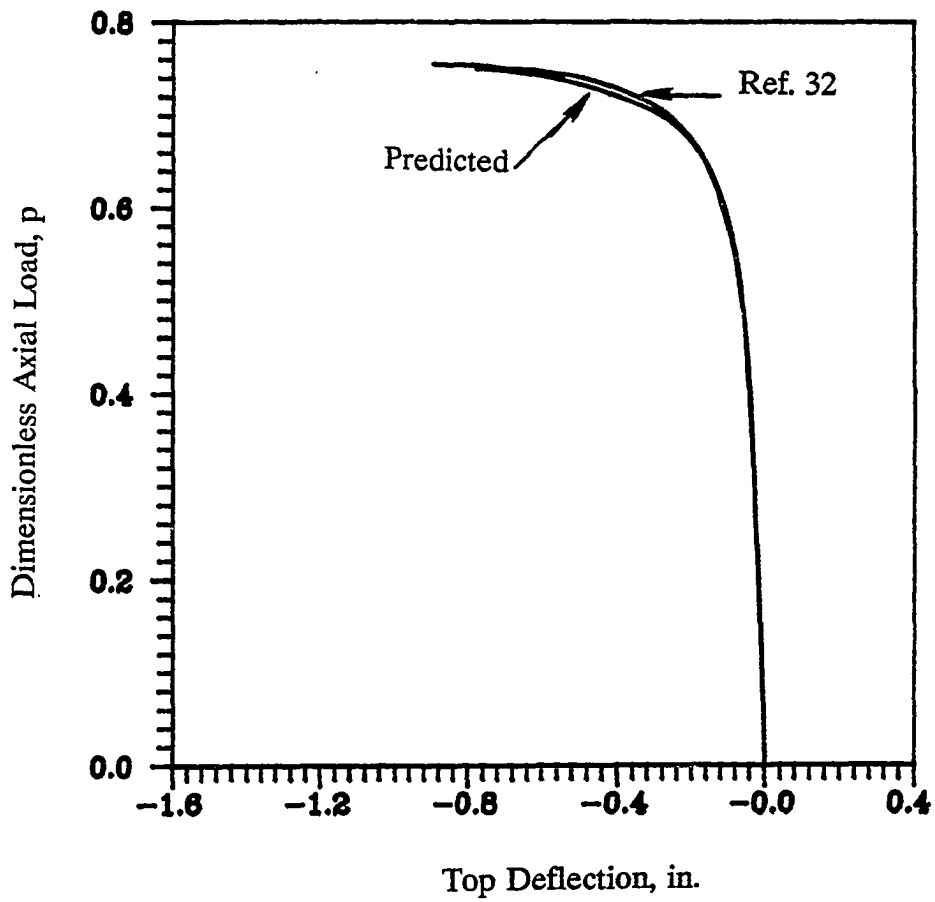


Figure 14. Dimensionless axial load versus top deflection of imperfect column with $K_{By} = K_d$ and $K_{Ty} = K_d$

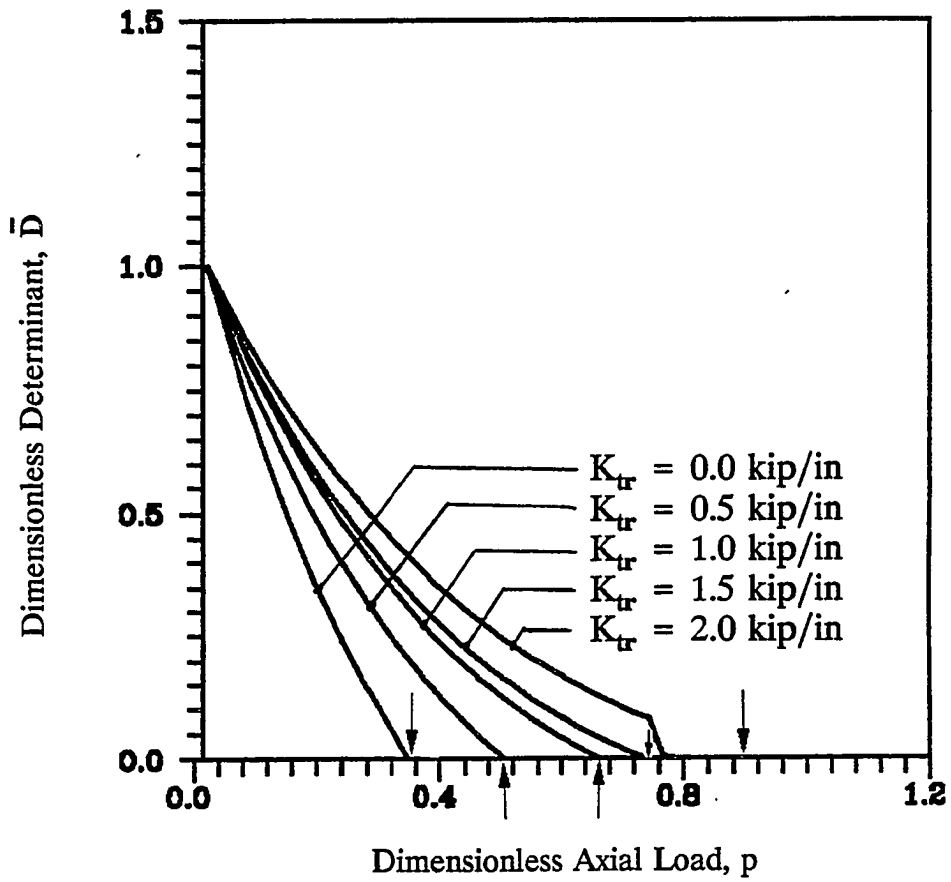


Figure 15. Stiffness degradation curves for uniaxially loaded sway beam-columns BC1, BC3, BC4, BC5, and BC6, with $K_{Bx} = K_{Tx} = K_2$

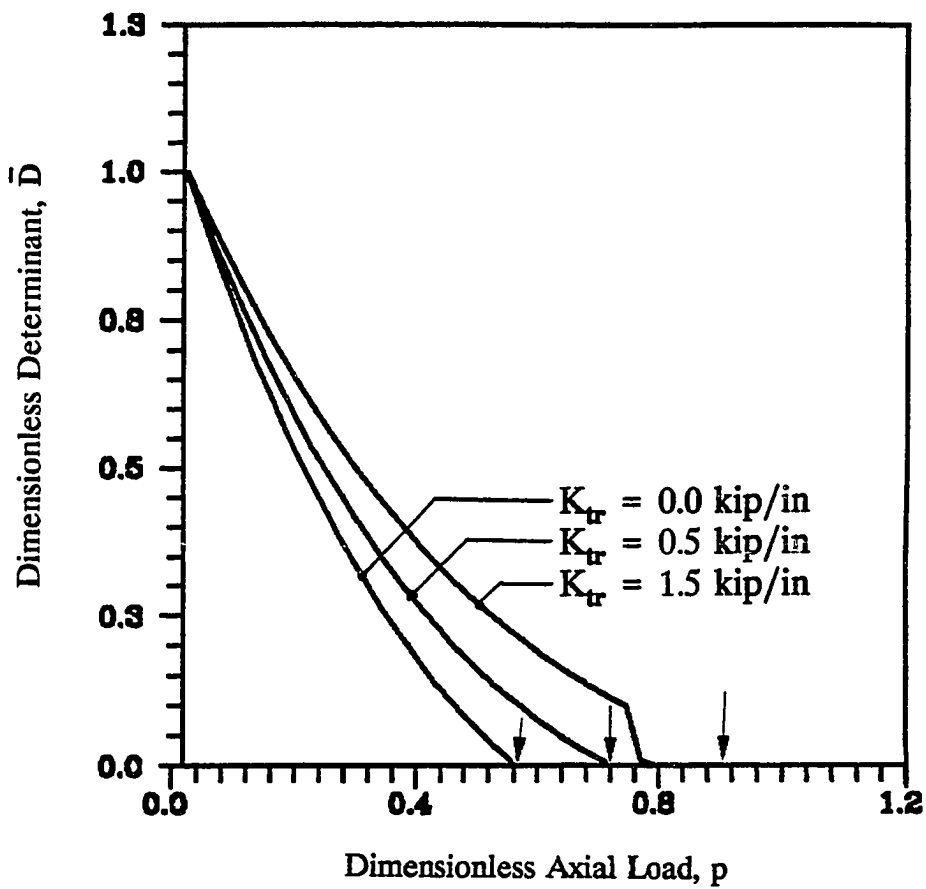


Figure 16. Stiffness degradation curves for uniaxially loaded sway beam-columns BC7, BC8, and BC10, with $K_{Bx} = K_{Tx} = K_3$

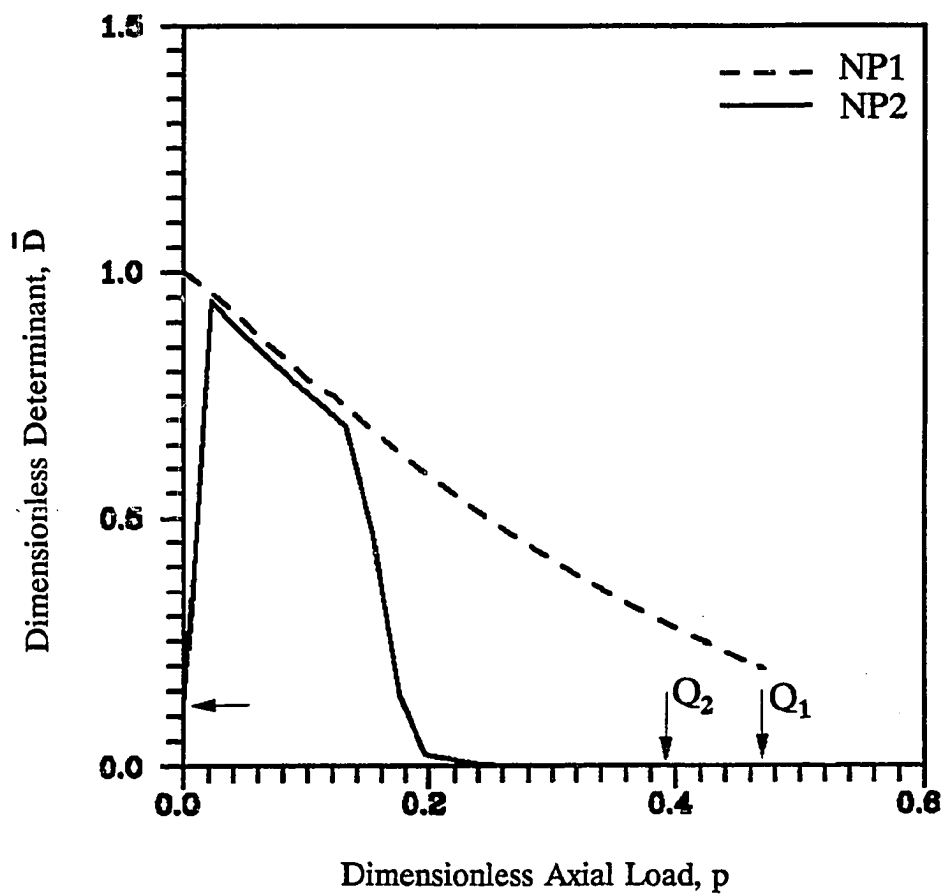


Figure 17. Stiffness degradation curves (\bar{D} - p) for uniaxially loaded sway beam-column BC5, for load paths NP1 and NP2, with $K_{Bx} = K_{Tx} = K_2$

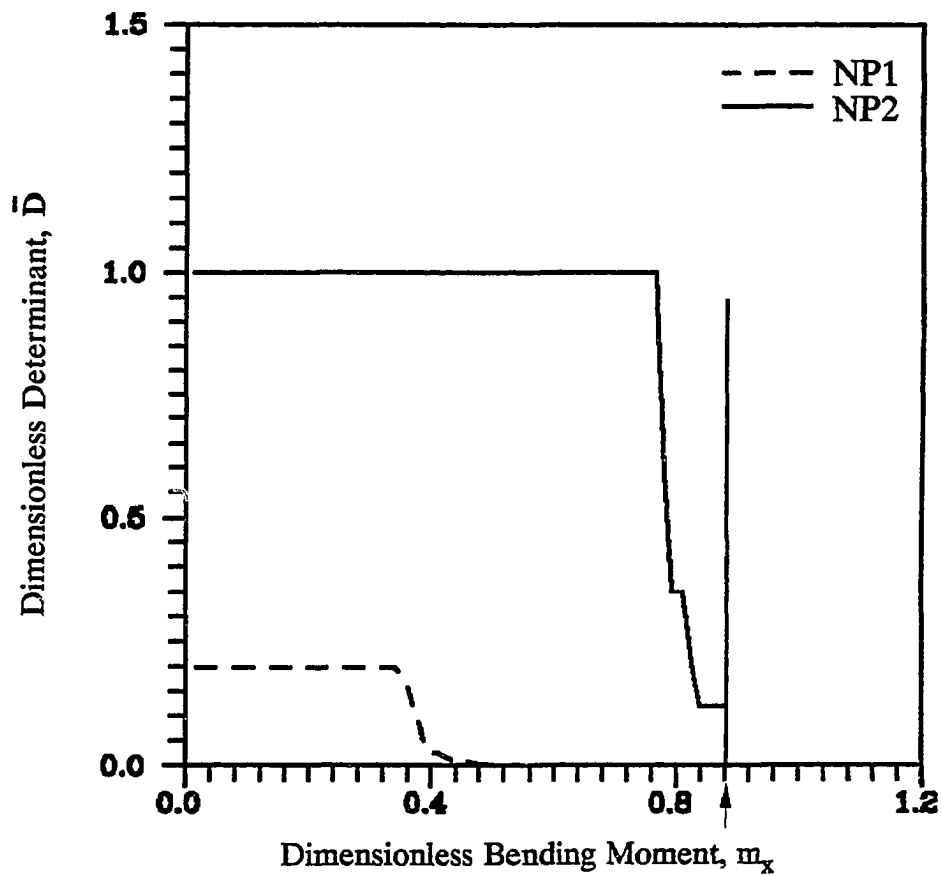


Figure 18. Stiffness degradation curves (\bar{D} - m_x) for uniaxially loaded sway beam-column BC5, for load paths NP1 and NP2, with $K_{Bx} = K_{Tx} = K_2$

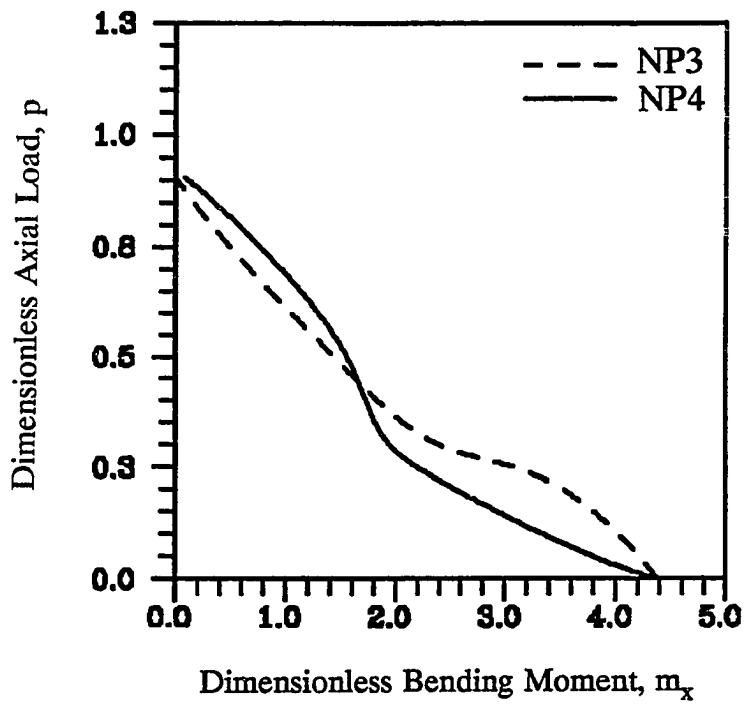


Figure 19. Interaction curve for uniaxially loaded sway beam-column BC10 for load paths NP3 and NP4, with $K_{Bx} = K_{Tx} = K_3$

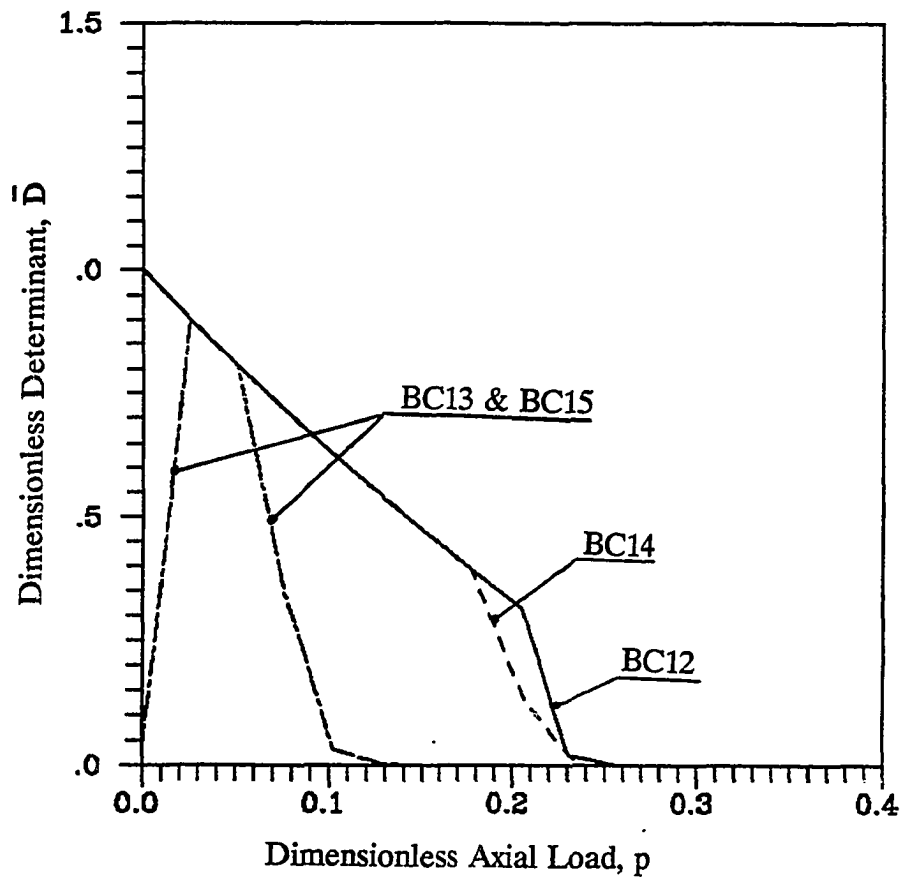


Figure 20. Stiffness degradation curves (\bar{D} - p) for uniaxially loaded sway beam-columns BC12, BC13, BC14, and BC15

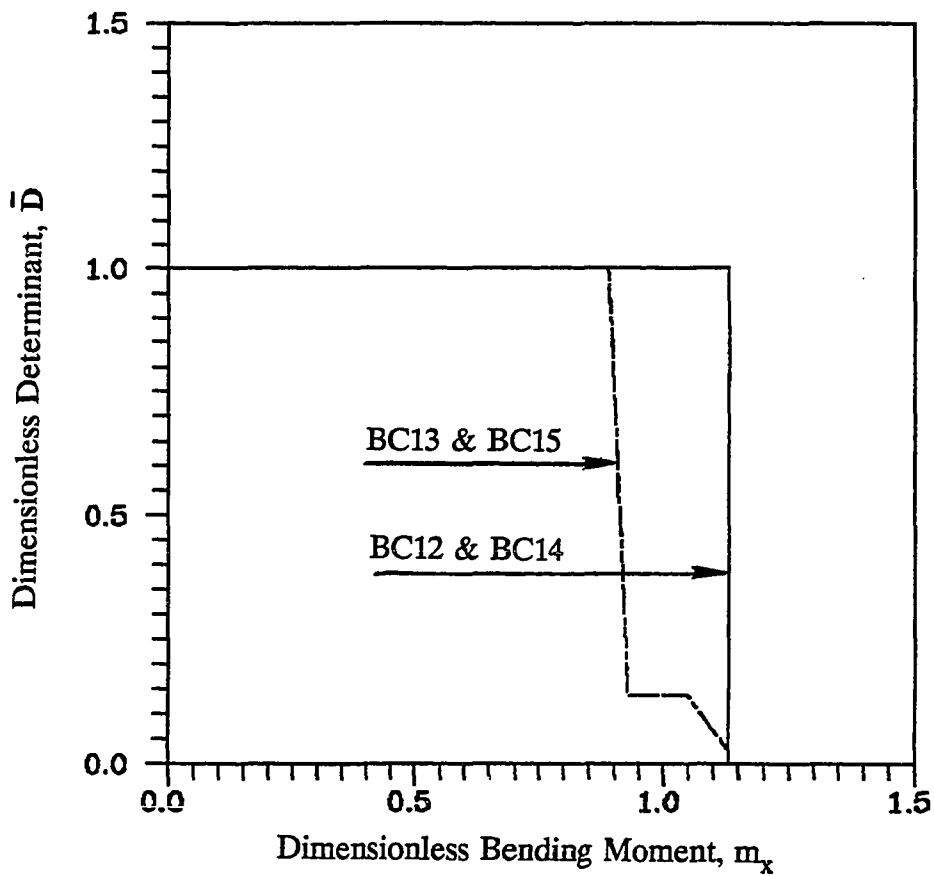


Figure 21. Stiffness degradation curves (\bar{D} - m_x) for uniaxially loaded sway beam-columns BC12, BC13, BC14, and BC15

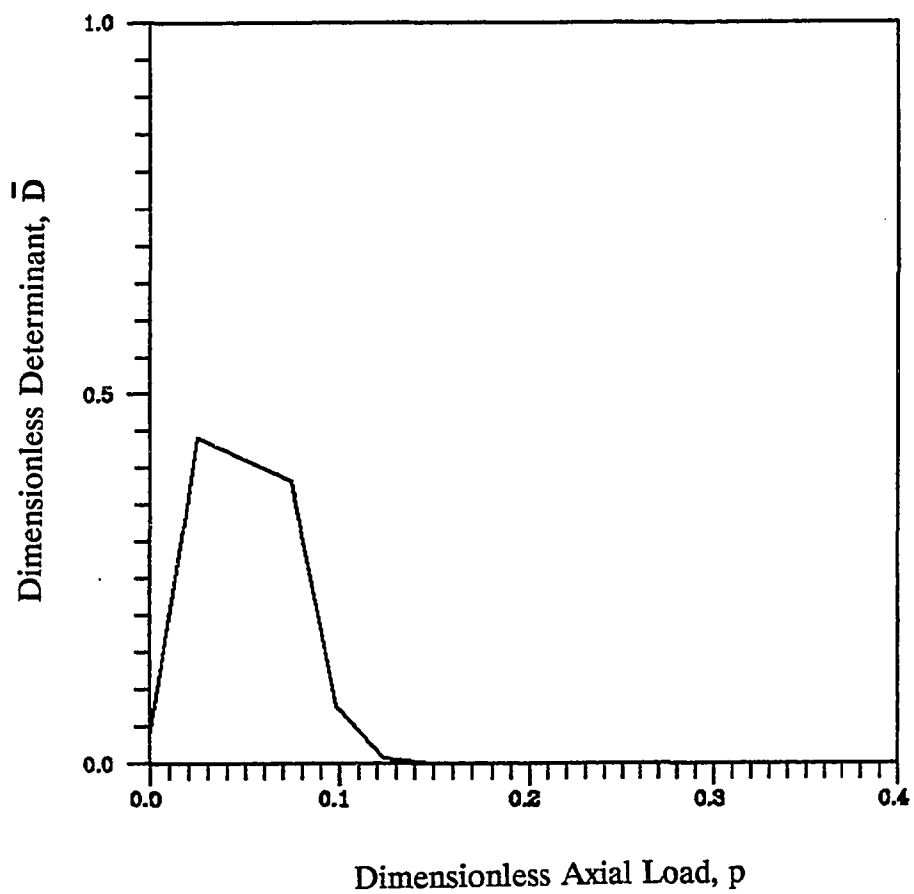


Figure 22. Stiffness degradation curve ($\bar{D} - p$) for uniaxially loaded sway beam-column BC30, with bilinear rotational restraints and load path NP3

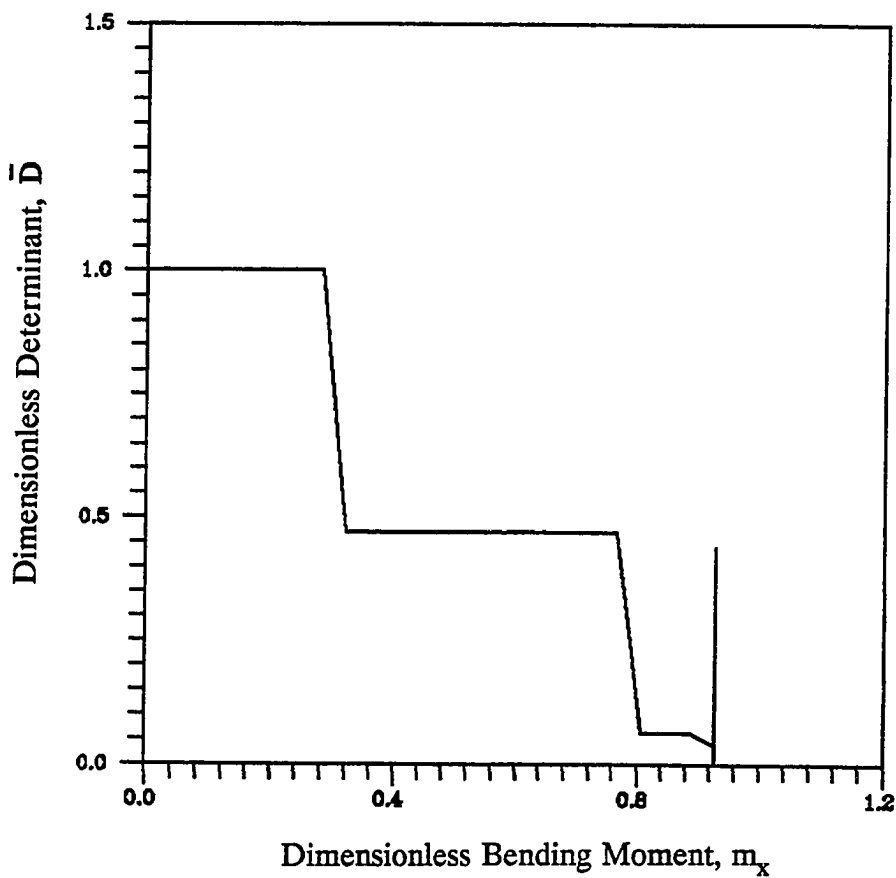


Figure 23. Stiffness degradation curve ($\bar{D} - m_x$) for uniaxially loaded sway beam-column BC30, with bilinear rotational restraints and load path NP3

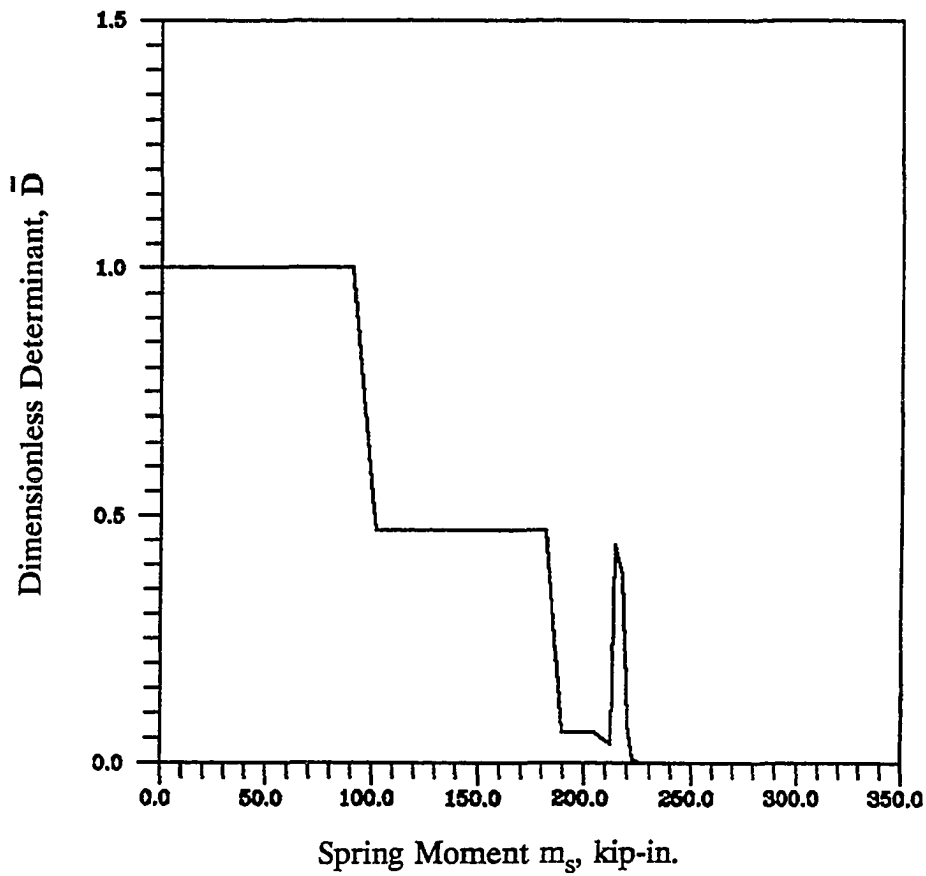


Figure 24. Stiffness degradation versus spring moment for uniaxially loaded sway beam-column BC30, with with bilinear rotational restraints and load path NP3

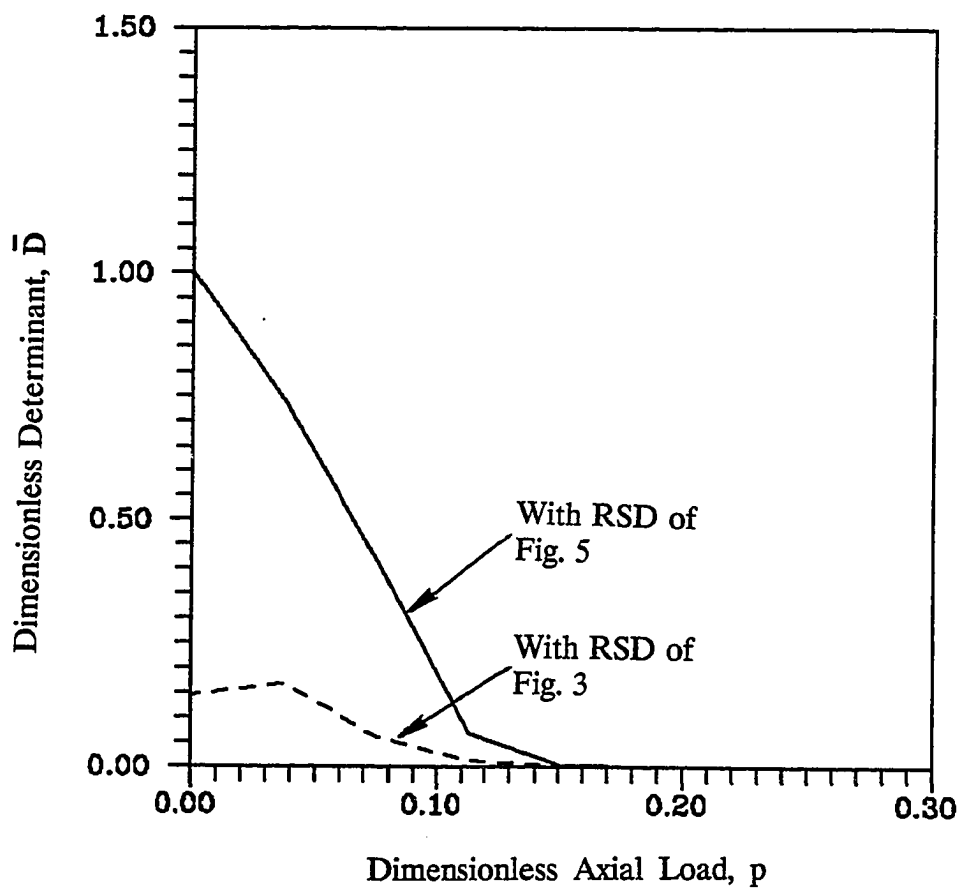


Figure 25. Effect of the type of residual stress distribution (RSD) on stiffness degradation ($\bar{D} - p$) of uniaxially loaded sway beam-column

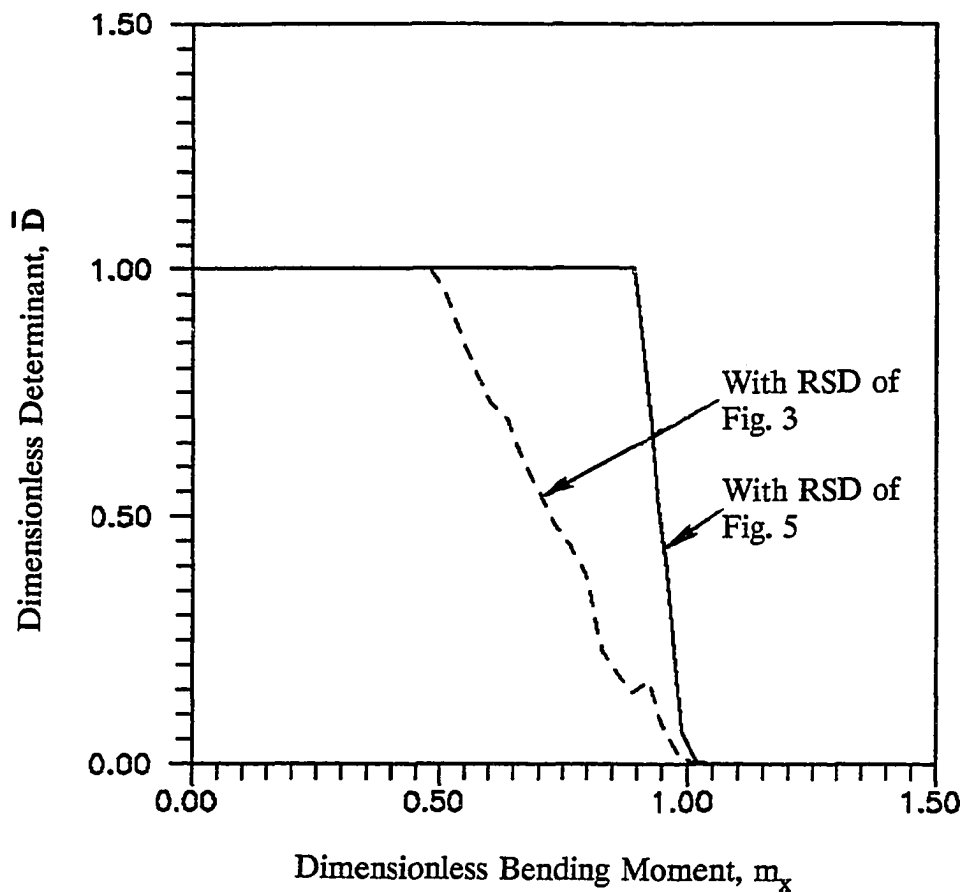


Figure 26. Effect of the type of residual stress distribution (RSD) on stiffness degradation ($\bar{D} - m_x$) of uniaxially loaded sway beam-column

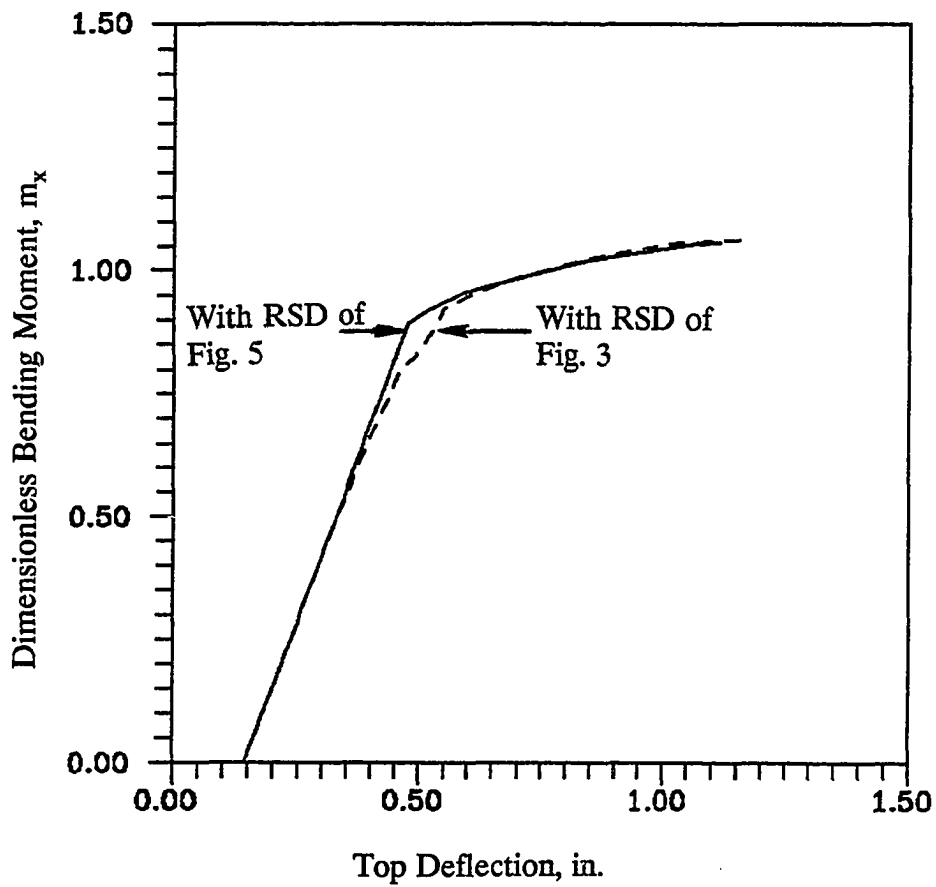


Figure 27. Dimensionless bending moment versus top deflection for uniaxially loaded sway beam-columns with two different residual stress distributions (RSD)

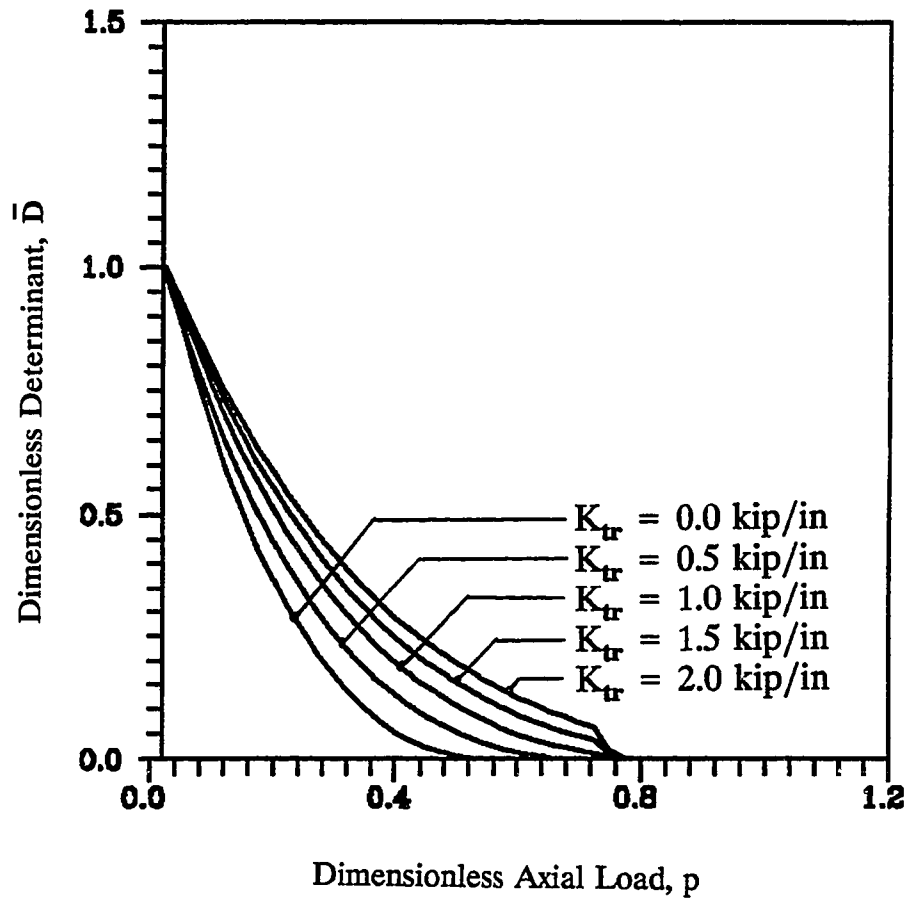


Figure 28. Stiffness degradation curve (\bar{D} - p) for biaxially loaded sway beam-columns BC32 through BC36

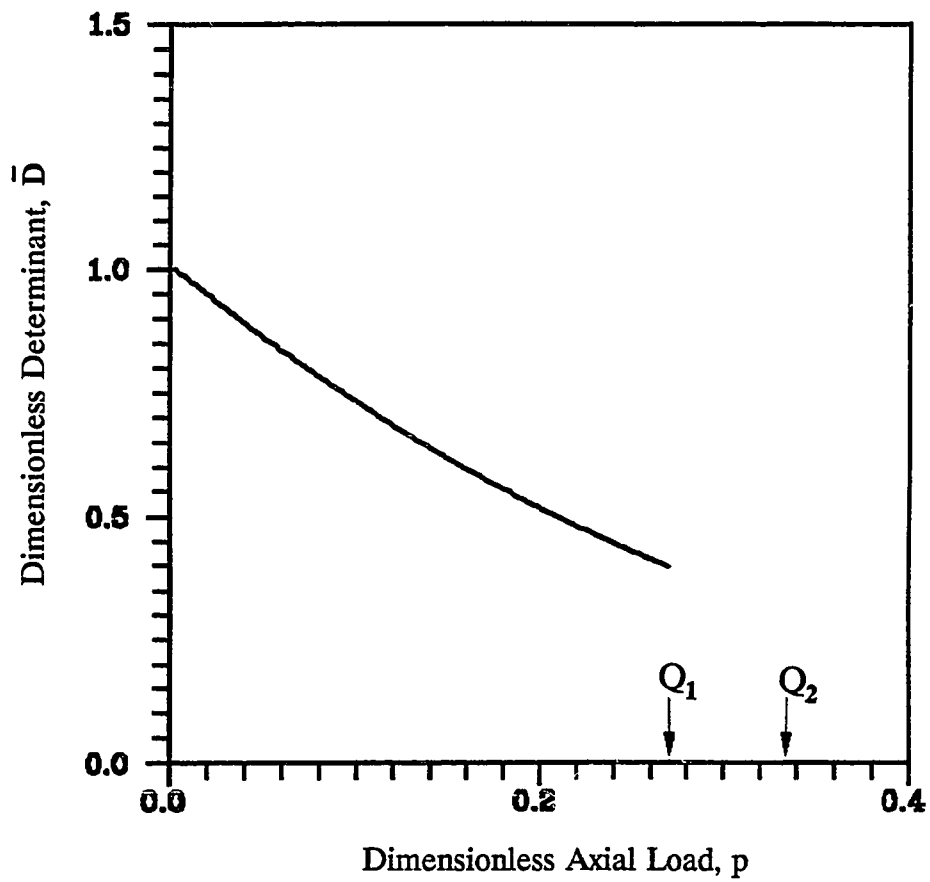


Figure 29. Stiffness degradation curve (\bar{D} - p) for biaxially sway loaded sway beam-column BC35 with LP1 load path

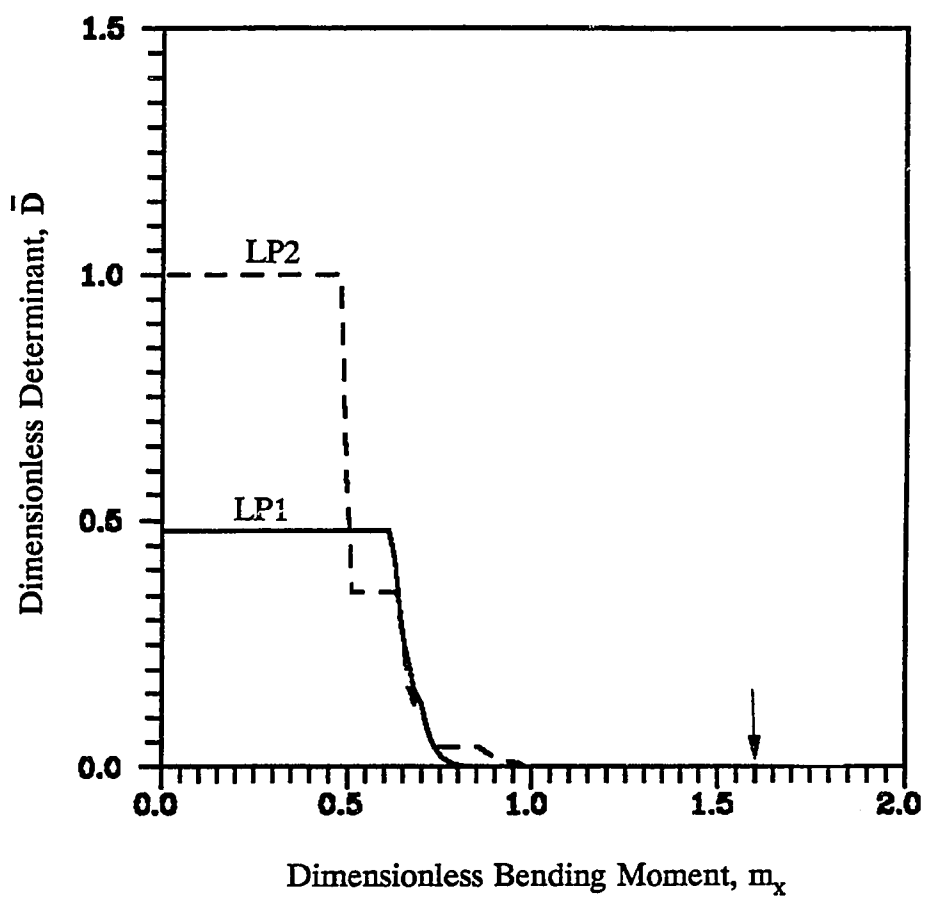


Figure 30. Stiffness degradation curve (\bar{D} - m_x) for biaxially loaded sway beam-column BC35 with LP1 and LP2 load paths

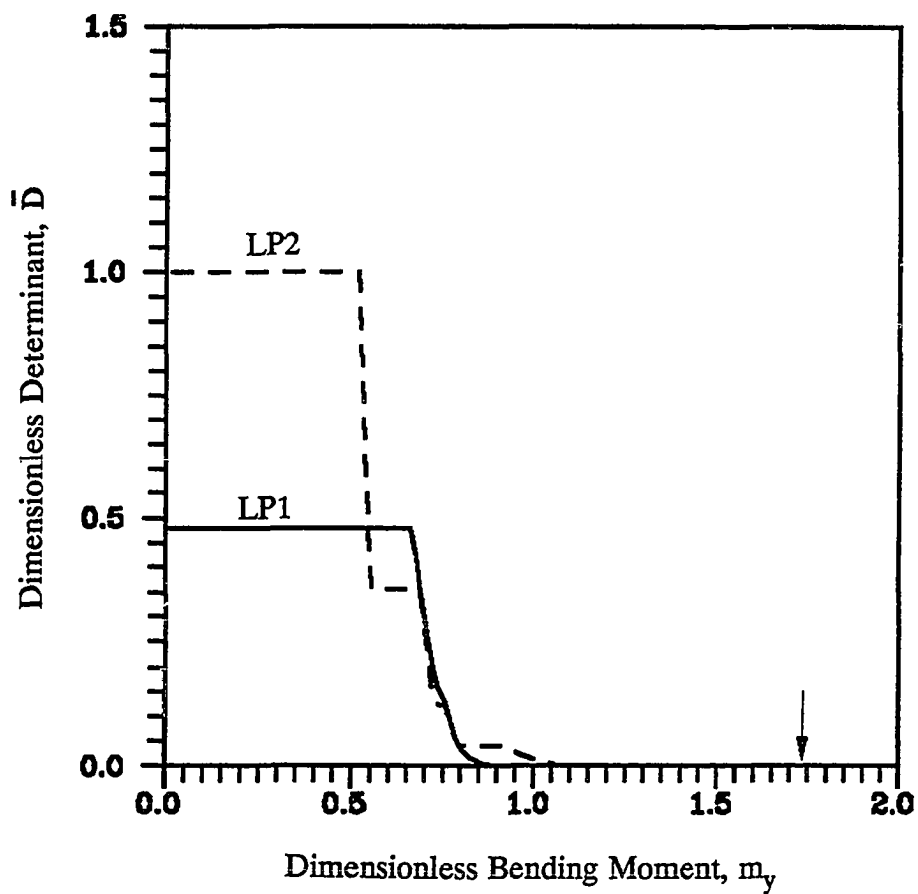


Figure 31. Stiffness degradation curve (\bar{D} - m_y) for biaxially loaded sway beam-column BC35 with load paths LP1 and LP2

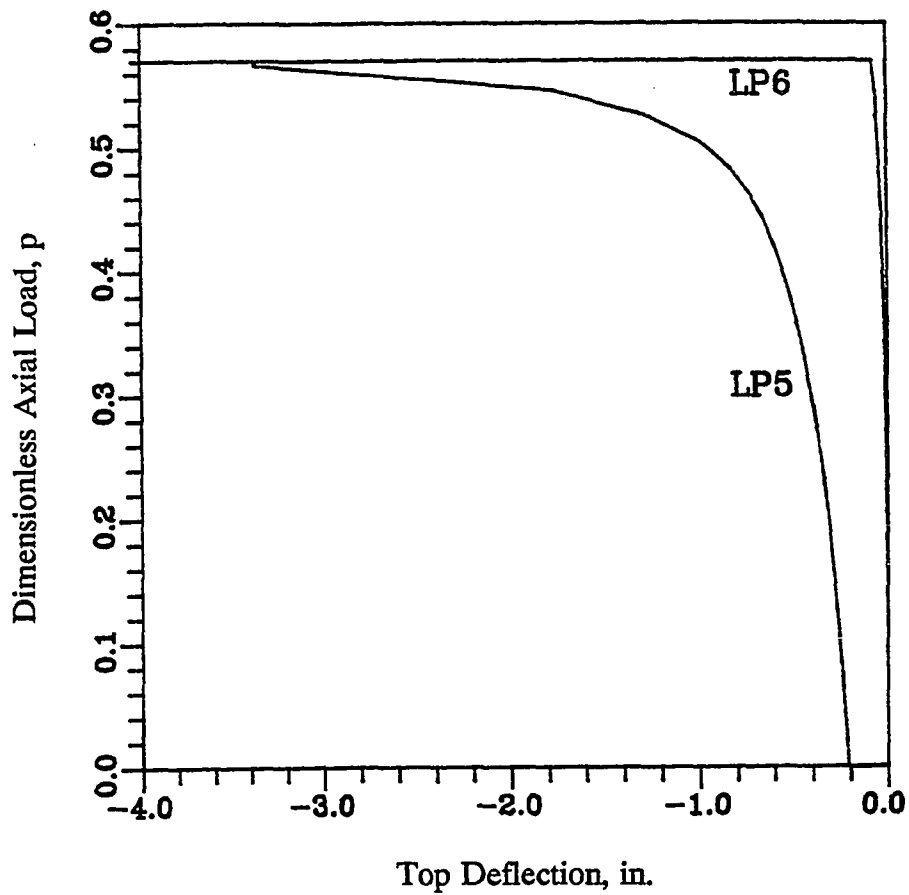


Figure 32. Axial load versus top deflection for biaxially loaded sway beam-column BC39 with equal end restraints and with load paths LP5 and LP6

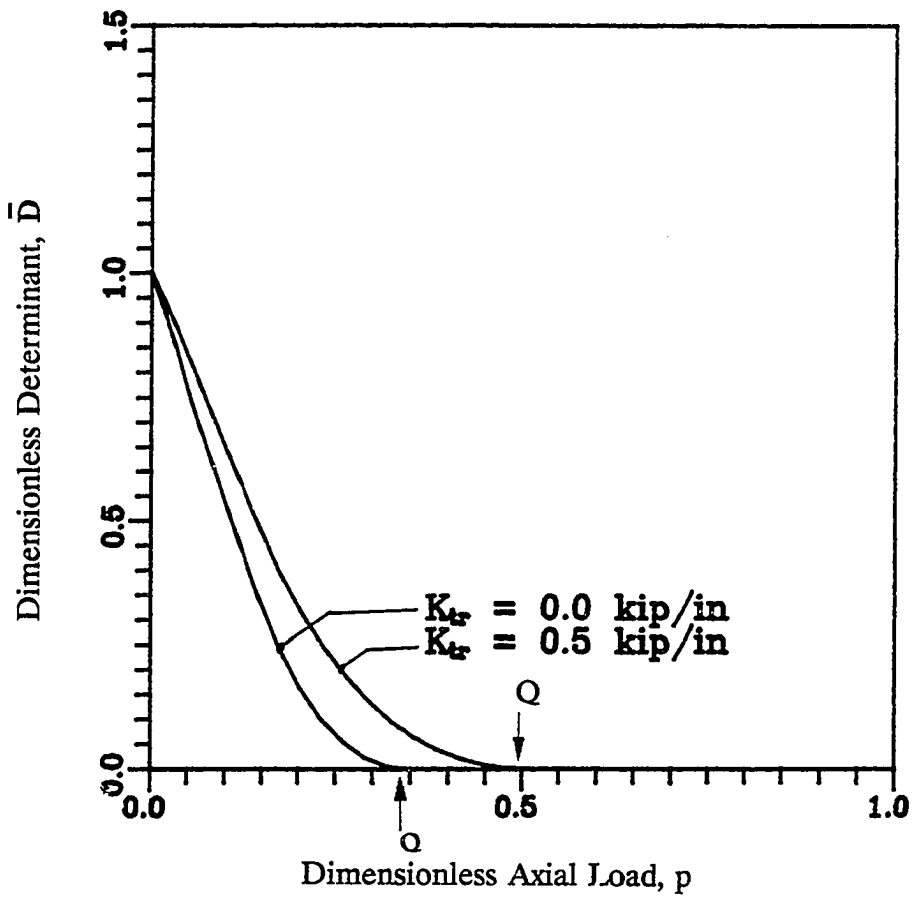


Figure 33. Stiffness degradation curve (\bar{D} - p) for biaxially loaded sway beam-columns BC42 and BC43

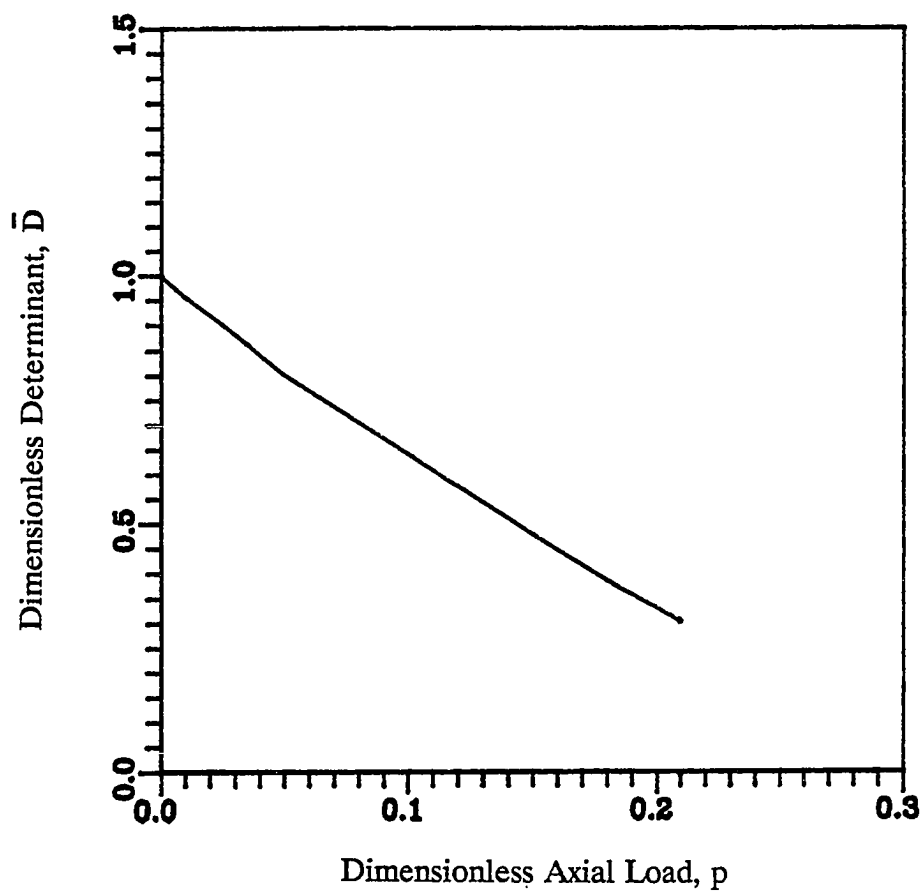


Figure 34. Stiffness degradation curve for member BC42 with load path LP3, $m_x = 1.38$ and $m_y = 1.12$

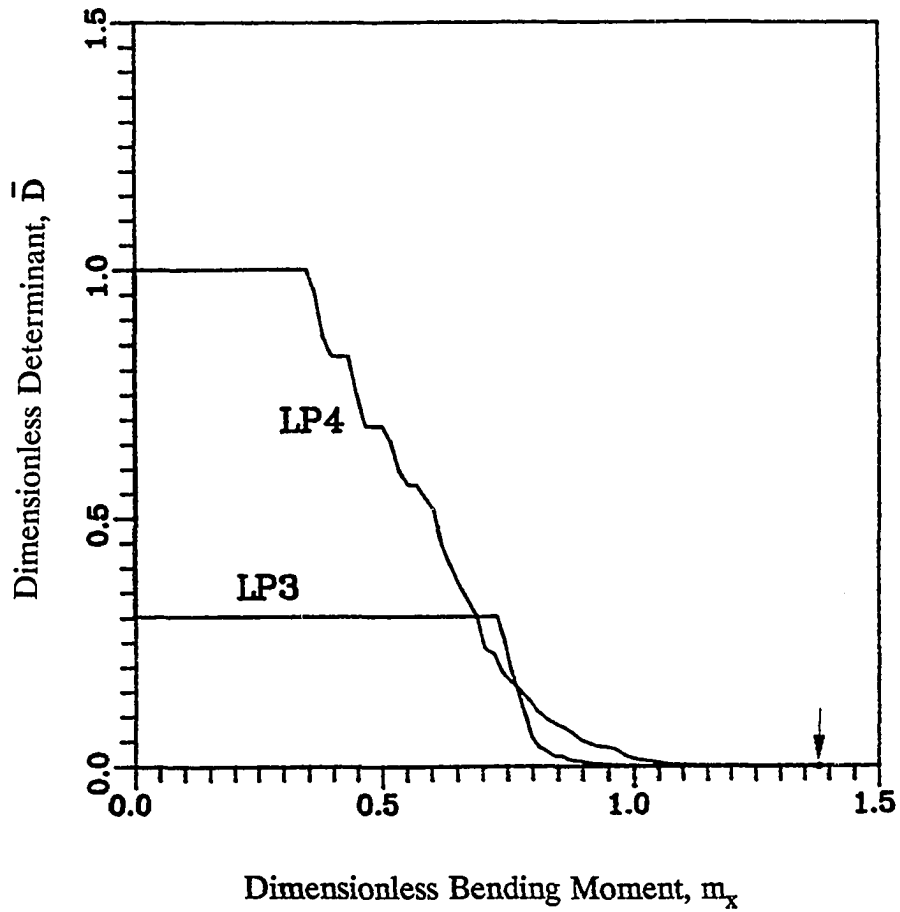


Figure 35. Stiffness degradation curve ($\bar{D} - m_x$) for member BC42 with load paths LP3 and LP4

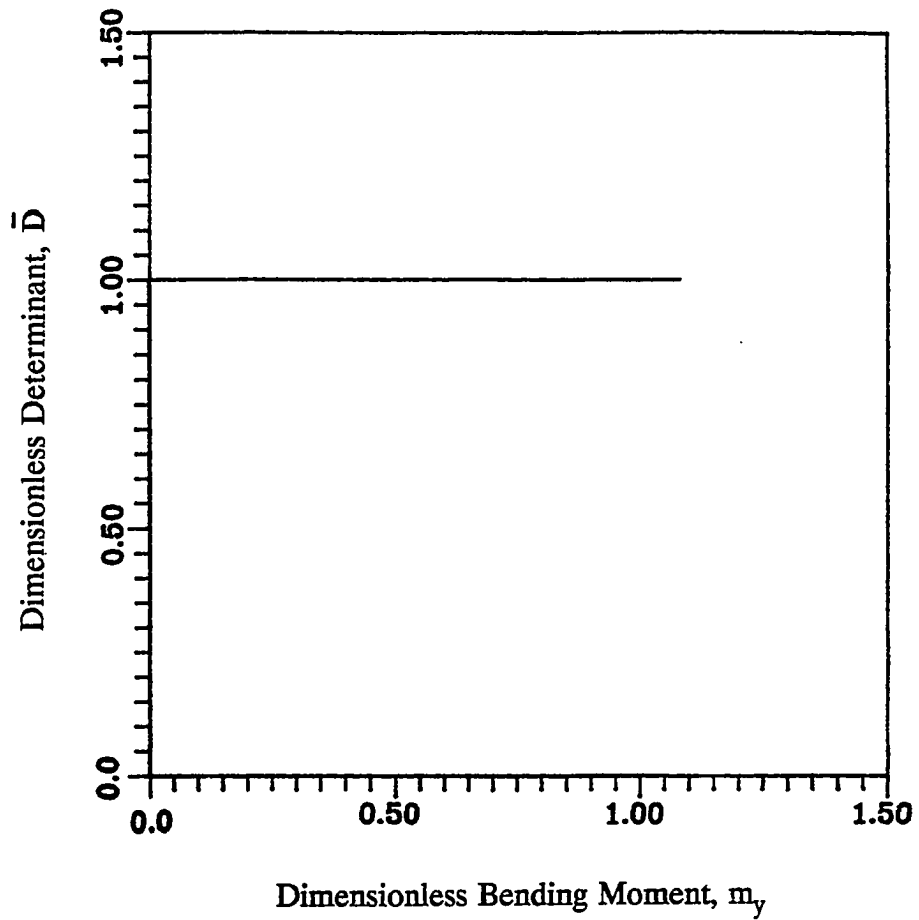


Figure 36. Stiffness degradation curve ($\bar{D} - m_y$) for member BC42 with load path LP4

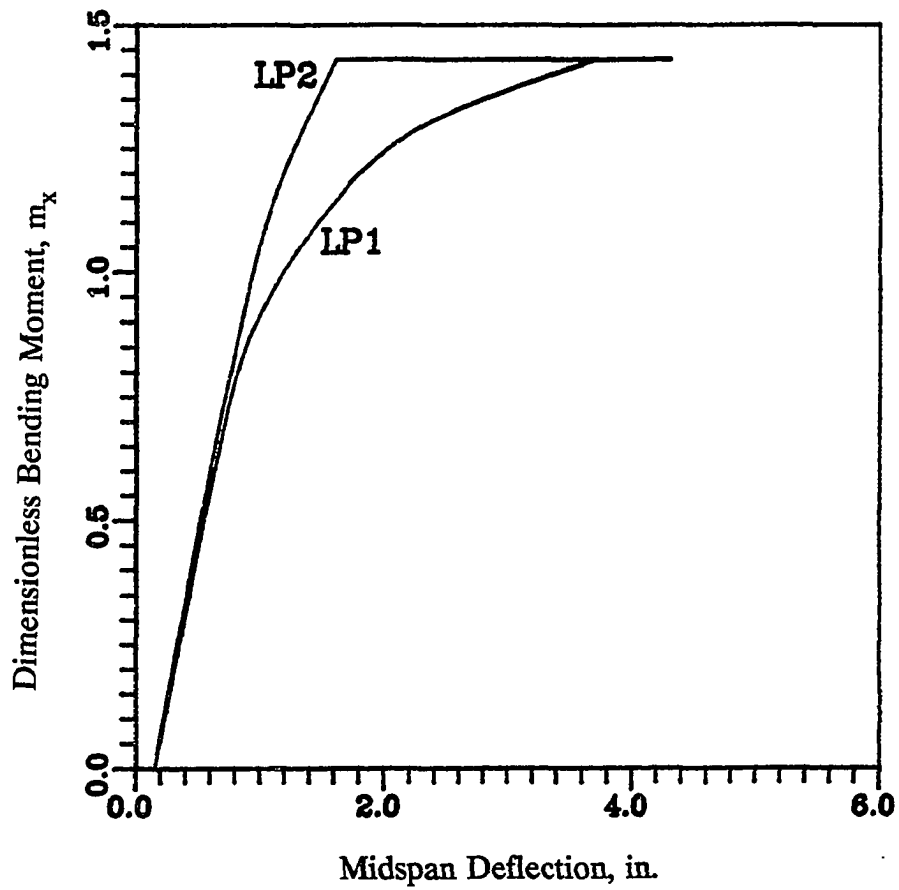


Figure 37. Moment versus midspan deflection for biaxially loaded sway beam-column BC42 with equal end restraints and with load paths LP1 and LP2

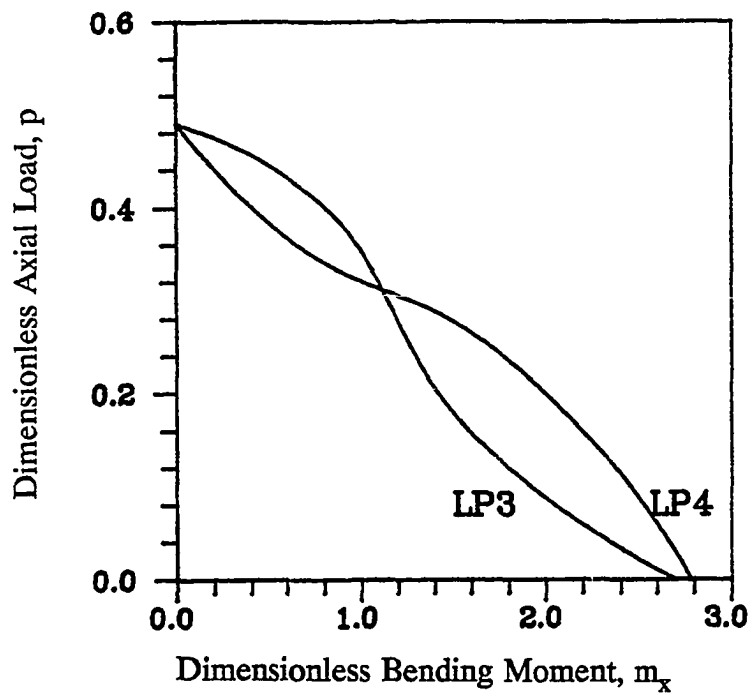


Figure 38. Interaction diagrams for biaxially loaded sway beam-column BC43 with equal end restraints and with load paths LP3 and LP4

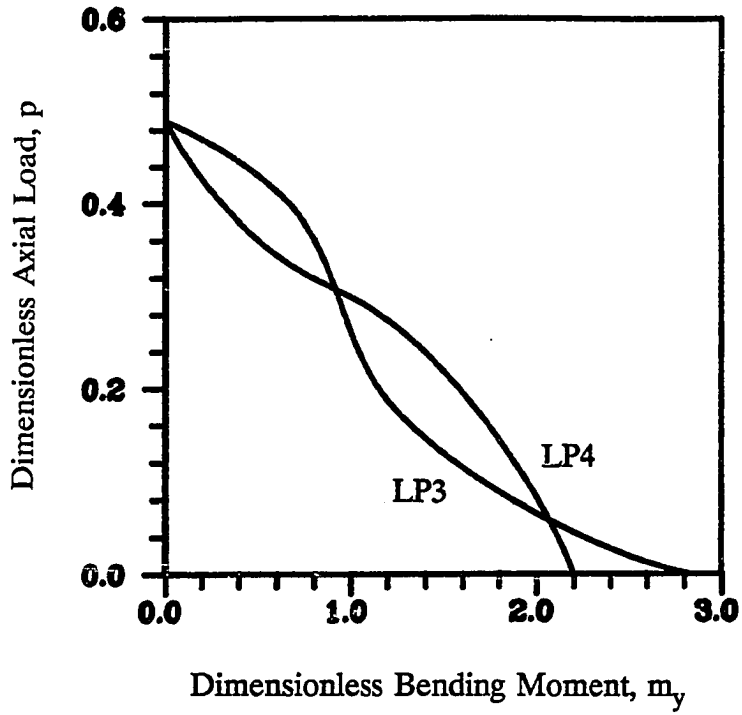


Figure 39. Interaction curves for biaxially loaded sway beam-column BC43 with equal end restraints and with load paths LP3 and LP4

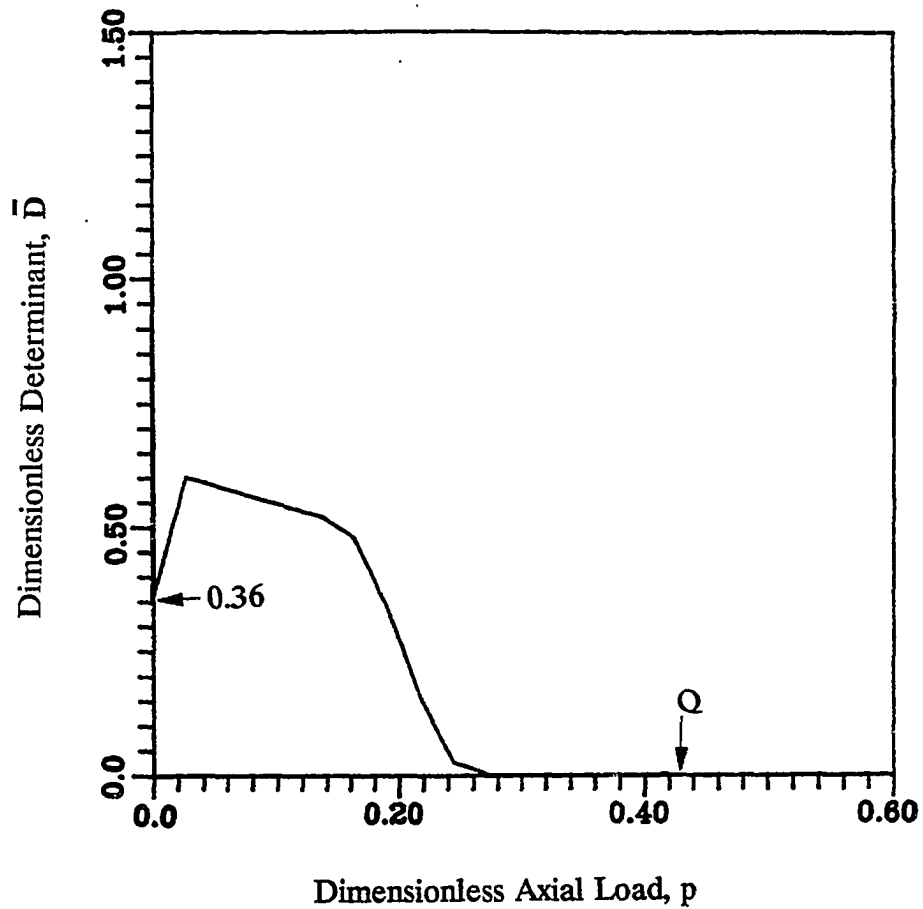


Figure 40. Stiffness degradation curve (\bar{D} - P) for biaxially loaded imperfect sway beam-column with end rotational restraints of type K_2 and with load path LP7

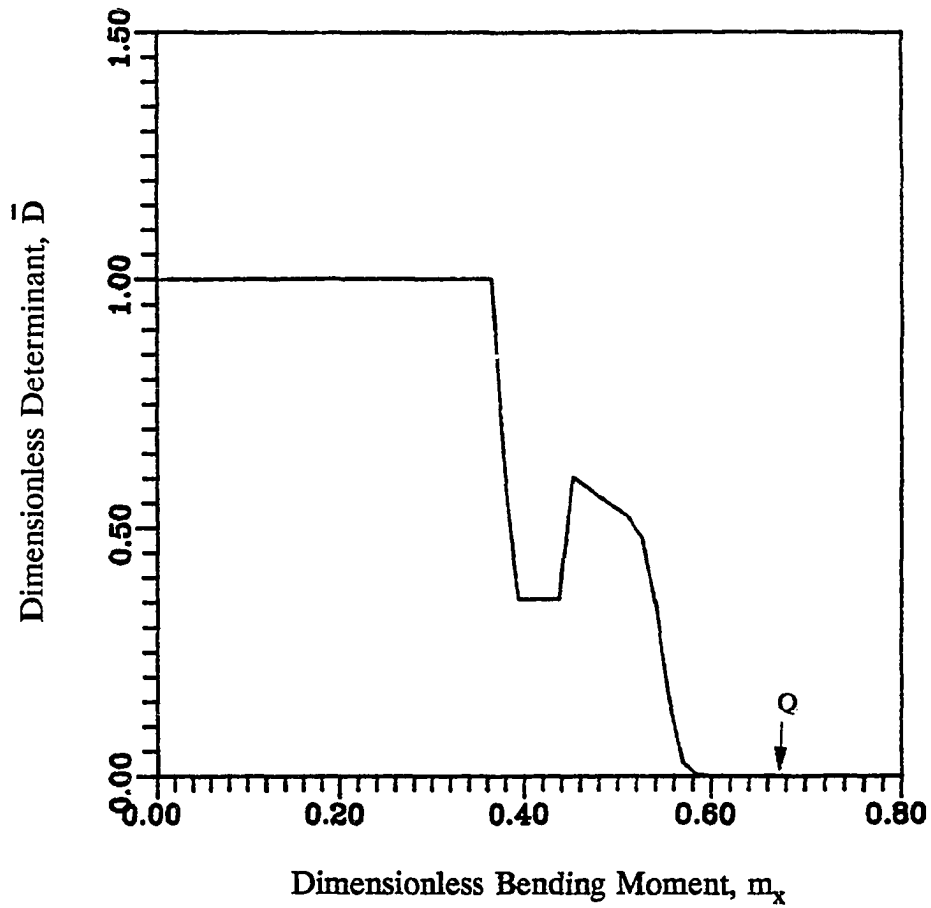


Figure 41. Stiffness degradation curve (\bar{D} - m_x) for biaxially loaded imperfect sway beam-column with end rotational restraints of type K_2 and with load path LP7

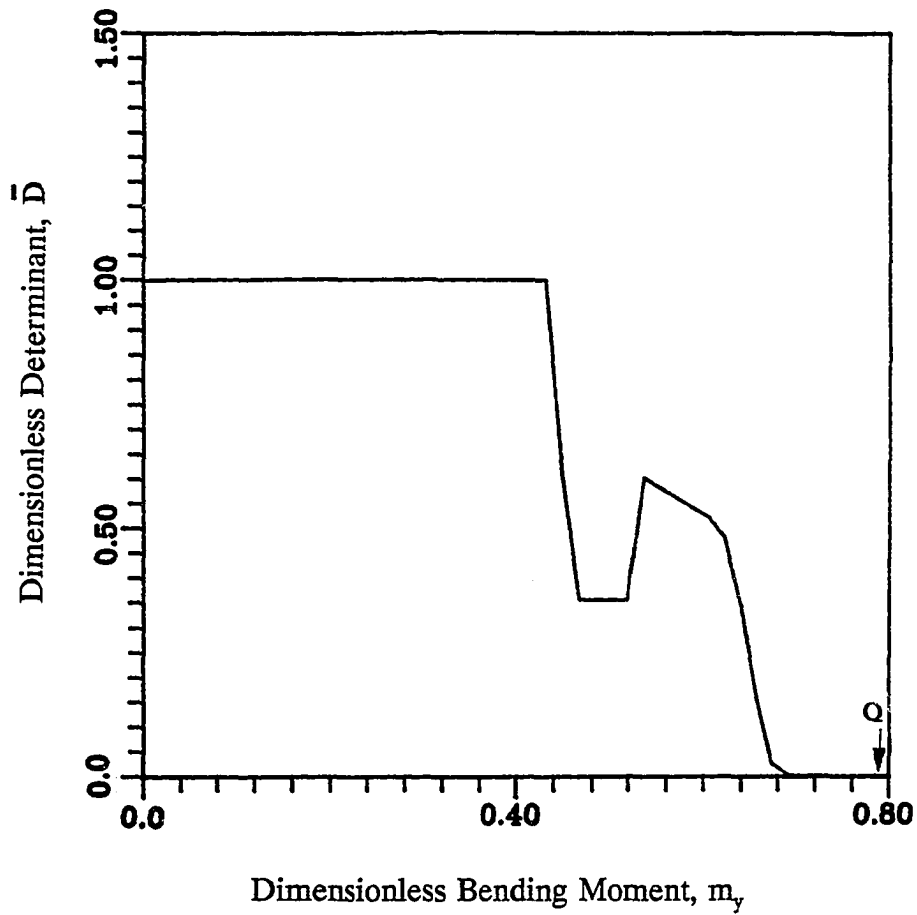


Figure 42. Stiffness degradation curve (\bar{D} - m_y) for biaxially loaded sway beam-column with rotational spring of K_2 type and with load path LP7

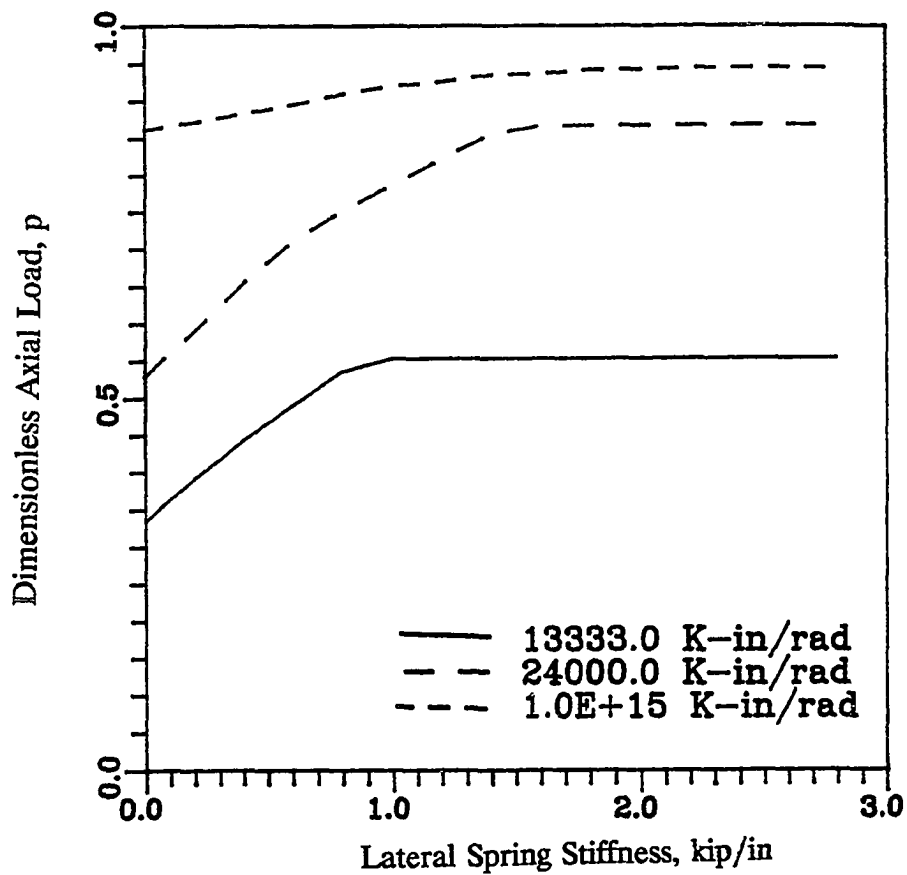


Figure 43. Dimensionless axial load versus lateral spring stiffness for biaxially loaded sway beam-column with various rotational end restraints, with $m_x = 0.5$, and load path NP2

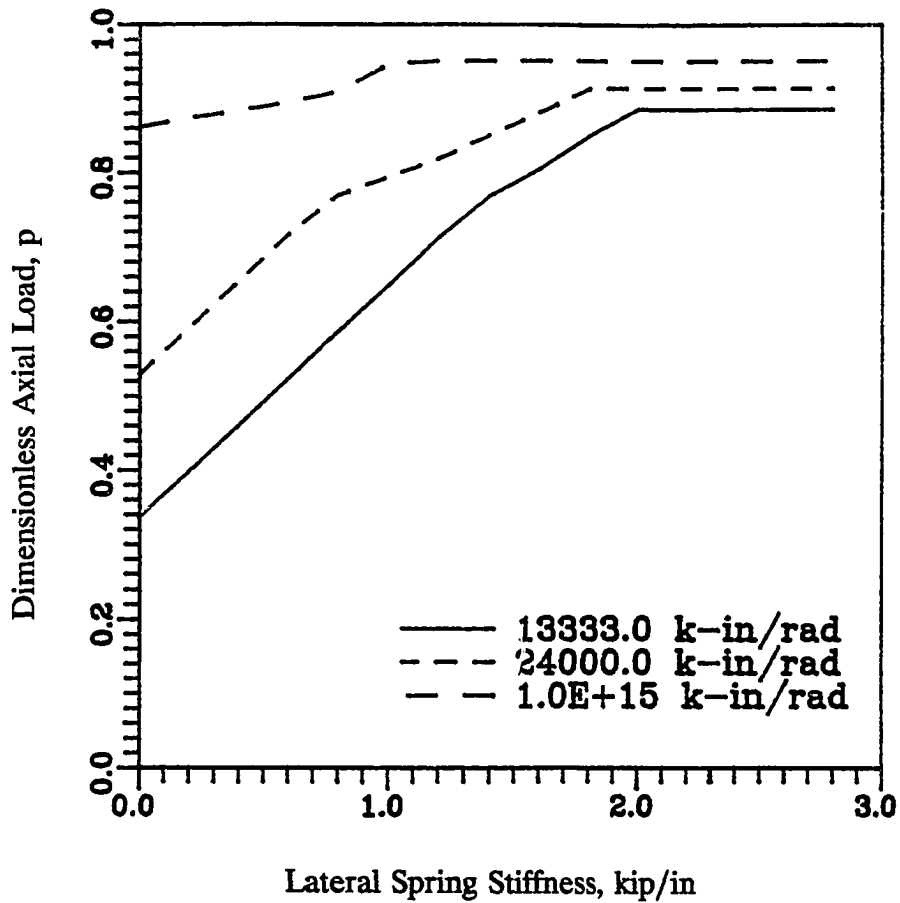


Figure 44. Dimensionless axial load versus lateral spring stiffness for biaxially loaded sway column with various rotational end restraints

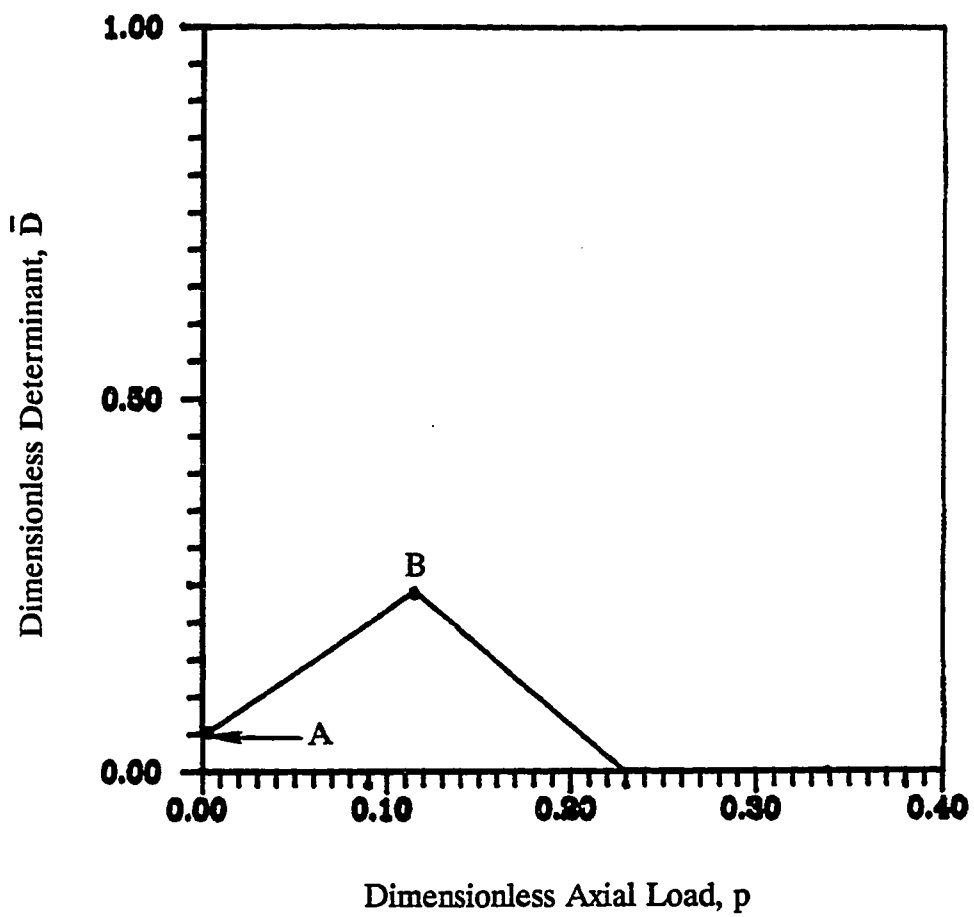


Figure 45. Stiffness degradation curve (\bar{D} - P) for biaxially loaded sway beam-column with load path LP7

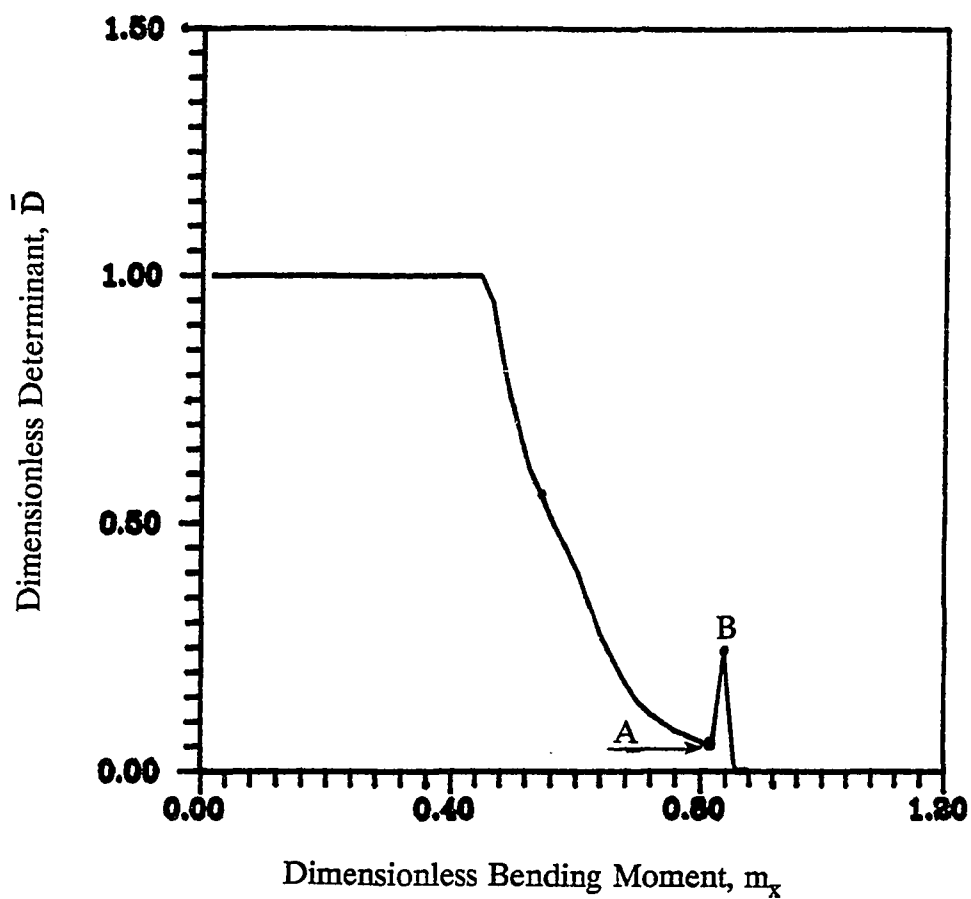


Figure 46. Stiffness degradation curve (\bar{D} - m_x) for biaxially loaded sway beam-column with load path LP7

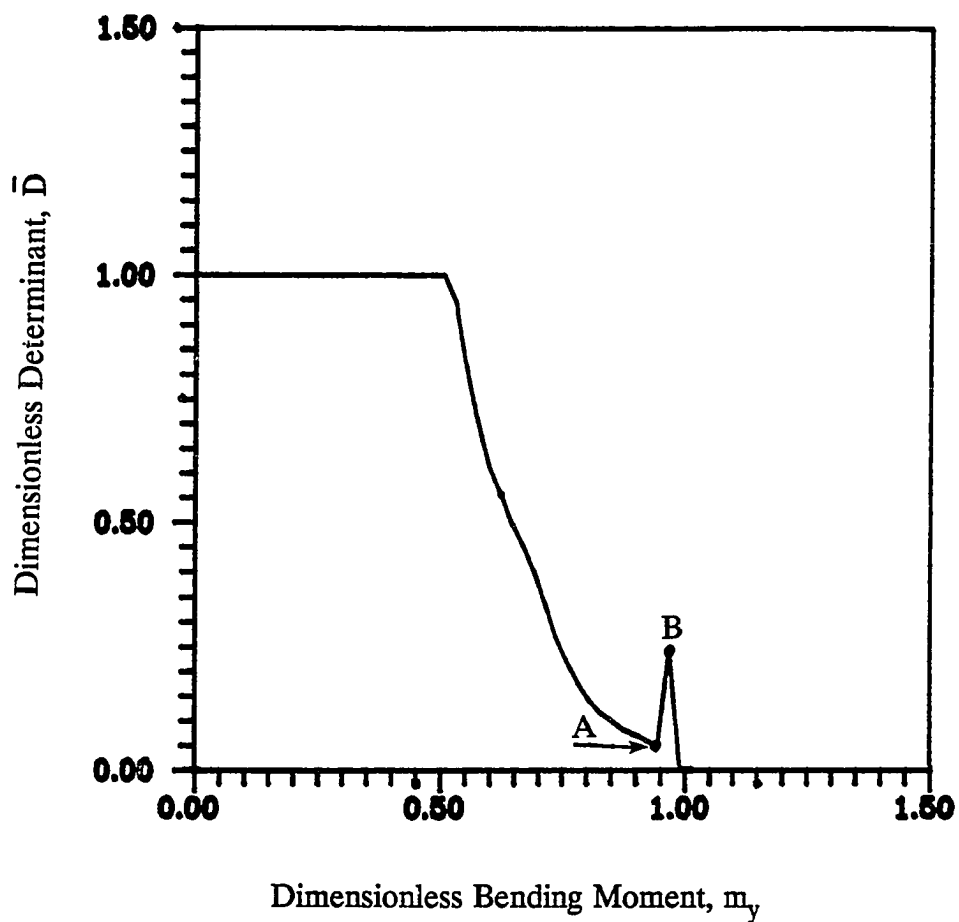


Figure 47. Stiffness degradation curve (\bar{D} - m_y) for biaxially loaded sway beam-column with load path LP7

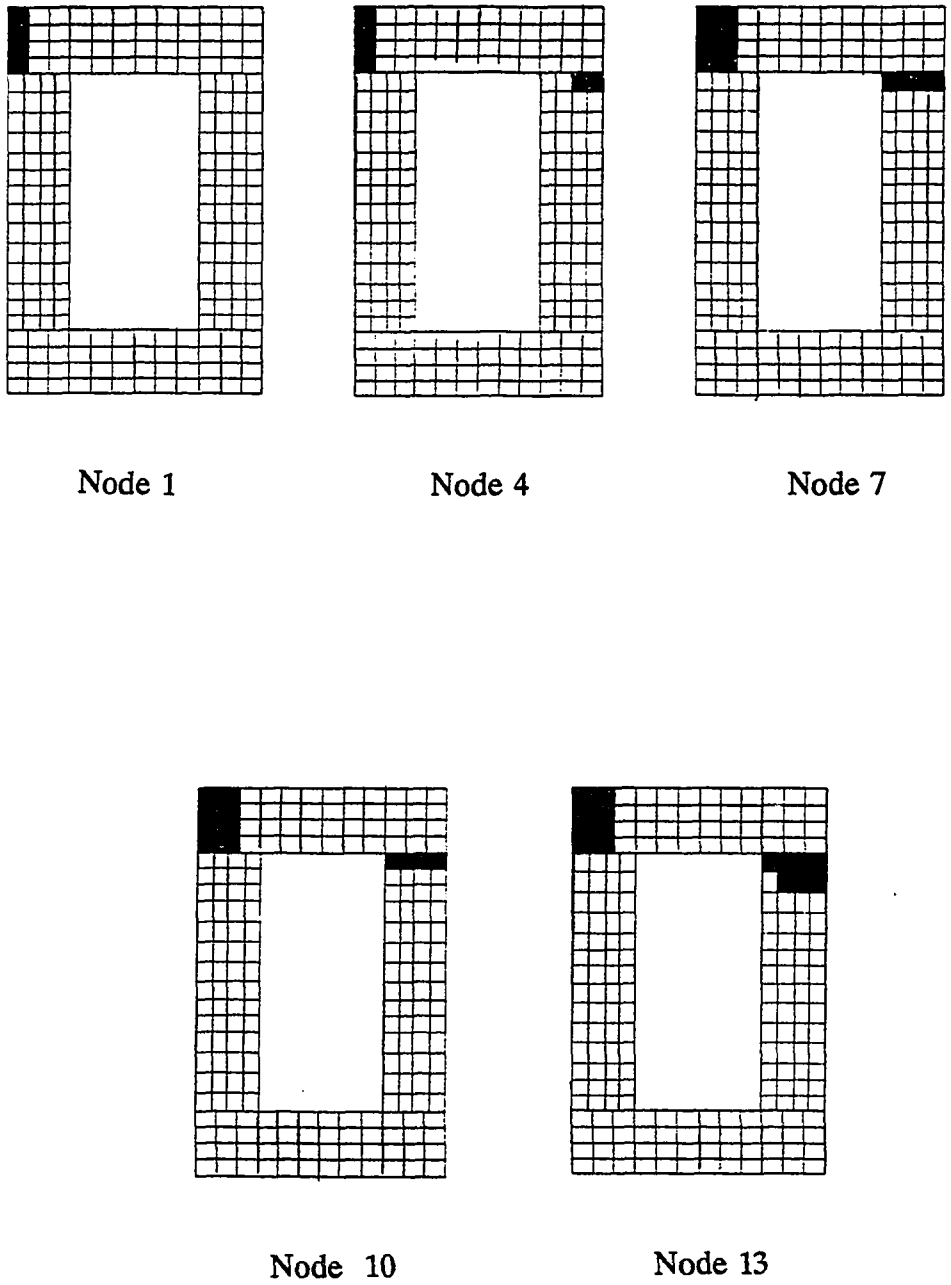
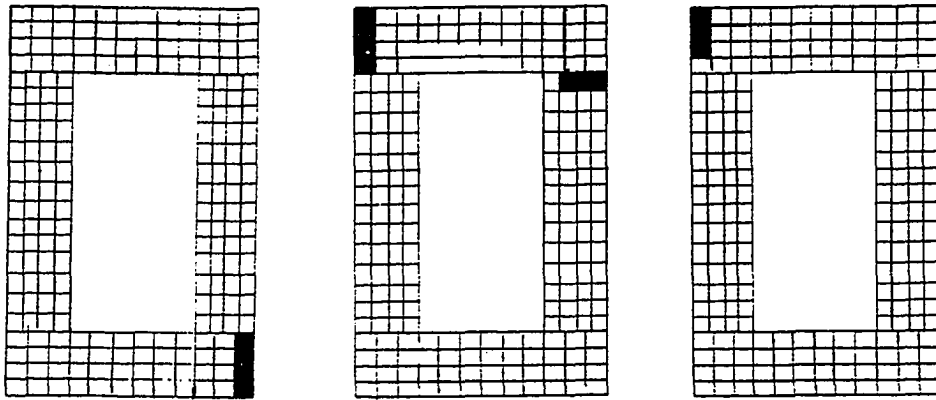


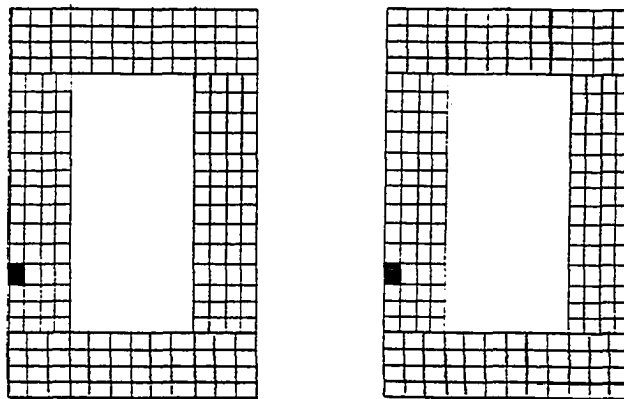
Figure 48. Spread of plasticity in the cross sections before axial load is incremented (corresponding to point A in Figures 47 - 49)



Node 1

Node 4

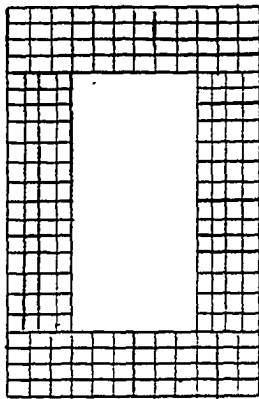
Node 7



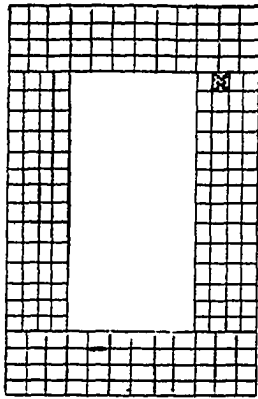
Node 10

Node 13

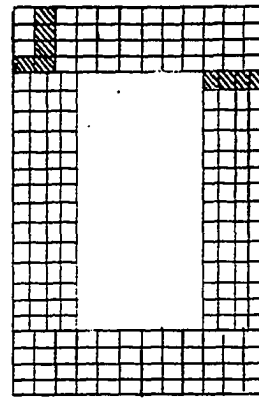
Figure 49. Spread of plasticity in the cross sections after axial load is incremented (corresponding to point B in Figures 47 - 49)



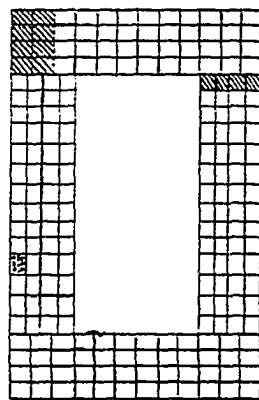
Node 1



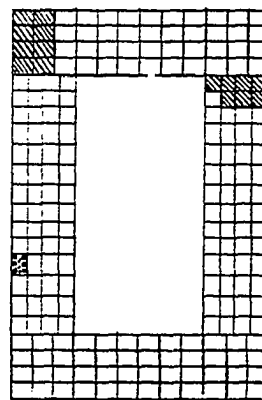
Node 4



Node 7



Node 10



Node 13

Figure 50. Unloaded elements in the section (dashed) and newly plastified elements (dotted)

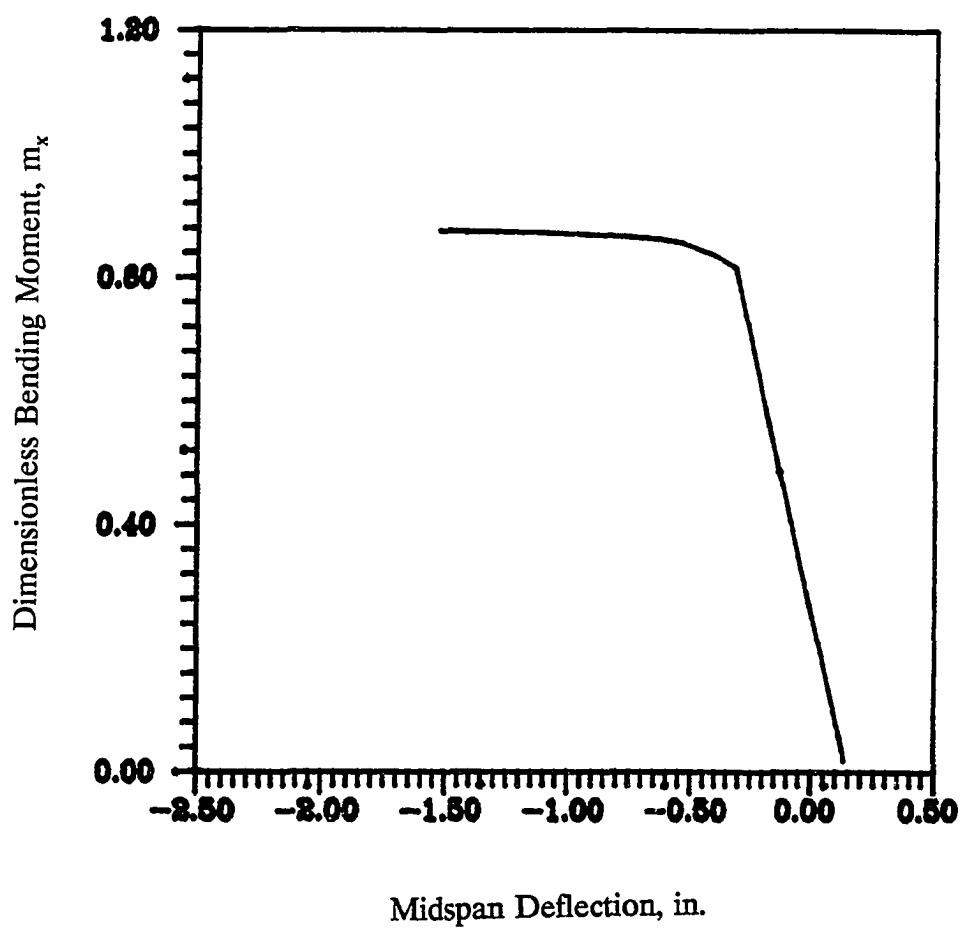


Figure 51. Dimensionless bending moment versus midspan deflection in yz plane for a biaxially loaded sway beam-column

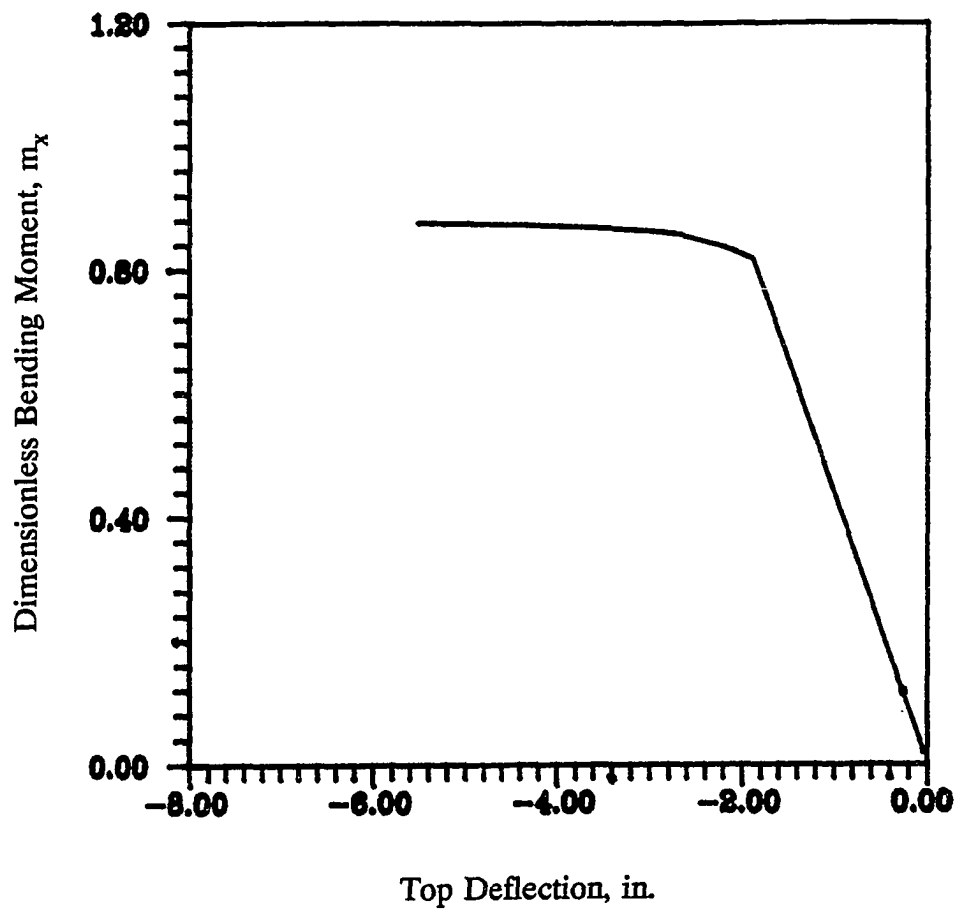


Figure 52. Dimensionless bending moment versus top deflection in yz plane for a biaxially loaded sway beam-column

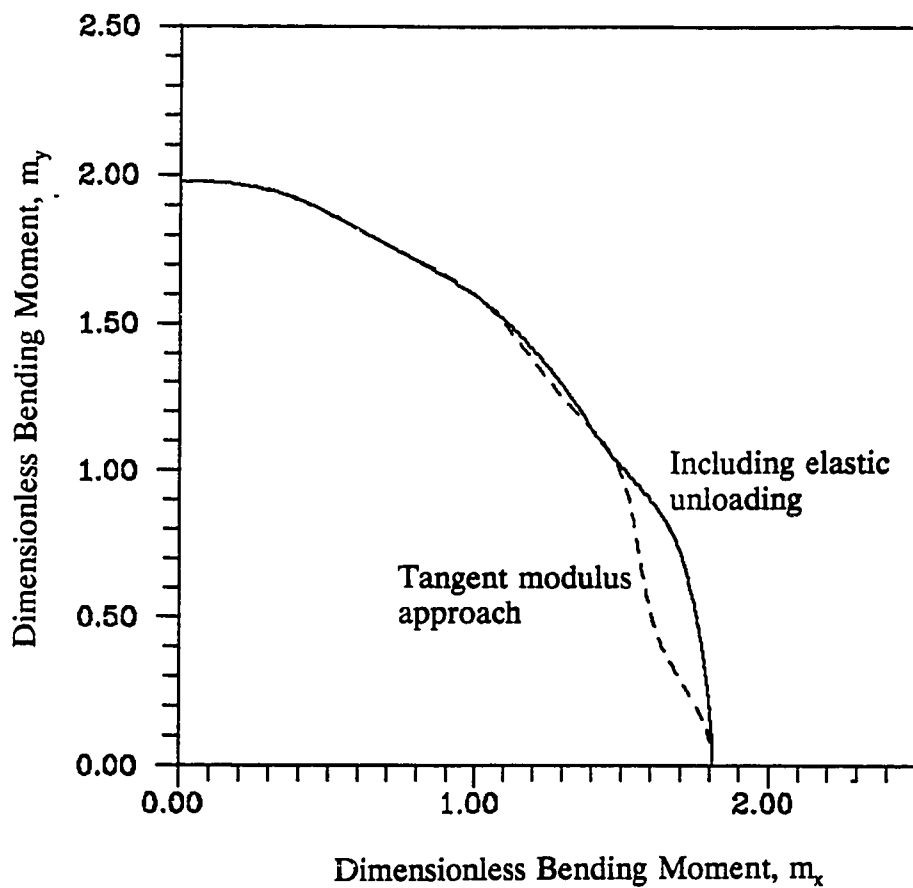


Figure 53. Interaction curves for biaxially loaded sway beam-column based on tangent modulus approach, and including elastic unloading

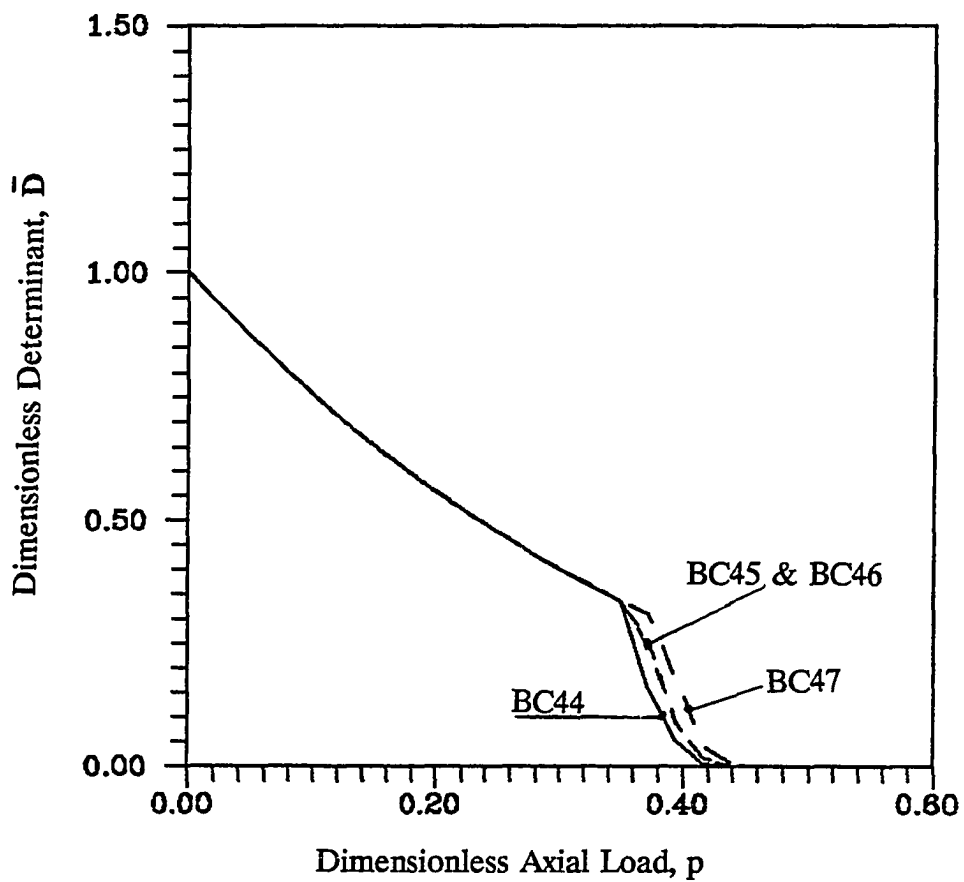


Figure 54. Effect of residual stresses and crookedness on the stiffness degradation of biaxially loaded sway beam-columns with load path LP5

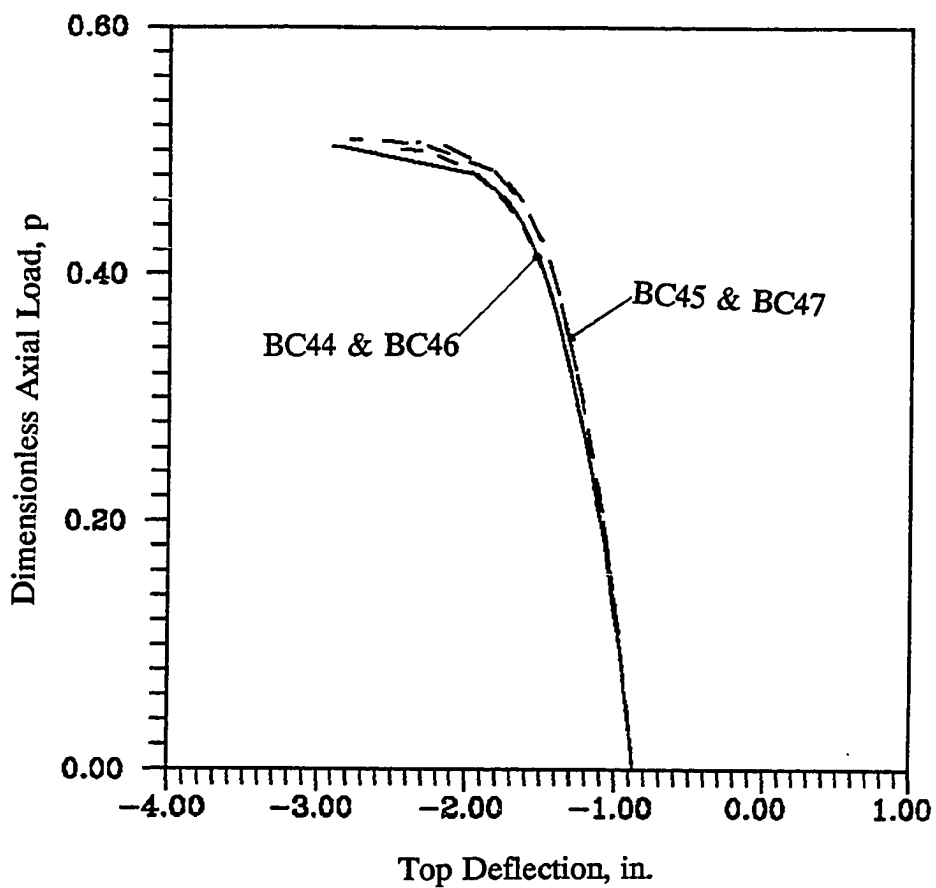


Figure 55. Dimensionless axial load versus top deflection of biaxially loaded sway beam-column with residual stresses and/or crookedness and with load path LP5

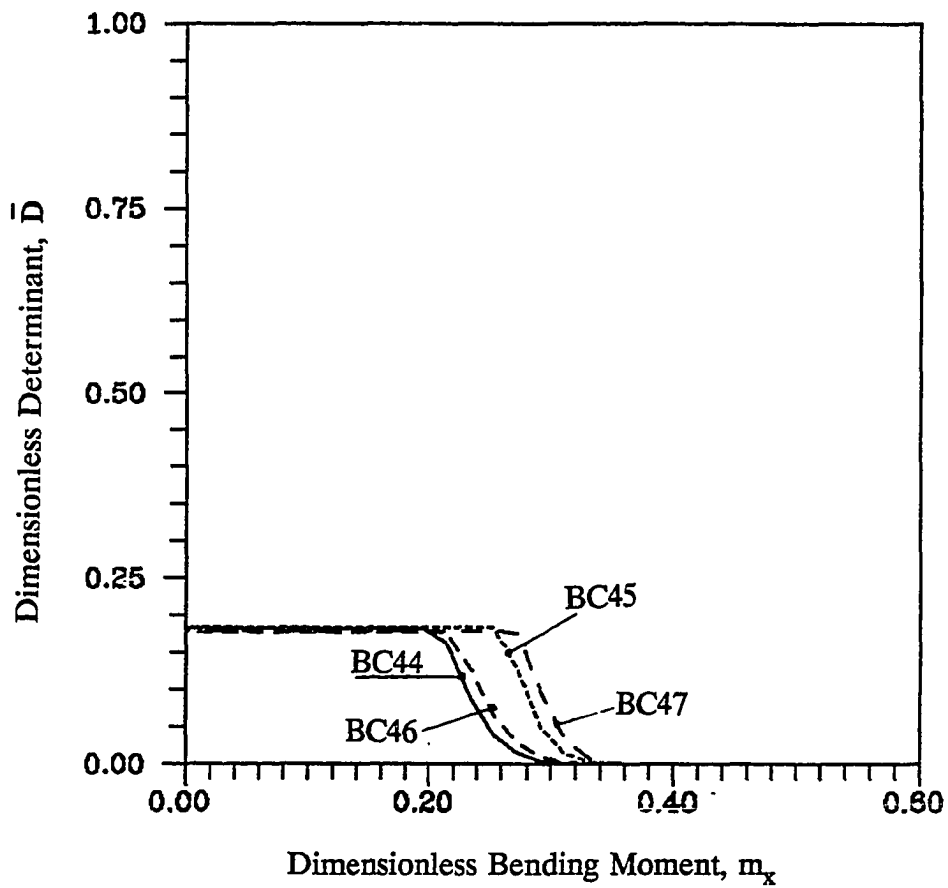


Figure 56. Stiffness degradation ($\bar{D} - m_x$) for biaxially loaded sway beam-column with residual stresses and/or crookedness and with load path LP6

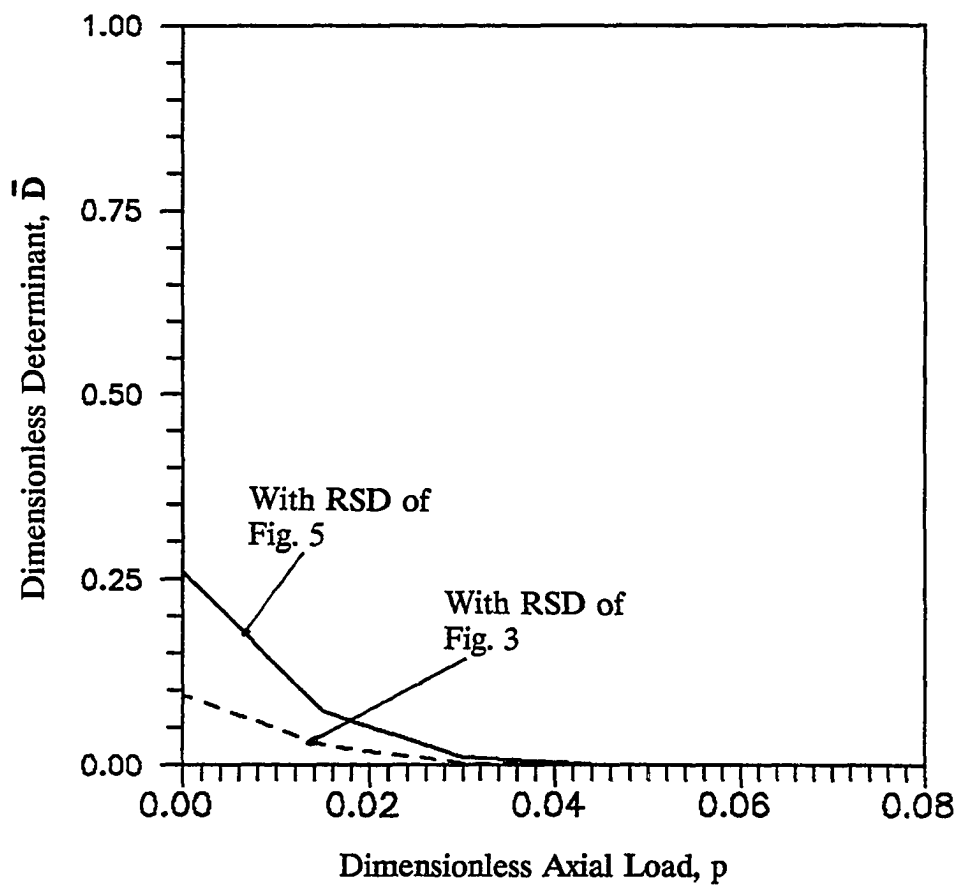


Figure 57. Effect of the type of residual stress distribution (RSD) on stiffness degradation ($\bar{D} - p$) of biaxially loaded sway beam-column

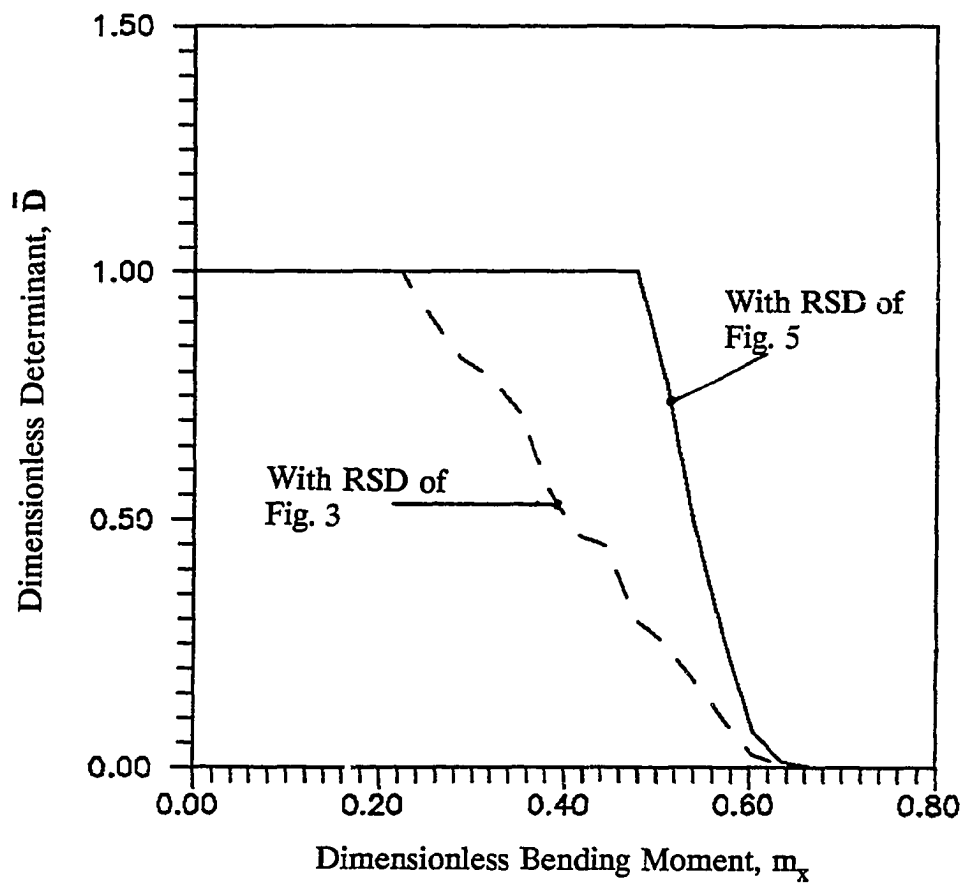


Figure 58. Effect of type residual stress distribution (RSD) on stiffness degradation ($\bar{D} - m_x$) of biaxially loaded sway beam-column

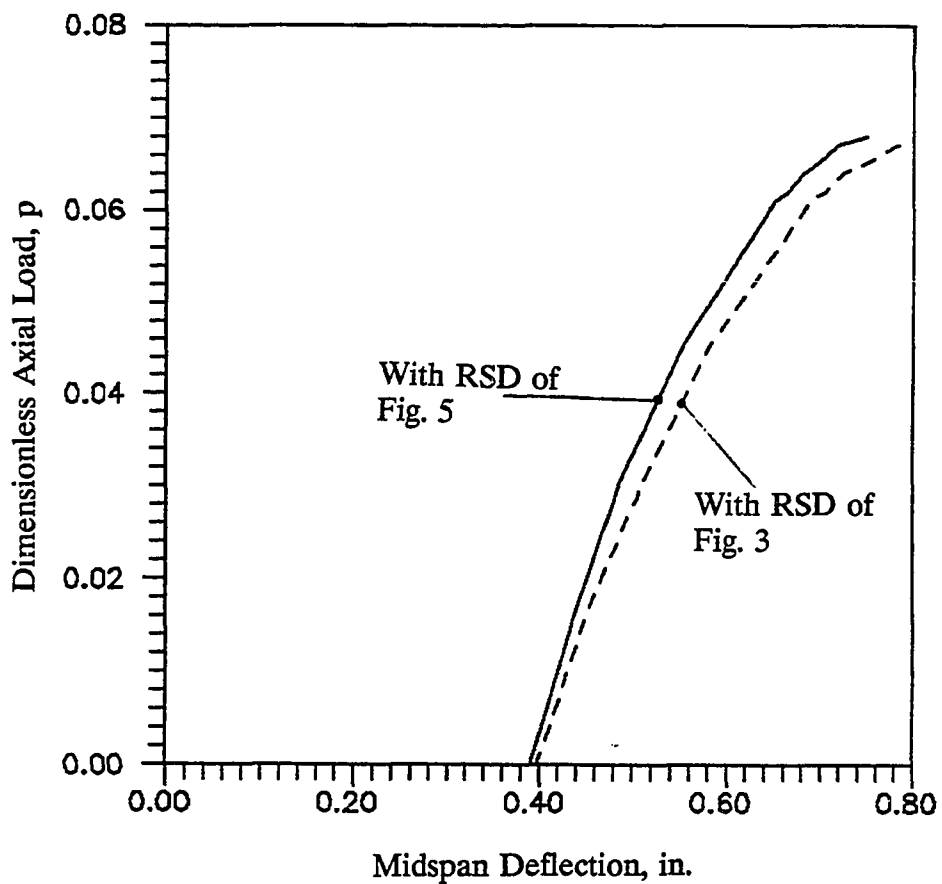


Figure 59. Dimensionless axial load versus midspan deflection of biaxially loaded sway beam-column with different residual stress distributions (RSD)

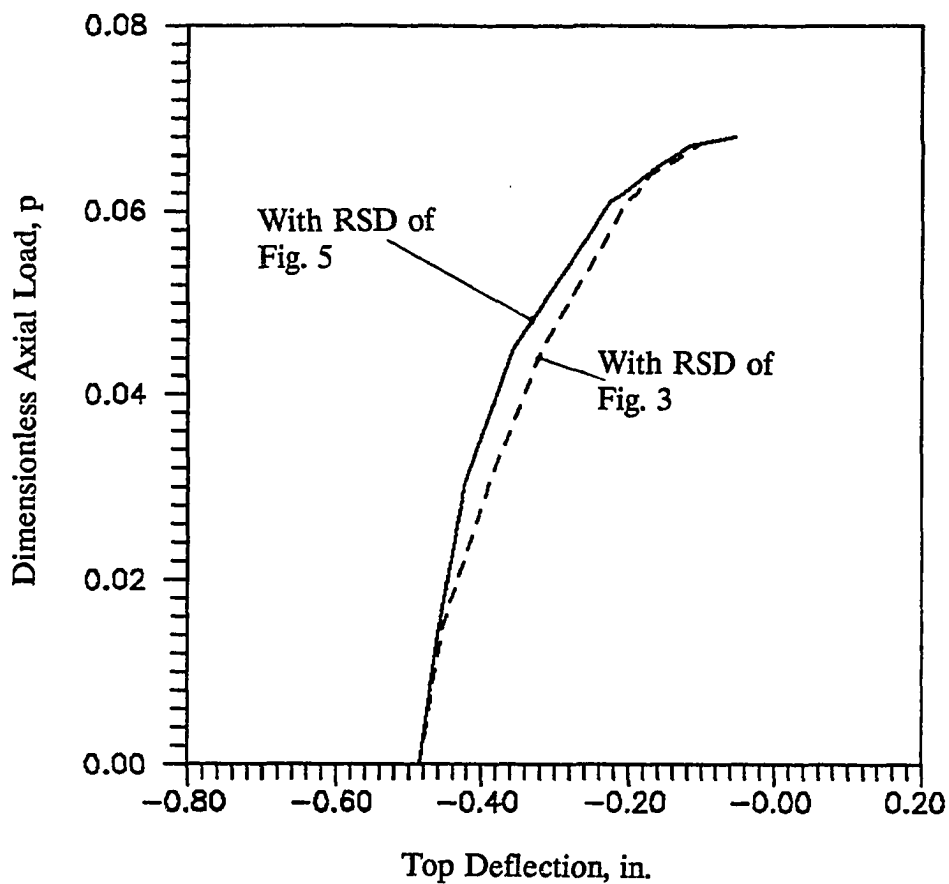


Figure 60. Dimensionless axial load versus top deflection of biaxially loaded sway beam-column with different residual stress distributions (RSD)

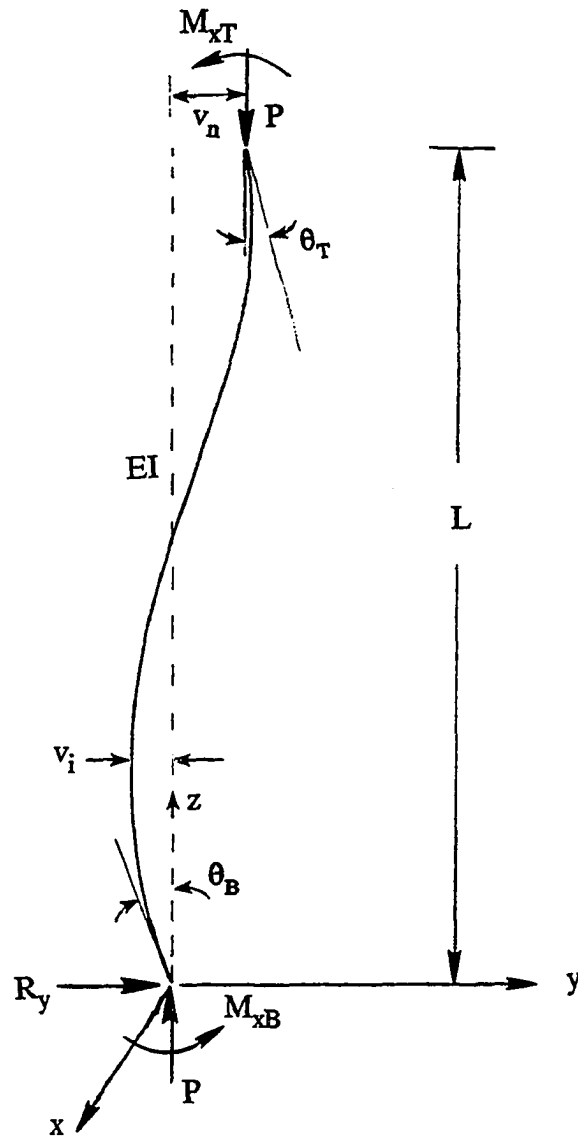


Figure 61. Sway beam-column subjected to uniaxial loading

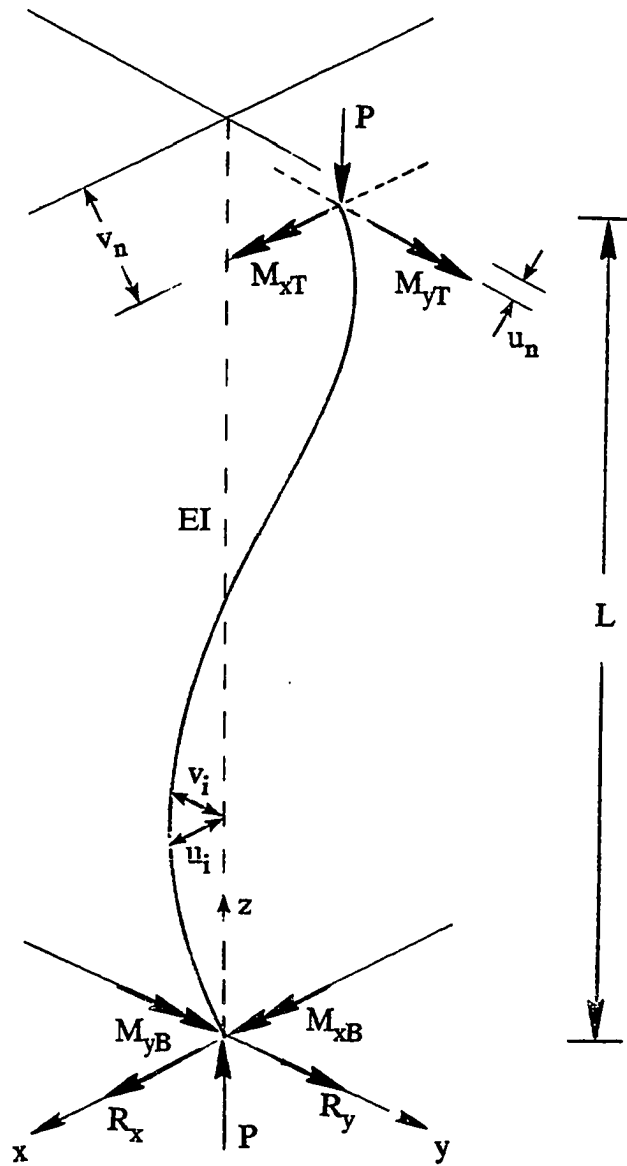


Figure 62. Sway beam-column subjected to biaxial loading

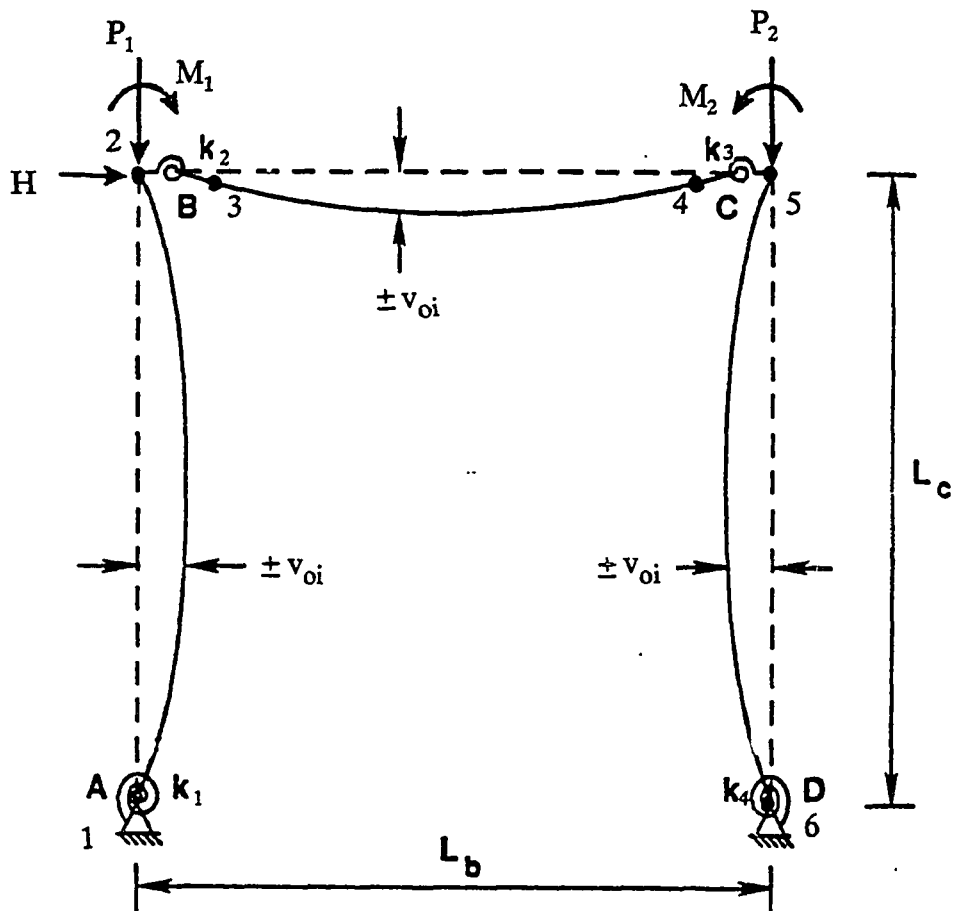


Figure 63. Imperfect unbraced portal frame with loading

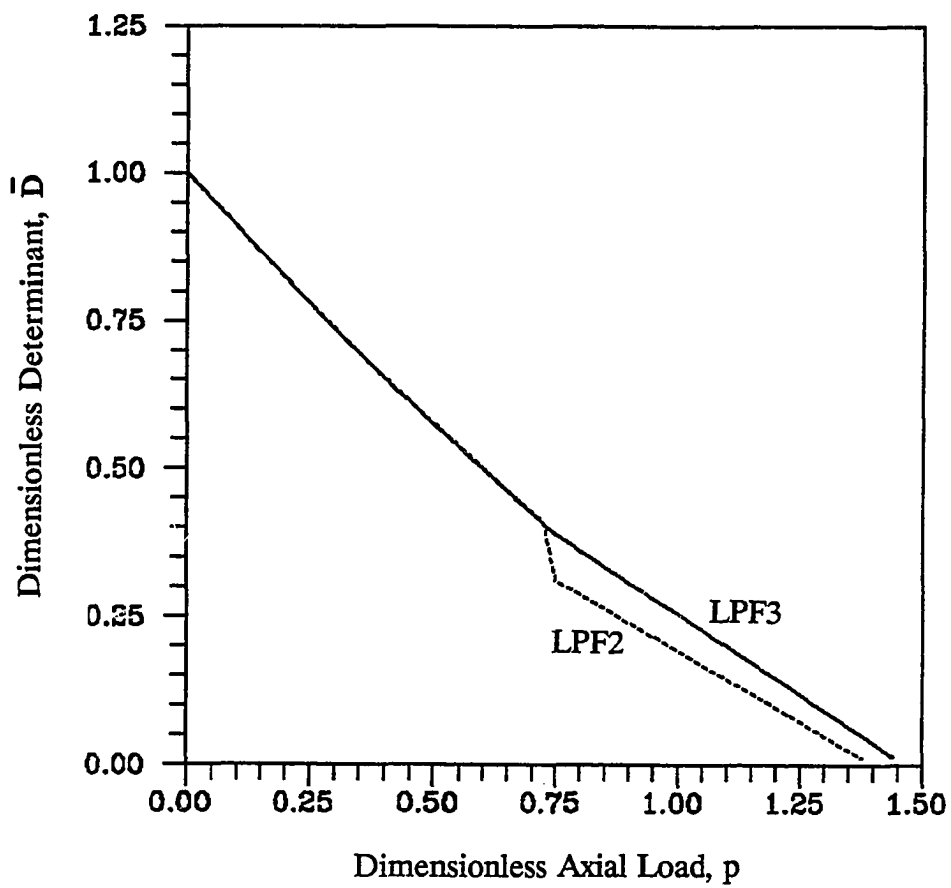


Figure 64. Stiffness degradation (\bar{D} - p) for sway plane frame PF9 with load paths LPF2 and LPF3

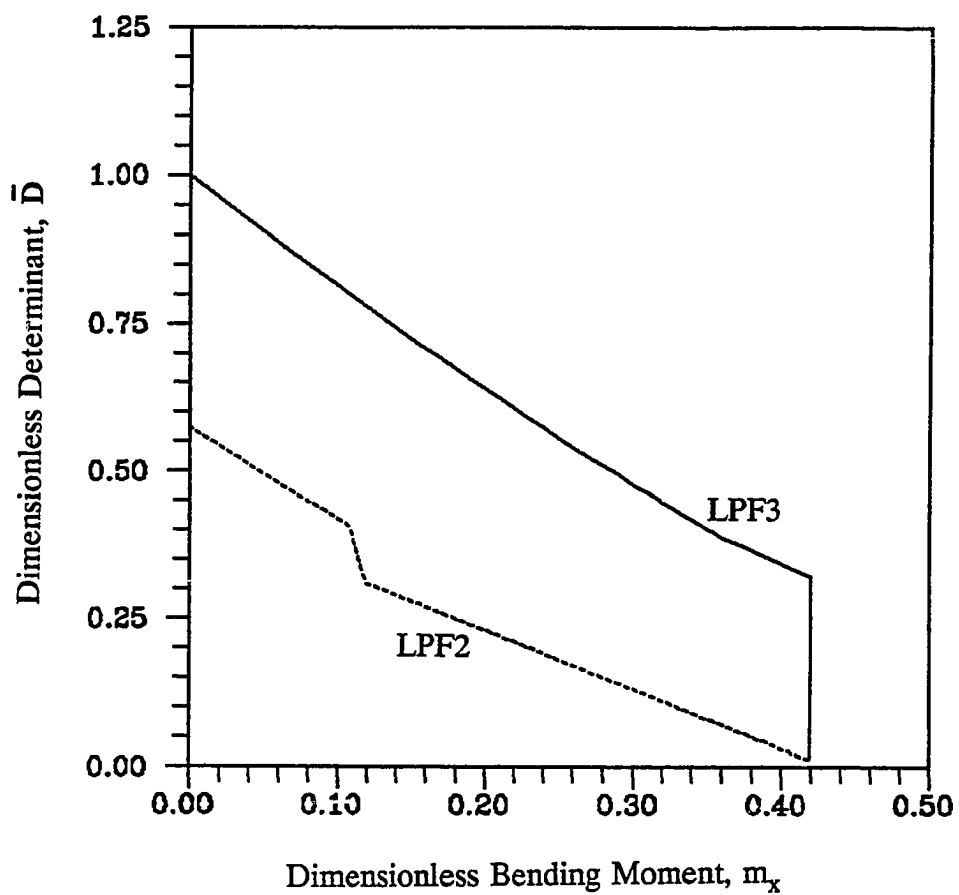


Figure 65. Stiffness degradation ($\bar{D} - m_x$) for sway plane frame PF9 with load paths LPF2 and LPF3

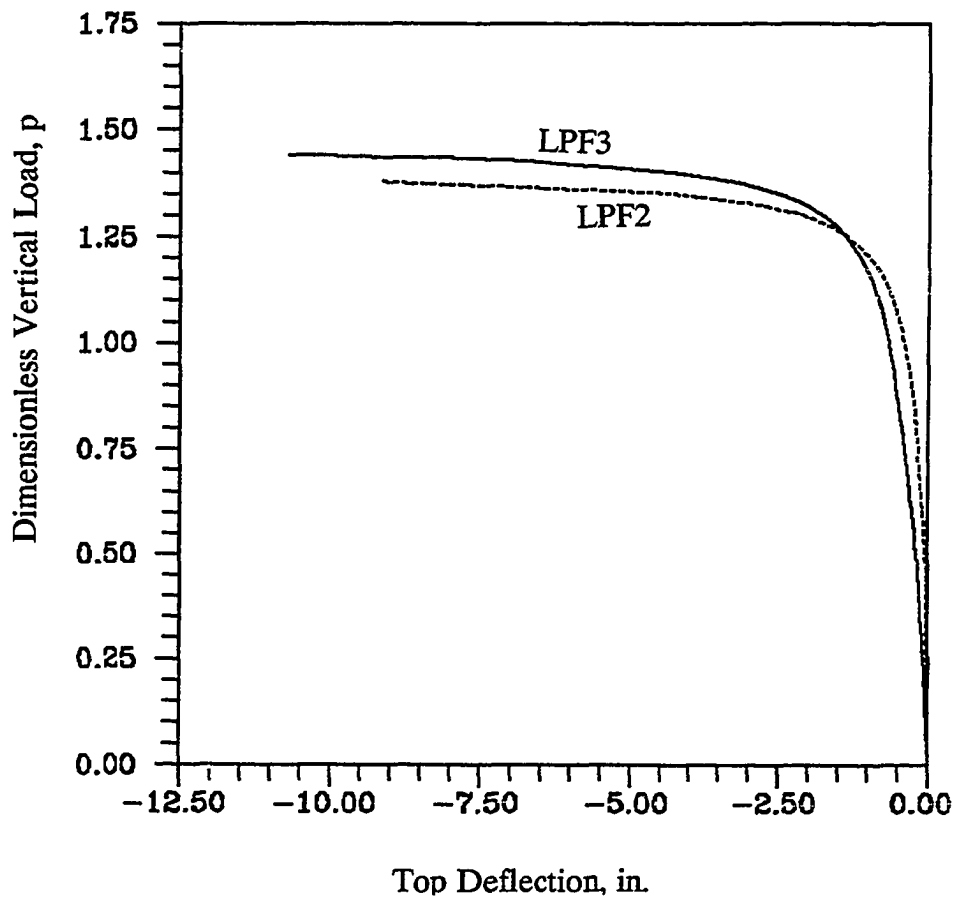


Figure 66. Dimensionless vertical load versus top deflection curves for sway portal frame PF9 with load paths LPF2 and LPF3

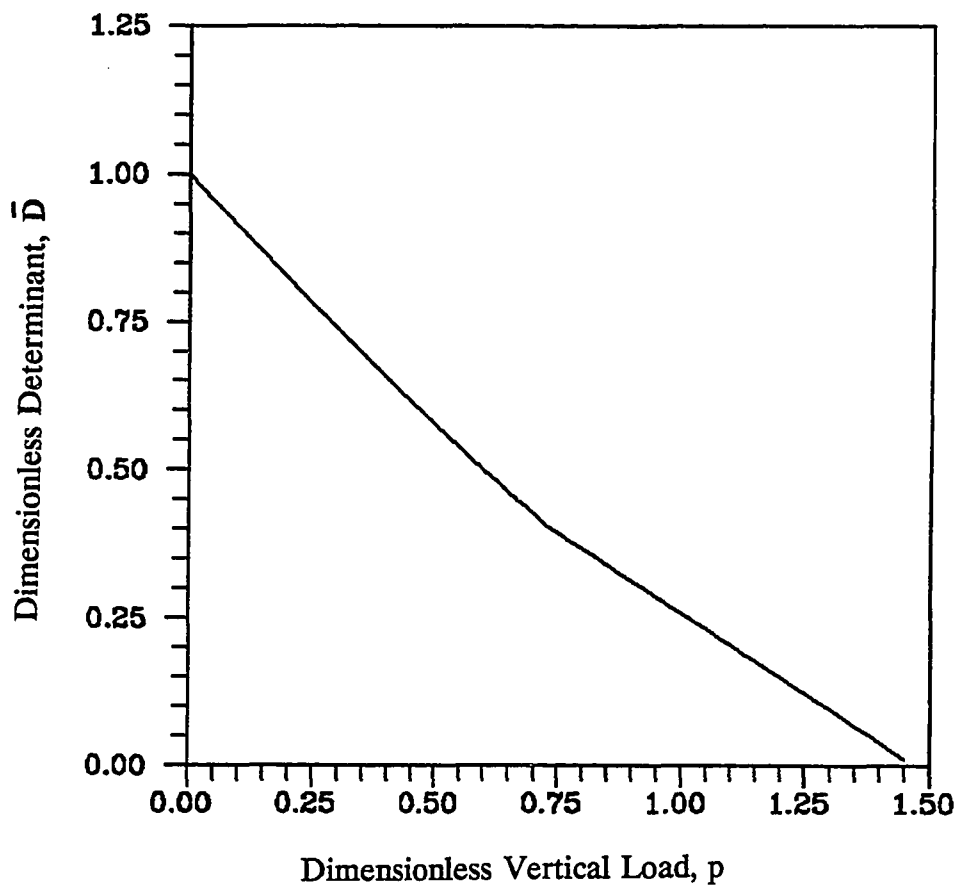


Figure 67. Stiffness degradation (\bar{D} - p) for sway plane frame PF10 with load path LPF2

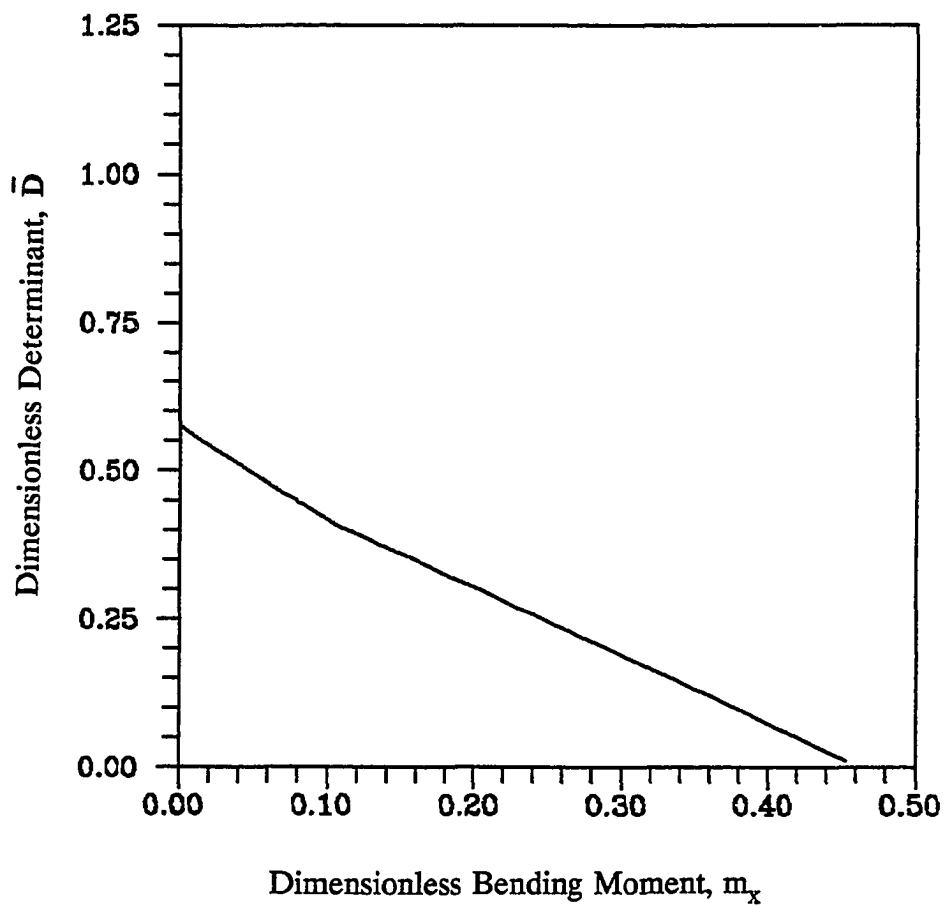


Figure 68. Dimensionless stiffness degradation ($\bar{D} - m_x$) for sway plane frame PF10 with load path LPF2

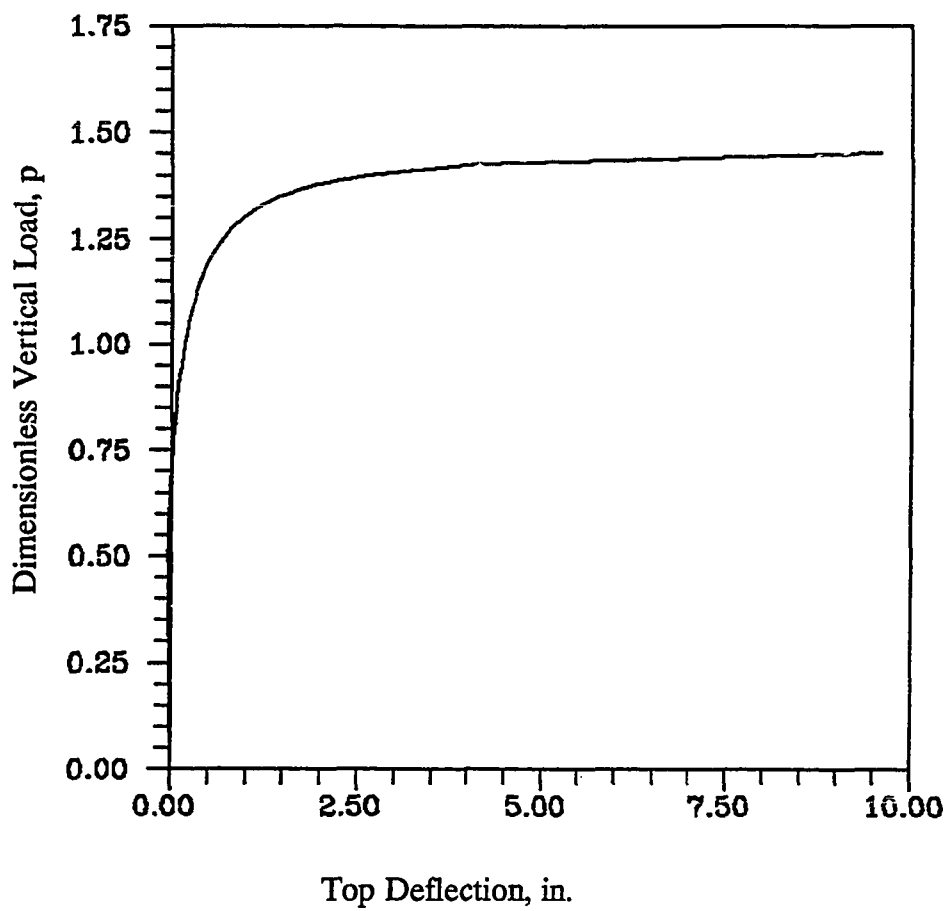


Figure 69. Dimensionless vertical load versus top deflection of plane frame PF10 with load path LPF2

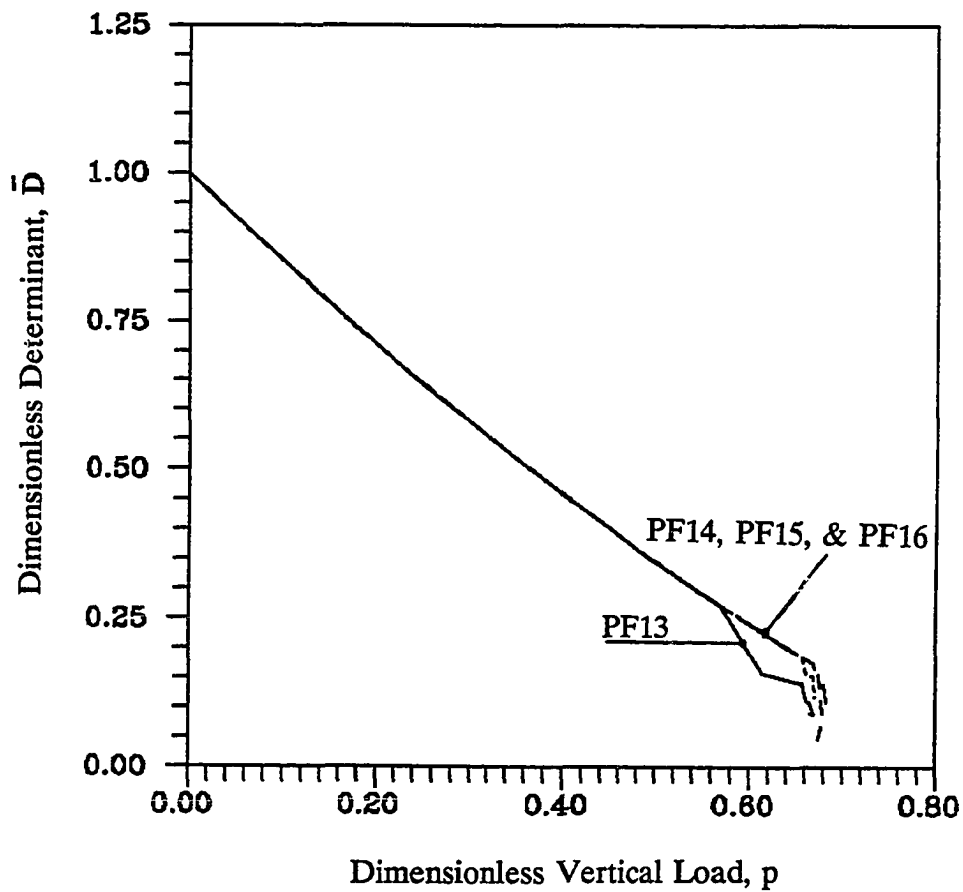


Figure 70. Effect of residual stresses and/or crookedness on stiffness degradation of sway portal frames under load path LPF1

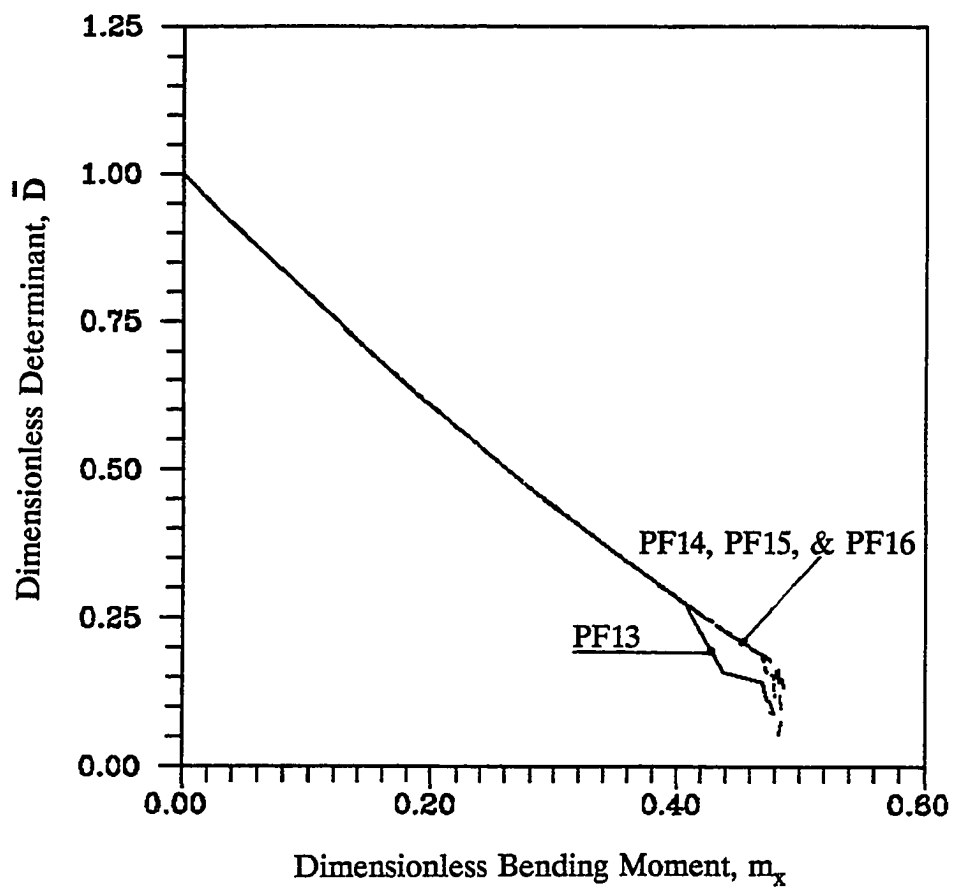


Figure 71. Stiffness degradation ($\bar{D} - m_x$) of sway portal frames with residual stresses and/or crookedness with load path LPF1

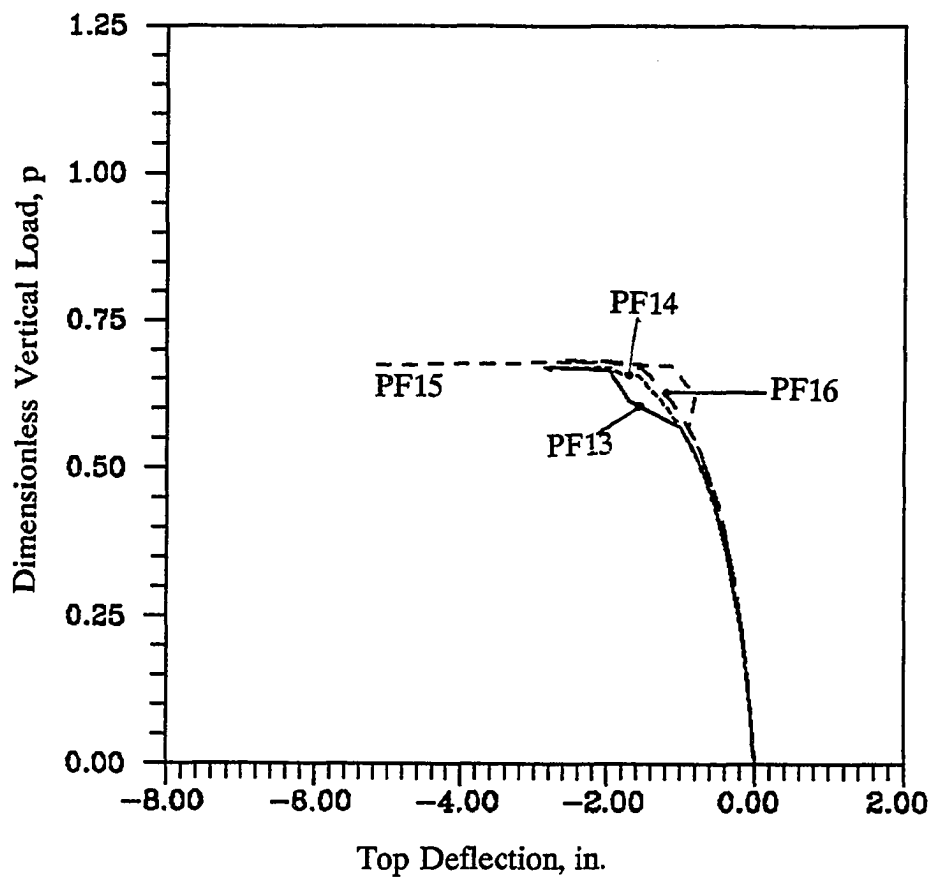


Figure 72. Dimensionless vertical load versus top deflection of plane frames with residual stresses and/or crookedness and with load path LPF1

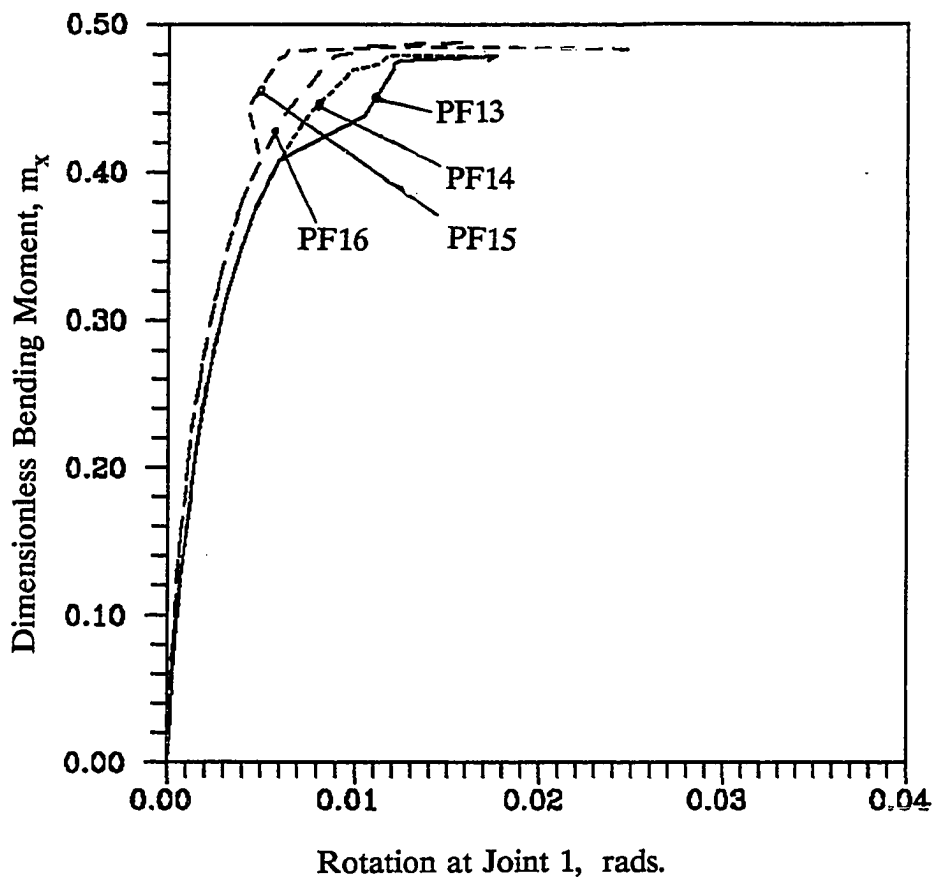


Figure 73. Dimensionless bending moment versus rotation at Joint 1 of plane frames with residual stresses and/or crookedness and with load path LPF1

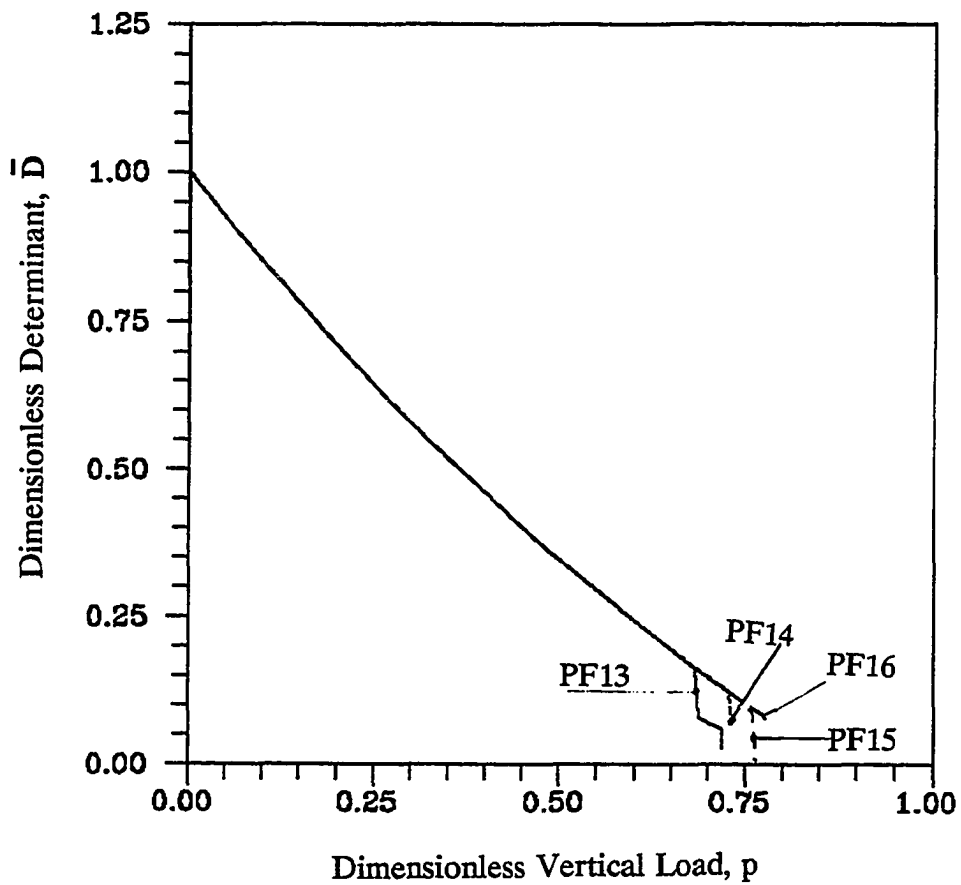


Figure 74. Stiffness degradation ($\bar{D} - p$) of sway portal frames with residual stresses and/or crookedness and with load path LPF2

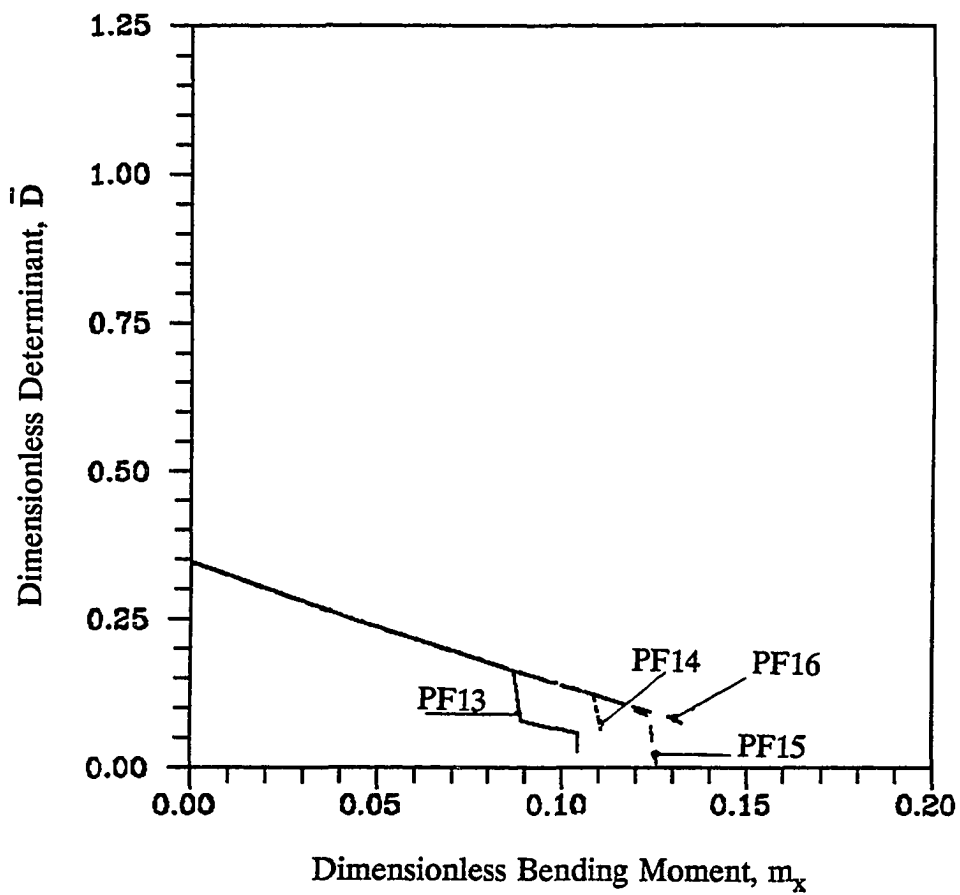


Figure 75. Stiffness degradation ($\bar{D} - m_x$) for sway portal frames with residual stresses and/or crookedness and with load path LPF2

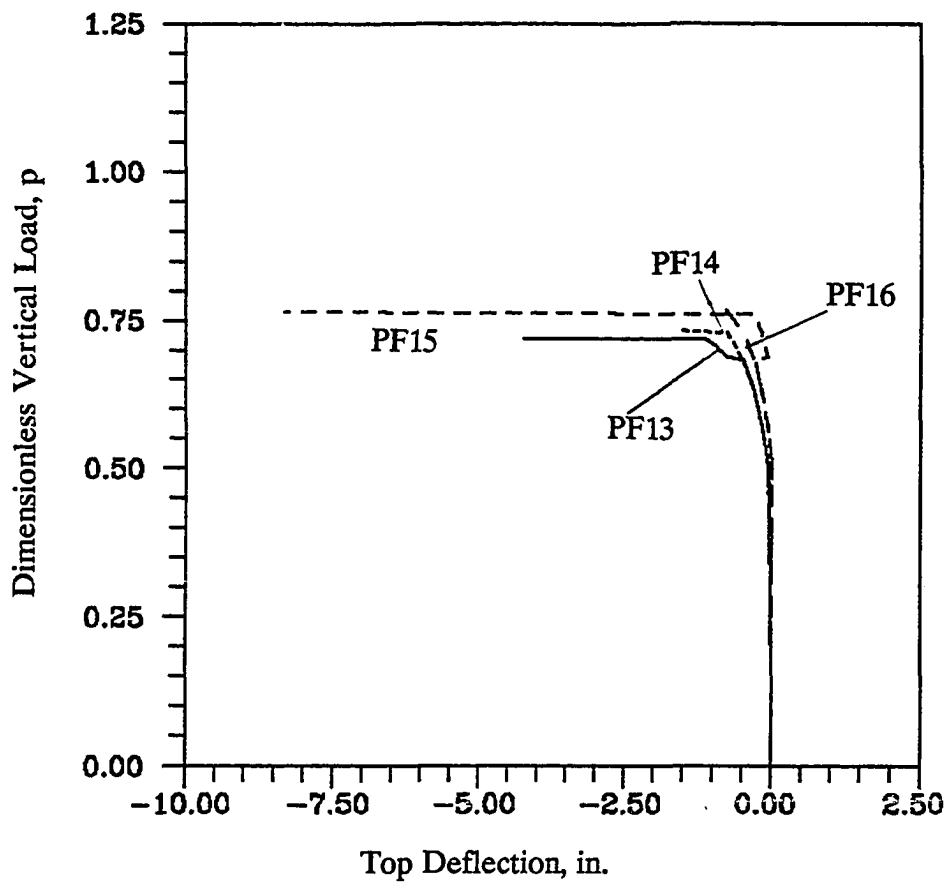


Figure 76. Dimensionless vertical load versus top deflection of plane frames with residual stresses and/or crookedness and with load path LPF2

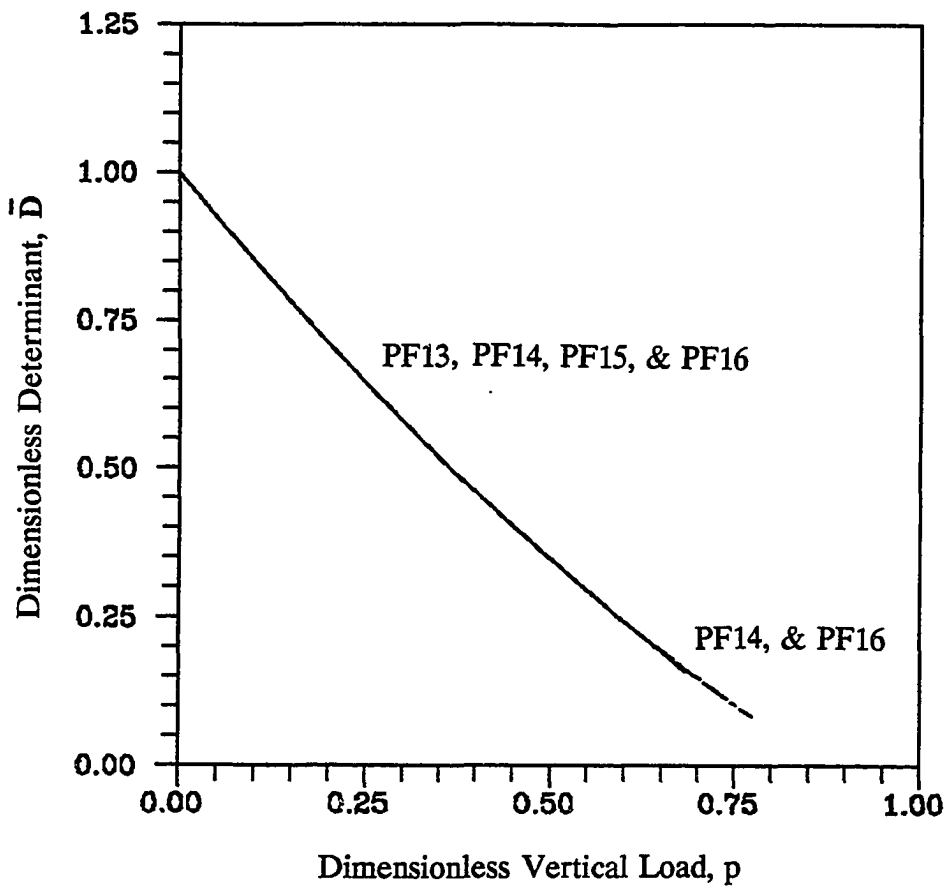


Figure 77. Stiffness degradation ($\bar{D} - p$) of sway portal frames with residual stresses and/or crookedness and with load path LPF3

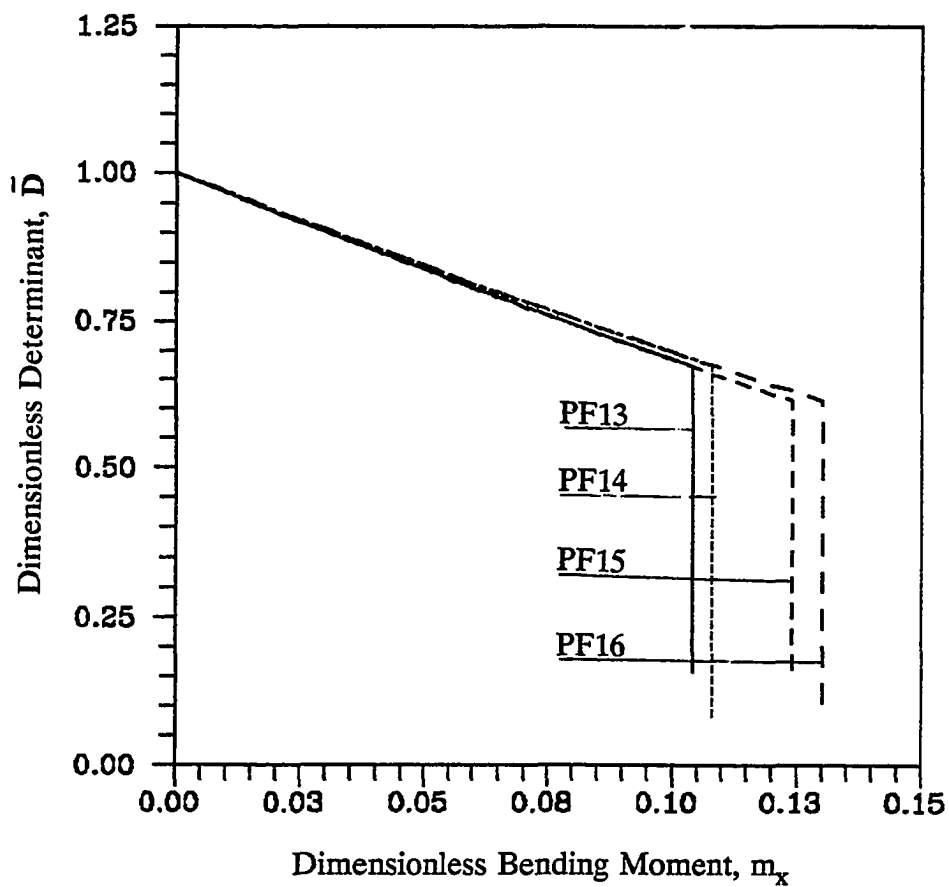


Figure 78. Stiffness degradation ($\bar{D} - m_x$) for sway portal frames with residual stresses and/or crookedness and with load path LPF3

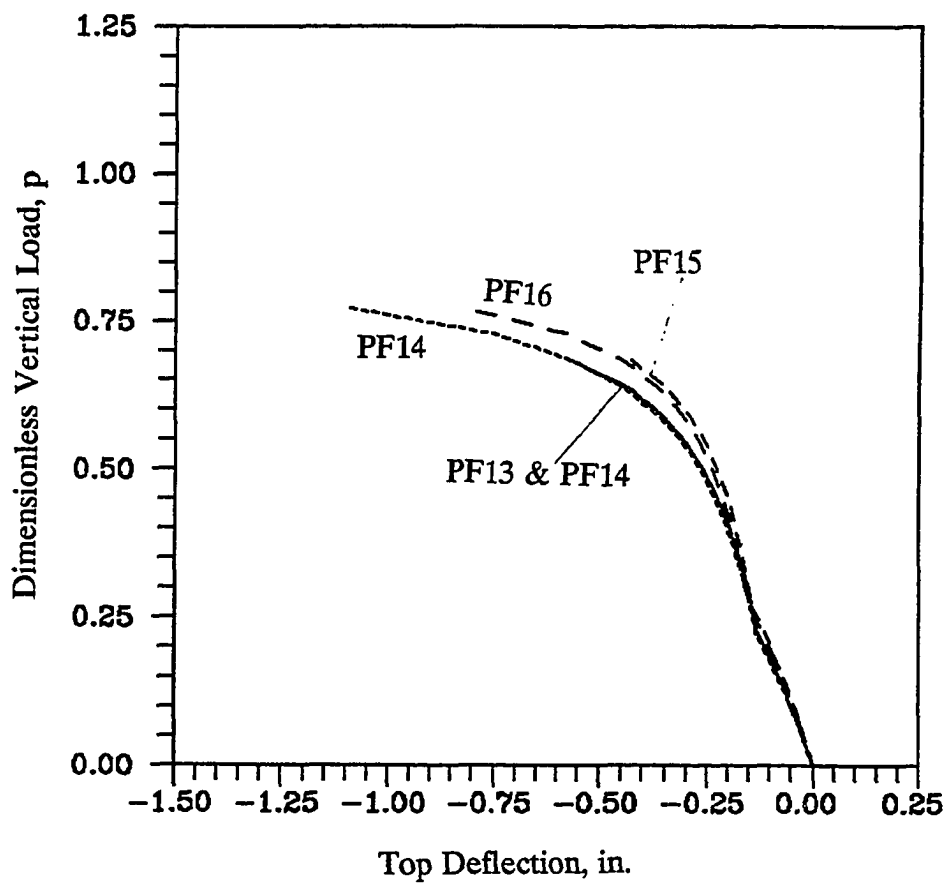


Figure 79. Dimensionless vertical load versus top deflection of plane frames with residual stresses and/or crookedness and with load path LPF3

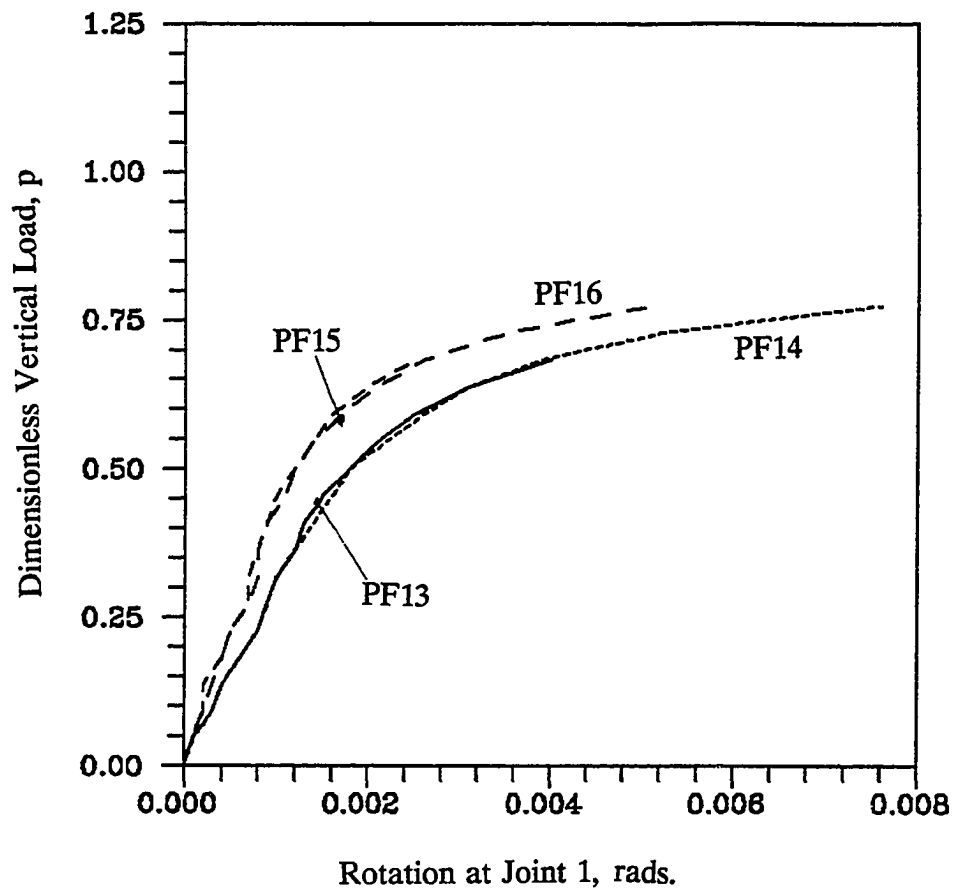


Figure 80. Dimensionless vertical load versus rotation at Joint 1 of sway plane frames with residual stresses and/or crookedness and with load path LPF3

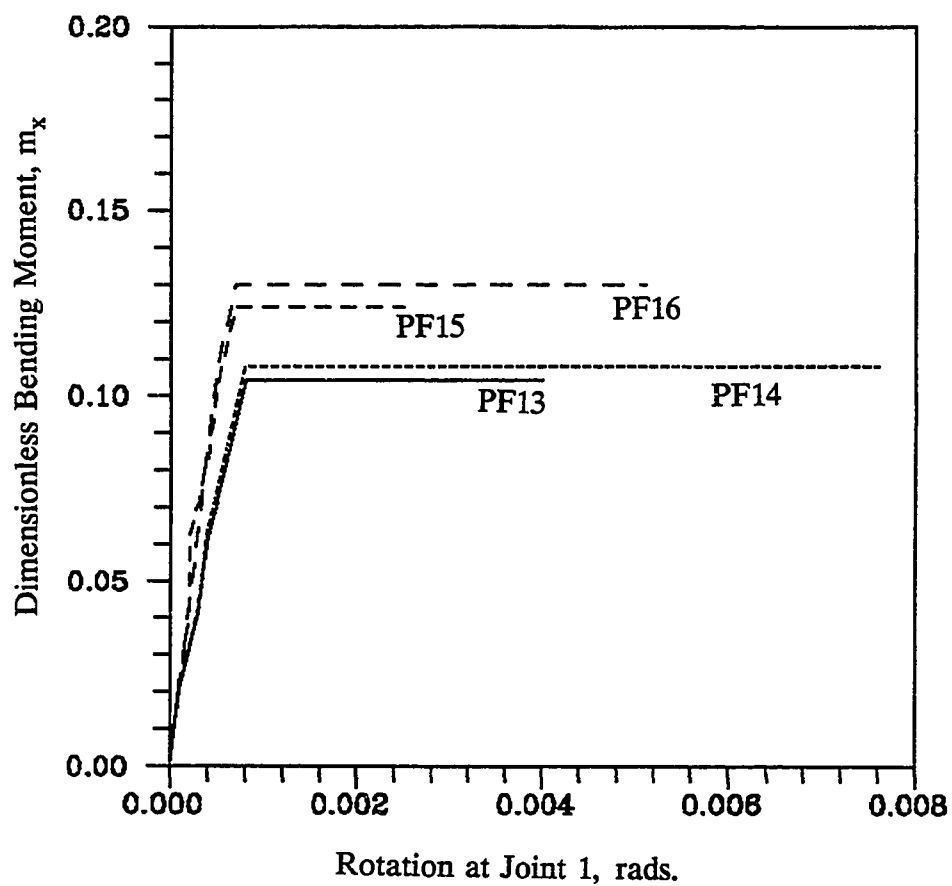


Figure 81. Dimensionless bending moment versus rotation at Joint 1 of sway plane frames with residual stresses and/or crookedness and with load path LPF3

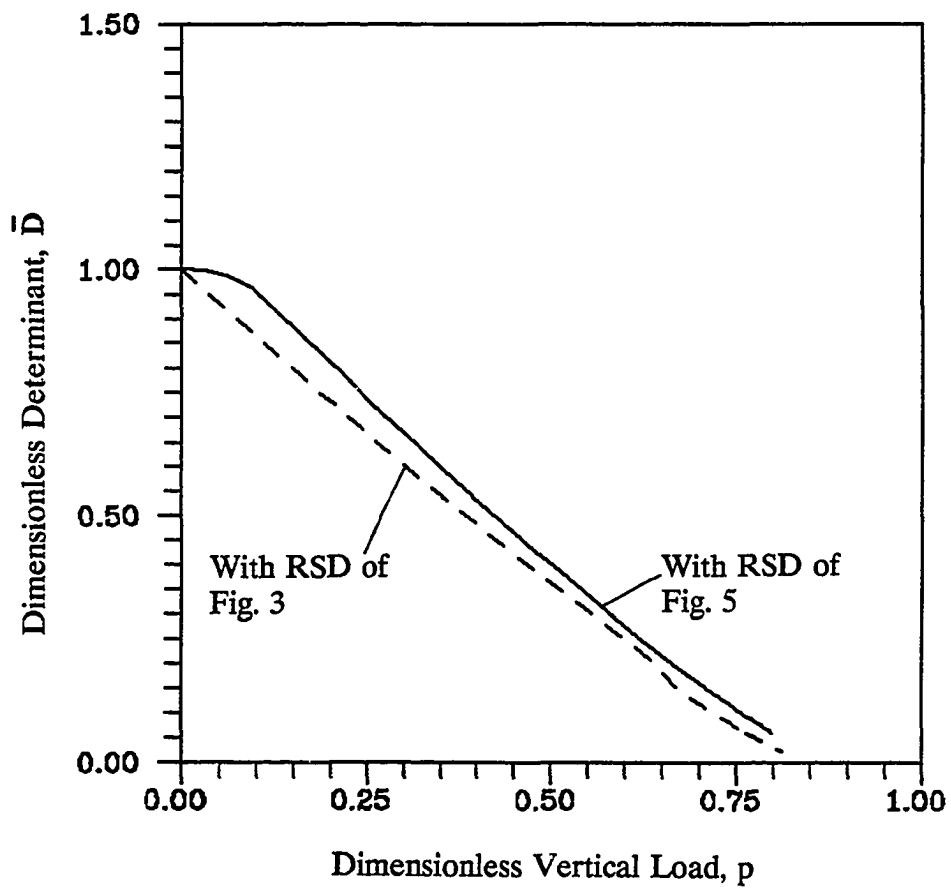


Figure 82. Stiffness degradation of sway portal frame with different residual stress distributions (RSDs) and load path LPF1

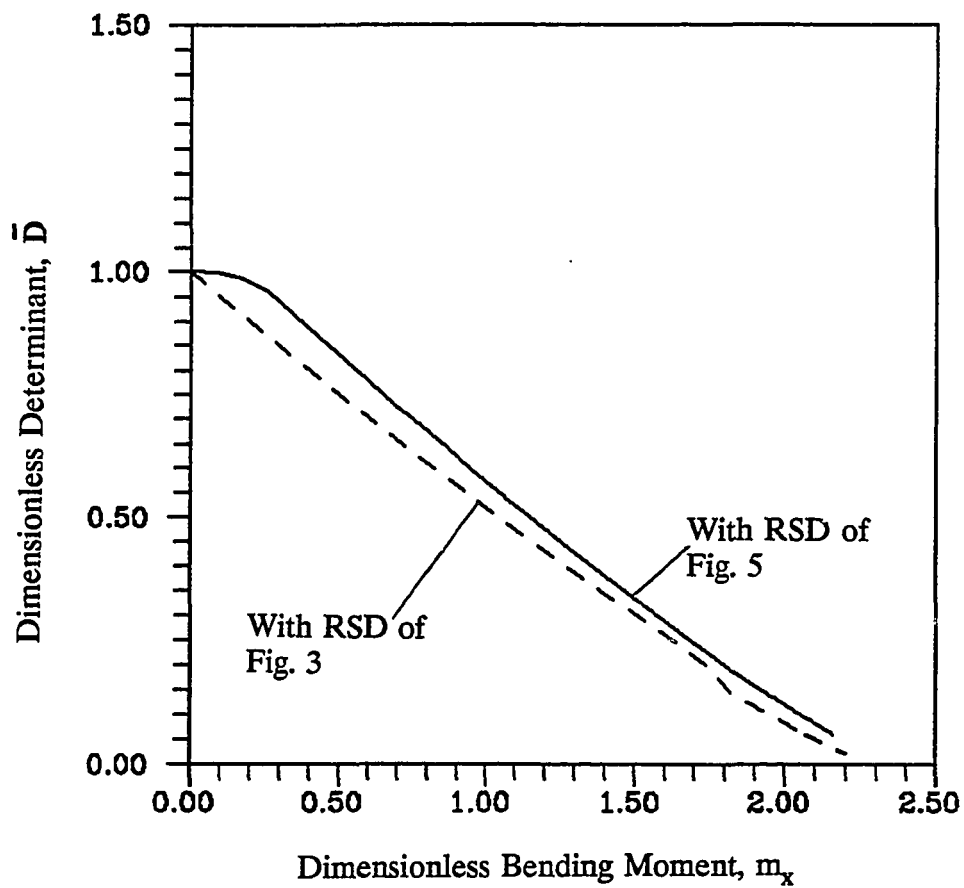


Figure 83. Stiffness degradation of sway portal frame with different residual stress distribution and load path LPF1

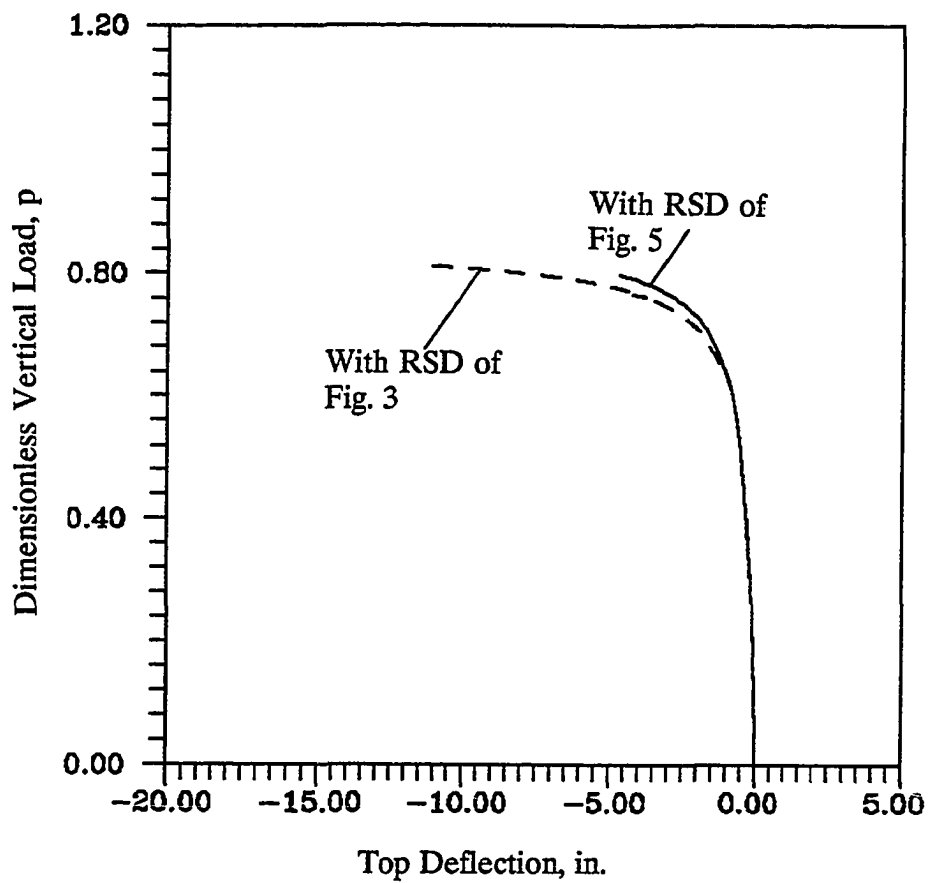


Figure 84. Dimensionless vertical load versus top deflection of sway portal frame with load path LPF1 and different residual stress distributions (RSDs)

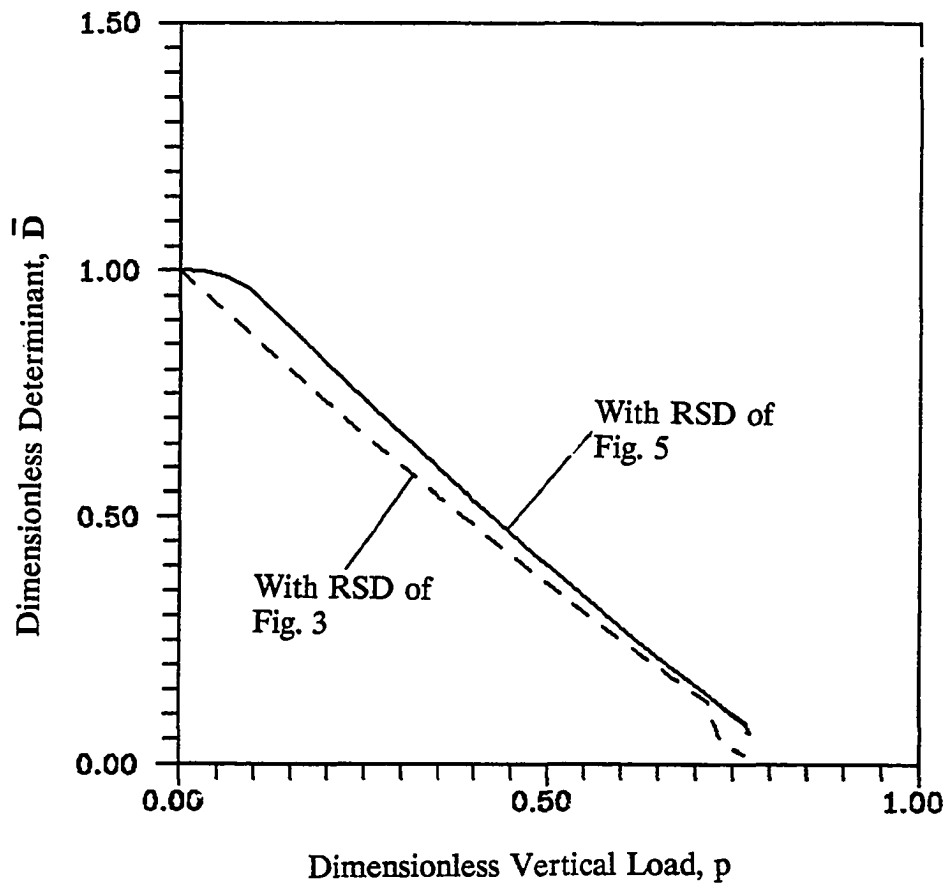


Figure 85. Stiffness degradation ($\bar{D} - p$) of sway portal frame with load path LPF2 and different residual stress distributions (RSDs)

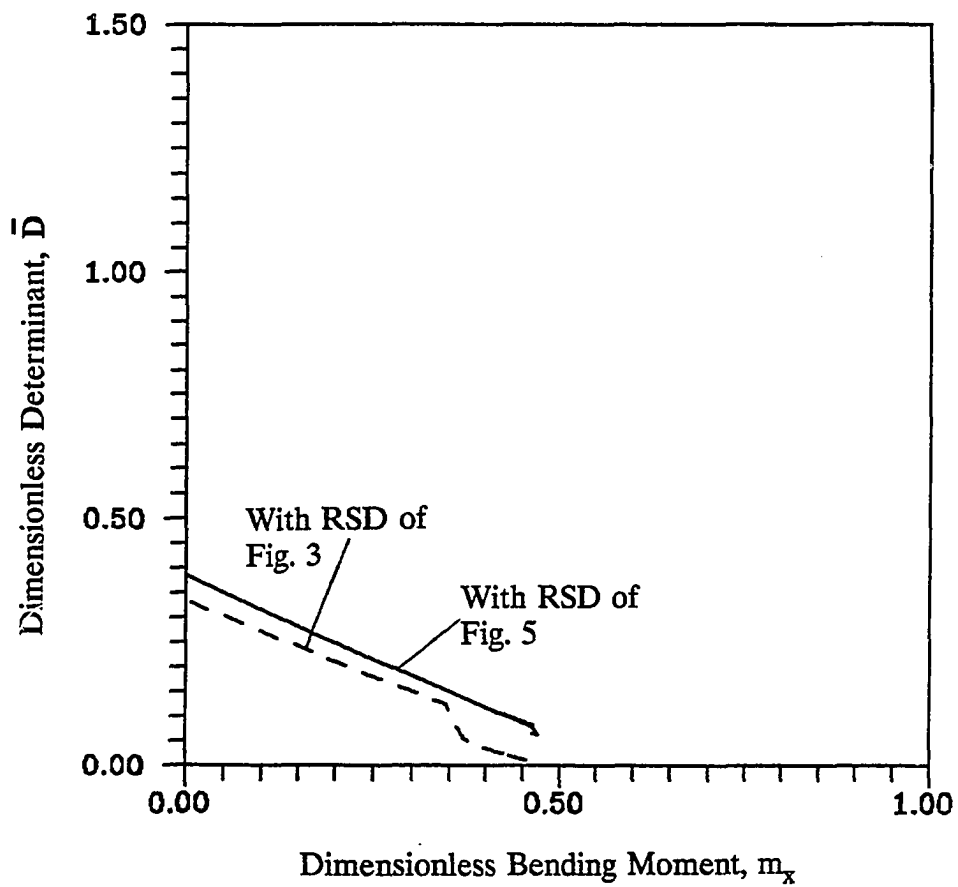


Figure 86. Stiffness degradation ($\bar{D} - m_x$) of sway portal frame with load path LPF2 and different residual stress distributions (RSDs)

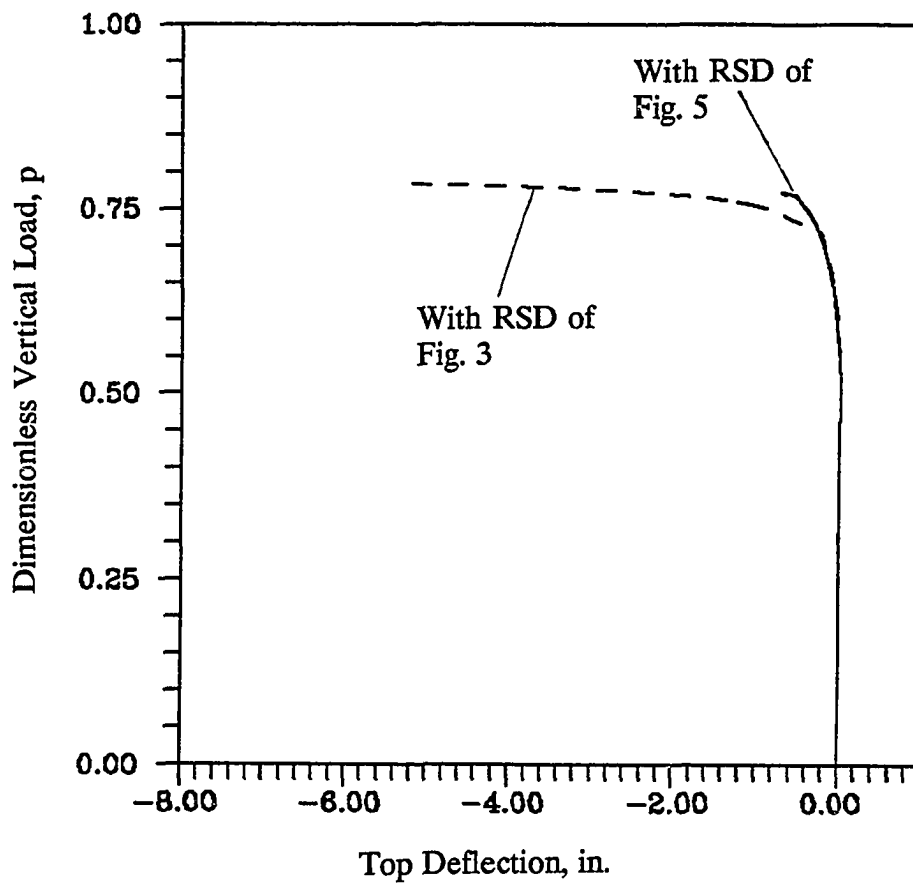


Figure 87. Dimensionless vertical load versus top deflection of sway portal frame with load path LPF2 and different residual stress distributions (RSDs)

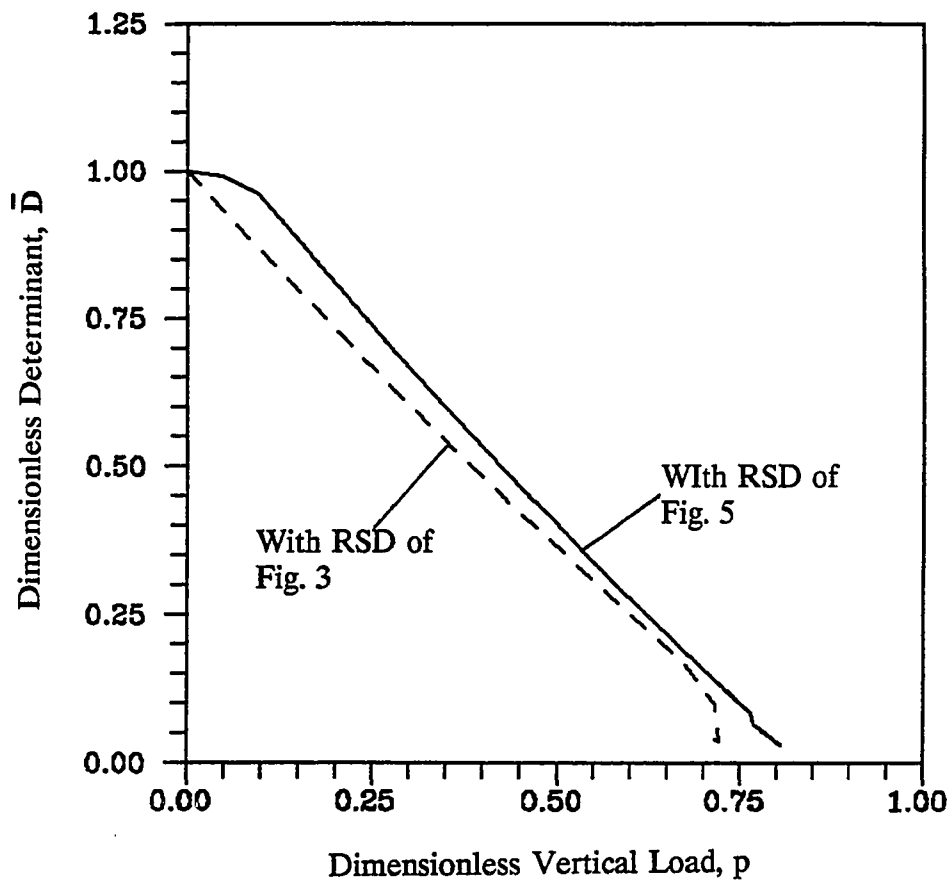


Figure 88. Stiffness degradation ($\bar{D} - p$) of sway portal frame with load path LPF3 and different residual stress distributions (RSDs)

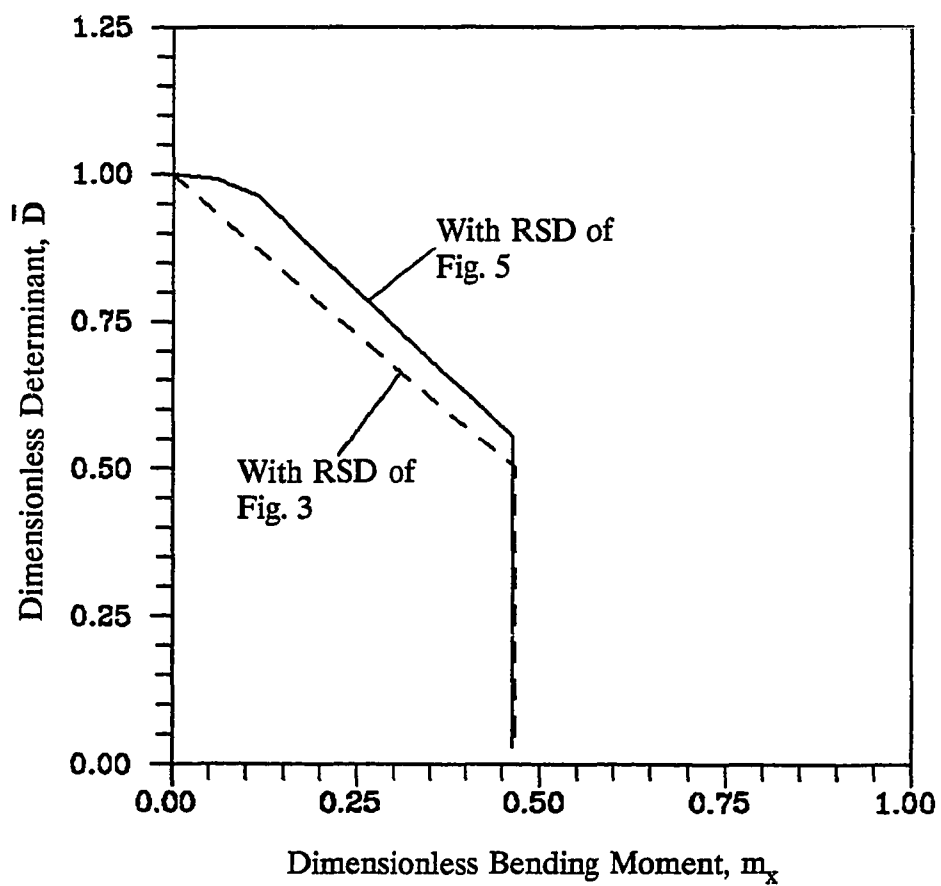


Figure 89. Stiffness degradation ($\bar{D} - m_x$) of sway portal frame with load path LPF3 and different residual stress distributions (RSDs)

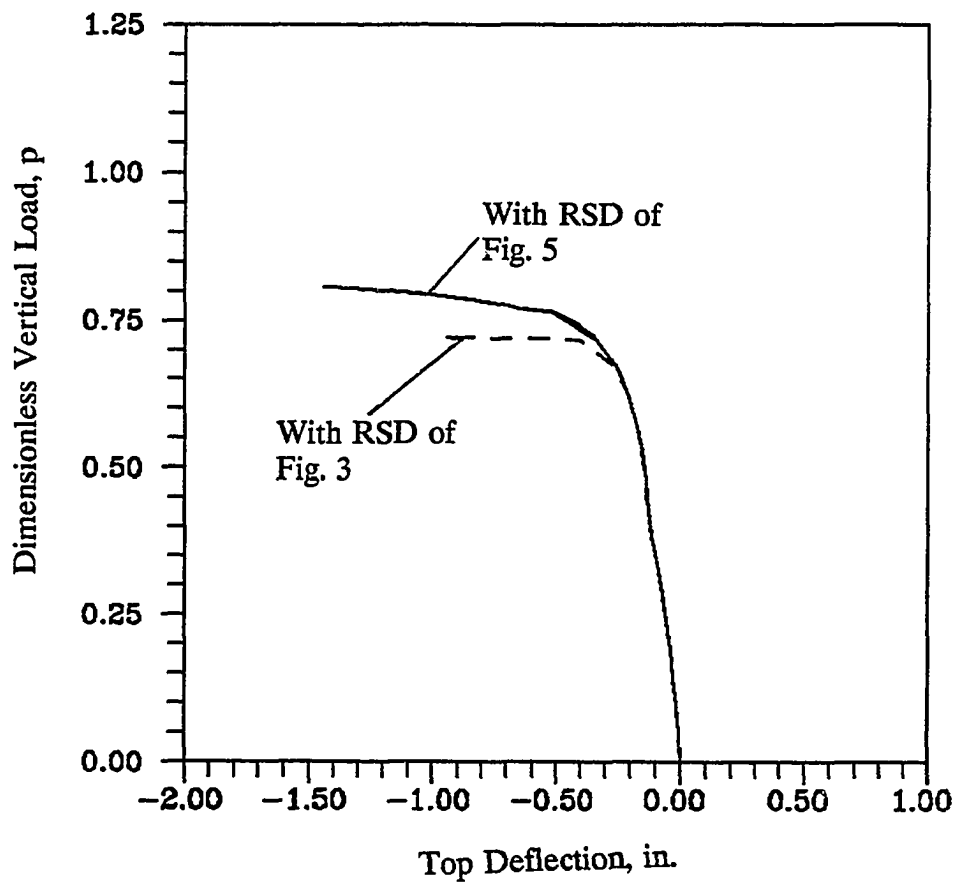


Figure 90. Dimensionless vertical load versus top deflection of sway portal frame with load path LPF3 and different residual stress distribution (RSDs)

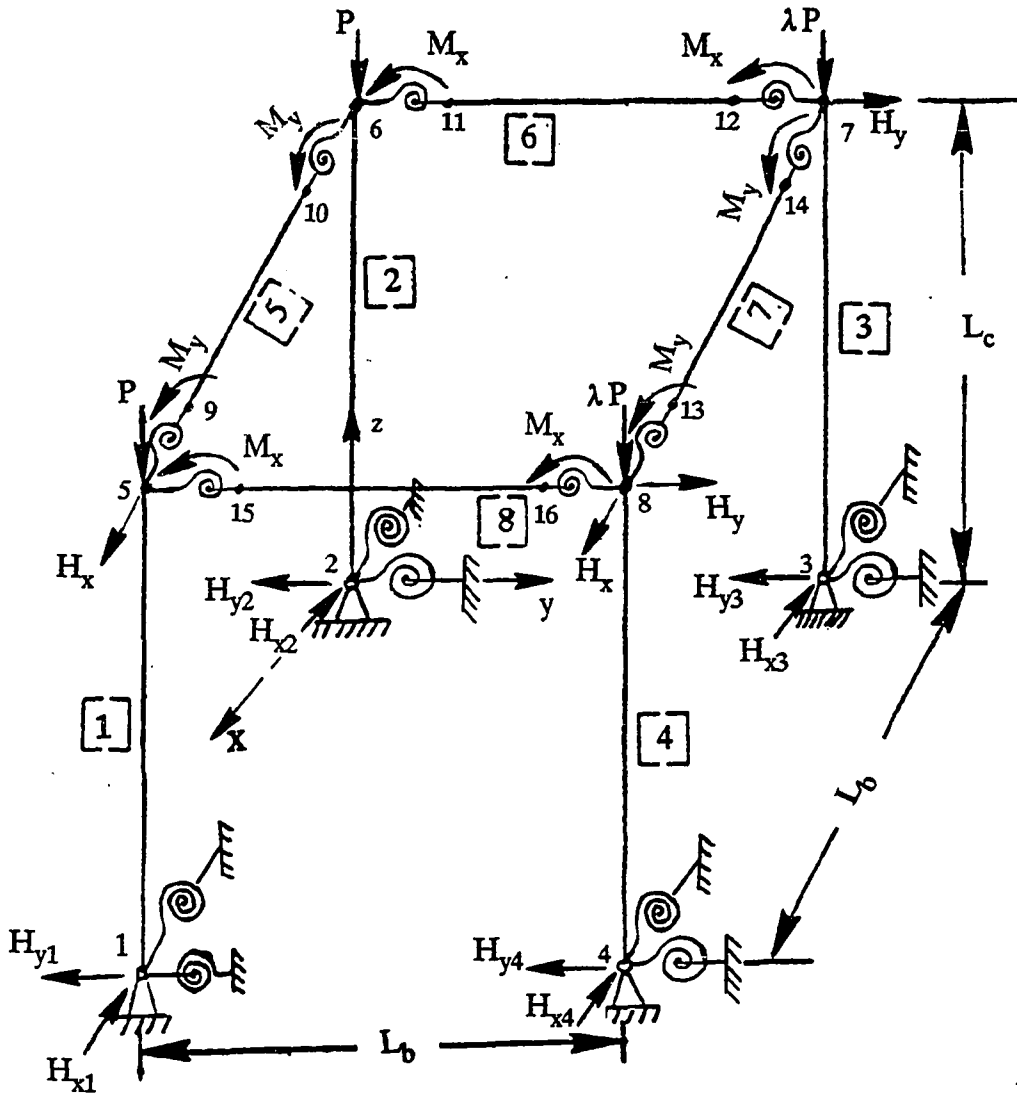
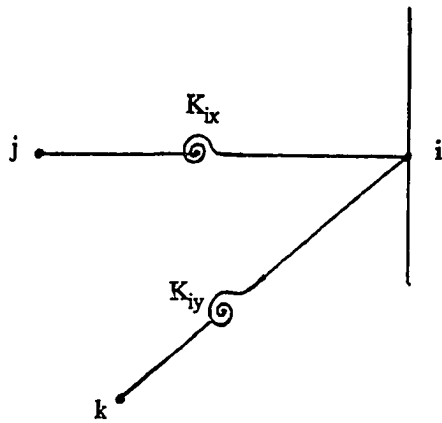
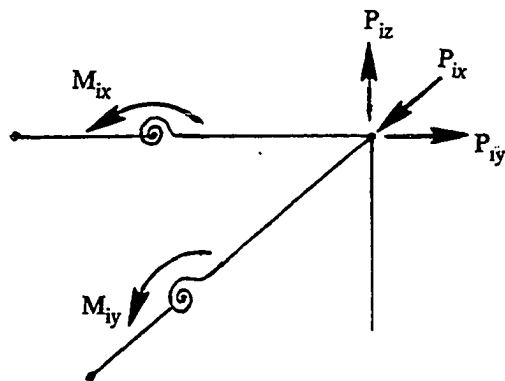


Figure 91. Flexibly-connected single-story single-bay unbraced sway space frame



(a) Spring and nodes



(b) Joint loads

Figure 92. Typical space frame joint

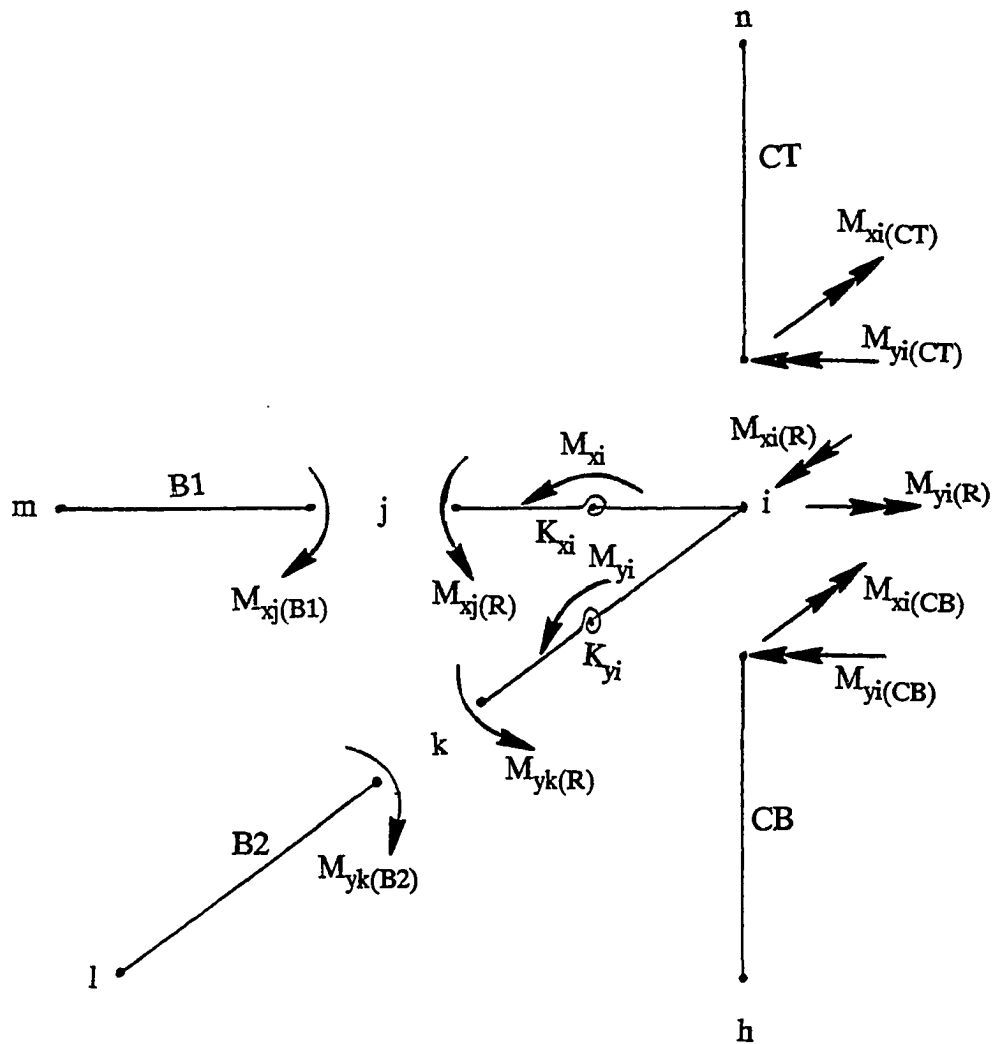


Figure 93. Space frame joint moments used in slope-deflection formulation

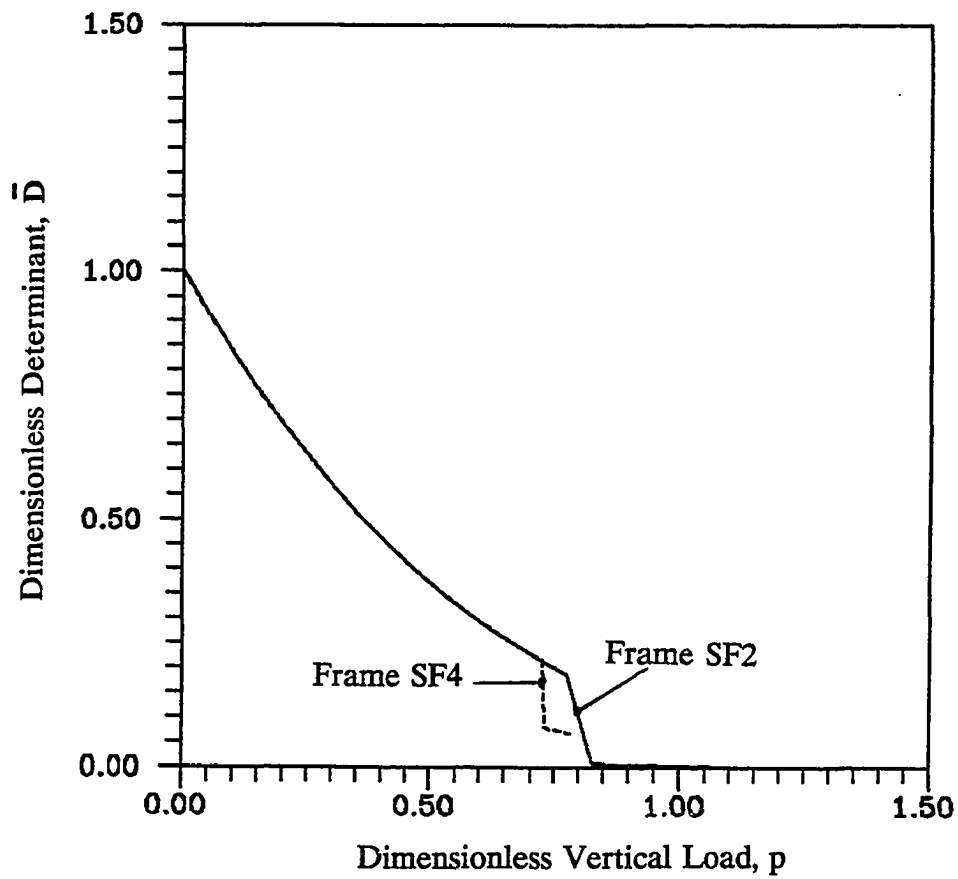


Figure 94. Stiffness degradation ($\bar{D} - p$) of single-story single-bay sway space frames SF2 and SF4

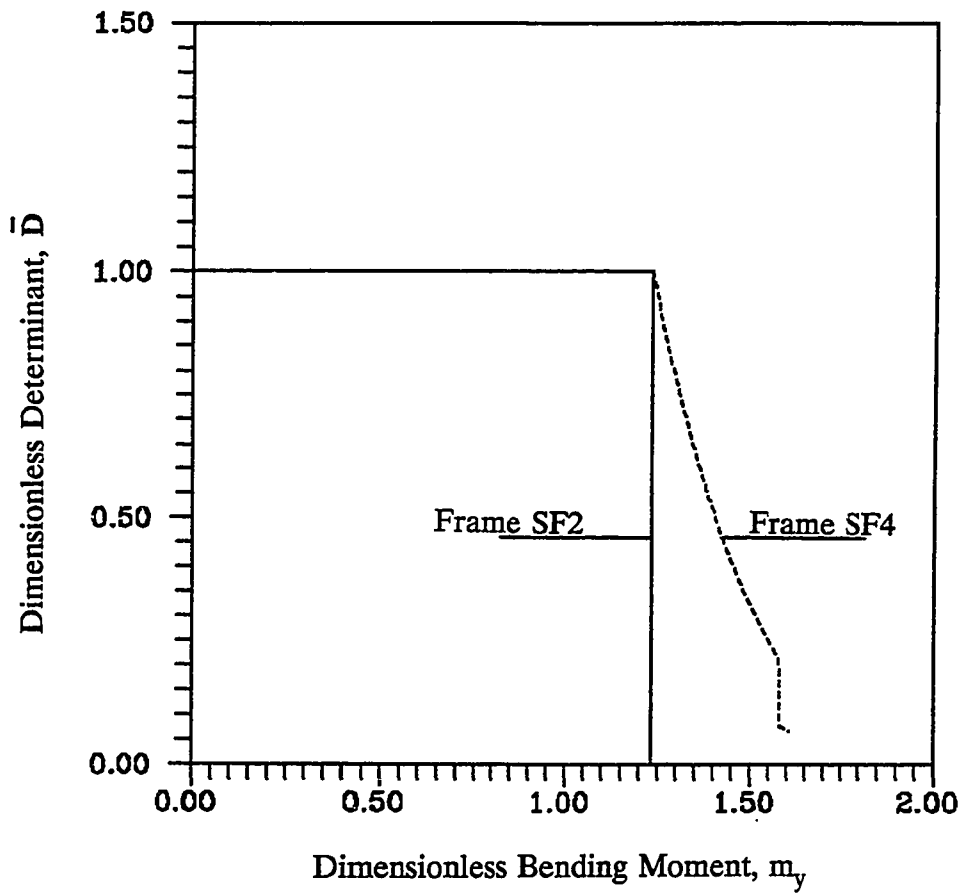


Figure 95. Stiffness degradation ($\bar{D} - m_y$) of single-story single-bay sway space frames SF2 and SF4

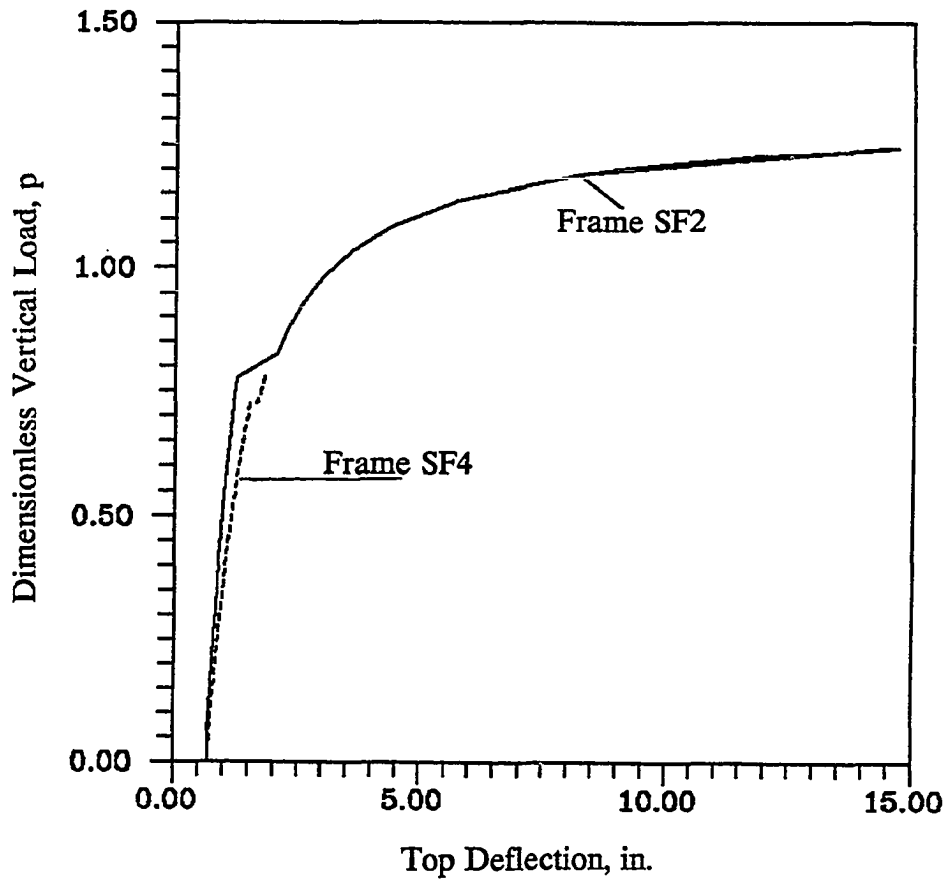


Figure 96. Dimensionless vertical load versus top deflection ($p - \Delta_x$) of single-story single-bay sway space frames SF2 and SF4

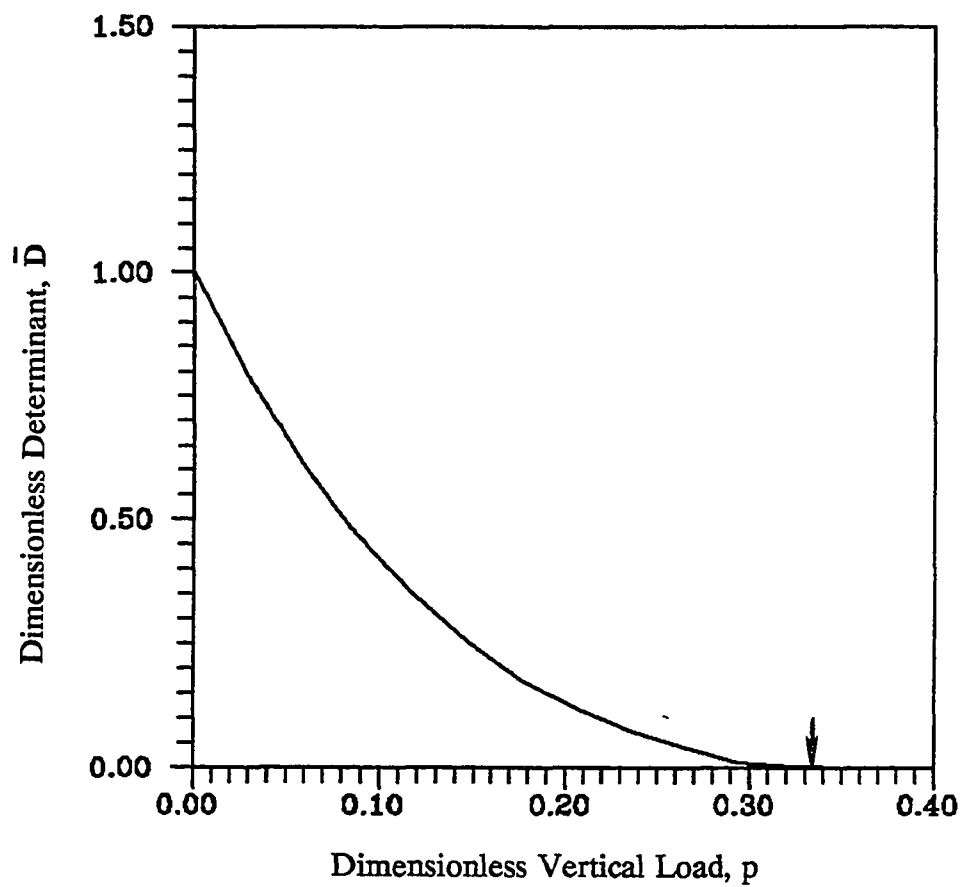


Figure 97. Stiffness degradation ($\bar{D} - p$) of single-story single-bay sway space frame SF24

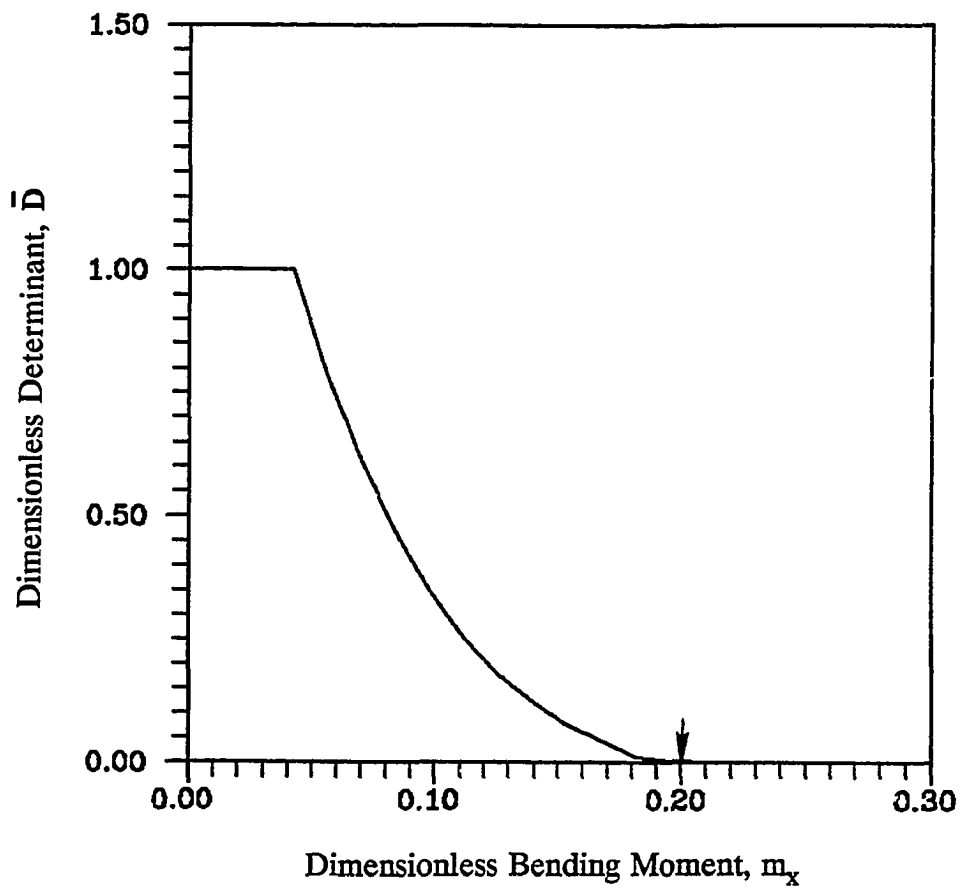


Figure 98. Stiffness degradation ($\bar{D} - m_x$) of single-story single-bay sway space frame SF24

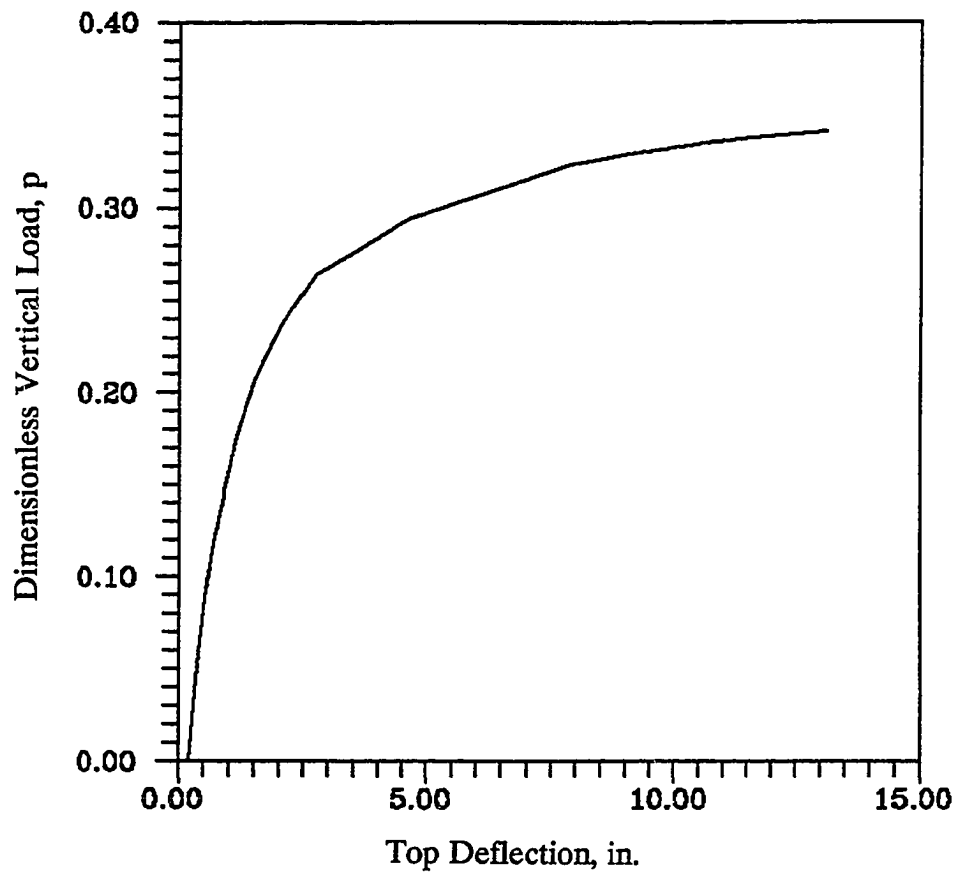


Figure 99. Dimensionless vertical load versus top deflection ($p - \Delta_x$) of single-bay single-story sway space frame SF24

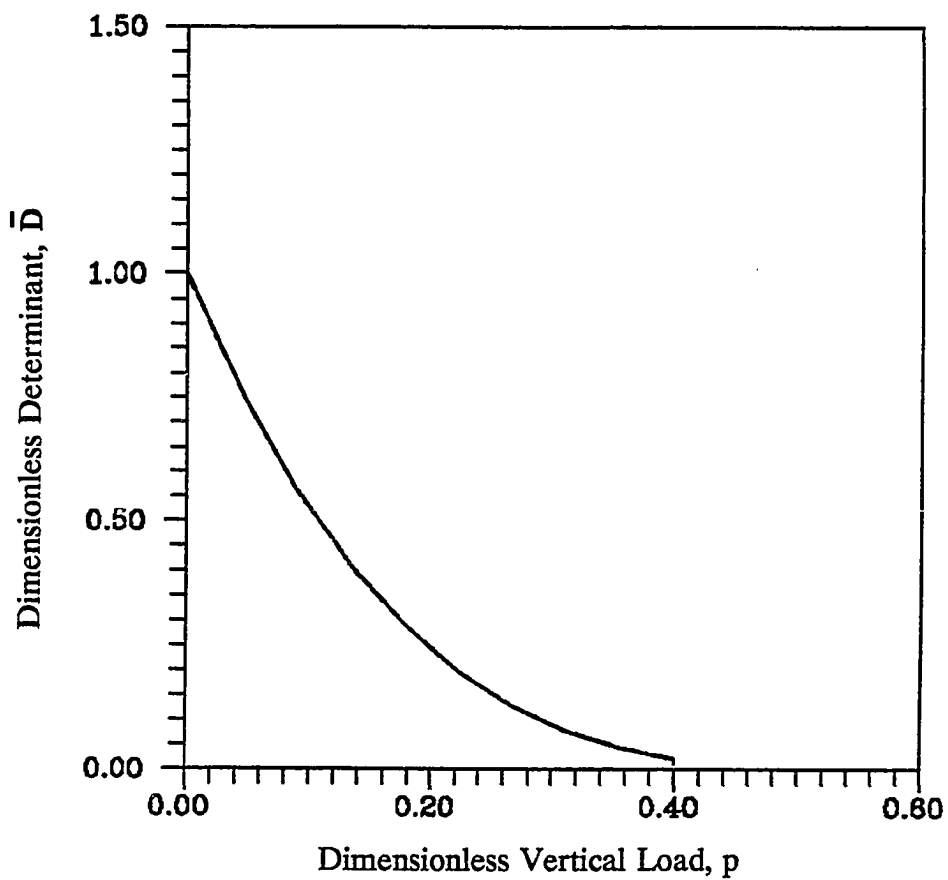


Figure 100. Stiffness degradation ($\bar{D} - p$) for single-story single-bay sway space frames with various combinations of residual stresses and crookedness, with load path SL1

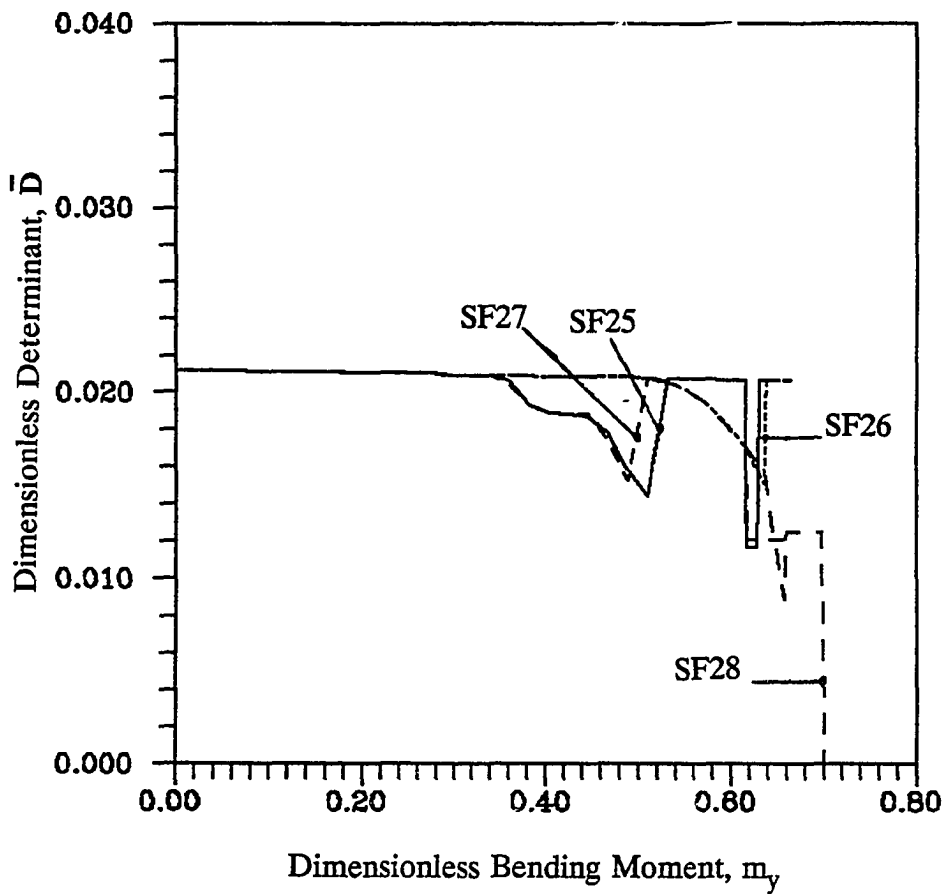


Figure 101. Stiffness degradation ($\bar{D} - m_y$) for single-story single-bay sway space frames with various combinations of residual stresses and crookedness, with load path SL1

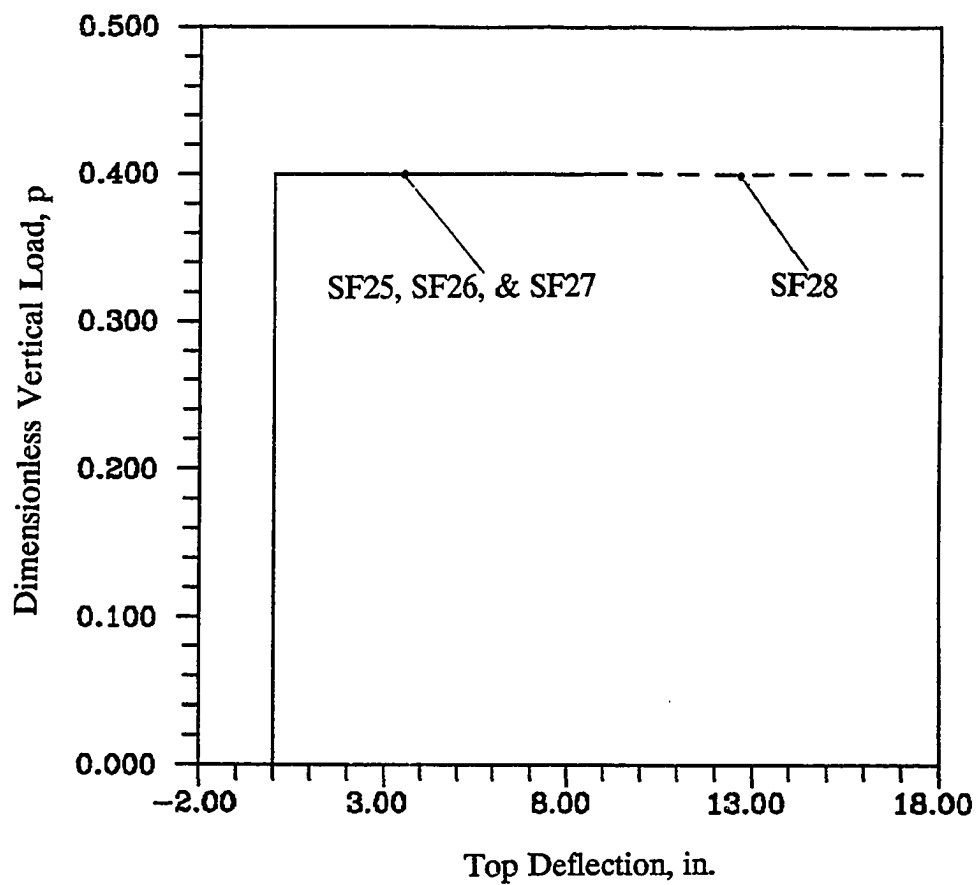


Figure 102. Dimensionless vertical load versus top deflection ($p - \Delta_x$) for single-story single-bay sway space frames with various combinations of residual stresses and crookedness; with load path SL1

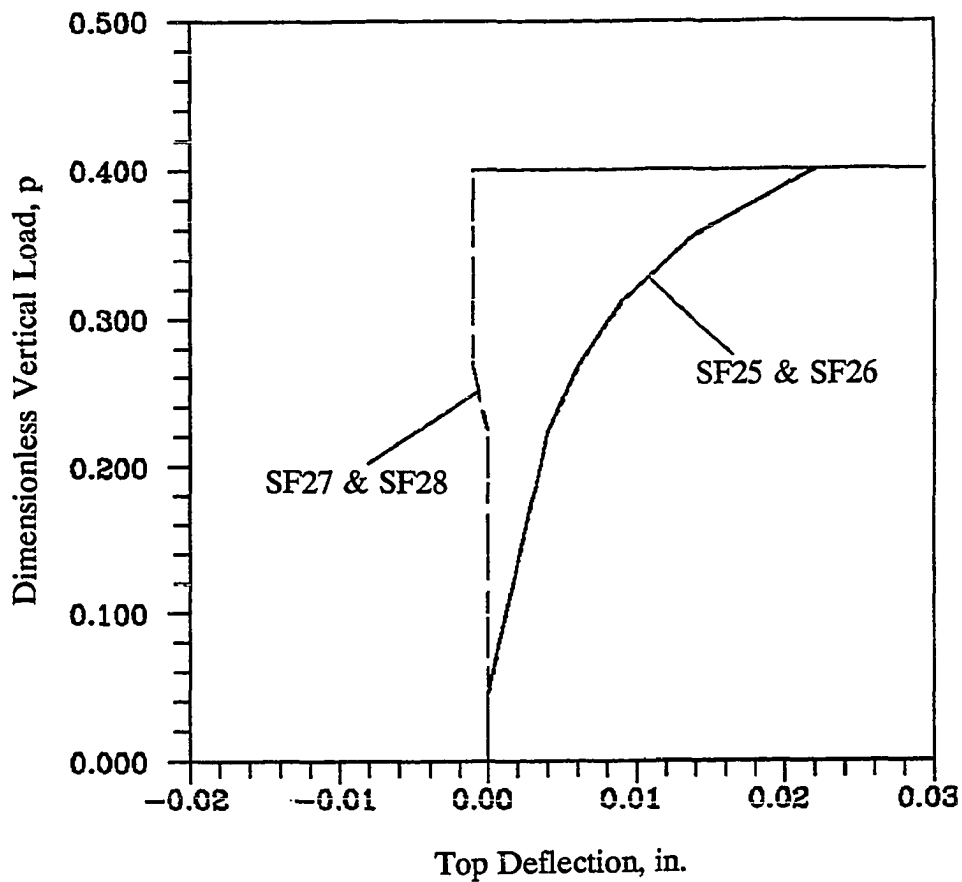


Figure 103. Dimensionless vertical load versus top deflection ($p - \Delta_x$) relationships of Figure 102 with horizontal scale magnification

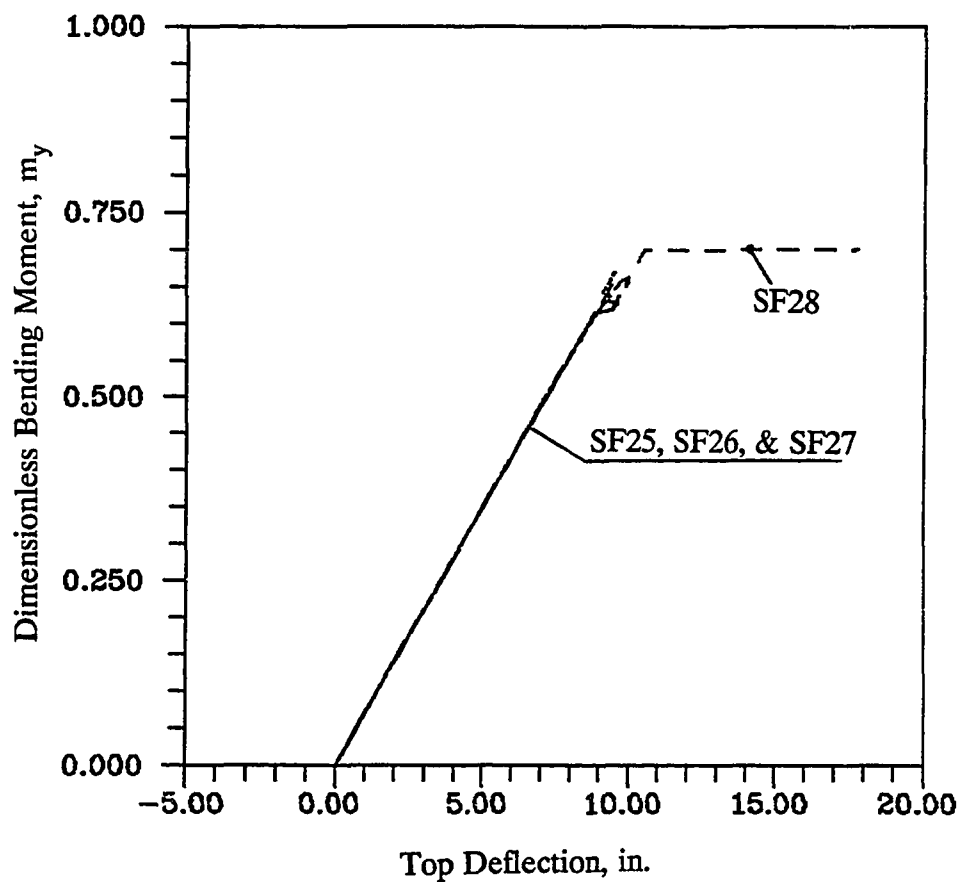


Figure 104. Dimensionless bending moment versus top deflection ($m_y - \Delta_x$) for single-story single-bay sway space frames with various combinations of residual stresses and crookedness, with load path SL1

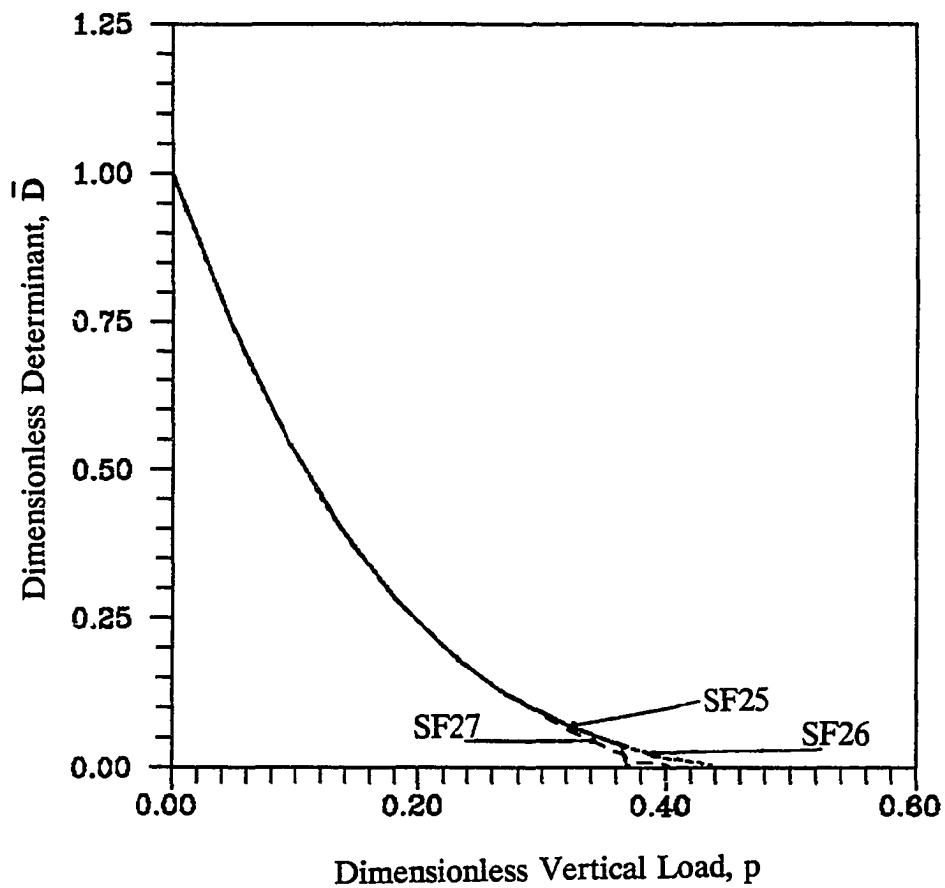


Figure 105. Stiffness degradation ($\bar{D} - p$) for a single-bay single-story space frames with different combination of residual stresses and crookedness, with load path SL2

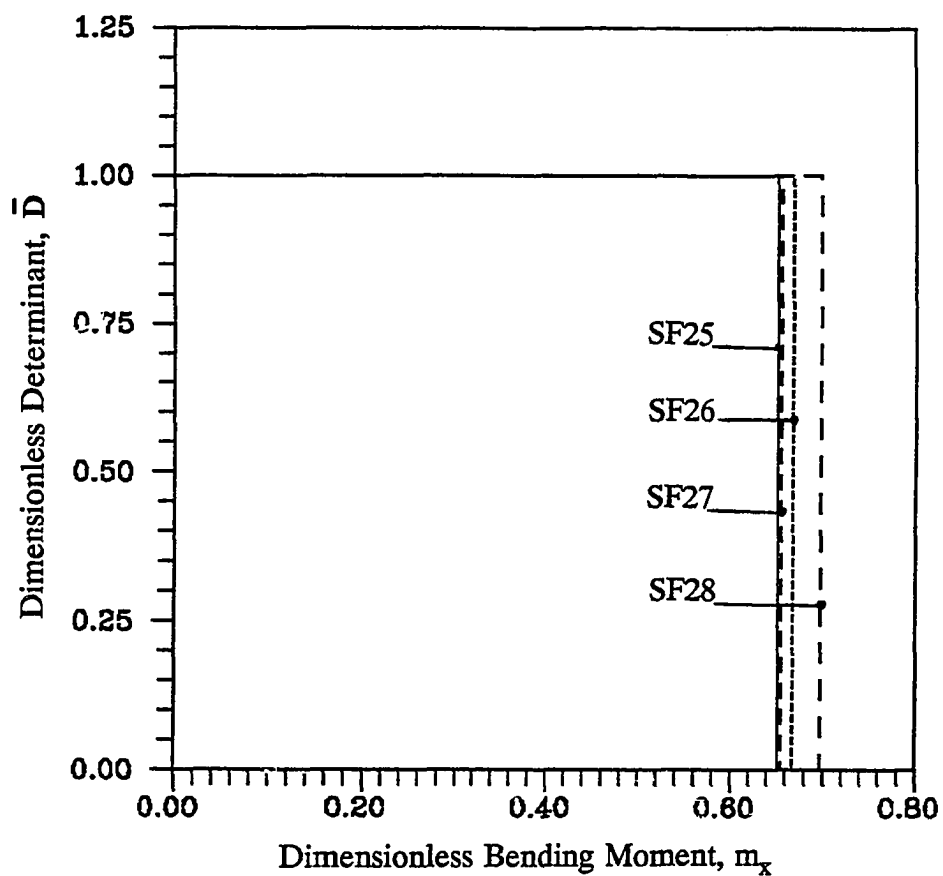


Figure 106. Stiffness degradation ($\bar{D} - m_x$) for single-story single-bay sway space frames with various combinations of residual stresses and crookedness, with load path SL2

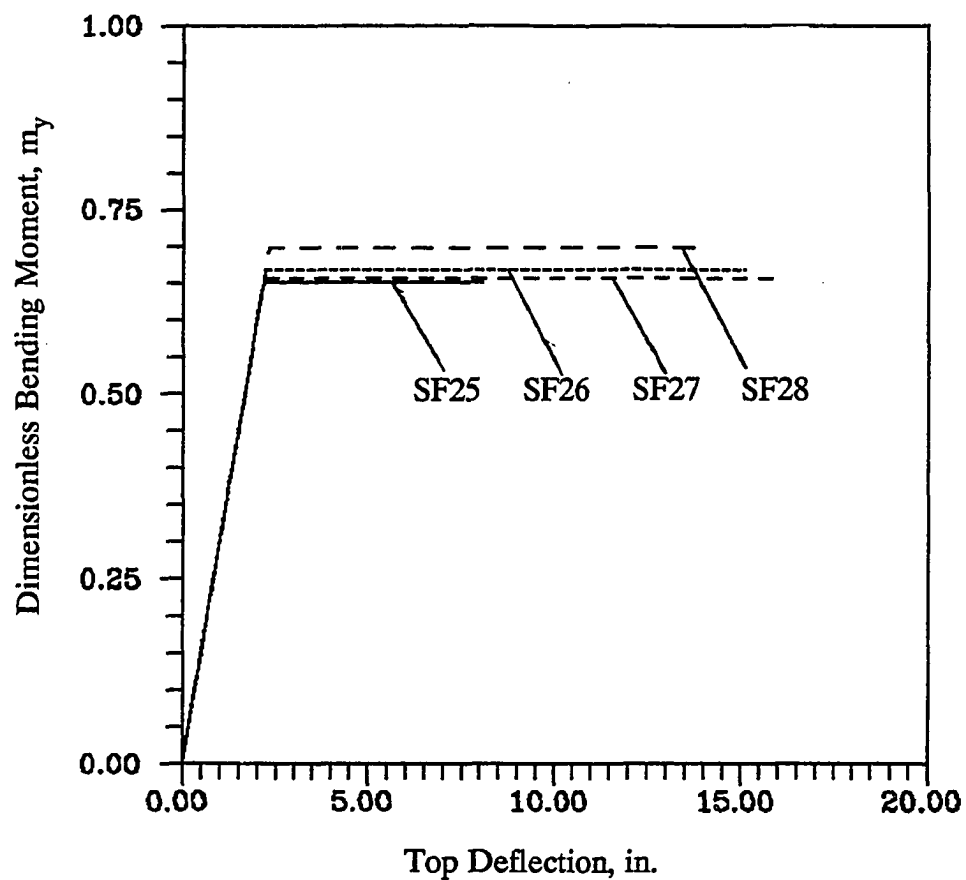


Figure 107. Bending moment versus top deflection ($m_y - \Delta_x$) for single-story single-bay sway space frames with various combinations of residual stresses and crookedness, with load path SL2

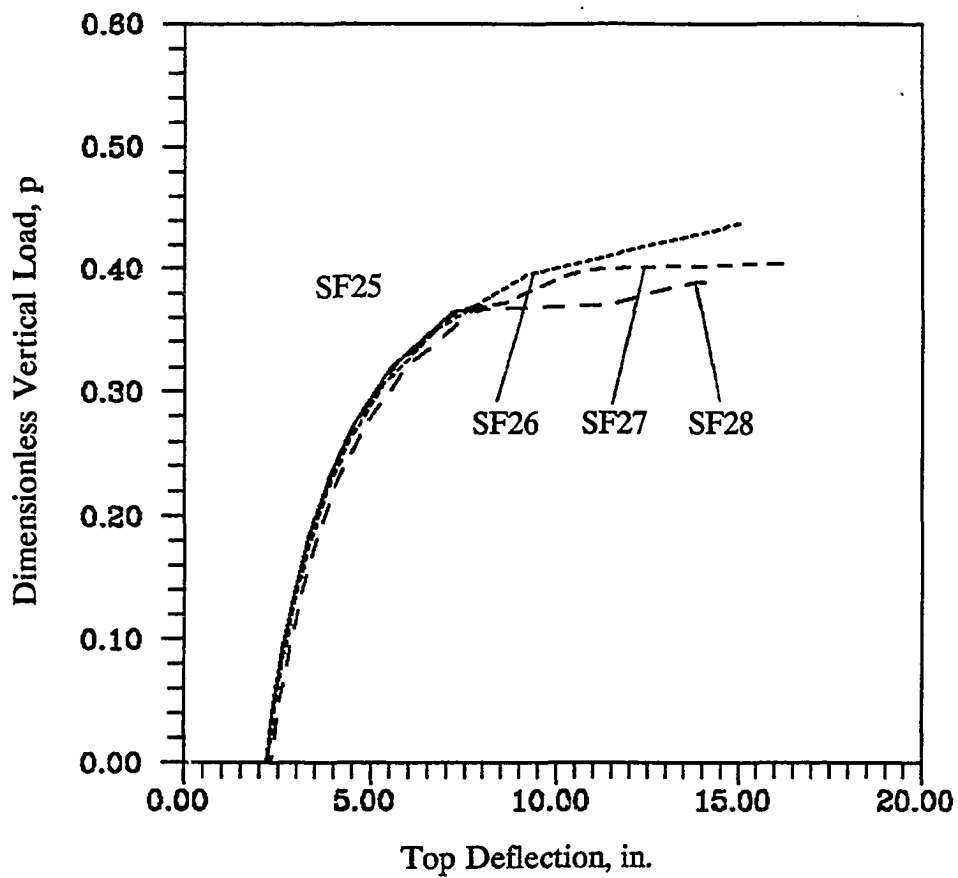


Figure 108. Dimensionless vertical load versus top deflection ($p - \Delta_x$) for single-story single-bay sway space frames with various combinations of residual stresses and crookedness, with load path SL2

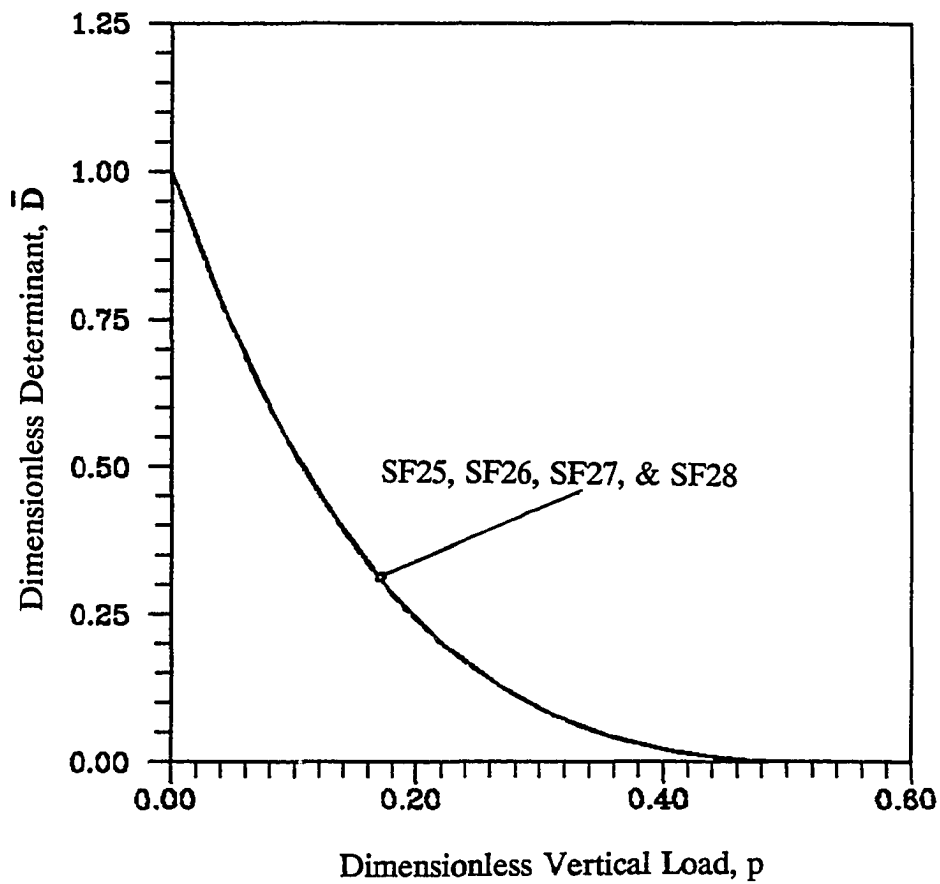


Figure 109. Stiffness degradation ($\bar{D} - p$) for single-story single-bay sway space frames with various combinations of residual stresses and crookedness, with load path SL3

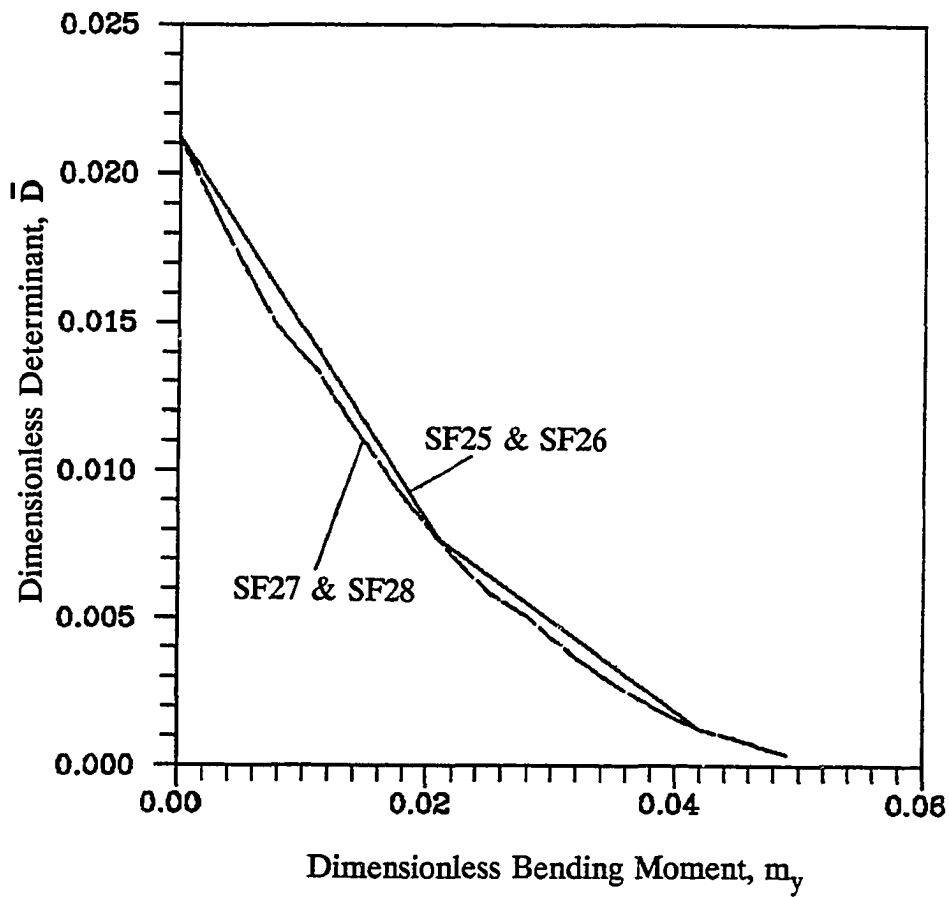


Figure 110. Stiffness degradation ($\bar{D} - m_y$) for single-story single-bay sway space frames with various combinations of residual stresses and crookedness, with load path SL3

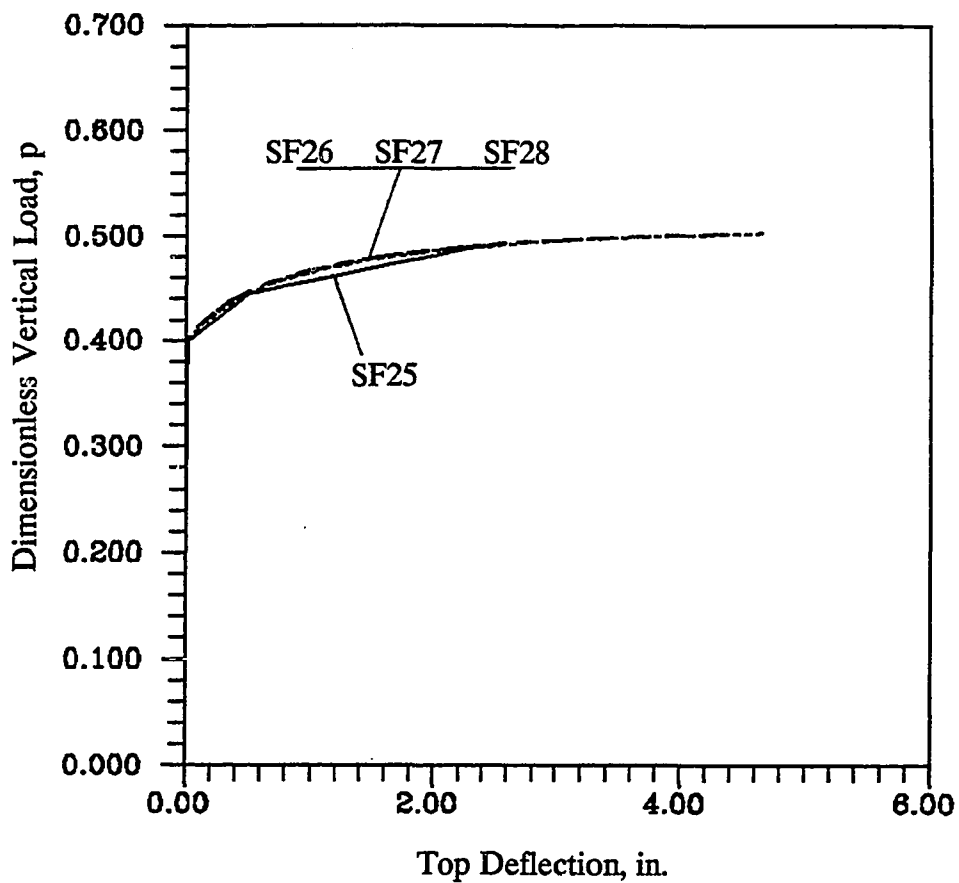


Figure 111. Dimensionless vertical load versus top deflection ($p - \Delta_x$) for single-story single-bay sway space frames with various combinations of residual stresses and crookedness, with load path SL3

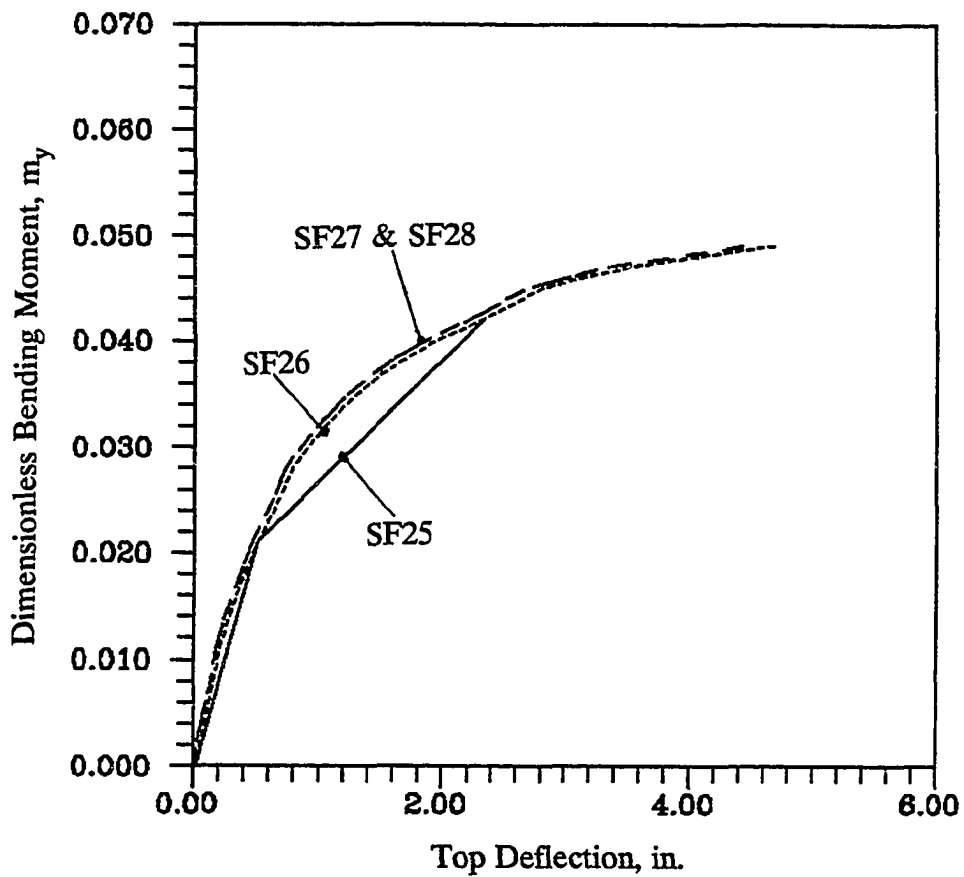


Figure 112. Bending moment versus top deflection ($m_y - \Delta_x$) for single-story single-bay sway space frames with various combinations of residual stresses and crookedness, with load path SL3

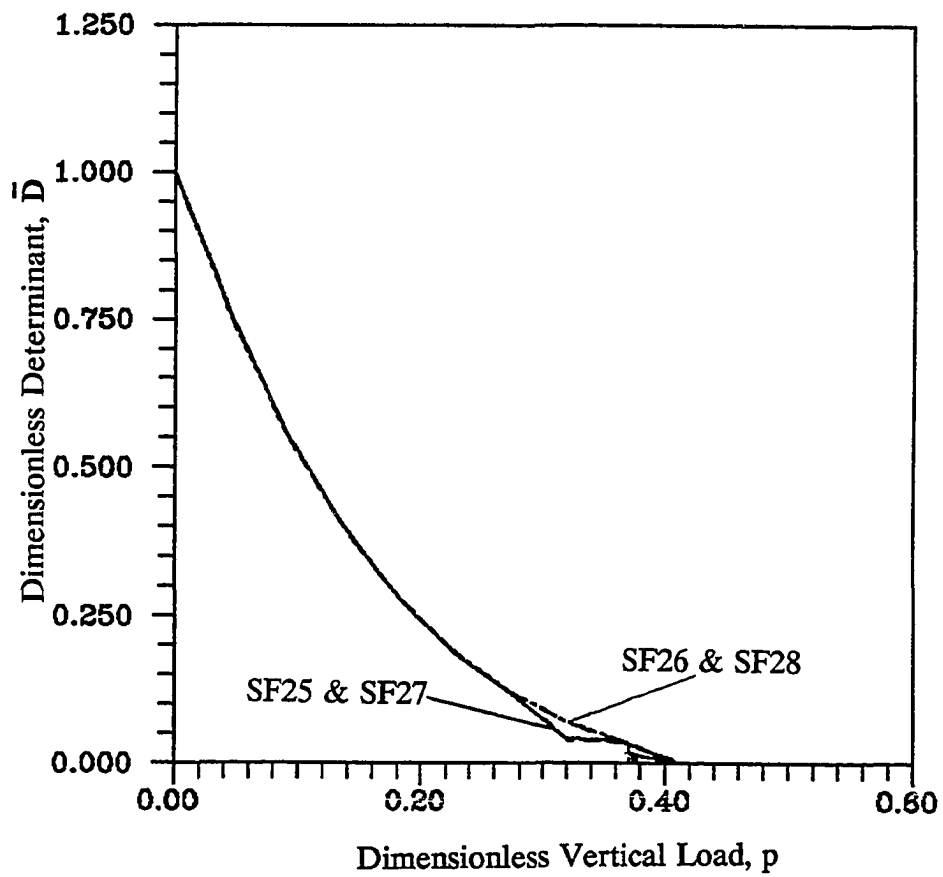


Figure 113. Stiffness degradation ($\bar{D} - p$) for single-story single-bay sway space frame with various combinations of residual stresses and crookedness, with load path SL4

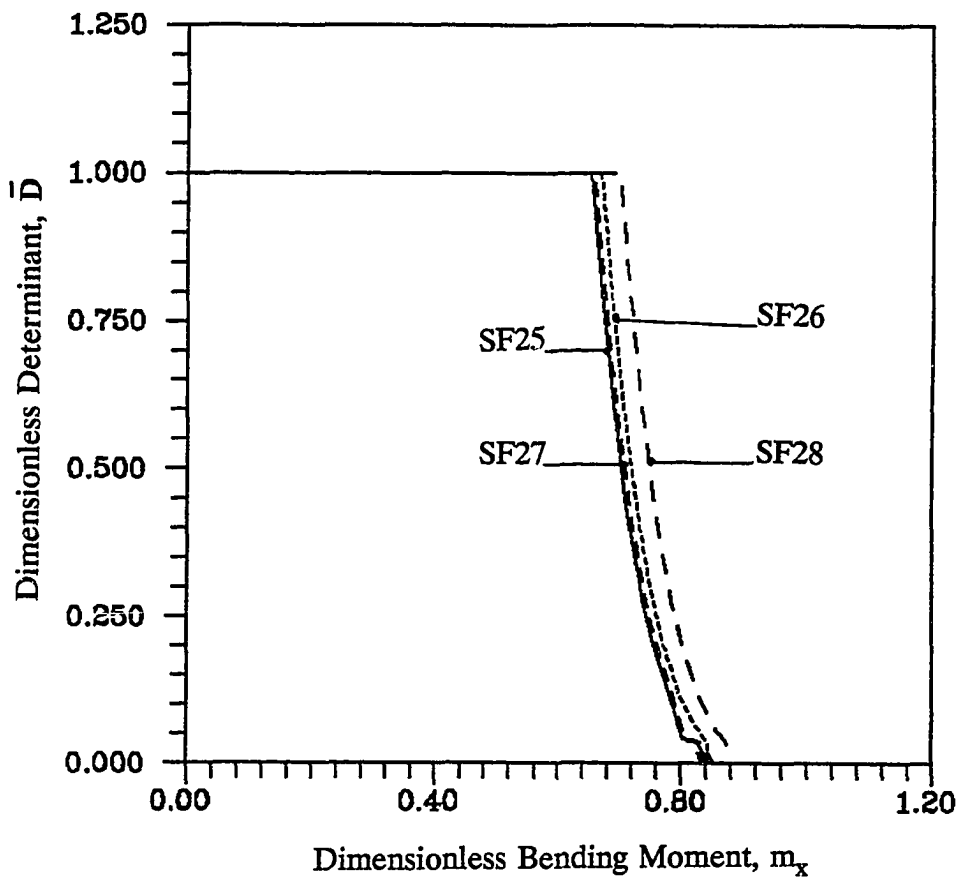


Figure 114. Stiffness degradation ($\bar{D} - m_x$) for single-story single-bay space sway frames with various combinations of residual stresses and crookedness, with load path SL4

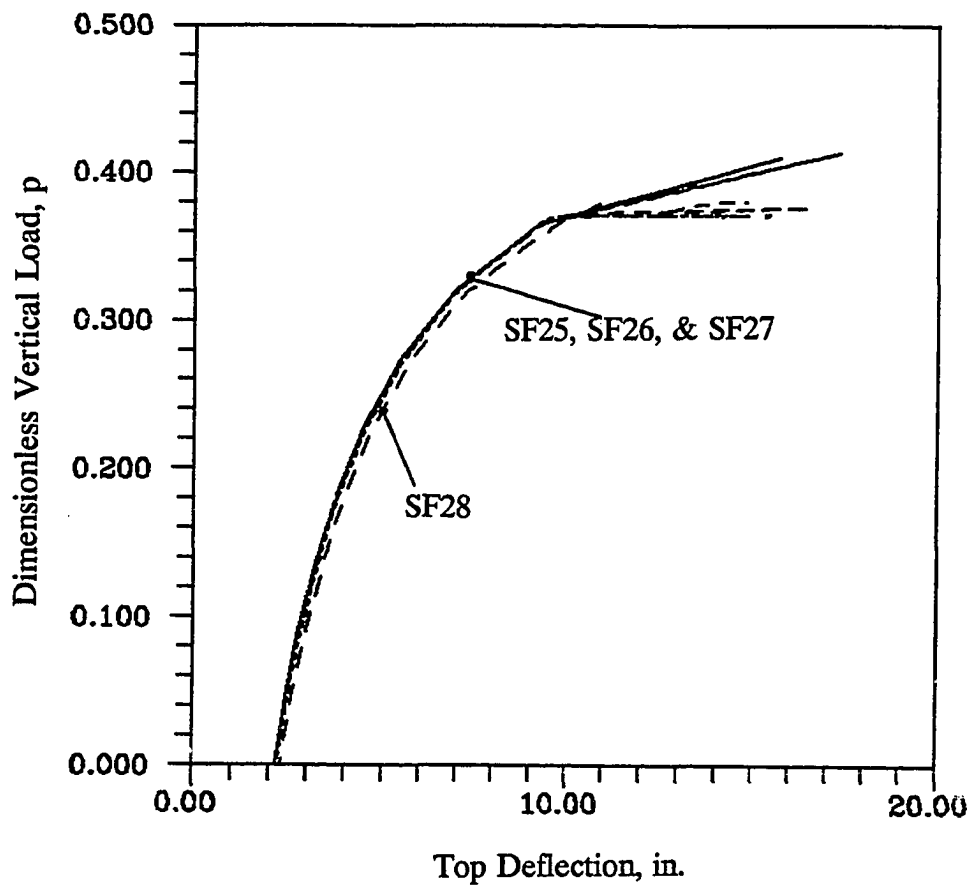


Figure 115. Dimensionless vertical load versus top deflection ($p - \Delta_x$) for single-story single-bay sway space frames with various combinations of residual stresses and crookedness, with load path SL4

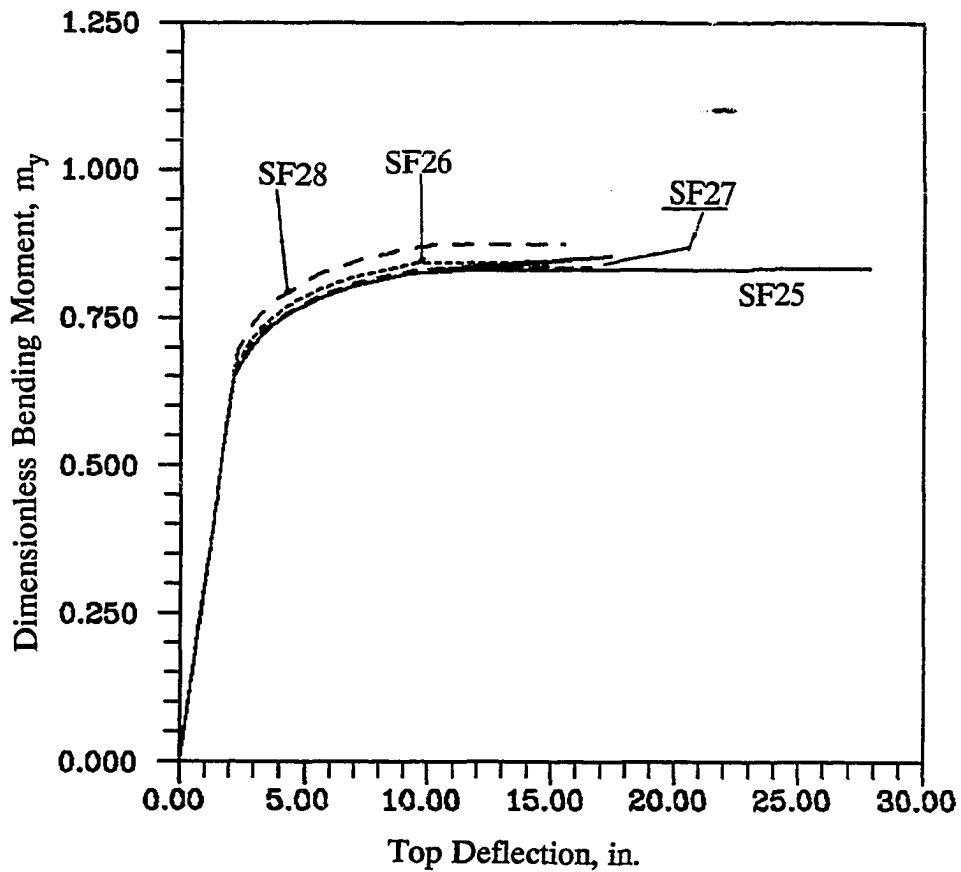


Figure 116. Bending moment versus top deflection ($m_y - \Delta_x$) for single-story single-bay sway space frames with various combinations of residual stresses and crookedness, with load path SL4

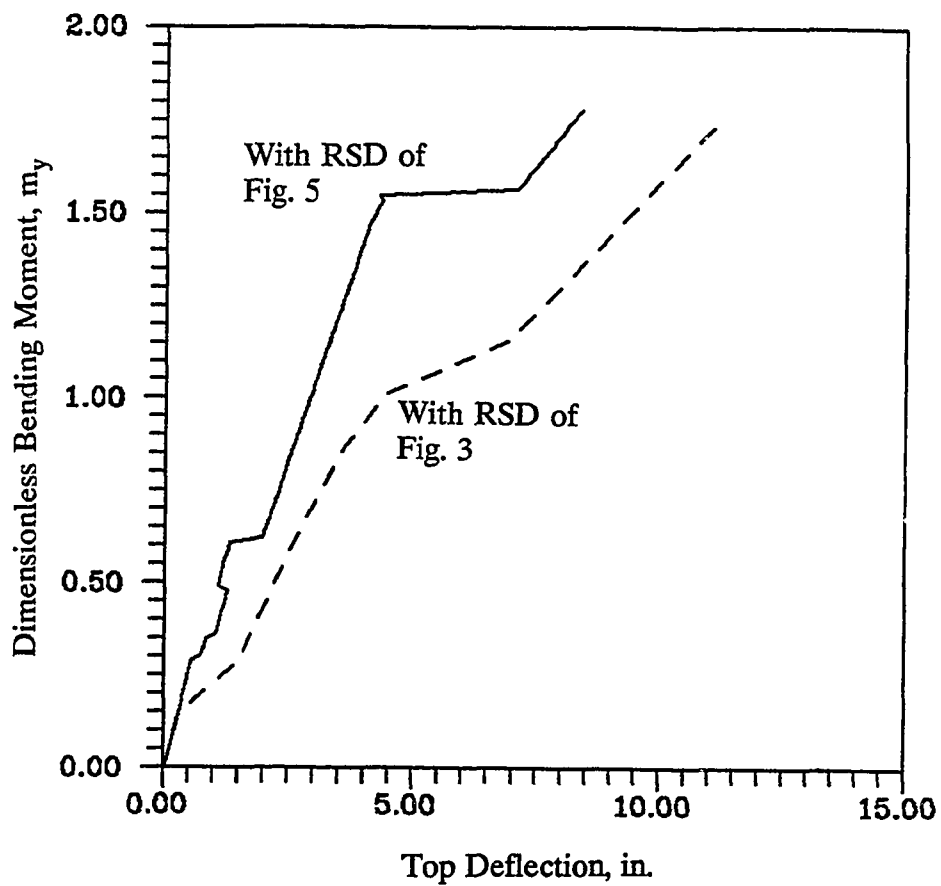


Figure 117. Dimensionless bending moment versus top deflection ($\bar{m}_y - \Delta_x$) for single-story single-bay sway space frames with various residual stress distributions and load path SL1

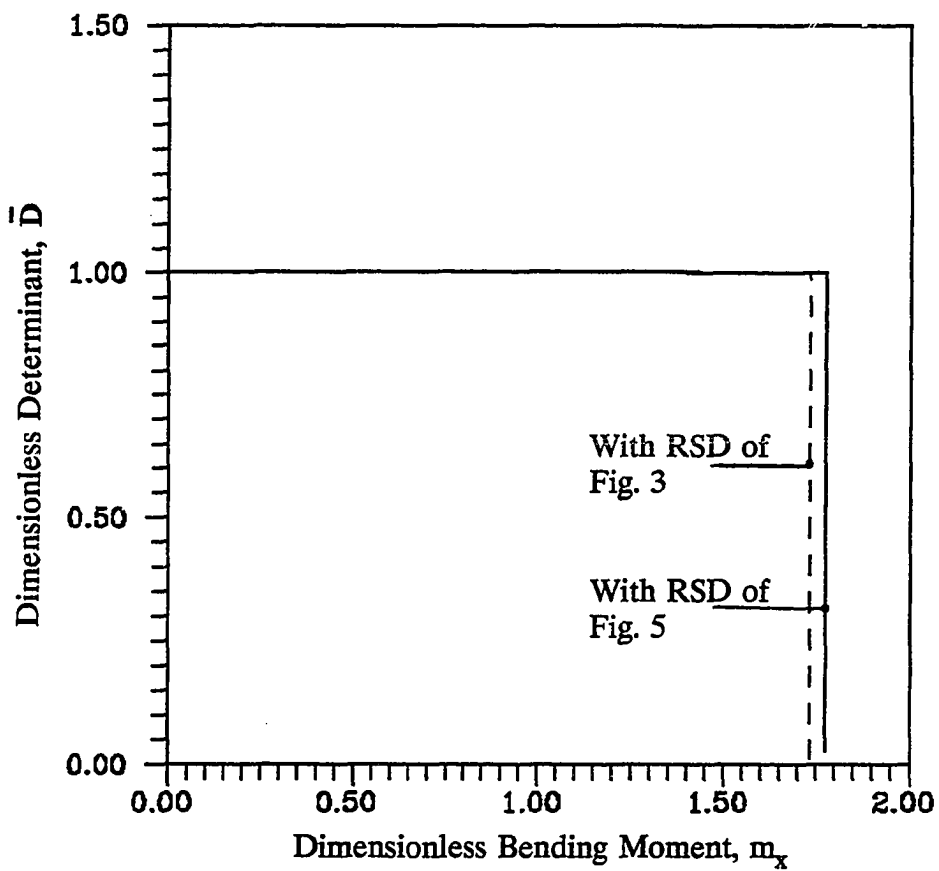


Figure 118. Stiffness degradation ($\bar{D} - m_x$) for single-story single-bay sway space frames with various residual stress distributions and with load path SL2

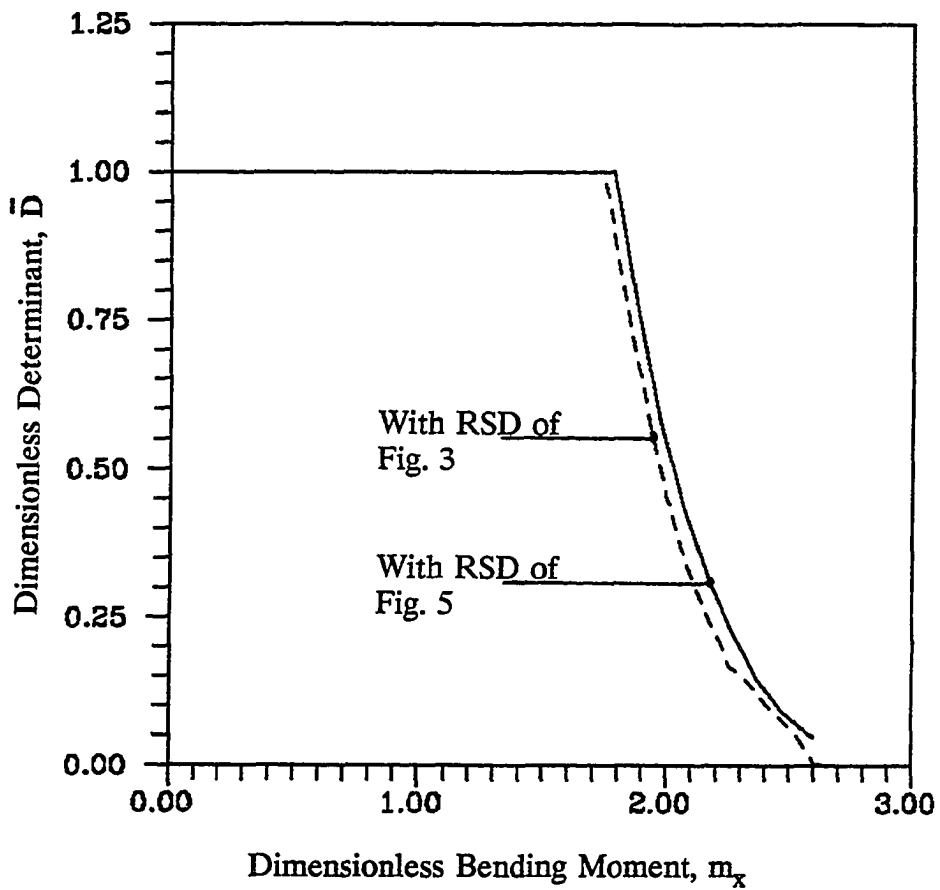


Figure 119. Stiffness degradation ($\bar{D} - m_x$) for single-story single-bay sway space frames with various residual stress distributions and load path SL4

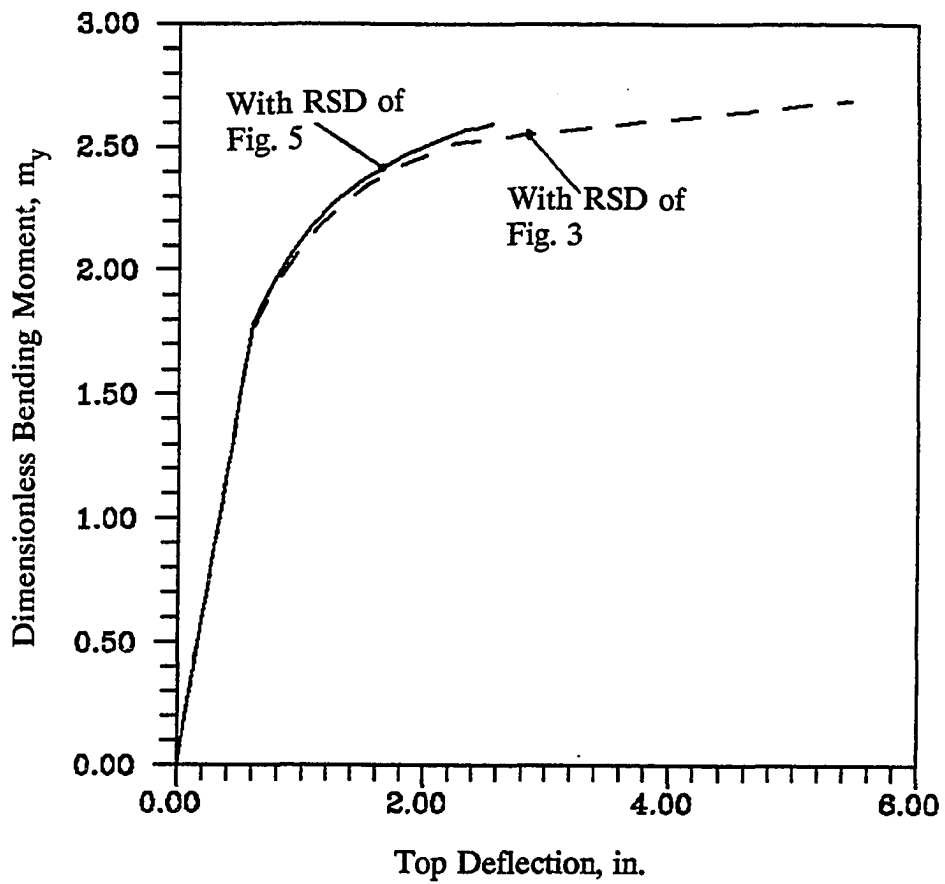


Figure 120. Bending moment versus top deflection ($m_y - \Delta_x$) for single-story single-bay sway space frames with various residual stress distributions and load path SL4

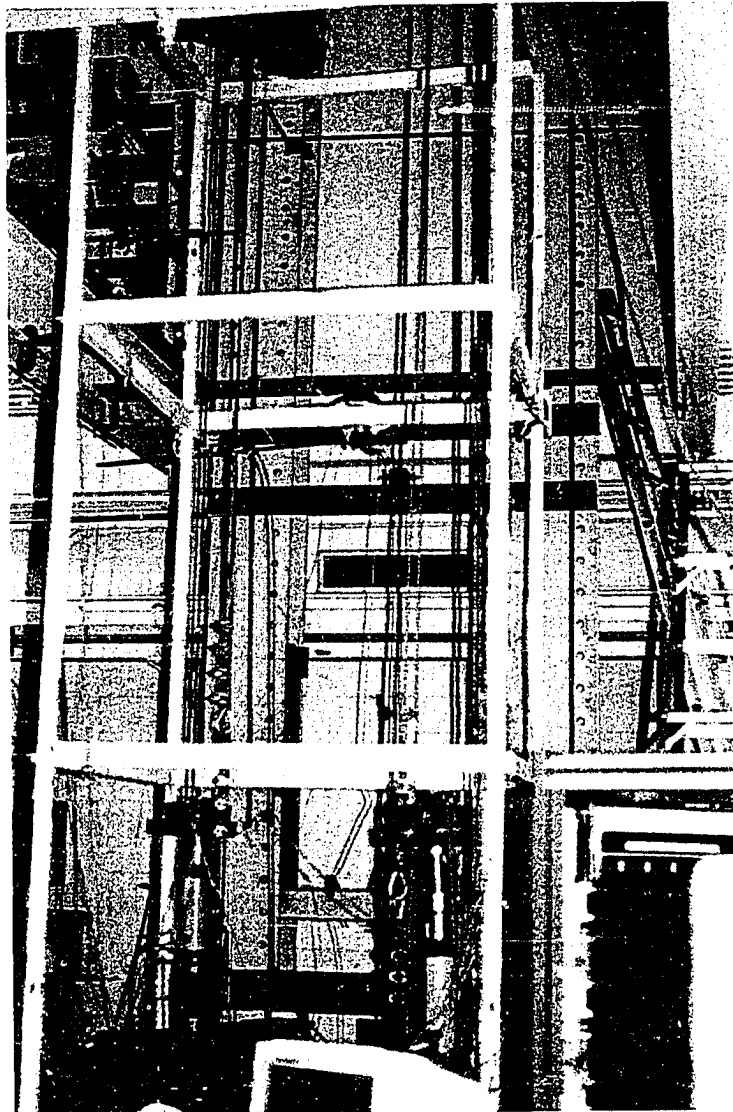


Figure 121. Tested Frame with Jacks and Cables Arrangement

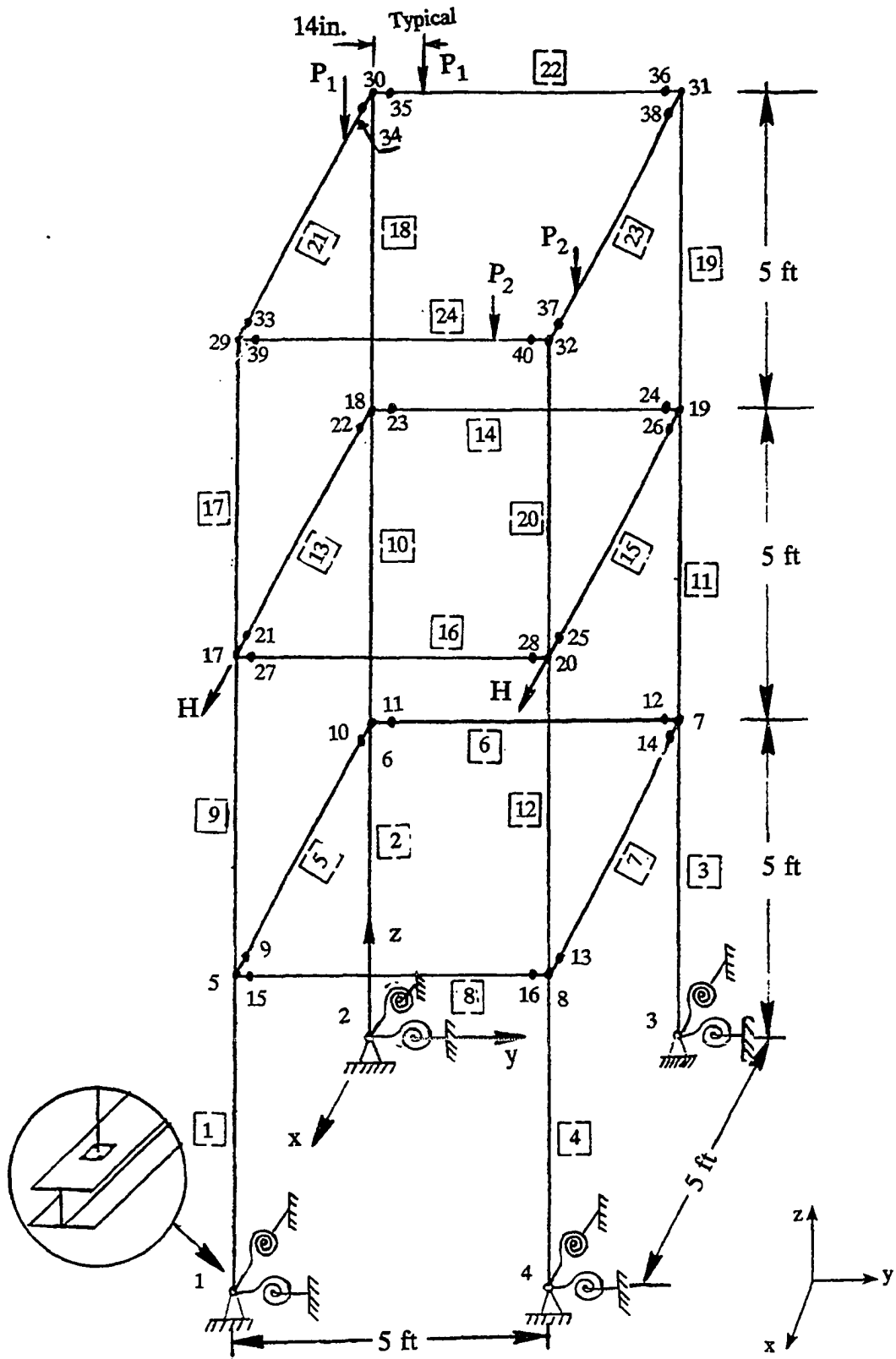


Figure 122. Three-story single-bay space frame



Figure 123. Stub column with center strain gages

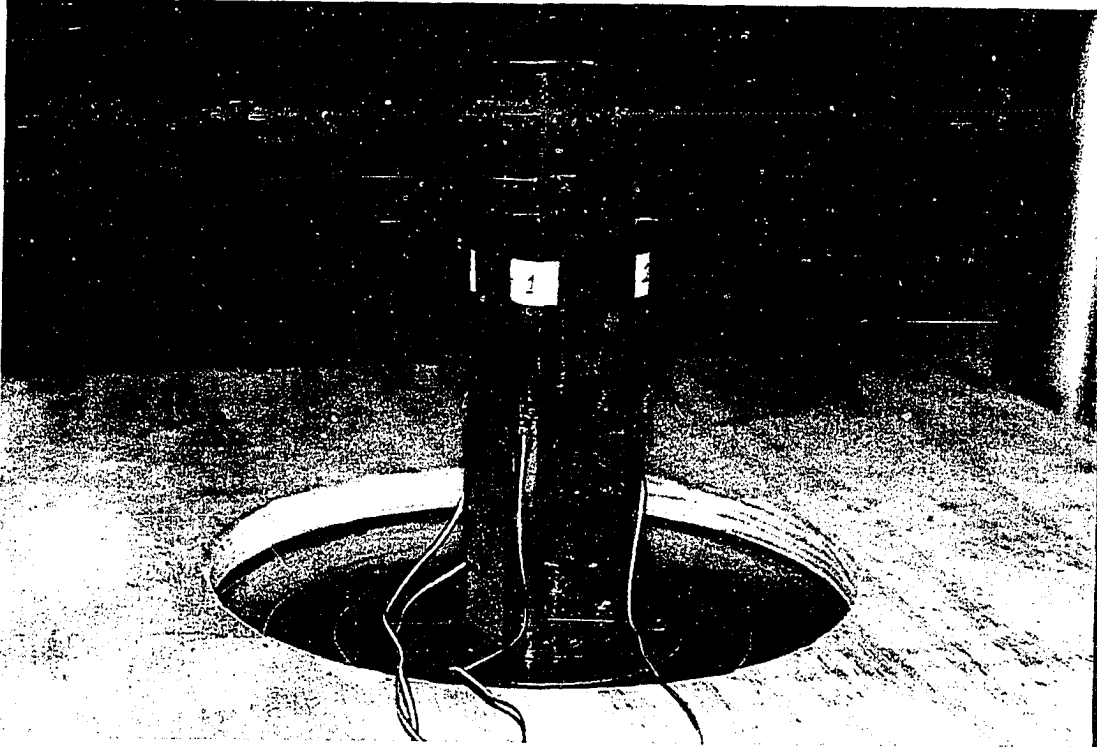


Figure 124. Stub column with corner strain gages

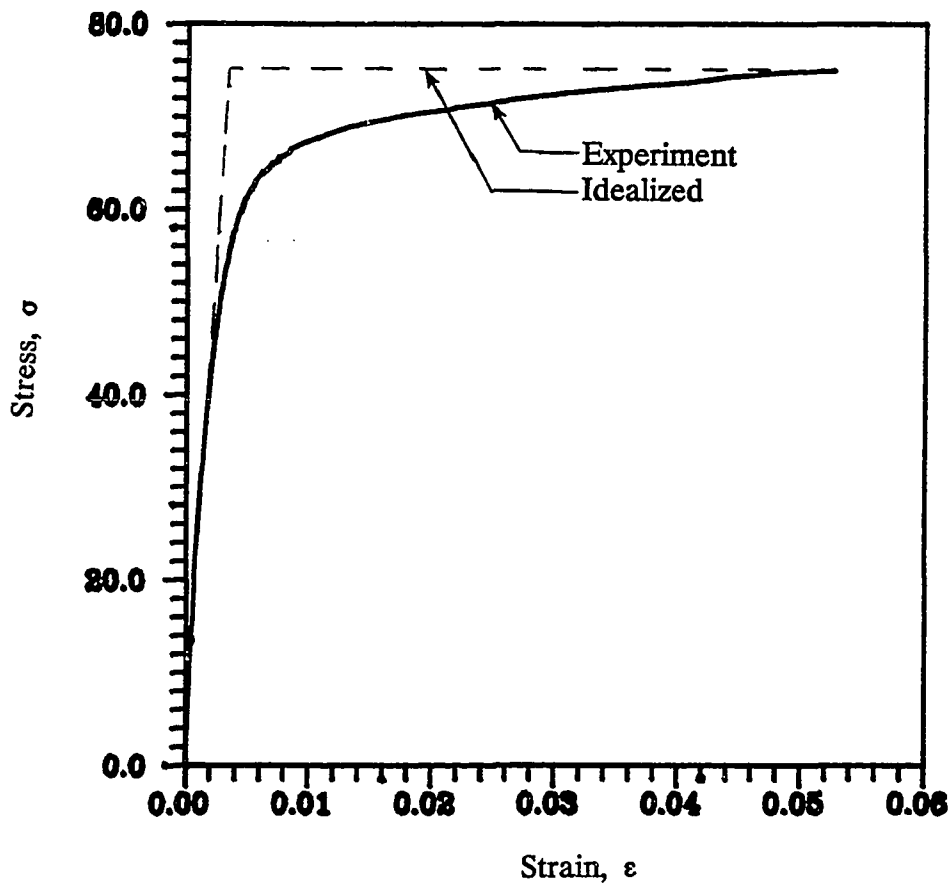


Figure 125. Stress-strain curve the stub column with strain gages at member corners

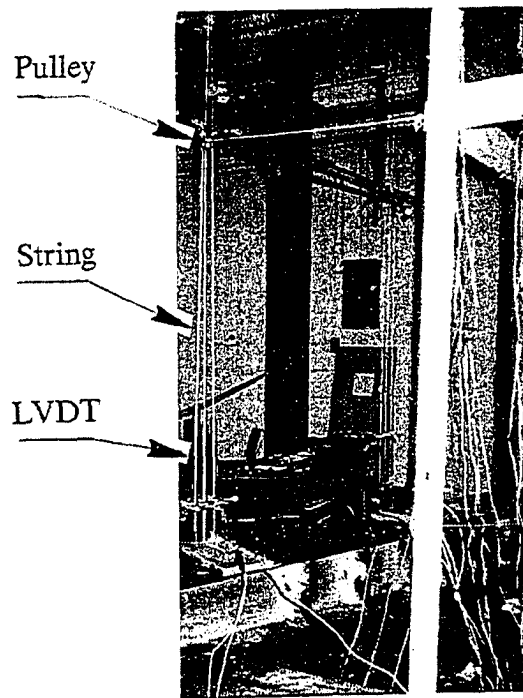


Figure 126. Setup for LVDTs

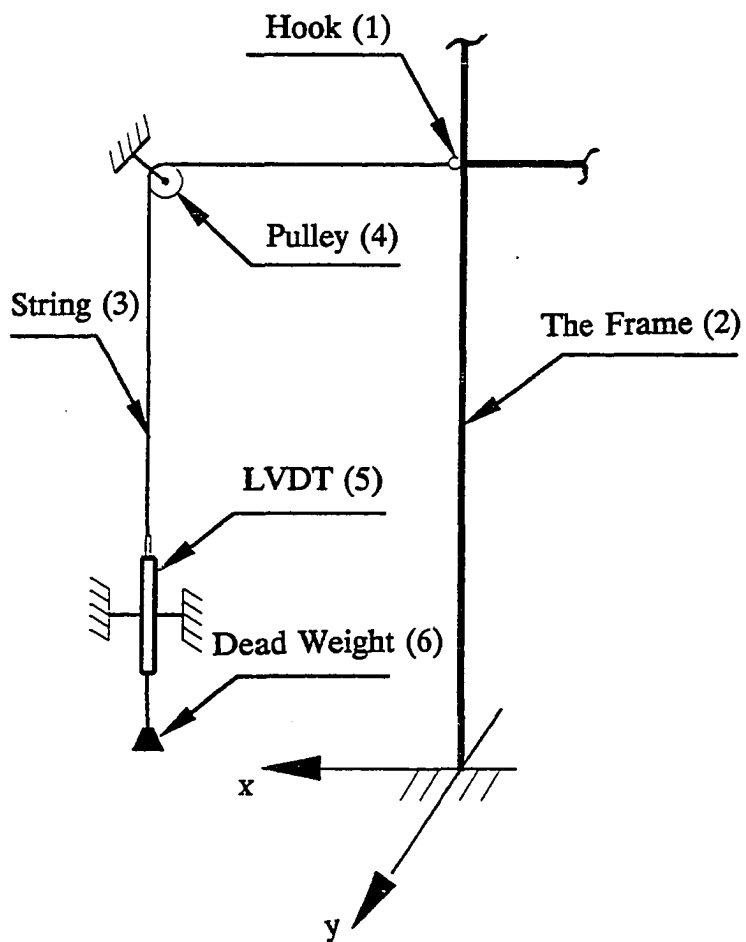


Figure 127. Schematic diagram for LVDTs setup

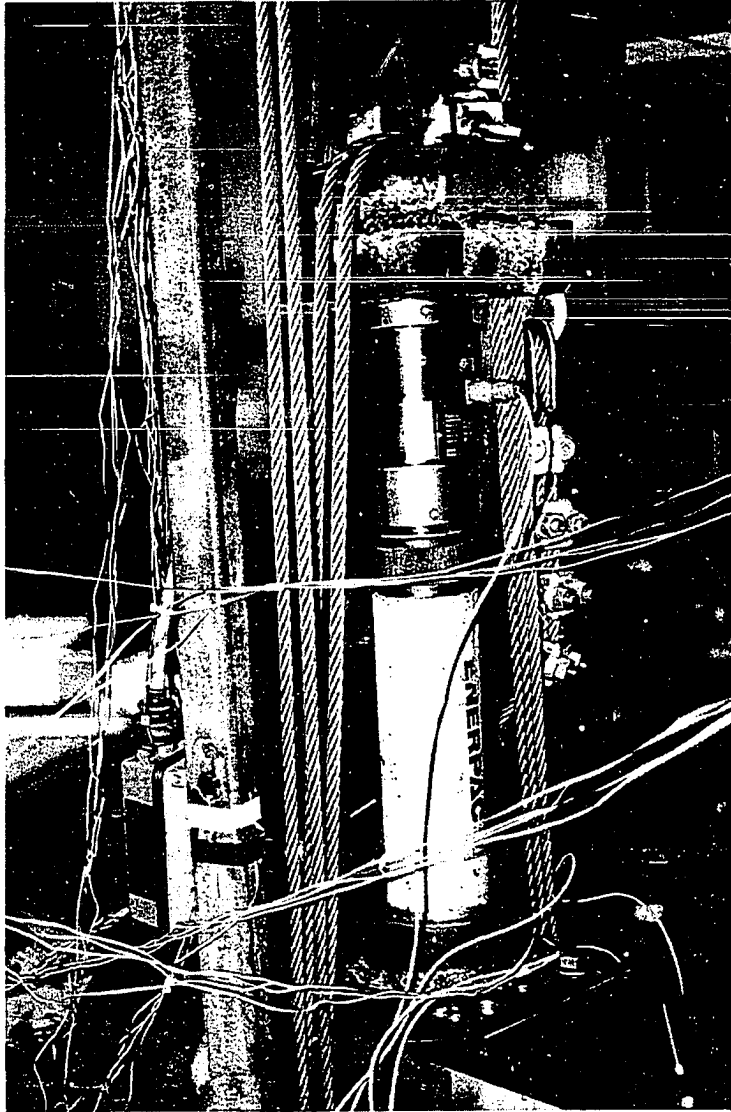


Figure 128. Jack, load cell and looped cable

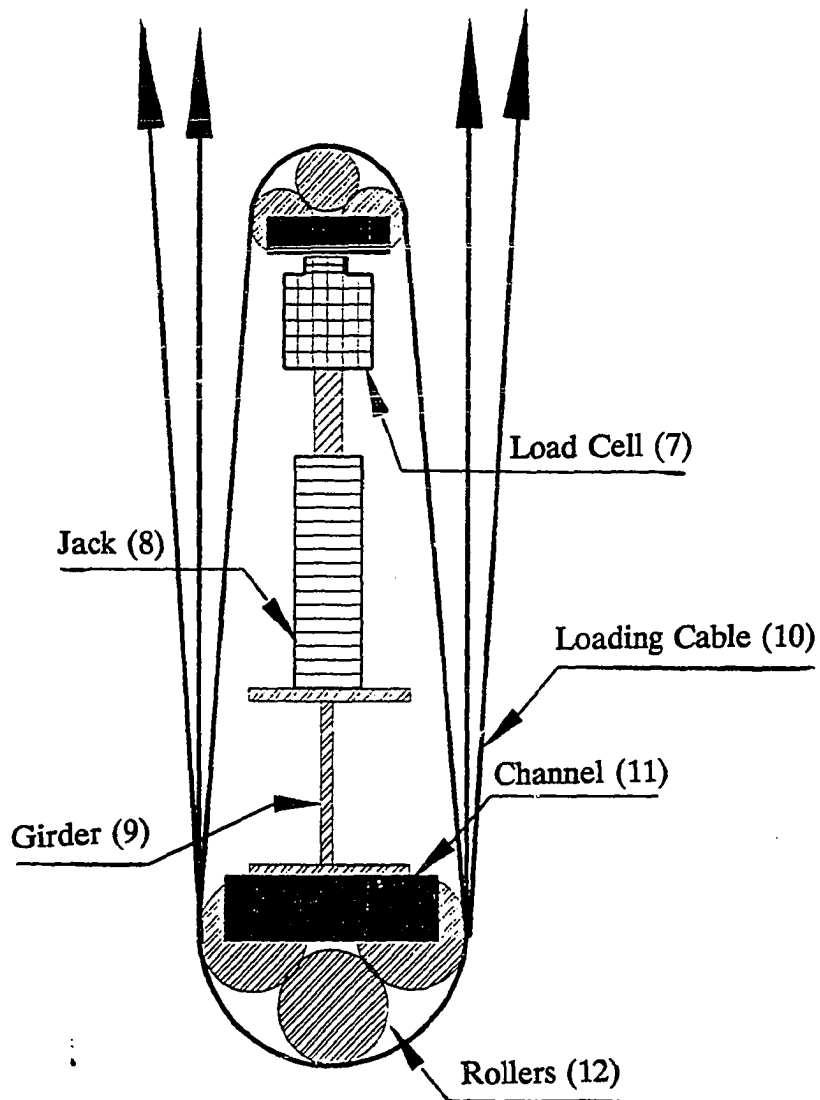


Figure 129. Schematic diagram showing the jack and cable

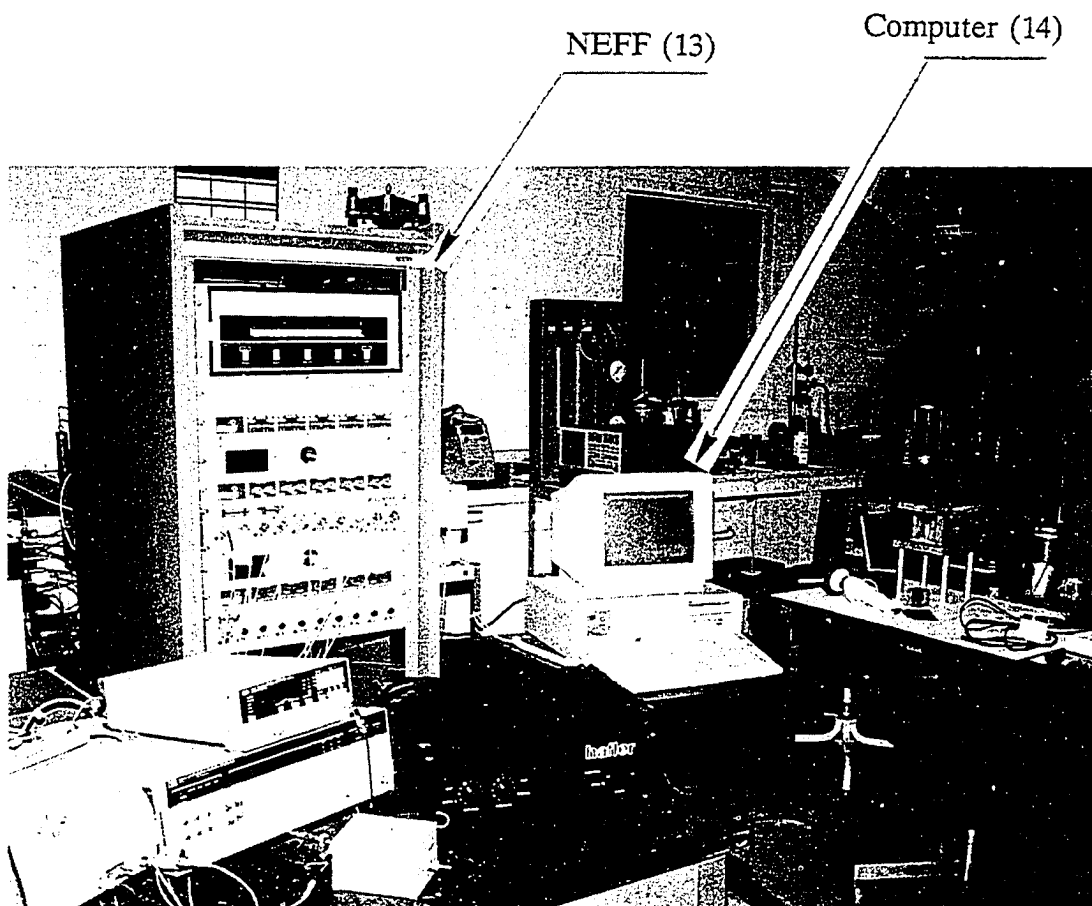


Figure 130. NEFF hardware and the personal computer used

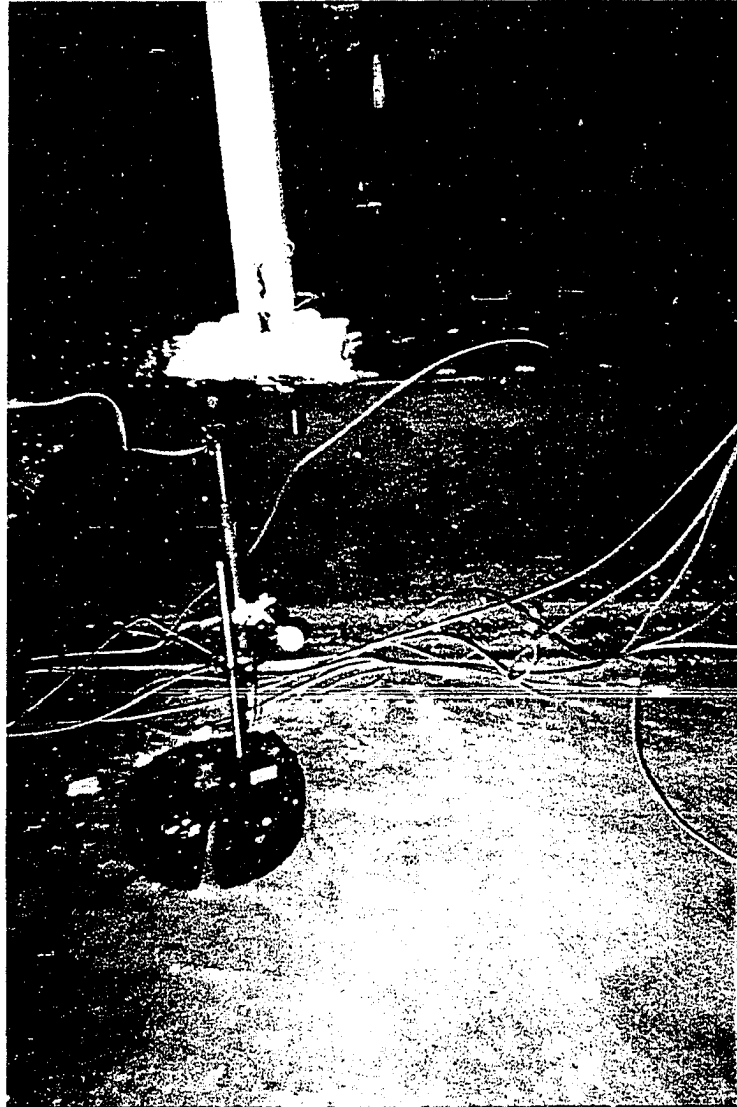


Figure 131. Bases connection detail

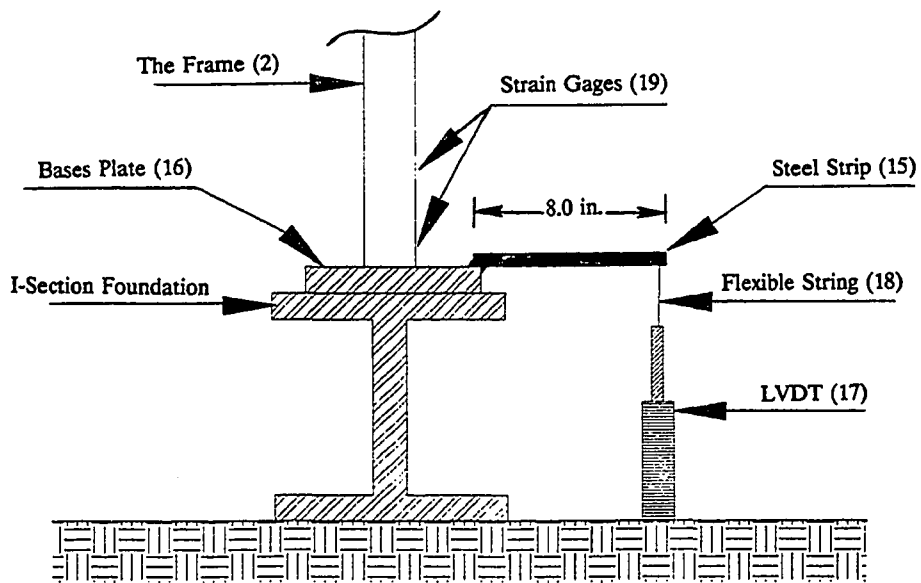


Figure 132. Schematic diagram showing setup for base joint rotation measurement

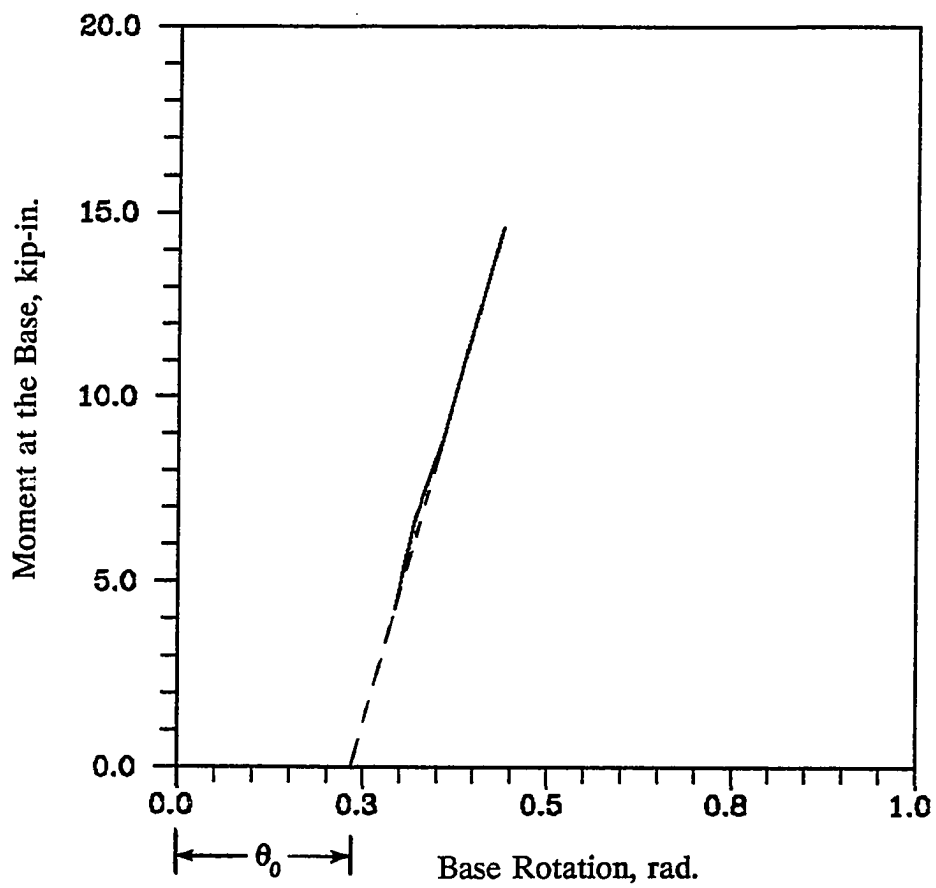


Figure 133. Base moment-rotation relationship

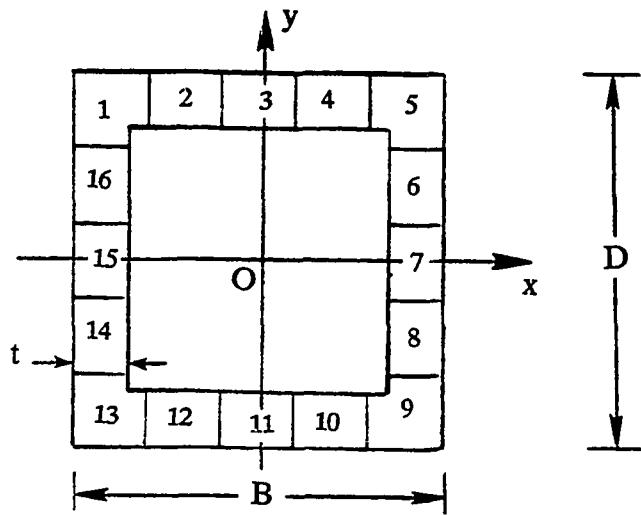


Figure 134. Strips numbering for the square section

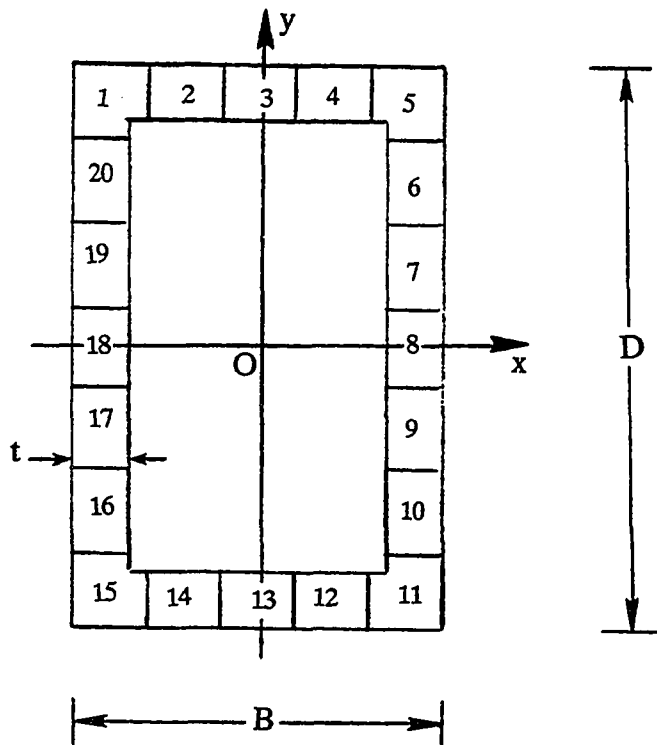


Figure 135. Strips numbering for the rectangular section

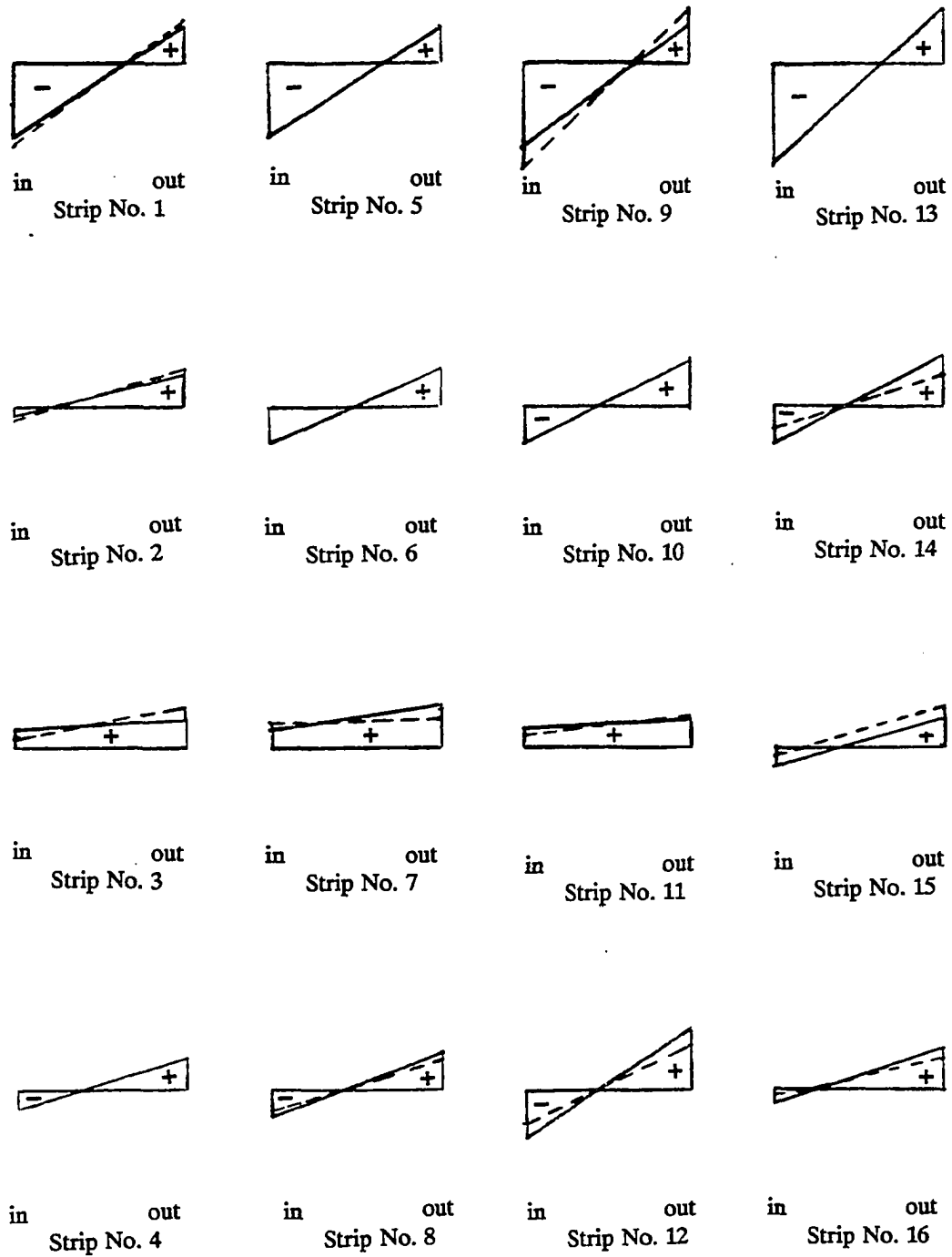


Figure 136. Distribution of residual stresses across wall thickness for square section
(Vertical scale: 1 in = 100 ksi)

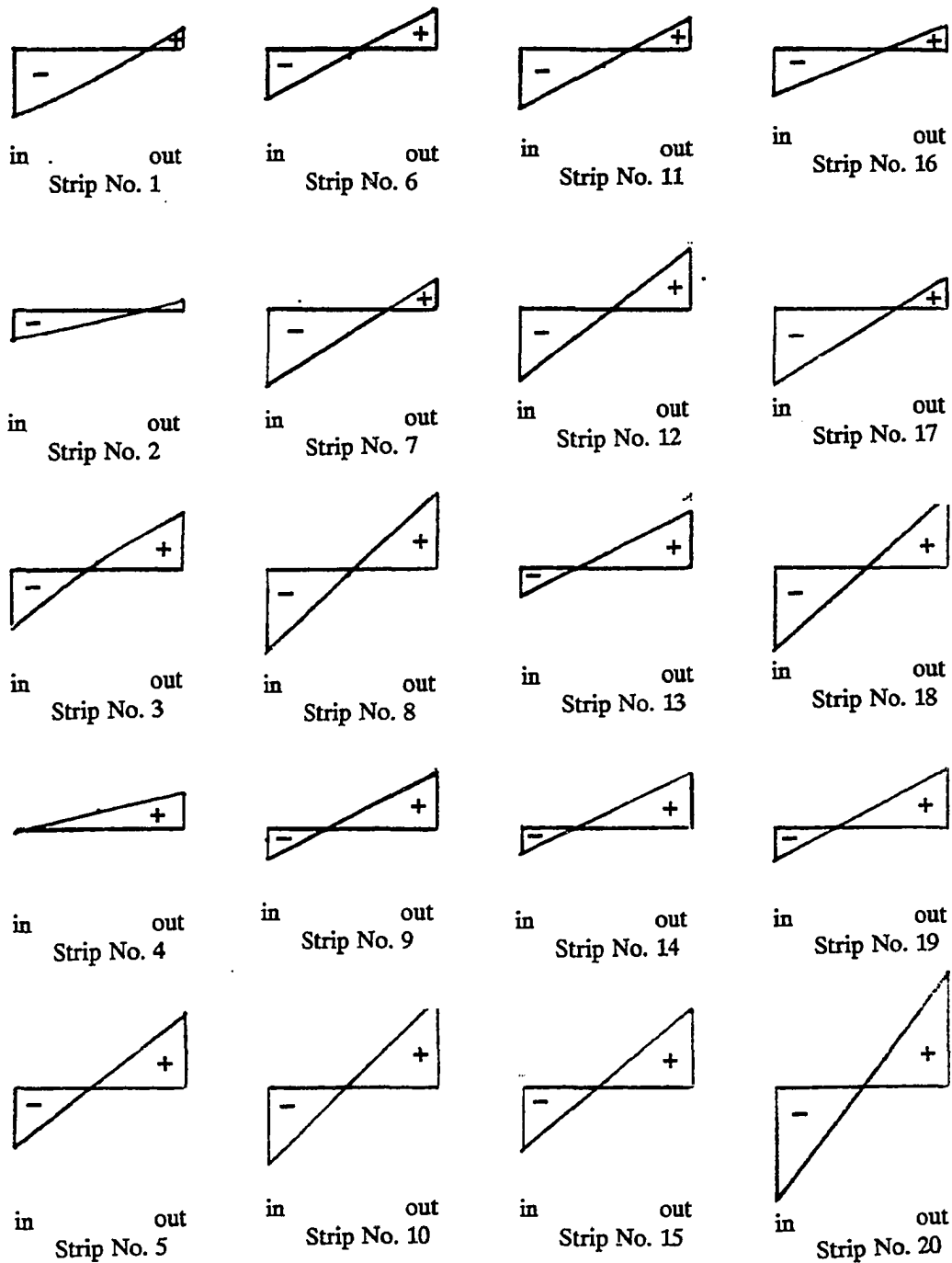


Figure 137. Distribution of residual stresses across wall thickness for rectangular section (Vertical scale: 1 in = 100 ksi)

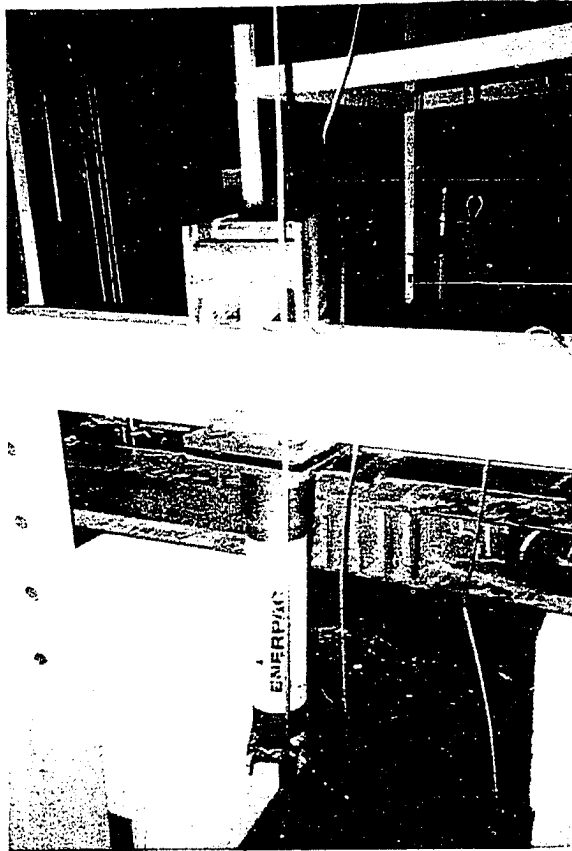


Figure 138. Loading jack (27) and cable arrangement for frame horizontal load application

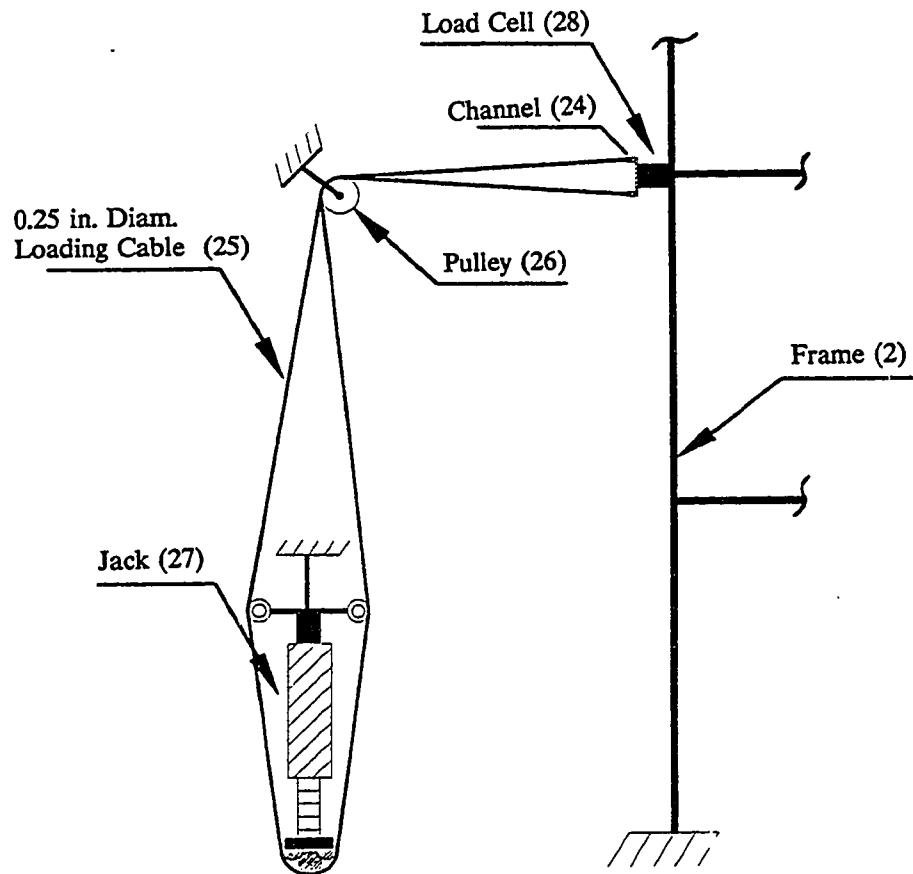


Figure 139. Schematic diagram of setup for lateral force application

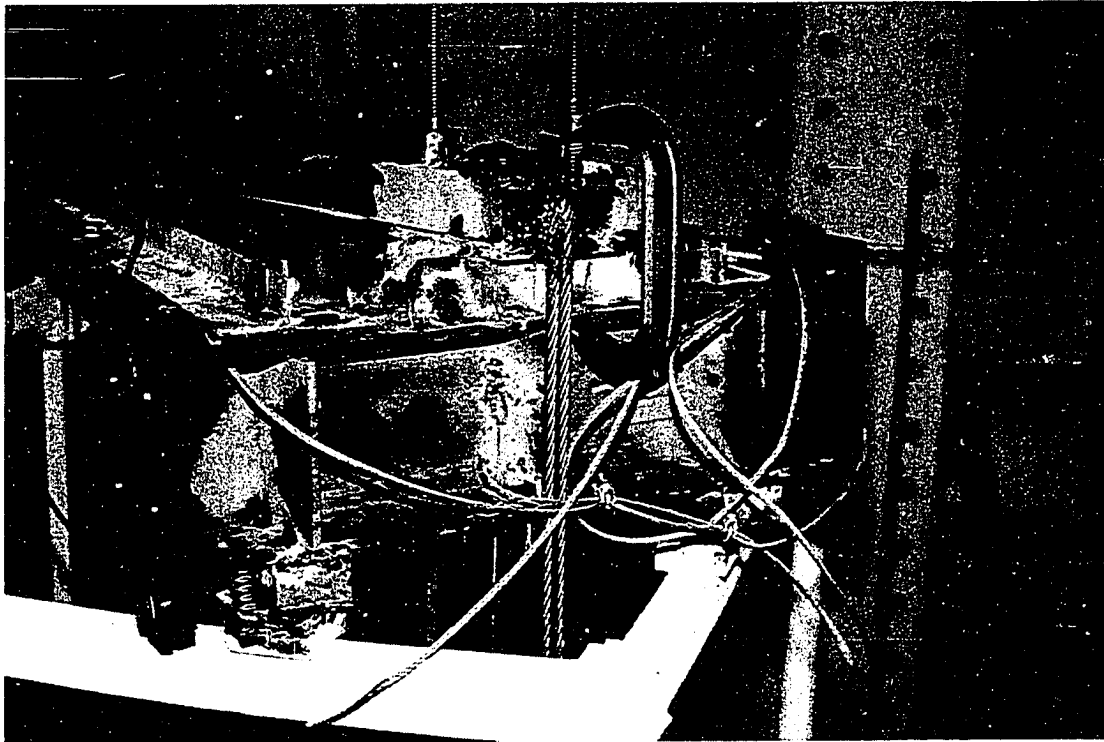


Figure 140. Loading beam assembly at frame top

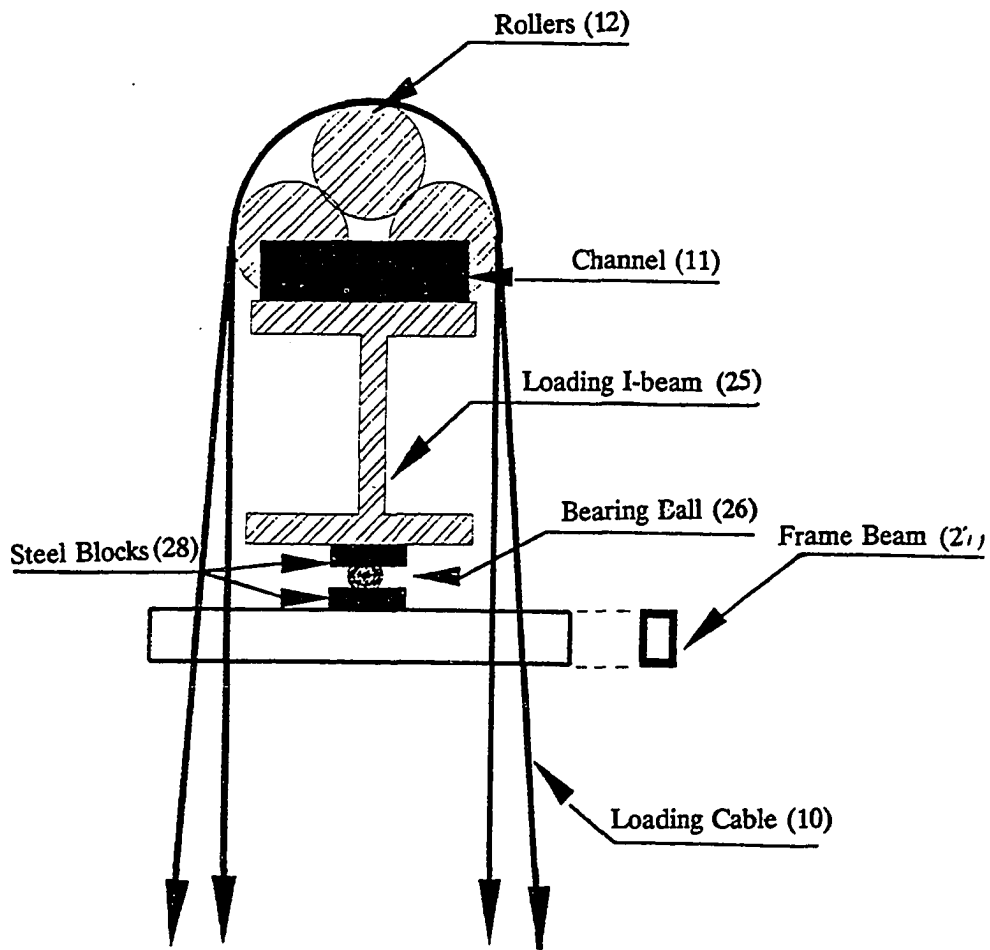


Figure 141. Schematic diagram of loading beam assembly at frame top

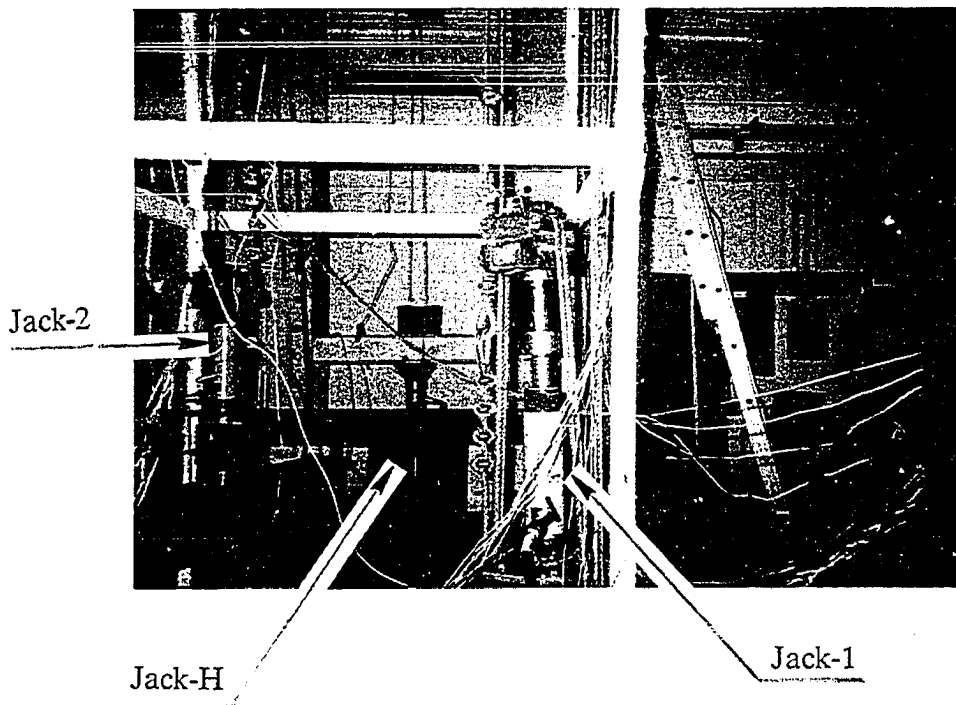


Figure 142. Loading jacks in frame test

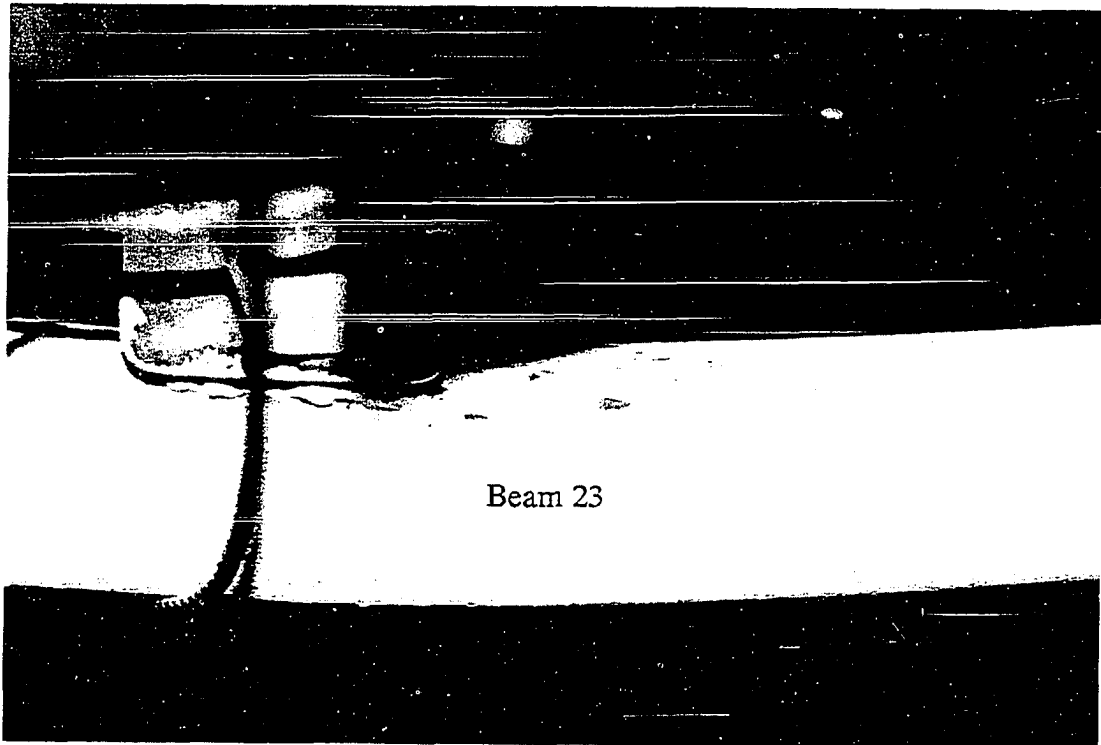


Figure 143. Start of plastification in Beam 23 at $P_2 = 19.5$ kips

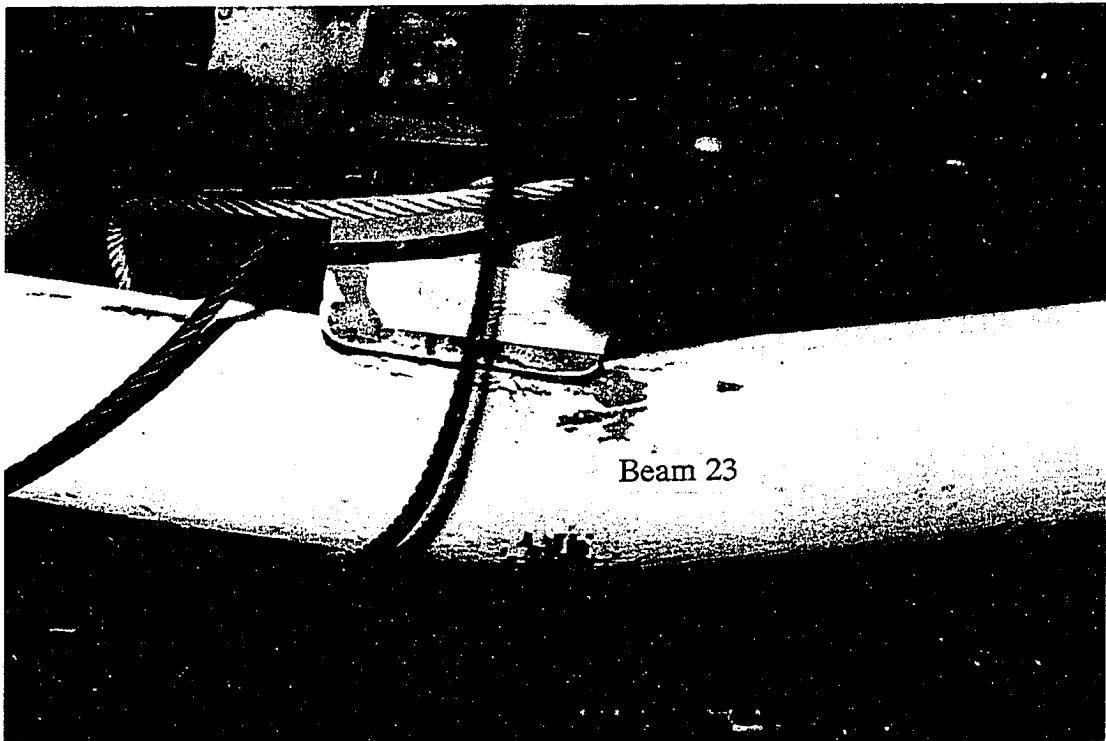


Figure 144. Nearly complete plastification of Beam 23 at $P_2 = 23.0$ kips

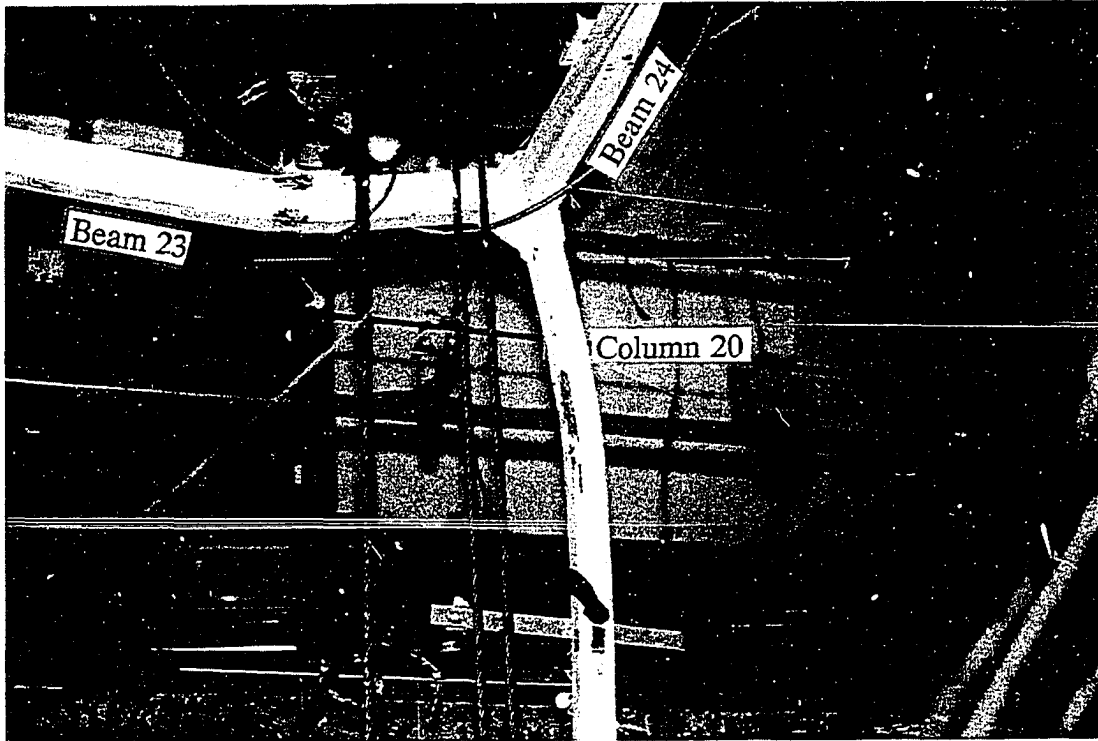


Figure 145. Plastification of Beam 23, Beam 24, and Column 20

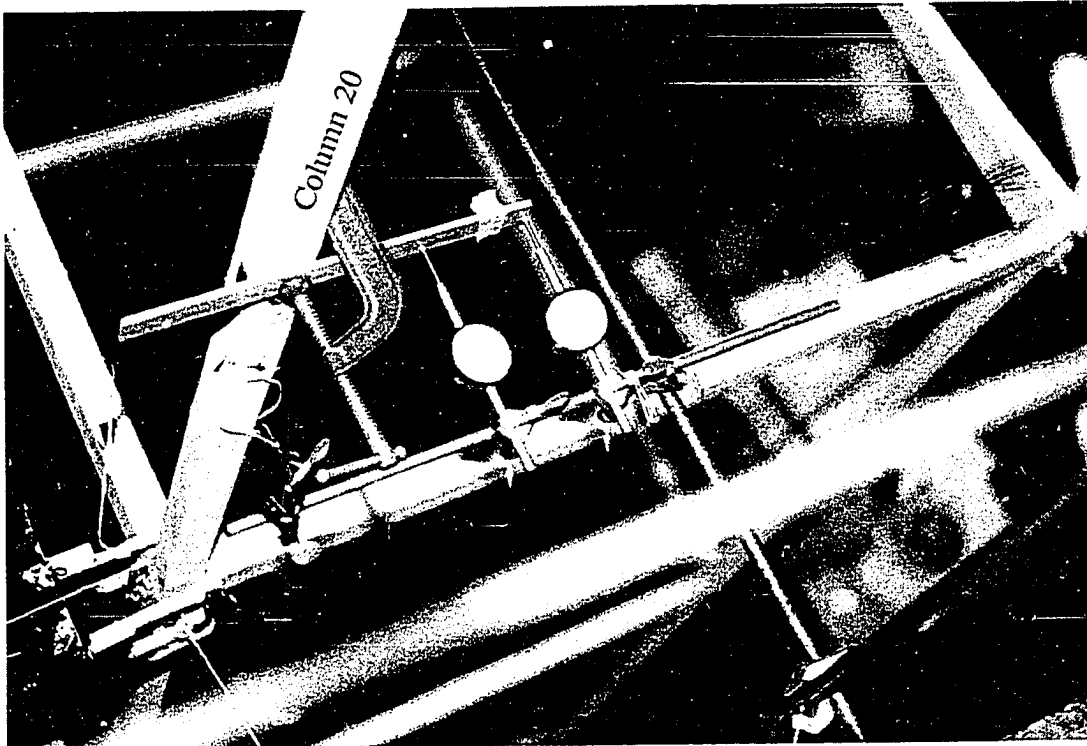
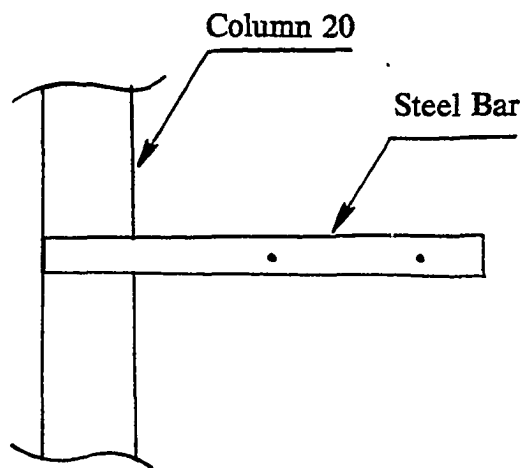
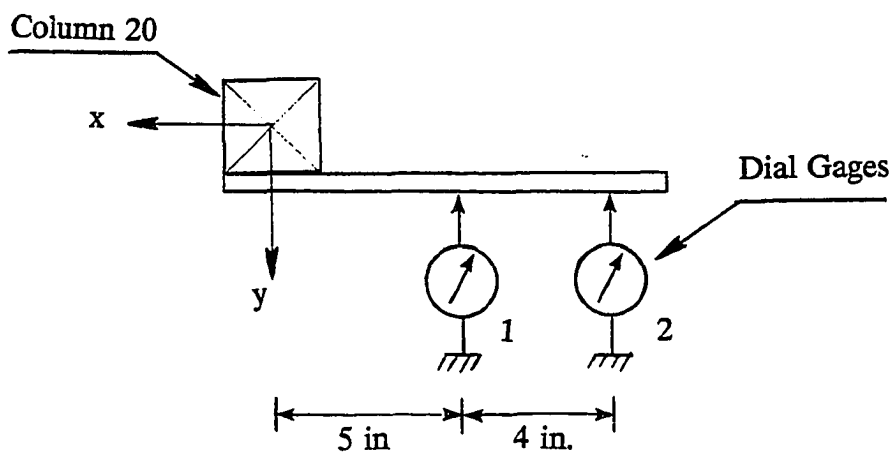


Figure 146. Dial gages attached to Column 20 for measuring torsional angle



(a) Elevation View



(b) Plan View

Figure 147. Schematic diagram for dial gages on Column 20 for measuring torsional angle

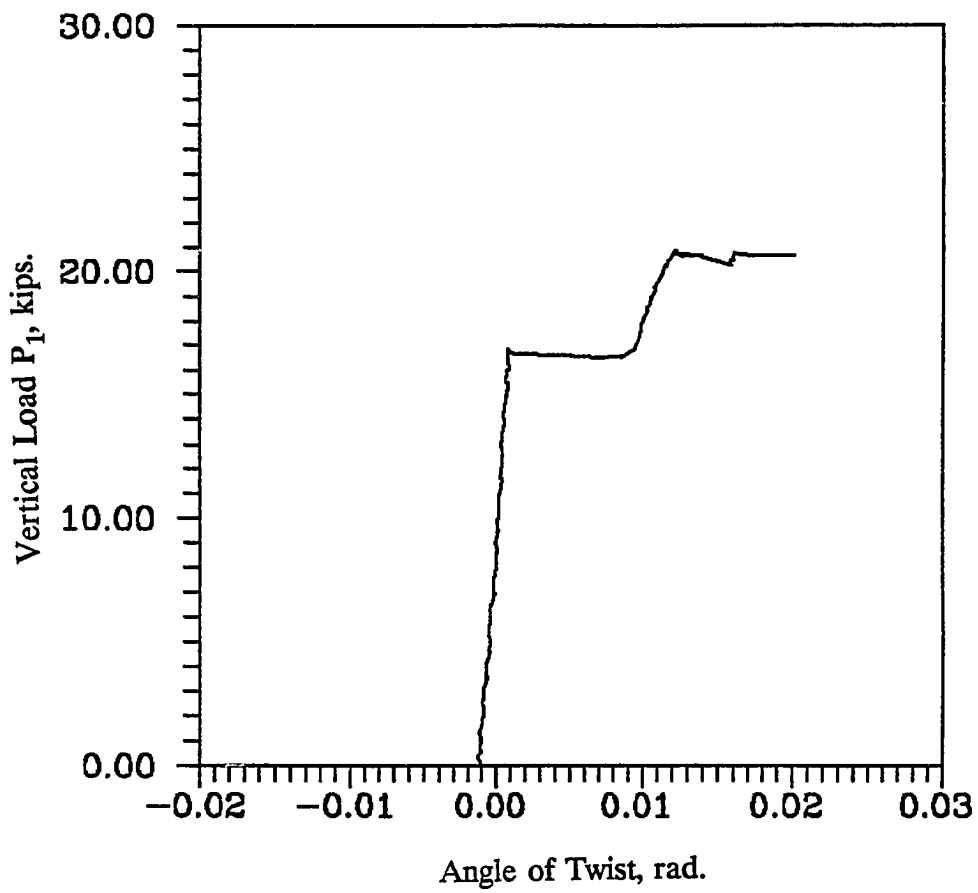


Figure 148. Experimental vertical load P_1 versus angle of twist of the test frame

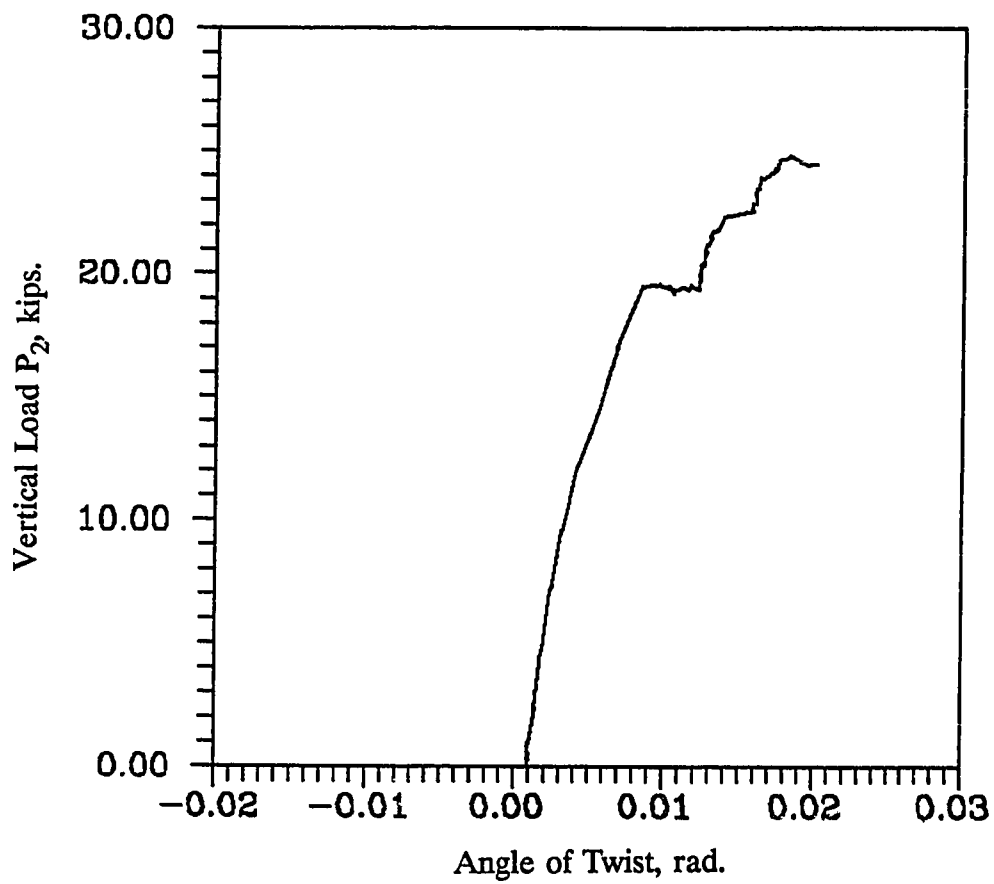


Figure 149. Experimental vertical load P_2 versus angle of twist of the test frame

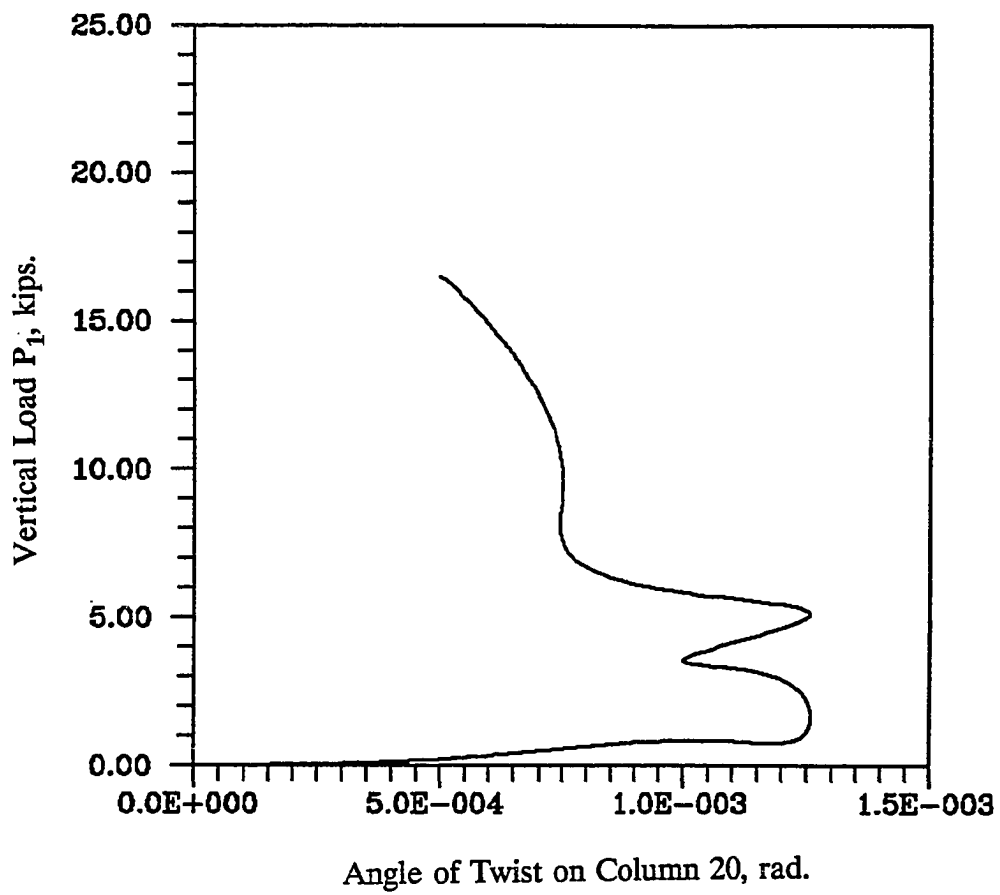


Figure 150. Experimental vertical load P_1 versus angle of twist of Column 20

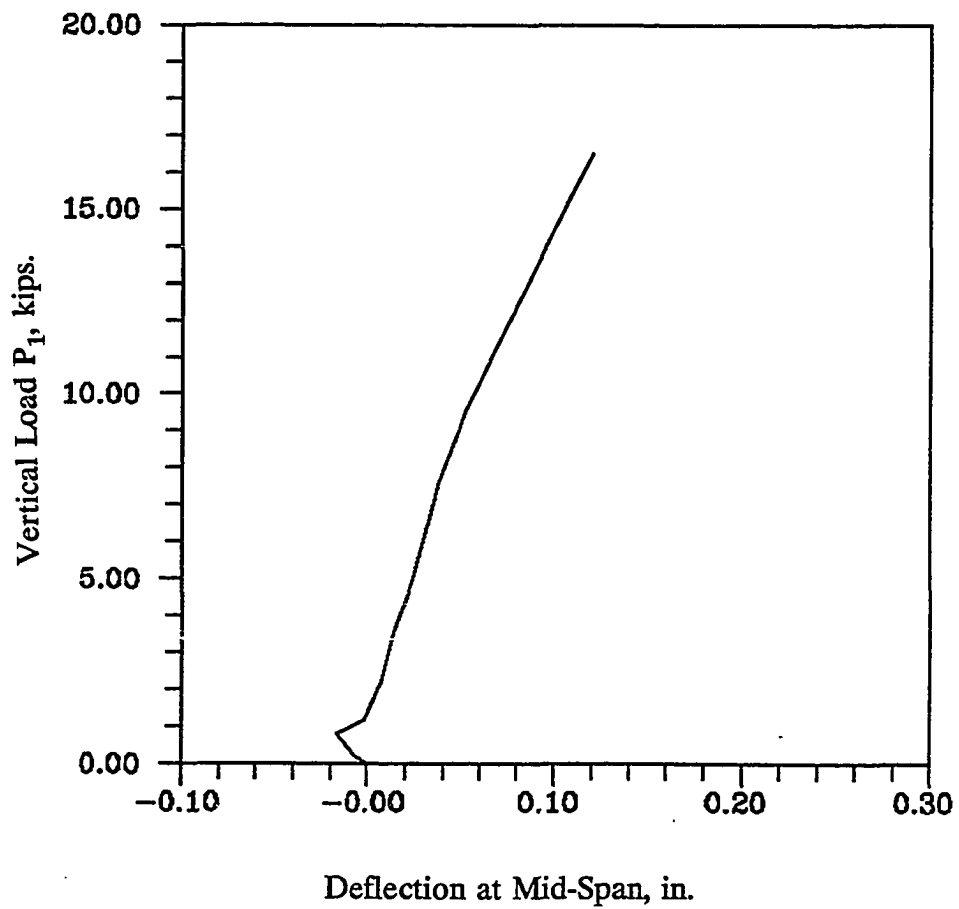


Figure 151. Experimental vertical load P_1 versus horizontal deflection at midspan of Column 20 in the y-direction

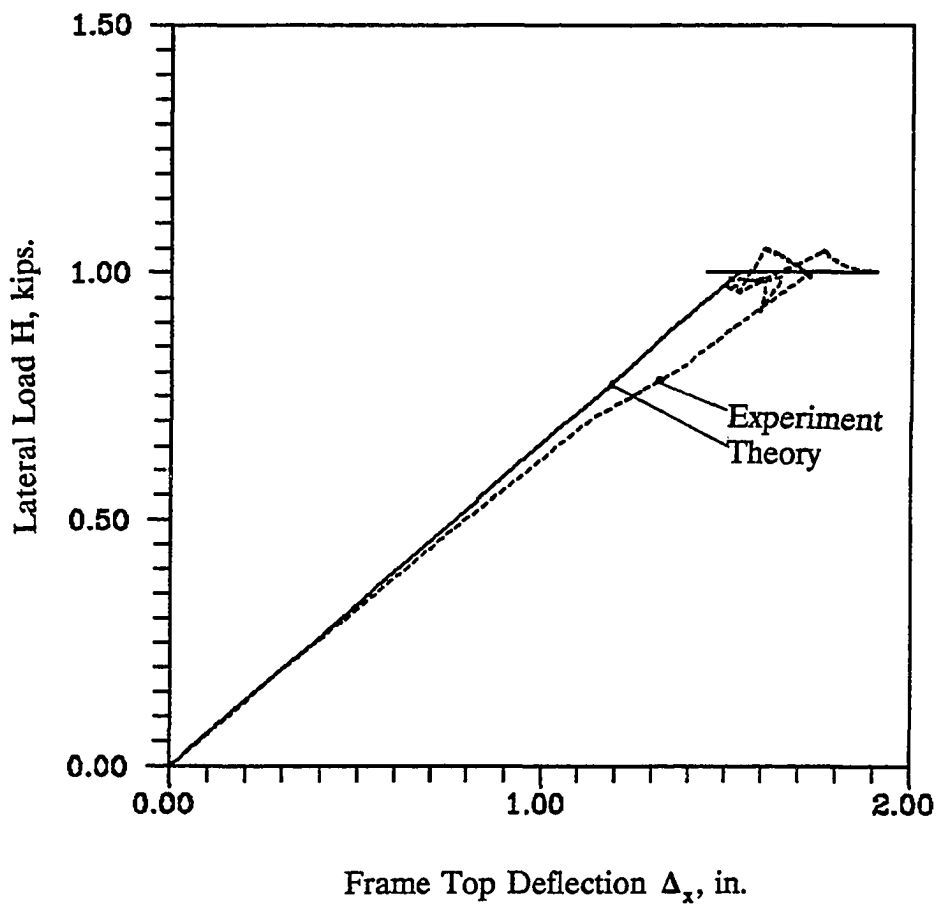


Figure 152. Lateral load versus frame top deflection Δ_x

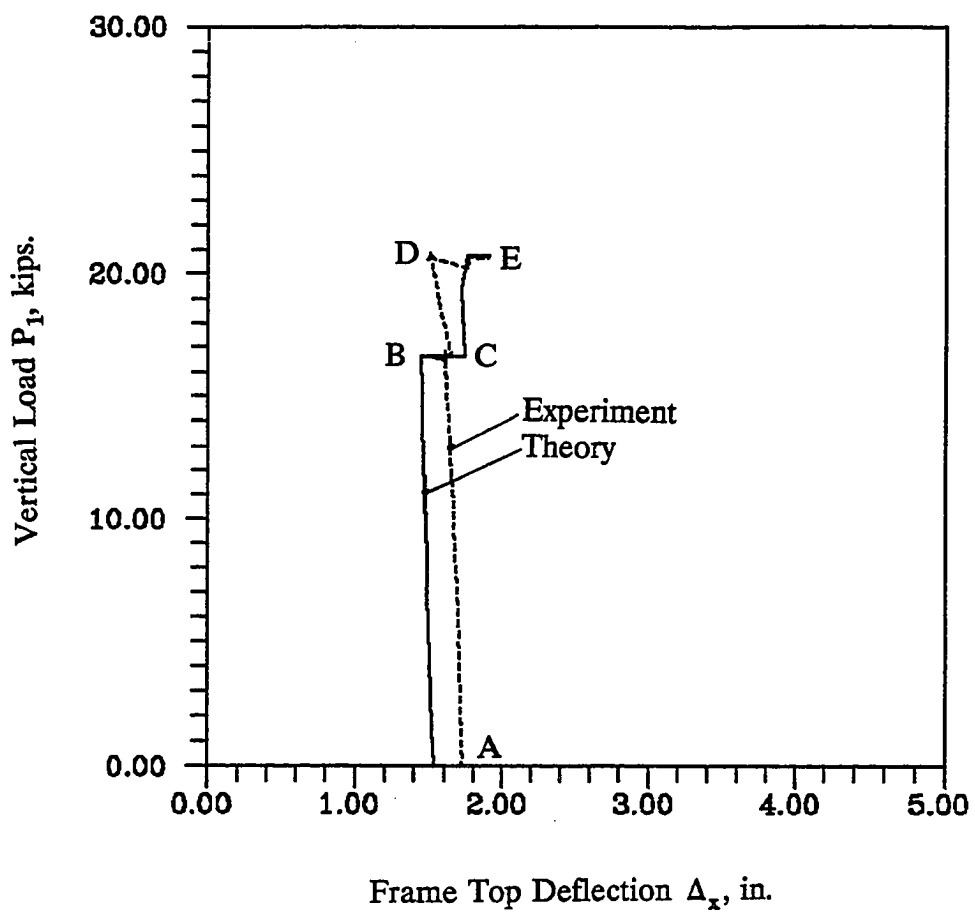


Figure 153. Vertical load P_1 versus frame top deflection Δ_x

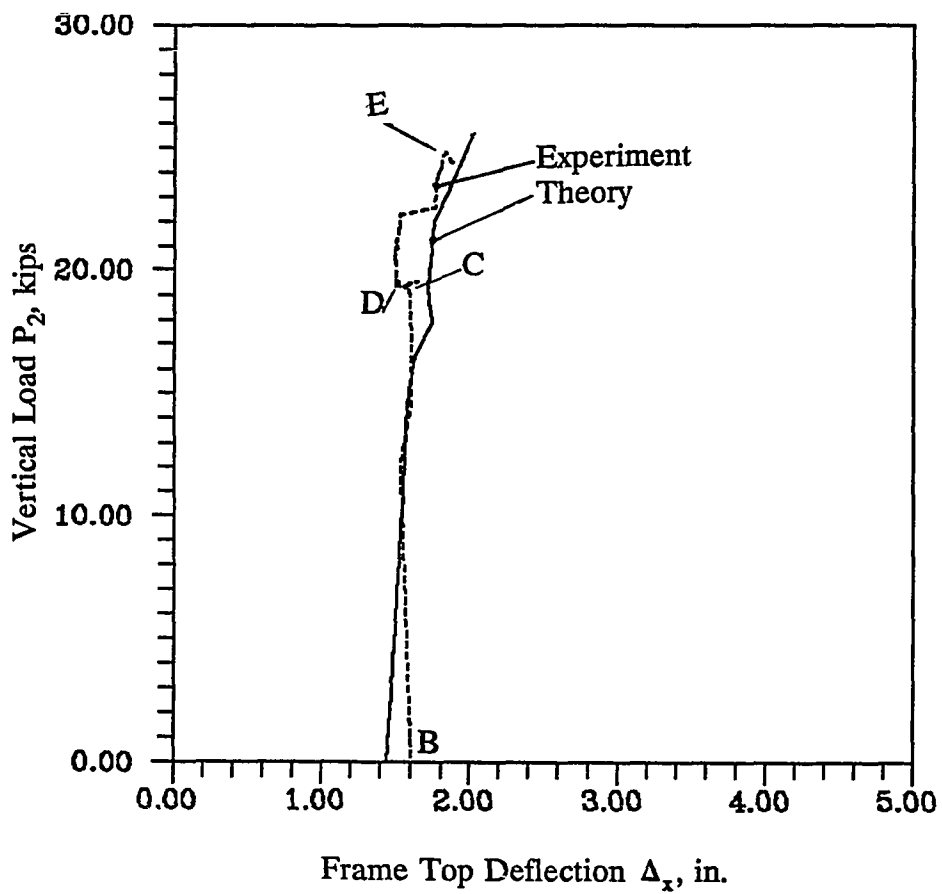


Figure 154. Vertical load P_2 versus frame top deflection Δ_x

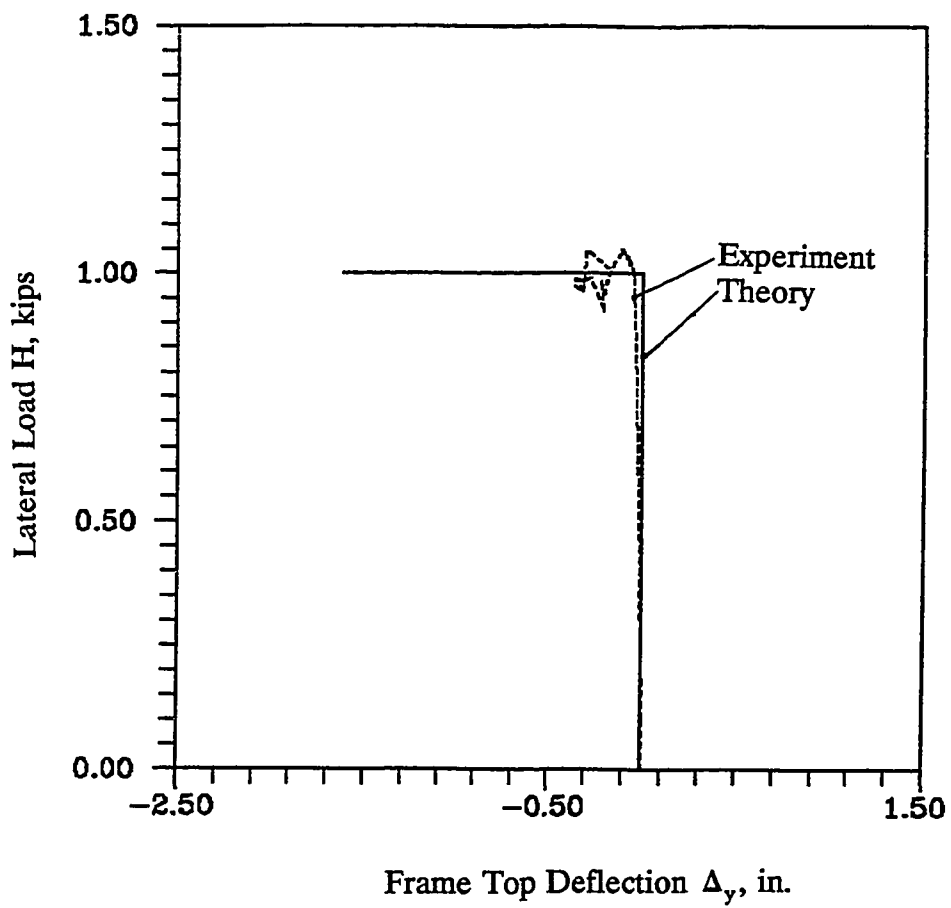


Figure 155. Lateral load H versus frame top deflection Δ_y

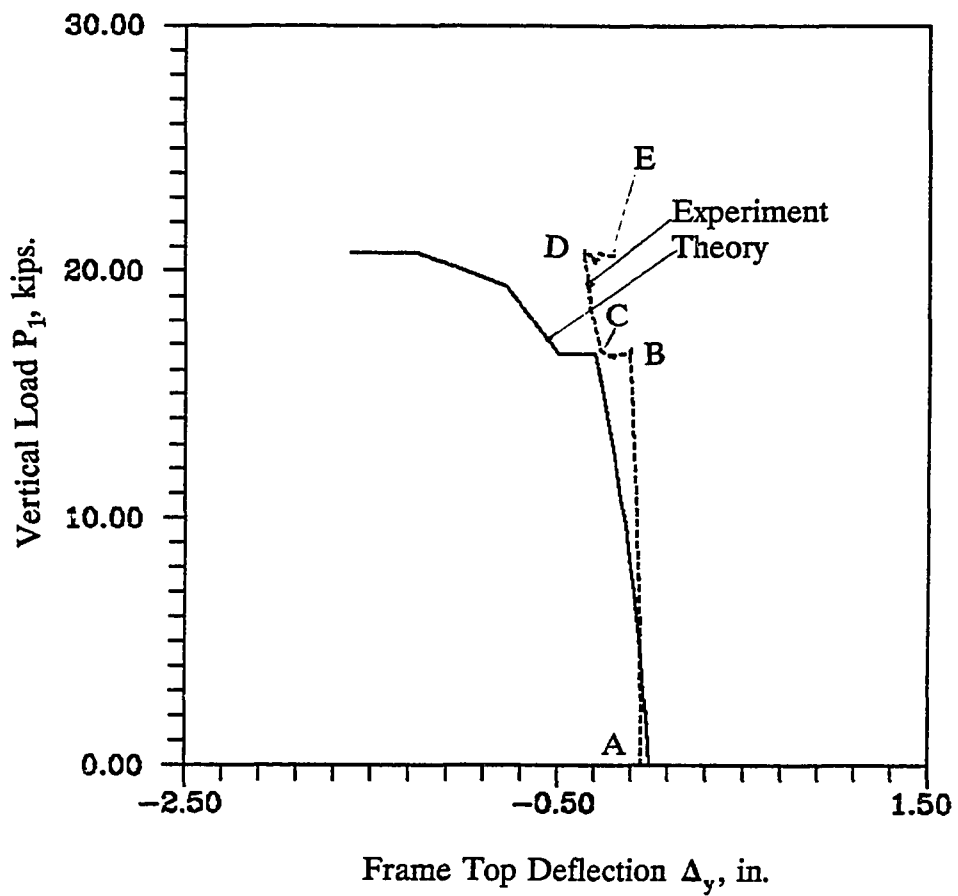


Figure 156. Vertical load P_1 versus frame top deflection Δ_y

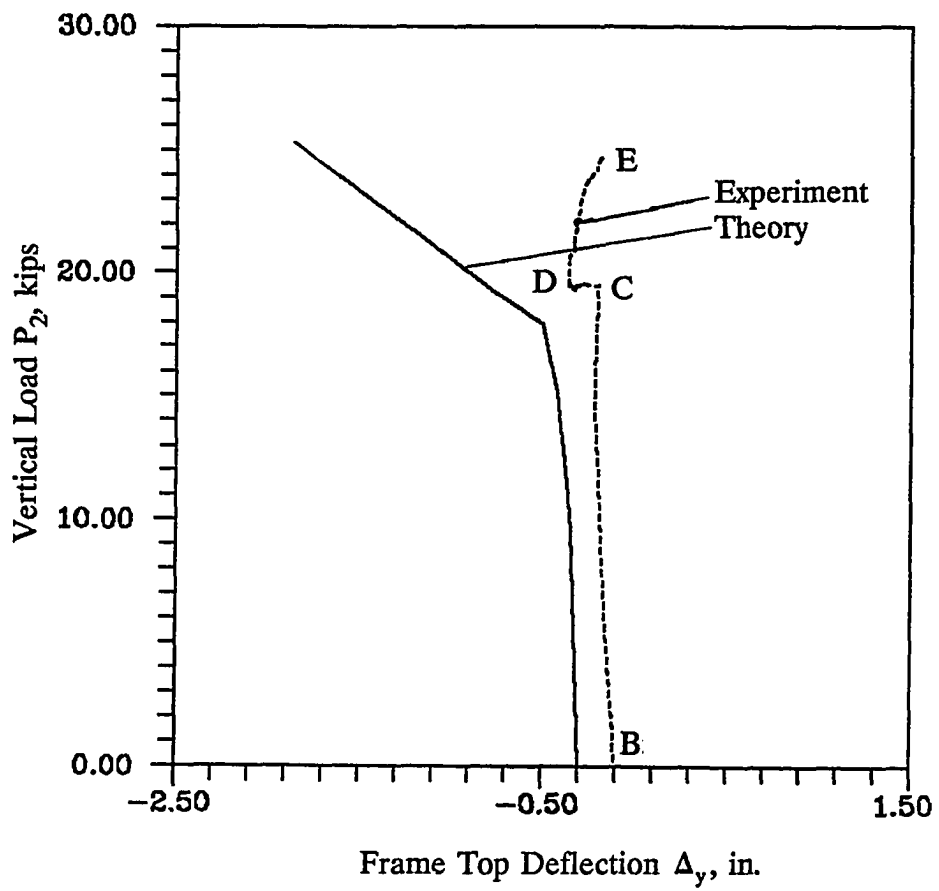


Figure 157. Vertical load P_2 versus frame top deflection Δ_y

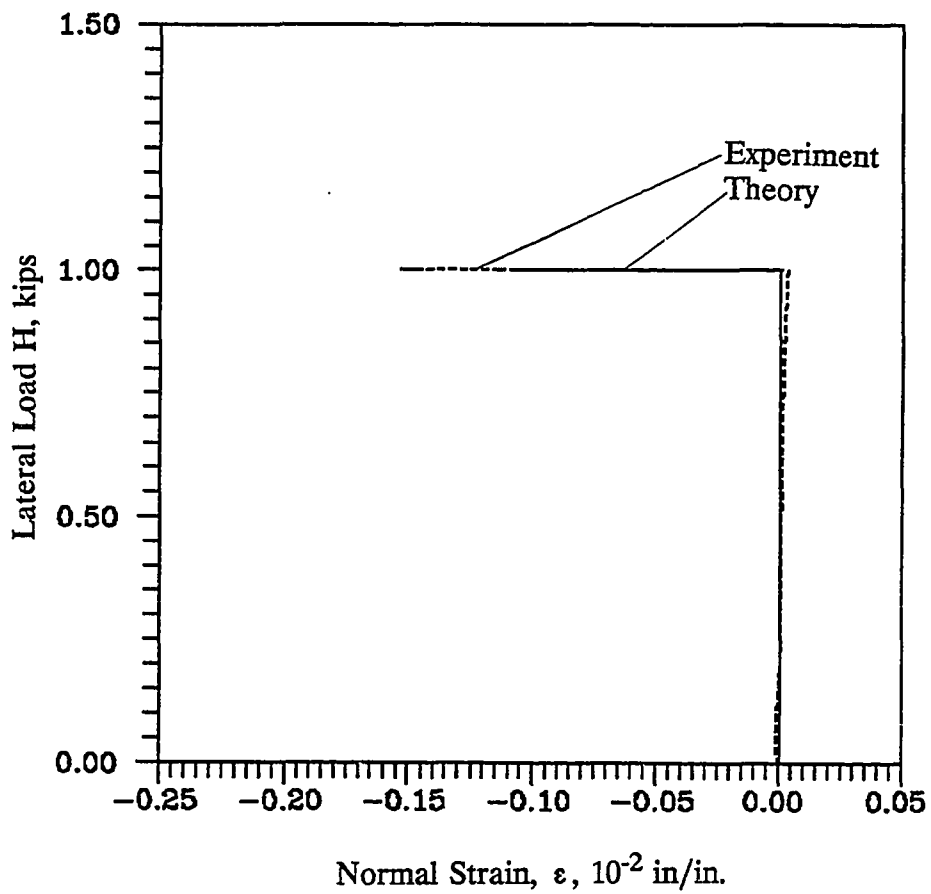


Figure 158. Lateral load H versus normal strain in column 18 at location S1

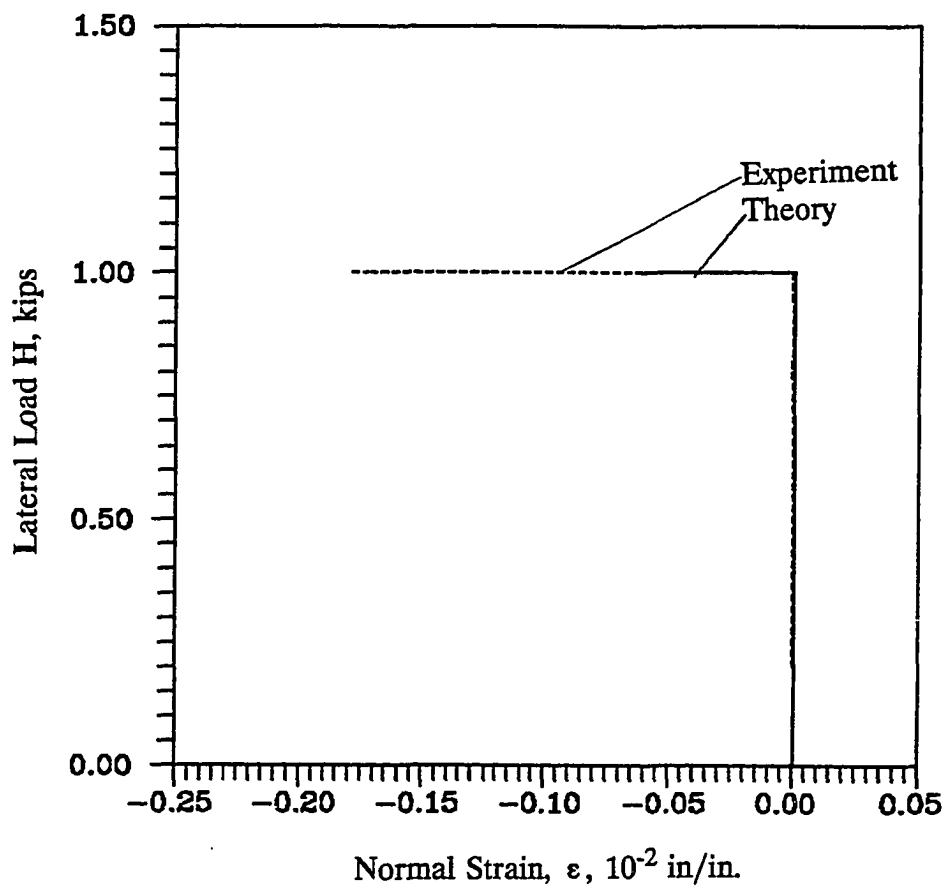


Figure 159. Lateral load H versus normal strain in column 18 at location S2

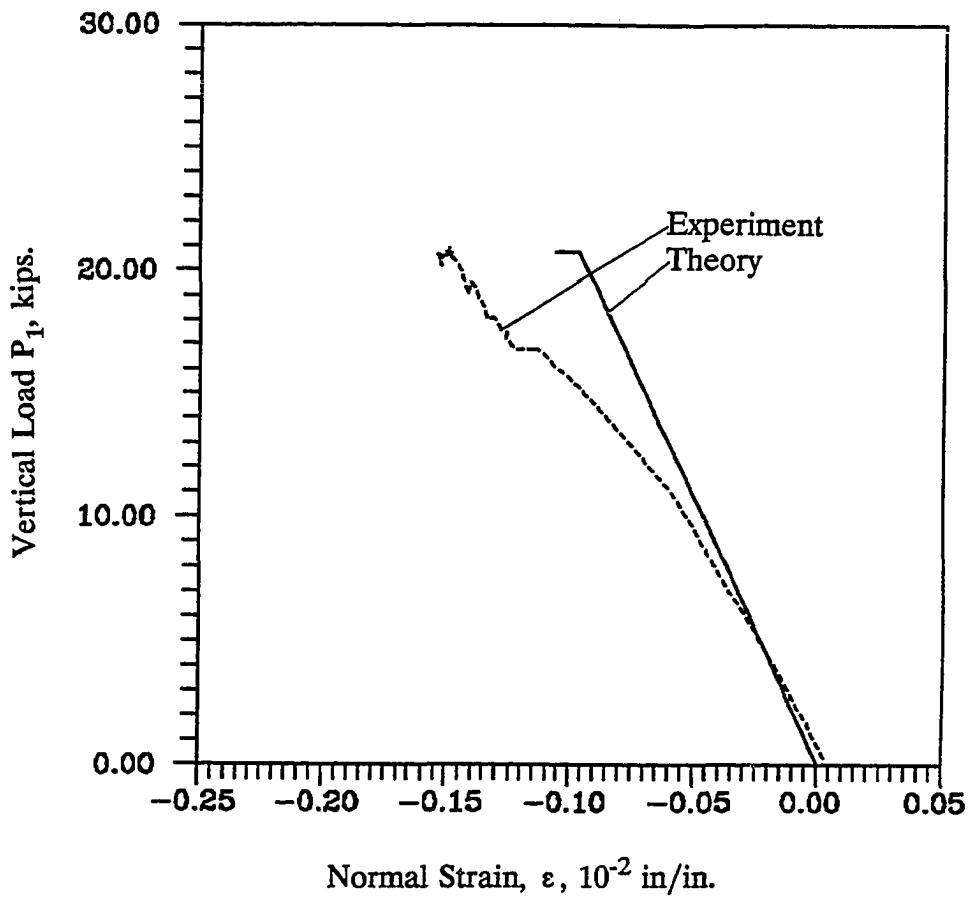


Figure 160. Vertical load P_1 versus normal strain in column 18 at location S1

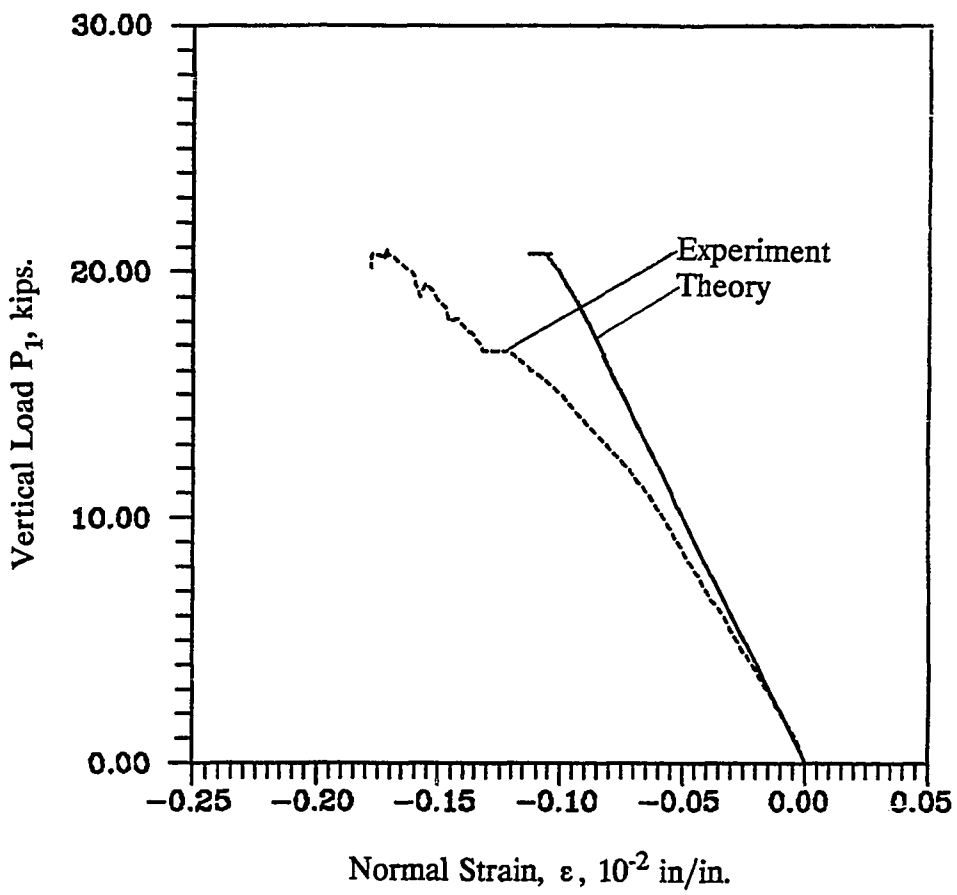


Figure 161. Vertical load P_1 versus normal strain in column 18 at location S2

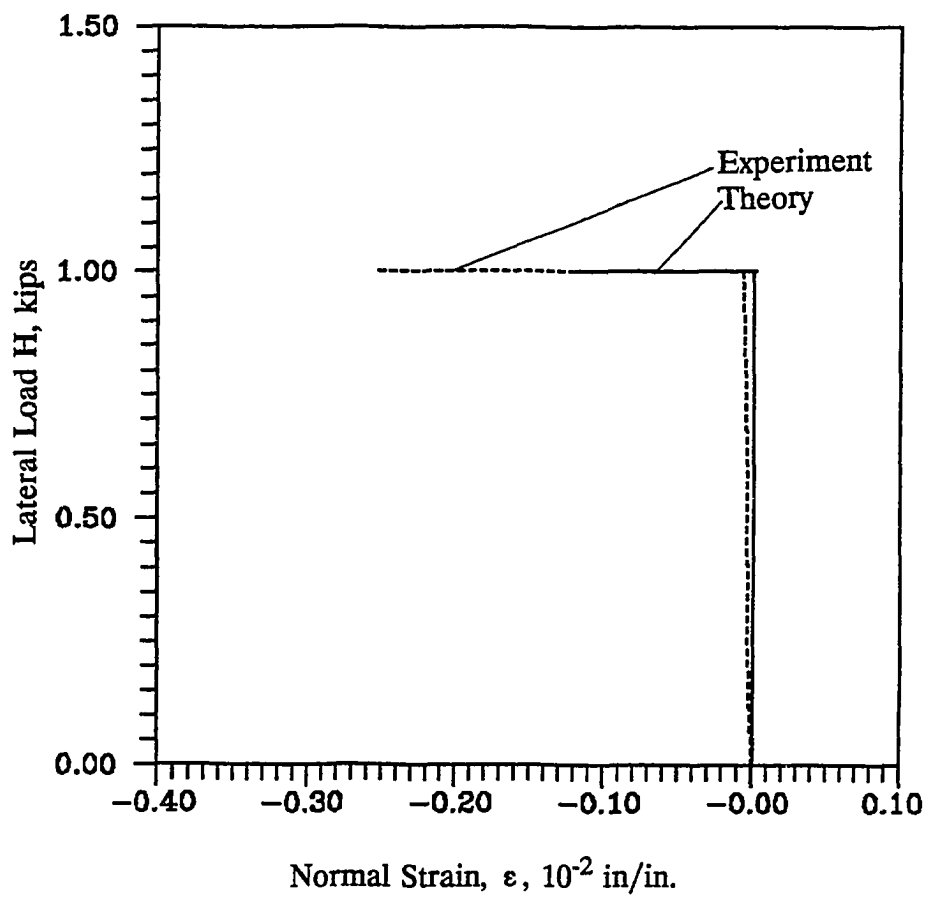


Figure 162. Lateral load H versus normal strain in column 20 at location S3

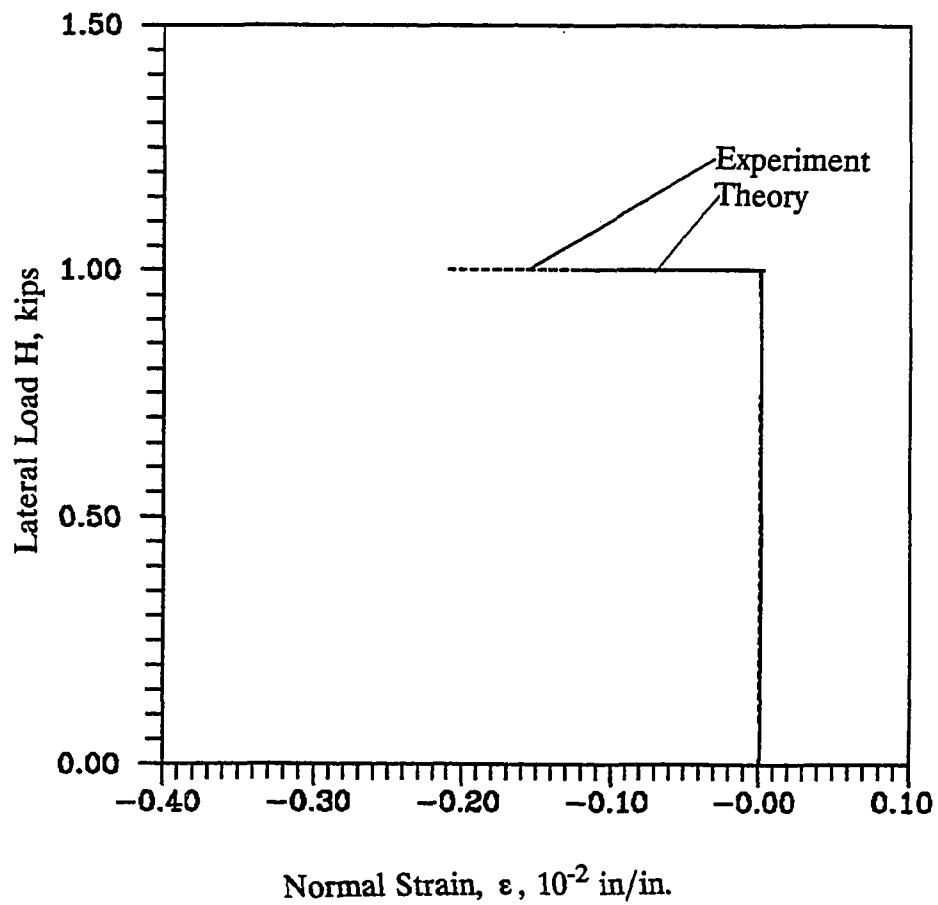


Figure 163. Lateral load H versus normal strain in column 20 at location S4

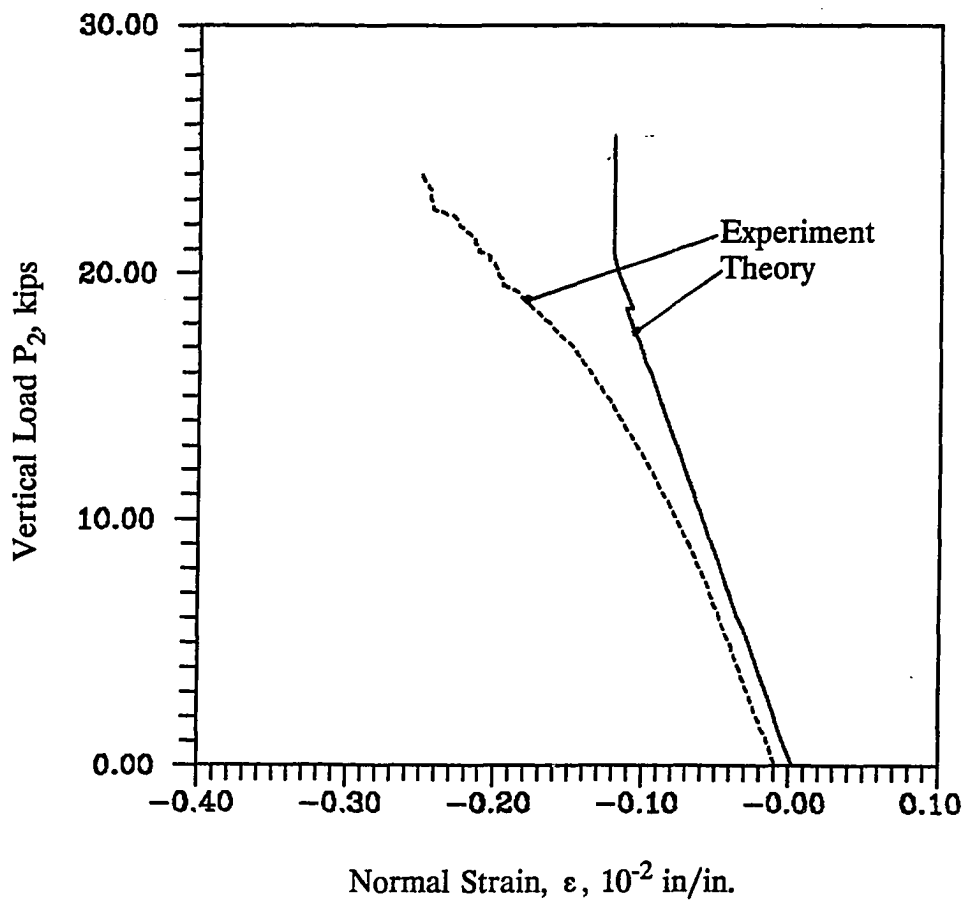


Figure 164. Vertical load P_2 versus normal strain in column 20 at location S3

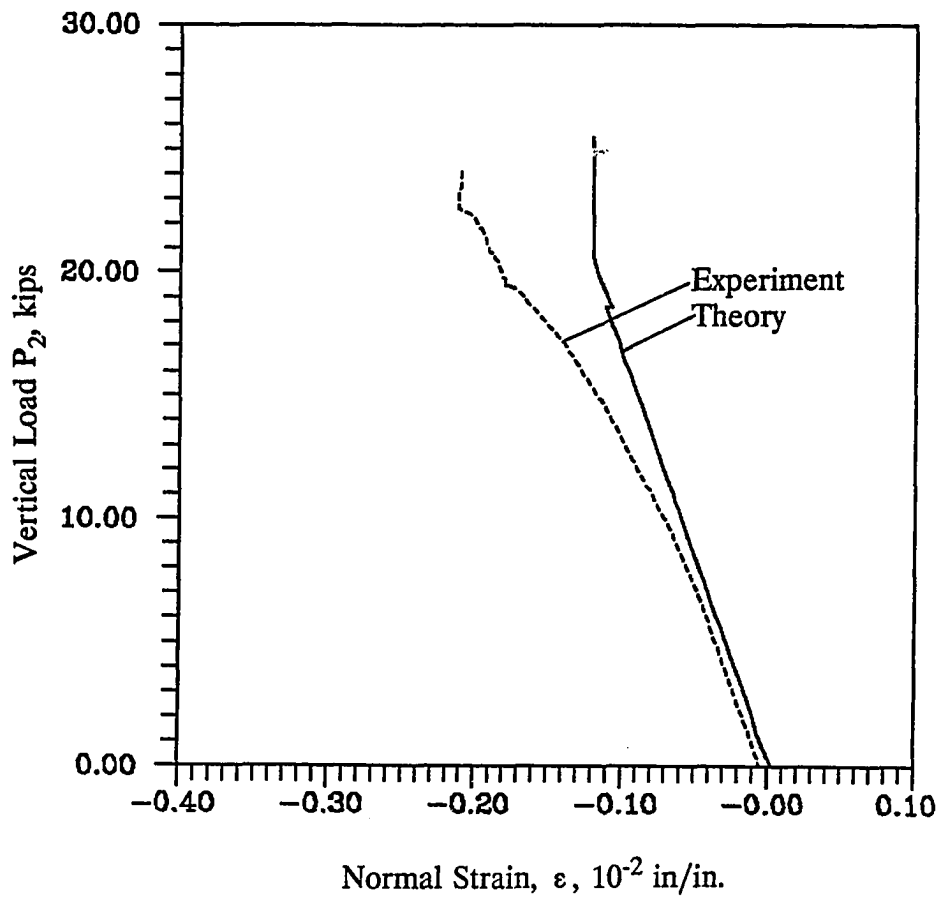


Figure 165. Vertical load P_2 versus normal strain in column 20 at location S4

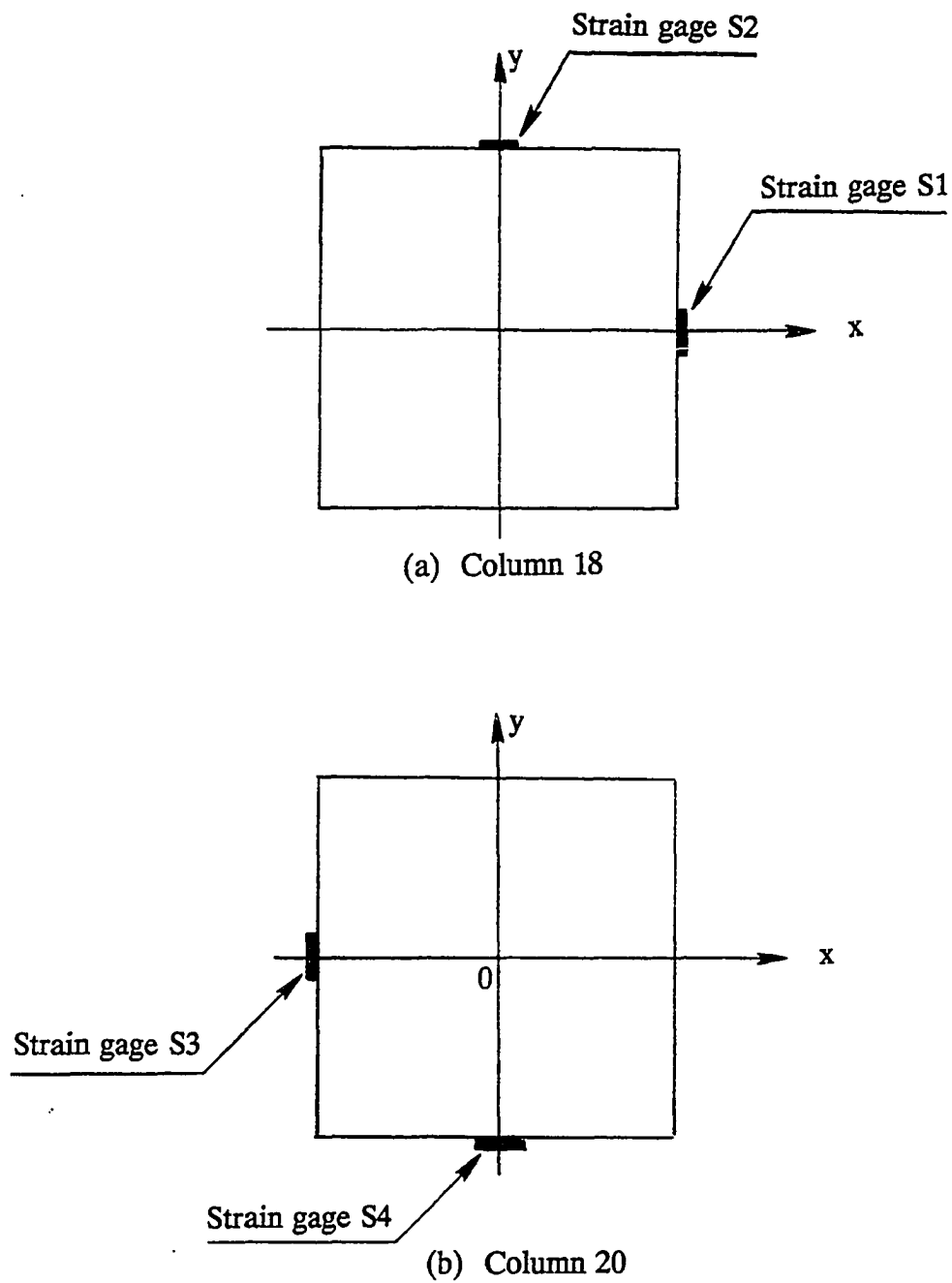


Figure 166. Locations of strain gages on Columns 18 and 20

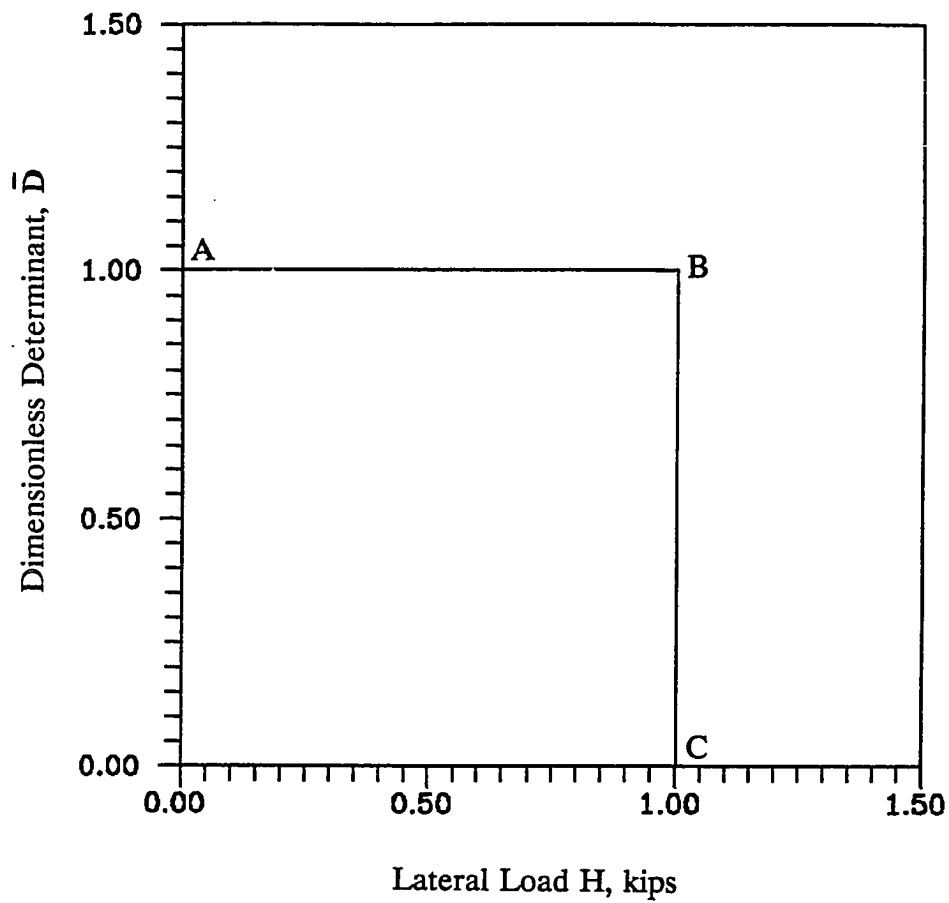


Figure 167. Stiffness degradation curve (\bar{D} -H) for three-story single bay sway space frame with the load path used in experiment

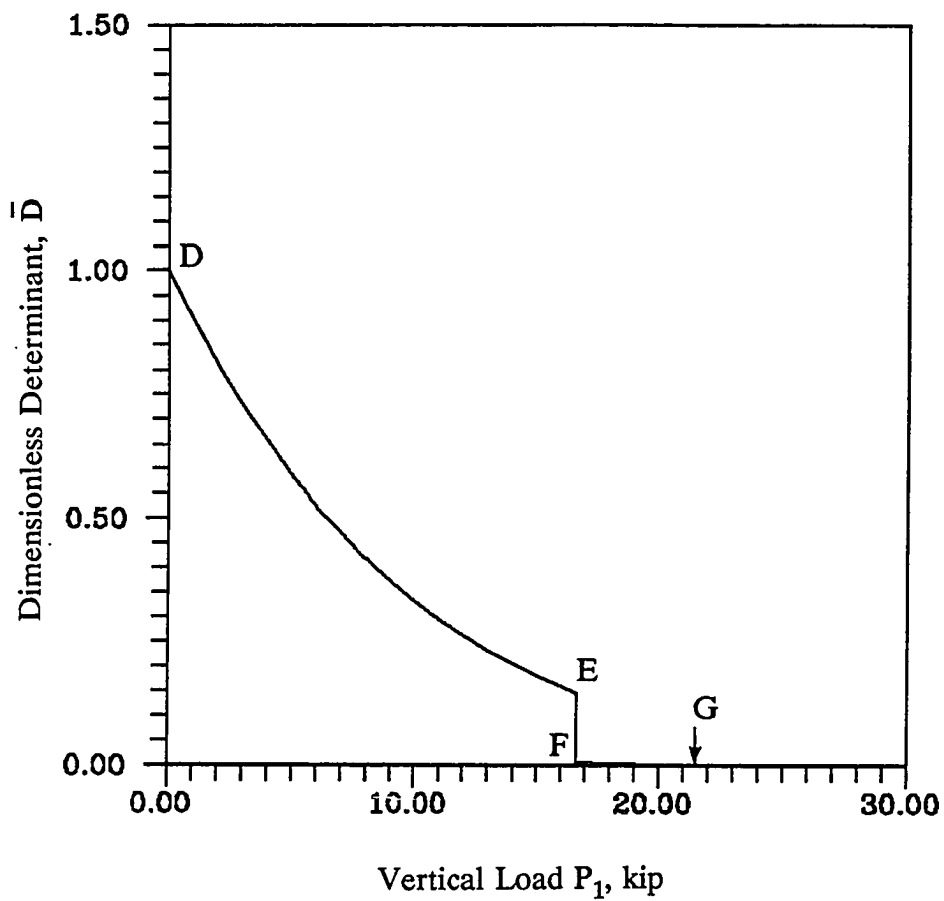


Figure 168. Stiffness degradation curve ($\bar{D}-P_1$) for three-story single bay sway space frame with the load path used in experiment

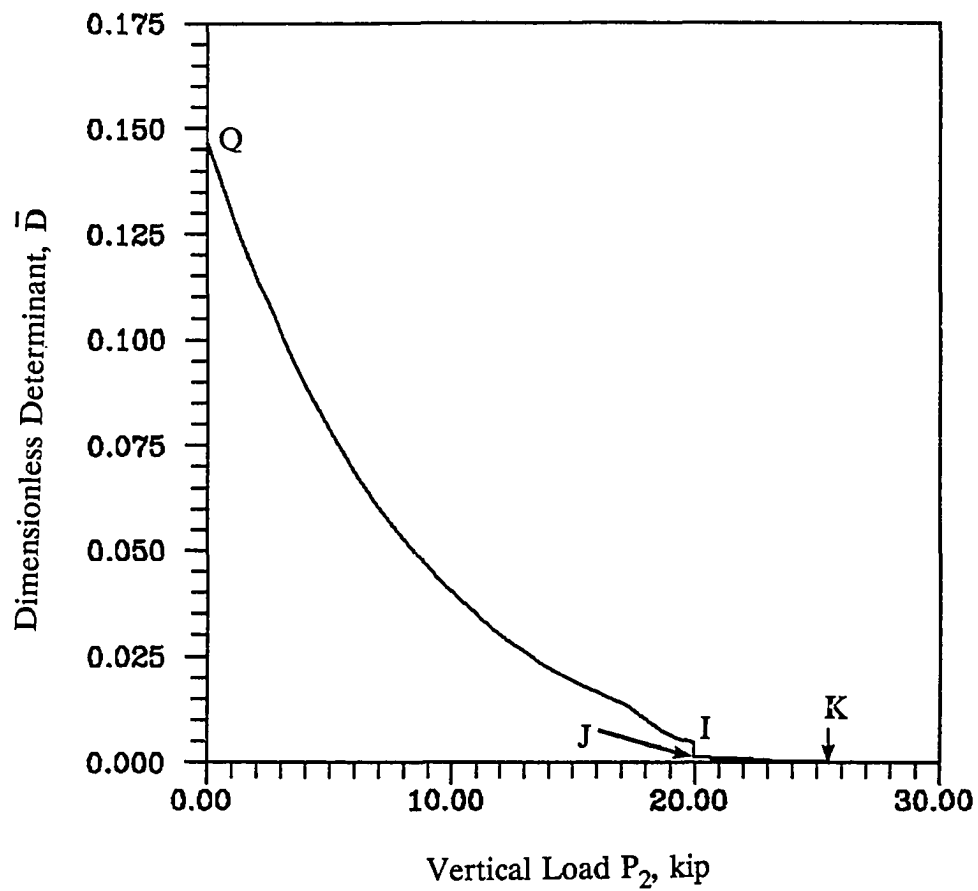


Figure 169. Stiffness degradation curve ($\bar{D}-P_2$) for three-story single bay sway space frame with the load path used in experiment

APPENDIX A

Cross-Sectional Inelastic Rate Equation

The various terms and the incremental equations used in the tangent stiffness procedure for the problem shown in Figure 1 are summarized in this appendix. It can be shown that the dimensionless rate form of Equations 3, 4, and 5 can be expressed in the matrix form given by Equation 8. The various terms of Equation 8 are defined as follows:

$$\{\dot{\mathbf{f}}\} = \{\dot{\mathbf{p}} \quad \dot{\mathbf{m}}_x \quad \dot{\mathbf{m}}_y\} \quad (\text{A-1})$$

$$[\mathbf{K}_t] = \begin{bmatrix} \int \bar{E}_t \frac{da}{A} & \int \bar{E}_t y \frac{da}{A} & \int \bar{E}_t x \frac{da}{A} \\ \int \bar{E}_t y \frac{da}{I_x} & \int \bar{E}_t y^2 \frac{da}{I_x} & \int \bar{E}_t xy \frac{da}{I_x} \\ \int \bar{E}_t x \frac{da}{I_y} & \int \bar{E}_t xy \frac{da}{I_y} & \int \bar{E}_t x^2 \frac{da}{I_y} \end{bmatrix} \quad (\text{A-2})$$

$$\{\dot{\delta}\} = \{\dot{\epsilon}_0 \quad \dot{\Phi}_x \quad \dot{\Phi}_y\} \quad (\text{A-3})$$

where:

$$\mathbf{p} = \frac{\mathbf{P}}{A \sigma_Y} \quad (\text{A-4})$$

$$m_x = \frac{M_x}{M_{xY}} \quad (\text{A-5})$$

$$m_y = \frac{M_y}{M_{yY}} \quad (\text{A-6})$$

$$\bar{\varepsilon}_0 = \frac{\varepsilon_0}{\varepsilon_Y} \quad (\text{A-7})$$

$$\bar{\varphi}_x = \frac{\Phi_x}{\Phi_{xY}} \quad (\text{A-8})$$

$$\bar{\varphi}_y = \frac{\Phi_y}{\Phi_{yY}} \quad (\text{A-9})$$

$$da = d\bar{x} d\bar{y} \quad (\text{A-10})$$

$$\bar{x} = \frac{X}{B/2} \quad (\text{A-11})$$

$$\bar{y} = \frac{Y}{D/2} \quad (\text{A-12})$$

$$\bar{A} = \frac{4A}{BD} \quad (\text{A-13})$$

$$\bar{I}_x = \frac{16I_x}{BD^3} \quad (\text{A-14})$$

$$\bar{I}_y = \frac{16I_y}{B^3D} \quad (\text{A-15})$$

$$M_{xY} = \frac{2\sigma_Y I_x}{D} \quad (\text{A-16})$$

$$M_{yY} = \frac{2 \sigma_Y I_y}{B} \quad (\text{A-17})$$

$$\varepsilon_Y = \frac{\sigma_Y}{E} \quad (\text{A-18})$$

$$\Phi_{xY} = \frac{2 \varepsilon_Y}{D} \quad (\text{A-19})$$

$$\Phi_{yY} = \frac{2 \varepsilon_Y}{B} \quad (\text{A-20})$$

where A is the area of the cross section, and I_x and I_y are the moments of inertia values about the x and the y axes, respectively. The integrals in Equation A-2 are evaluated by numerical summation over the discrete elemental areas shown in Figure 1.

APPENDIX B

Inelastic Parameters

The inelastic load and moments parameters a_{ij} used in Equations 17,18, and 19 are defined as follows:

$$a_{11} = -EA_e \quad (\text{B-1})$$

$$a_{12} = ES_{xe} \quad (\text{B-2})$$

$$a_{13} = ES_{ye} \quad (\text{B-3})$$

$$a_{21} = a_{12} \quad (\text{B-4})$$

$$a_{22} = -EI_{xe} \quad (\text{B-5})$$

$$a_{23} = -EI_{xye} \quad (\text{B-6})$$

$$a_{31} = -a_{13} \quad (\text{B-7})$$

$$a_{32} = -a_{23} \quad (\text{B-8})$$

$$a_{33} = EI_{ye} \quad (\text{B-9})$$

where:

$$A_c = \int_{A_c} dA \quad (\text{B-10})$$

$$S_{xc} = \int_{A_c} y dA \quad (\text{B-11})$$

$$S_{yc} = \int_{A_c} x dA \quad (\text{B-12})$$

$$I_{xc} = \int_{A_c} y^2 dA \quad (\text{B-13})$$

$$I_{yc} = \int_{A_c} x^2 dA \quad (\text{B-14})$$

$$I_{xye} = \int_{A_c} xy dA \quad (\text{B-15})$$

$$P_r = \int_{A_c} \sigma_r dA \quad (\text{B-16})$$

$$P_p = \int_{A_p} \sigma_Y dA \quad (\text{B-17})$$

$$M_{xrc} = \int_{A_c} \sigma_r y dA \quad (\text{B-18})$$

$$M_{yrc} = \int_{A_c} \sigma_r x dA \quad (\text{B-19})$$

$$M_{xp} = \int_{A_p} \sigma_Y y dA \quad (\text{B-20})$$

$$M_{yp} = \int_{A_p} \sigma_Y x dA \quad (\text{B-21})$$

$$\sigma_r = E \epsilon_r \quad (\text{B-22})$$

The above integrals are evaluated numerically by summing over the discretized cross section of the type shown in Figure 1.

APPENDIX C

Portal Frame Shear Equilibrium Equation

The terms used in Equation 107 are defined in this appendix. Substituting Equation 94, 95, 98, and 99 into Equation 107, the following equation is obtained:

$$\begin{aligned}
 & R_{x(11,1)} \theta_{x1} + R_{x(12,1)} \theta_{x2} + R_{x(13,1)} v_n - R_{xs(1,1)} - R_{xp(1,1)} + R_{x(21,1)} \theta_{x1} + \\
 & R_{x(22,1)} \theta_{x2} + R_{x(23,1)} v_n - R_{xs(2,1)} - R_{xp(2,1)} + R_{x(11,3)} \theta_{x5} + R_{x(12,3)} \theta_{x6} + \\
 & R_{x(13,3)} v_n - R_{xs(1,3)} - R_{xp(1,3)} + R_{x(21,3)} \theta_{x5} + R_{x(22,3)} \theta_{x6} + R_{x(23,3)} v_n - \\
 & R_{xs(2,3)} - R_{xp(2,3)} + (P_{c1} + P_{c3}) v_n = HL_c
 \end{aligned} \tag{C-1}$$

where P_{c1} and P_{c3} are the axial loads in columns 1 and 3, respectively. By using the condensed notation:

$$\Psi_{x1} = R_{x(11,1)} + R_{x(21,1)} \tag{C-2}$$

$$\Psi_{x2} = R_{x(12,1)} + R_{x(22,1)} \tag{C-3}$$

$$\Psi_{x3} = R_{x(11,3)} + R_{x(21,3)} \tag{C-4}$$

$$\Psi_{x4} = R_{x(12,3)} + R_{x(22,3)} \tag{C-5}$$

$$\Psi_{x5} = R_{x(13,1)} + R_{x(23,1)} + R_{x(23,3)} + P_{c1} + P_{c3} \quad (C-6)$$

$$\Psi_{x6} = -R_{xs(1,1)} - R_{xs(2,1)} - R_{xs(1,3)} - R_{xs(2,3)} - \\ R_{xp(1,1)} - R_{xp(2,1)} - R_{xp(1,3)} - R_{xp(2,3)} \quad (C-7)$$

Equation C-1 is expressed as:

$$\Psi_{x1} \theta_{x1} + \Psi_{x2} \theta_{x2} + \Psi_{x3} \theta_{x5} + \Psi_{x4} \theta_{x6} = HL_c + \Psi_6 \quad (C-8)$$

which is Equation 108 presented in Section 3.1.1

APPENDIX D

Computer Programs

This appendix presents the complete listing of the following computer programs based on the theory presented in this dissertation:

Program D.1 Biaxial Sway Beam-Column

Program D.2 Sway Portal Frame (SPF)

Program D.3 Sway Space Frame (SSF)

The input parameters for the programs are defined below.

For Program D.1:

ANG	Bilinear angle of rotation in radian (θ_s)
B	Cross section width (B)
B1	Equal D for tube and equal zero for I-section
CODE	Beam-column Identification code
COX	Coefficient for maximum moment applied about x axis
COY	Coefficient for maximum moment applied about y axis
D	Cross section depth (D)
DELX	Initial crookedness in the x direction (u_{01})
DELY	Initial crookedness in the y direction (v_{01})
DTOL	Determinant tolerance
E	Young modulus (E)

EL	Beam-column length, (L)
EMXBSXB	Incremental applied moment about x axis at bottom
EMXTSXT	Incremental applied moment about x axis at top
EMYBSYB	Incremental applied moment about y axis at bottom
EMYTSYT	Incremental applied moment about y axis at top
EPSAVE	Axial load increment
FT	Flange thickness of the cross section (t)
FY	Yield stress (σ_y)
INPT	Number of nodes along the beam-column length (n)
ITANG	Equal 1.0 for tangent modulus
KX	Lateral restraint in the x direction (K_x)
KY	Lateral restraint in the y direction (K_y)
KBX	Rotational restraint about x axis at B (K_{Bx})
KTX	Rotational restraint about x axis at T (K_{Tx})
KBY	Rotational restraint about y axis at B (K_{By})
KTY	Rotational restraint about y axis at T (K_{Ty})
LP	Load Path (LP or NP)
MBAX	Initial applied moment at end B about x axis
MTAX	Initial applied moment at end T about x axis
MBAY	Initial applied moment at end B about y axis
MTAY	Initial applied moment at end T about y axis
NELAST	Coefficient used as 1 for elastic problem
NFH	Number of layers in each flange

NFV	Number of elements across the flange
NWH	Number of layers in each web
NWV	Number of elements across the web
PB1	Initial applied axial load
SRC	Compressive residual stress (σ_{rc})
TTOL	Equal to 10.0 (incremental force reduction factor)
WT	Web thickness of the cross section (t)

For Program D.2 and D.3:

In addition to the input data for the beam-columns, the following input parameters are required in the programs for the frames:

I Story number (= 1, 2, 3)

J Joint number (= 5, 6, 7, 8, 17, 18, 19, 20, 29, 30, 31, 32)

ALPPXI Coefficient controlling the lateral load at joint i in x-direction; I=1,2,3

ALPPYI Coefficient controlling the lateral load at joint i in y-direction; I=1,2,3

ALPPZJ Coefficient controlling the vertical load at joint j in z-direction; I=1,2,3

FRATIOP Coefficient for maximum P load

FRATIOM Coefficient for maximum M load

NXJ Coefficient controlling the moments at joint J about x-direction;
J=5,6,7,....

NYJ Coefficient controlling the moments at joint J about y-direction;
J=5,6,7,....

KXJ Rotational restraints about x axis at joint J (Kx^j); J=5,6,7,....

KYJ	Rotational restraints about y axis at joint J (Ky^J); J=5,6,7,....
LPF	Load path for frames
MAPL	Initial applied moments (M_x and M_y)
MAPLINC	Incremental load for moments
P21	Initial applied load on top of beam 21 (P_1)
P22	Initial applied load on top of beam 22 (P_1)
P23	Initial applied load on top of beam 23 (P_2)
P24	Initial applied load on top of beam 24 (P_2)
P21INC	Incremental load for P_1
P22INC	Incremental load for P_1
P23INC	Incremental load for P_2
P24INC	Incremental load for P_2
P21MAX	Maximum load for experimental use
PAPL	Initial applied lateral (H) and vertical loads (P)
PAPLINC	Incremental loads for lateral and vertical
X21	Distance between P_1 on beam 21 and joint 30
X22	Distance between P_1 on beam 22 and joint 30
X23	Distance between P_2 on beam 23 and joint 32
X24	Distance between P_2 on beam 24 and joint 32

Sample output are presented at the end of each of the programs.

D.1 Biaxial Sway Beam-Column

```

C PROGRAM SWAY BIAXIALLY LOADED BEAM-COLUMN
INCLUDE 'PROJECT'
READ(12,7)CODE
7 FORMAT(A7)
PRINT 193,CODE
193 FORMAT(' * LOADING NUMBER * ','A9,')
READ(12,*)ALPHAP,ALPHAM,ALPHA1,ALPHA2,COEFP,COX,COY
READ(12,*)LP,ITANG,TOLG
PRINT *,
EMAX=0.0
INNN=0
CALL READ
CALL SEC
TR=TOTAL-NWV*NWH
IF ( B1 .EQ. 0.0 ) THEN
DO 66 I=1,TOTAL
IF( I .LE. TR )THEN
STR(I)=-ABS(SRC)+SRT*ABS(X(I))+SRT
ELSE
STR(I)=SRT
ENDIF
66 CONTINUE
ENDIF
IF ( B1 .LE. 0.0 ) GO TO 68
QL=2.0*SRC*(BR+DR)/(8.0*SRC-4.0*SRT+4.0*SRC*ABS(SRC)/SRT)
FQQ=4.*SRT*FT+4.*WT*SRT+8.*SRC*ABS(SRC)*FT/SRT-8.*SRC*FT
+8.*FT*SRC*ABS(SRC)/SRT-8.*WT*SRC-8.*FT*SRC*ABS(SRC)/SRT
FQ=4.0*SRC*(BR*FT+DR*WT)
F=SRT*(FT*WT**2+WT*FT**2)
QL=0.5*(-FQ+SQR(FQ**2-4.0*F*FQQ))/FQQ
Z=ABS(SRC)*QL/SRT
QQ=QL+Z
DO 67 I=1,TOTAL
IF ( I .LE. TR ) THEN
STRM=SRT*(1+WT/(2.*QL))
SOUT=-ABS(SRC)/Z*B/2.0-STRM
STR(I)=ABS(X(I))*B/2.0*(STRM+AES(SOUT))*2.0/B-ABS(SOUT)
IF ( STR(I) .LT. SRC ) STR(I)=SRC
ELSE
DR=D-2.0*FT
STRM=SRT*(1-0.5*FT/QL)
SOUT=-ABS(SRC)/Z*DR/2.0-STRM
STR(I)=ABS(Y(I))*D/2.0*2.0/DR*(STRM+ABS(SOUT))-ABS(SOUT)
IF ( STR(I) .LT. SRC ) STR(I)=SRC
ENDIF
67 CONTINUE
68 FCC=0.0
DO 32 I=1,TOTAL
32 FCC=FCC+AD(I)*STR(I)*B*D/4.0
IYYY=0
JCHEK=0
JJ=1

```

```

IF ( ABS(SRC) .LE. 0.00001 ) THEN
DO 333 I=1,TOTAL
333 STR(I)=0.0
ENDIF
IF ( ELIMT .NE. 900000.) GO TO 922
NS1=NFV*NFH
NS2=NS1*2-NFV+1
NS3=2*NS1
922 CALL EXT
END
c The next subroutine is as a second main program
SUBROUTINE EXT
INCLUDE 'PROJECT'
PIY=99999.0
ICHI=0
IDL=0
IXEE=0
RATIO=1.0
READ(12,*)KTX,KTY,KBX,KBY,KX,KY,MATX,MATY,MABX,MABY,PBI
READ(12,*)TTOL,ANG
9911 PY=FY*A
ADXX=IX*10.0
LAXI=0
DET0=0.0
IYYY=0
ICHI=0
IDL=0
IXEE=0
JCHEK=0
IDD=0
IEE=0
PA=0.0
DO 95 I=1,INPT
AE(I)=A
MYR(I)=0.0
UNL1(I)=0.0
UNL2(I)=0.0
UNL3(I)=0.0
MXA(I)=0.0
MYA(I)=0.0
ST1(I)=0.0
ST2(I)=0.0
95 ST3(I)=0.0
DO 96 J=1,INPT
DO 96 I=1,TOTAL
IT(J,I)=0
ITR(J,I)=0
STRPRE(J,I)=STR(I)/FY
96 STRPAS(J,I)=STR(I)/FY
TTOL=10.
CURMX=0.0
CUTS=0.0
ATX=1.0

```

```

ABX=1.0
ATY=1.0
ABY=1.0
BTX=0.0
BBX=0.0
BTY=0.0
BBY=0.0
ICH=0
NR=INFT*2
NG=NR+4
NC=NG+1
DO 829 I=1,NG
829 DEI=0.0
DO 529 I=1,NG+1
V(I)=0.0
U(I)=0.0
529 XI(I)=0.0
DO 419 I=1,INFT+2
XI(I)=0.0
419 XG(I)=0.0
Z=0.0
DO 219 I=1,INFT
Z=(I)*H
CUP(I)=0.0
CUX(I)=0.0
CUY(I)=0.0
XL(I)=DELY*SIN(P1*Z/EL)
XGT(I)=DELX*SIN(P1*Z/EL)
V(I)=DELY*SIN(P1*Z/EL)
U(I)=DELX*SIN(P1*Z/EL)
XL(I)=DELY*SIN(P1*Z/EL)
219 XG(I)=DELX*SIN(P1*Z/EL)
CEN=INFT/2+1
MXYX=(2*FY*IX)/D
MYXX=(2*FY*TY)/B
PRINT *,MXY,MYX,MXXY,MYXY
PRINT *,PY ,PY
MXT=KTX*XL(INFT+2)
MXBB=KBX*XL(INFT+1)
MYT=KTY*XG(INFT+2)
MYBB=KBY*XG(INFT+1)
ISTT=0
PMAX=COEFF*PY
MMAX=COEFM*MYXY
UMX=COX*MXXY
UMY=COY*MYXY
EP=EPSAVE
EMXT=EMXTSXT
EMYT=EMYSYX
EMXB=EMXBSXB
EMYB=EMYSYB
EP*ALPHAP
EMYT=EMYT*ALPHAI*ALPHAM
EMXT=EMXT*ALPHA2*ALPHAM
PBI=EP
MATX=EMXT*ALPHA2
MATY=EMYT*ALPHAI
MABX=EMXB*ALPHA2
MABY=EMYB*ALPHAI
ILP=0
969 CONTINUE
67 DO 491 NL=1,100
DO 492 NT=1,20000
STOPTR=MAX(ABS(EP),ABS(EMXT),ABS(EMYT),ABS(EMXB),ABS(EMYB))
IF ( STOPTR .LT. 0.1000) GO TO 999
IEEL=0
IF ( LP .GT. 20) GO TO 201
IF ( ILP .EQ. 1 ) GO TO 838
IF ( ILP .EQ. 13 ) GO TO 838
IF ( LP .EQ. 10 ) GO TO 839
IF ( LP .EQ. 11 ) GO TO 839
IF ( LP .EQ. 1 .AND. CONV1 .GE. PMAX ) THEN
PBI=PBI*EP
EP=0.0
EMXT=EMXTSXT
EMYT=EMYSYX
EMXB=EMXBSXB
MATY=EMYT
ALPHAP=0.0
ALPHAM=1.0
ILP=1
ELSE IF ( LP .EQ. 6 .AND. PBI .GE. PMAX ) THEN
EMXT=0.0
EMXB=0.0
EMYB=0.0
EMYT=0.0
ILP=77
ELSE IF ( LP .EQ. 3 .AND. PBI .GE. PMAX ) THEN
ALPHAM=1.0
EMXT=EMXTSXT
EMYT=EMYSYX
EMXB=EMXBSXB
EMYB=EMYSYB
ILP=1
ELSE IF (LP.EQ. 2 .AND. CONVMY.GE. UMY
+ .OR. LP .EQ. 2 .AND. CONVMX .GE. UMX) THEN
ALPHAP=1.0
ALPHAI=0.0
ALPHA2=0.0
ALPHAM=0.0
MATX=MATX-EMXT
MATY=MATY-EMYT
MABX=MABX-EMXB
MABY=MABY-EMYB
EMXT=0.0
EMYT=0.0
EMXB=0.0

```

```

EMYB=0.0
EP=EPSAVE
PB1=EP
ILP=1
ELSE IF ( LP .EQ. 7 .AND. PB1 .GE. PMAX ) THEN
EP=1.0E-15
ILP=1
ELSE IF (LP .EQ. 4 .AND. CONVMX .GE. UMX ) THEN
ALPHAP=1.0
EP=EPSAVE
PB1=EP
ILP=1
ENDIF
IF ( LP .EQ. 8 .AND. ABS(MATX) .GE. MMAX ) THEN
ALPHA2=0.0
ALPHA1=1.0
EMYT=EMYSYT
EMYB=EMYSYB
MATY=EMYT
MABY=MABY
EMXT=0.0
EMXB=0.0
ILP=1
ENDIF
IF ( LP .EQ. 9 .AND. ABS(MATX) .GE. UMX ) THEN
ALPHA1=1.0
ALPHA2=0.0
EMYT=EMYSYT
EMYB=EMYSYB
ILP=9
ENDIF
839 IF (LP .EQ. 11 ) GO TO 836
IF (LP .EQ. 10 .AND. CONVP .GE. PMAX ) THEN
PB1=PB1-EP
EP=0.0
EMXT=EMXTSXT
EMXB=EMXBSXB
MATX=EMXT
MABX=EMXB
ALPHA1=0.0
ALPHA2=1.0
ALPHAP=0.0
ALPHAM=1.0
LP=11
ENDIF
836 CONTINUE
IF ( LP .EQ. 11 .AND. CONVMX .GE. UMX ) THEN
MATX=MATX-EMXT
MABX=MABX-EMXB
EP=0.0
ALPHP=0.0
EMYT=EMYSYT
EMYB=EMYSYB
MATY=EMYT
MABY=EMYB

```

```

EMXT=0.0
EMXB=0.0
ALPHA1=1.0
ALPHA2=0.0
ILP=13
ENDIF
IF ( LP .EQ. 12 .AND. CONVMY .GE. UMY ) THEN
MATY=MATY-EMYT
MABY=MABY-EMYB
ALPHA1=0.0
ALPHA2=1.0
EMXT=EMXTSXT
EMXB=EMXBSXB
MATX=EMXT
MABX=EMXB
EMYT=0.0
EMYB=0.0
LP=13
ENDIF
IF ( LP .EQ. 13 .AND. CONVMX .GE. UMX ) THEN
MATX=MATX-EMXT
MABX=MABX-EMXB
EMXT=0.0
EMXB=0.0
ALPHA2=0.0
ALPHAM=0.0
ALPHP=1.0
ILP=13
ENDIF
201 CONTINUE
838 PB1=PB1-EP+EP*ALPHAP
MATX=MATX-EMXT+EMXT*ALPHA2*ALPHAM*RATIO
MABX=MABX-EMXB+EMXB*ALPHA2*ALPHAM*RATIO
MATY=MATY-EMYT+EMYT*ALPHA1*ALPHAM
MABY=MABY-EMYB+EMYB*ALPHA1*ALPHAM
IF ( ILP .EQ. 2 ) THEN
EMXT=0.0
EMYT=0.0
EMXB=0.0
EMYB=0.0
ENDIF
IF (DET0 .EQ. 0.0 ) THEN
PB1=PB1/1000.0
MATY=MATY/1000.0
MABY=MABY/1000.0
ENDIF
PB=-PB1/PY
119 MXT=KTX*XL(INPT+2)
MXBB=+KBX*XL(INPT+1)
MYT=+KTY*XG(INPT+2)
MYBB=+KBY*XG(INPT+1)
DO 494 K=1,INPT
Z=(K-1)*H
MXB(K)=(+PB1*XL(K)+MXBB-MABX-Z/EL*(MXT+MXBB-MATX-
+MABX+PB1*XL(INPT)))/MXY

```

```

MYB(K) = (-PBI*XG(K) + MYBB*MBY + Z/EL*(-MVT*MYBB + MATY +
+MABY + PBI*XG(INFT)))/MYYY
494 CONTINUE
561 CONTINUE
ILOCC=0
JI=1
727 CONTINUE
77 CALL STRAINU
IF (NELAST.NE.1) GO TO 4455
DO 319 I=1,TOTAL
IT(I)=1
319 STRY(I)=0.0
4455 FDT(1)=PB-PA
FDT(2)=MXB(JI)-MXA(JI)
FDT(3)=MYB(JI)-MYA(JI)
ICRAMER=0
666 CALL STIF
IF (ICRAMER.EQ.1) GO TO 808
CALL STRAINU
IF (NELAST.EQ.1) THEN
DO 329 I=1,TOTAL
IT(I)=1
329 STRY(I)=0.0
ENDIF
CALL LOAD
IF (ELJMT.NE.900000.) GO TO 922
922 CONTINUE
IF (ABS(MATY).LE.99999.) GO TO 2299
PRINT 732JJ,MYA(JI),IXE(JI),IYE(JI)
PRINT 84MX,FDT(1)
PRINT 85MY,FDT(3)
43 FORMAT('INTERNAL AXIAL LOAD =',F74,' UNBALANCE P =',F7.5)
84 FORMAT('INTERNAL MX =',F74,' UNBALANCE MX =',F7.5)
85 FORMAT('INTERNAL MY =',F74,' UNBALANCE MY =',F7.5)
732 FORMAT('J MY IX IY',I3,F16.8)
2299 IF (ABS(FDT(1)).LT.TOL .AND. ABS(FDT(2)).LT.TOL
+ .AND. ABS(FDT(3)).LT.TOL ) GO TO 555
808 IF (ICRAMER.EQ.1) ICH=10
ICH=ICH+1
IF ( ICH.GE.10 ) THEN
ICHI=ICHI+1
DO 771 I=1,INPT
STI(I)=UNL1(I)
ST2(I)=UNL2(I)
ST3(I)=UNL3(I)
DO 198 I=1,INPT+2
V(I)=XLT(I)
U(I)=XGT(I)
XL(I)=XLT(I)
198 XG(I)=XGT(I)
DO 946 J=1,INPT
DO 946 I=1,TOTAL
946 ITT(I,J)=ITR(J,I)
IF ( ICHI.EQ.20 ) GO TO 999
GO TO 333
ELSE
ENDIF
797 GO TO 666
555 CONTINUE
IF(0000.NE.0)PRINT *,'%%%%%%%%% CONVERGE %%%%%%%%%%'
37 FORMAT('//////////')
JI=JI+1
IF ( JI.LE.INPT ) GO TO 7272
636 ISTIF=0
CALL GLOB
ISTIF=0
IF (IEE.EQ.1) THEN
C*VDIR: PREFER VECTOR
DO 193 I=1,INPT
STI(I)=UNL1(I)
ST2(I)=UNL2(I)
ST3(I)=UNL3(I)
ADXX=MIN(DXE(I),ADXX)
193 CONTINUE
DO 845 JI=1,INPT
DO 845 I=1,TOTAL
845 ITT(I,JI)=ITR(JI,I)
IEEI=IEEI+1
IF ( IEEI.GE.10 ) THEN
DO 295 I=1,INPT+2
V(I)=XLT(I)
U(I)=XGT(I)
XL(I)=XLT(I)
295 XG(I)=XGT(I)
GO TO 333
ENDIF
IF ( IREDFAC.NE.1 ) GO TO 565
IF ( ADXX.LT.AUX.AND. IAXI.EQ.0 ) THEN
DO 495 I=1,INPT+2
V(I)=XLT(I)
U(I)=XGT(I)
XL(I)=XLT(I)
495 XG(I)=XGT(I)
PBI=PBI*EP
MATX=MATX*EMXT
MABX=MABX*EMXB
MATY=MATY*EMYT
MABY=MABY*EMYB
EP=EP/TTOL
EMXT=EMXT/TTOL
EMXB=EMXB/TTOL
EMYT=EMYT/TTOL
EMYB=EMYB/TTOL
PBI=PBI+EP
MATX=MATX+EMXT
MABX=MABX+EMXB
MATY=MATY+EMYT

```

```

MABY=MABY+EMVB
PRINT *, REDUCING THE LOADS *
IAXI=1
GO TO 909
ENDIF
565 CONTINUE
GO TO 119
ENDIF
IF ( DETB .LT. 0.0 ) THEN
DO 965 JJ=1,INPT
DO 965 I=1,TOTAL
965 ITR(JJ)=ITR(JJ)
DO 197 I=1,INPT
STI(I)=UNL1(I)
ST2(I)=UNL2(I)
197 ST3(I)=UNL3(I)
DO 195 I=1,INPT+2
V(I)=XL(I)
U(I)=XGT(I)
XL(I)=XL(I)
195 XG(I)=XGT(I)
GO TO 333
ENDIF
PAR=PB1/PY
DO 749 I=1,INPT
DO 749 I=1,INPT
PIY=MIN(PIE(I),PIY)
749 CONTINUE
RMU=MXI-MATX
RMU=RMU/(MXXY*SHAPEX)
XMT=ABS(MATX/(MXXY*SHAPEX))
YMT=ABS(MATY/(MYYX*SHAPEY))
XMB=ABS(MABX/(MXXY*SHAPEX))
YMB=ABS(MABY/(MYYX*SHAPEY))
XMSX=ABS(MXSI/(MXXY*SHAPEX))
YMSY=ABS(MYSI/(MYYX*SHAPEY))
RAT10M=RATIO
IF (YMB.NE.0.0) RATIO=XMB/YMB
IF (IXAX.EQ.1) PRINT 6,PAR,MATX,MXT,XMT,XMB,XL(INPT),RMU
IF (IVAX.EQ.1) PRINT 6,DETB,PAR,YMT,XG(INPT)
6 FORMAT(E10.3,F8.4,F10.4,E10.6)
25 FORMAT(GGG',5E13.3)
56 FORMAT(E10.5,6F10.3)
IF (IXAX.EQ.2) PRINT 26,DETB,PAR,XMT,YMT,XG(CEN),XG(INPT),XL(CEN),
+XL(INPT)
126 FORMAT('Y',5E12.7)
IF (FLOTT.GT. 0.0) GO TO 3089
JUMB=0.0
DO 3089 K=1,INPT
IF (K.EQ.1.OR.K.EQ.4.OR.K.EQ.7.OR.K.EQ.10
+OR.K.EQ.13) THEN
DO 3089 J=1,TOTAL
STPLOT(K,J)=0.0
IF (ABS(STPRE(K,J)).GE.0.99990) STPLOT(K,J)=1.0
IF (STPLOT(K,J).EQ.1) JUMB=1
3089 CONTINUE

```

```

IF ( JUMB.NE.1 ) GO TO 3089
PRINT *, SECTION LOCATION IS ',K
DO 3088 J=1,TOTAL,8
3088 PRINT 6764,STPLOT(K,J),J+1,STPLOT(K,J+1),J+2,STPLOT(K,J+2)
+J+3,STPLOT(K,J+3),J+4,STPLOT(K,J+4),J+5,STPLOT(K,J+5)
+J+6,STPLOT(K,J+6),J+7,STPLOT(K,J+7)
ENDIF
3089 CONTINUE
6764 FORMAT(I4.0,F4.0,F4.0,F4.0,F4.0,F4.0,F4.0,F4.0,F4.0,F4.0,
+J,F4.0)
3087 IF (IVAX.EQ.3) PRINT 26,PAR,YMB,STI(CEN),ST3(CEN)
26 FORMAT(E8.3,F8.3,4F9.4)
CONVP=PB1
CONVMX=ABS(MATX)
CONVMY=ABS(MATY)
IF (IYYI.GT.0) IYYY=IYYI+1
IF (IYYI.GT. 8) GO TO 999
IF ( ABS(PB1) .GE.EJLMT .AND. IYYY .EQ. 0 ) THEN
EP=-EP
IYYY=1
ENDIF
IF ( ABS(MATY) .GE.EJLMT .AND. IYYY .EQ. 0 ) THEN
EMYT=-EMYT
EMVB=-EMVB
ENDIF
IF ( ABS(MATX) .GE.EJLMT .AND. IYYY .EQ. 0 ) THEN
EMXT=-EMXT
EMXB=-EMXB
IYYY=1
ENDIF
IF ( EMAX .LE. 0.000001 .AND. IAXI .EQ. 0 ) AXI=IXE(3)
PA=PB
DO 994 I=1,INPT
UNL1(I)=STI(I)
UNL2(I)=ST2(I)
UNL3(I)=ST3(I)
MXA(I)=MXB(I)
994 MYA(I)=MYB(I)
DO 196 I=1,INPT+2
XL(I)=XL(I)
196 XGT(I)=XG(I)
DO 993 JJ=1,INPT
DO 993 I=1,TOTAL
ITR(JJ)=ITR(JJ)
993 STPRE(JJ)=STPRE(JJ)
IF ( ABS(DETB) .GT. 1.0 ) THEN
GO TO 999
ELSE
ENDIF
IF ( DETB .LE. DTOL ) GO TO 999
FXX=DETB
PB1=PB1+EP
MATX=MATX+EMXT
MABX=MABX+EMXB
MATY=MATY+EMYT

```



```

MABY = MABY + EMYB
492 CONTINUE
333 TTOL = TTOL
IXBE = I
MATX = MATX + EMXT
MABX = MABX + EMXB
MATY = MATY + EMYT
MABY = MABY + EMYB
PBI = PBI + EP
EP = EP / TTOL
EMXT = EMXT / TTOL
EMXB = EMXB / TTOL
EMYT = EMYT / TTOL
EMYB = EMYB / TTOL
799 PBI = PBI + EP
MATX = MATX + EMXT
MABX = MABX + EMXB
MATY = MATY + EMYT
491 MABY = MABY + EMYB
KITX = KITX + YINC
KITV = KITV + YINC
KBY = KBY + YINC
IF ( KITX.LT. CRK ) GO TO 991
999 END
c The next subroutine is used to read the input data and calculate
c the residual stresses in sections.
SUBROUTINE READ
INCLUDE 'PROJECT'
READ(12,'J)BI,FT,D,WT,BI
READ(12,'J)FY,EL,SRC
SRC = SRC * FY
DT = D - 2.0 * FT
IF ( BI.EQ.0.0 ) THEN
SRT = (-WT * DT * ABS(SRC) + SQR((WT * DT * SRC)**2 + 4.0 * (FT * B * SRC)**2)
+ (B * FT + DT * WT)) / (2.0 * (B * FT + DT * WT))
TL = 0.5 * ABS(SRC) * B / (ABS(SRC) + SRT)
ELSE
SS = 1.0
IF ( ABS(SRC) .LT. 0.001 ) SS = 1.0E-15
SKT = -0.19 * FY * SS
ENDIF
READ(12,'J)NFV,NFH,NWV,NWH
READ(12,'J)DELX,DELY,INFT
READ(12,'J)NELAST,EFSAVE,EMXTXST,EMYSYTY,EMXBSXB,EMYSYB
READ(12,'J)DTOL,TOL
H = EL / (INFT - 1)
PA = 0.0
PI = D * ARCCOS(-1.0) / PIPAR
DI = BI - 2 * WT
IF ( BI.EQ.0.0 ) THEN
A = 2.0 * FT * B + WT * (D - 2 * FT)
IX = 2 * (B * FT)**3 / 12.0 + FT * B * (5 * D - 5 * FT)**2 + (D - 2 * FT)**3 * WT / 12.0
IY = FT * B**3 / 6 + (D - 2 * FT) * WT**3 / 12.0
ELSE
IX = B * D**3 / 12.0 - (B - 2.0 * WT) * (D - 2.0 * FT)**3 / 12.0
IY = D * B**3 / 12.0 - (D - 2.0 * FT) * (B - 2.0 * WT)**3 / 12.0
ENDIF
RATIO = SQR(IX / IY)
PRINT *, RATIO ,RATIO
SX = 2.0 * IX / D
SY = 2.0 * IY / B
IXB = (X**10) / (B * D**3)
IYB = (Y**10) / (B**3 * D)
SXB = 8.0 * SX / (B * D**2)
SYB = 8.0 * SY / (D * B**2)
AB = 4.0 * A / (B * D)
IF ( DI .LT. 0.0 ) DI = 0.0
IF ( BI .GT. 0.0 ) NWV = NWV * 2
FTOT = 2 * NFV * NFH
WTOT = NWV * NWH
TOTAL = FTOT + WTOT
FEW = B / FLOAT(NFV)
FET = FT / FLOAT(NFH)
WET = (D - 2 * FT) / FLOAT(NWV)
IF ( BI.EQ.0.0 ) THEN
WEW = WT / FLOAT(NWV)
ELSE
WEW = 2.0 * WT / FLOAT(NWV)
ENDIF
END
c The next subroutine is used to calculate the sectional
c dimensions and properties
SUBROUTINE SEC
INCLUDE 'PROJECT'
SR = FEW / 2.0
LI = 1
DO 35 K = 1,2 * NFH
NTOT = NFV * K
DO 10 I = LI,NTOT
SRI = SR + (I - LI) * FEW
L1 = LI + NFV
10 X(I) = (-B / 2.0 + SRI) * 2.0 / B
L1 = LI + NFV
35 SR = FEW / 2
L1 = 1
MR = 1
SR = FET / 2.0
DO 36 K = 1,2 * NFH
NTOT = NFV * K
IF( K.EQ. NFH + 1 ) MR = -1
IF( K.EQ. NFH + 1 ) SR = FET / 2
DO 11 I = LI,NTOT
AD(I) = (FET * FEW**4) / (B * D)
11 Y(I) = (MR * D / 2.0 - MR * SR) * 2.0 / D
SR = SR + FET
36 L1 = LI + NFV
L1 = NTOT + 1
L2 = L1
NTOT = NTOT + NWV
SR = WET / 2.0

```

```

DO 37 K=1,NWH
DO 13 I=1,L,NTOT
13 Y(I)=(((D-2*F)/2.0-SR)*2.0)/D
SR=SR+WET
NTOT=NTOT+NWV
37 L1=L1+NWV
IF (B1.GT.0.0) THEN
T1=B/2.0-D1/2.0-WT
ELSE
T1=B/2.0-WT/2.0
ENDIF
SR=WEW/2.0+T1
NTOT=NTOT+FTOT
DO 38 K=1,NWV
IF (B1.EQ.0.0) GO TO 300
IF (K.EQ.NWV/2+1) SR=(B+D1+WEW)/2.0
300 DO 14 I=L,NTOT,NWV
AD(I)=(WEW*WET*4)/(B*D)
14 X(I)=((B/2.0+SR)*2.0)/B
SR=SR+WEW
38 L2=L2+1
END
SUBROUTINE STIF
INCLUDE 'PROJECT'
ISTIF=0
Q1=0.0
Q2=0.0
Q3=0.0
Q4=0.0
Q5=0.0
Q6=0.0
Q7=0.0
Q8=0.0
Q9=0.0
DO 21 I=1,TOTAL
IT(I)=1
IF (ABS(STRPREF(J,I)).GE.1.0) IT(I)=0
IF (NELAST.EQ.1) IT(I)=1
21 CONTINUE
DO 20 I=1,TOTAL
Q1=Q1+IT(I)*AD(I)/AB
Q2=Q2+IT(I)*AD(I)*Y(I)/AB
Q3=Q3+IT(I)*AD(I)*X(I)/AB
Q4=Q4+IT(I)*AD(I)*Y(I)/IXB
Q5=Q5+IT(I)*AD(I)*Y(I)**2/IXB
Q6=Q6+IT(I)*AD(I)*X(I)*Y(I)/IXB
Q7=Q7+IT(I)*AD(I)*X(I)/IYB
Q8=Q8+IT(I)*AD(I)*X(I)*Y(I)/IYB
Q9=Q9+IT(I)*AD(I)*X(I)**2/IYB
888 F1=FDT(1)
F2=FDT(2)
F3=FDT(3)
DETCR=Q1*(Q5*Q9-Q6*Q8)-Q2*(Q4*Q9-Q6*Q7)+Q3*(Q4*Q8-Q5*Q7)
DETS1=F1*(Q5*Q9-Q6*Q8)-Q2*(F2*Q9-F3*Q6)+Q3*(F2*Q8-F3*Q5)
DETS2=Q1*(F2*Q9-F3*Q6)+Q3*(F3*Q4-F2*Q7)
DETS3=Q1*(F3*Q5-F2*Q8)-Q2*(F3*Q4-F2*Q7)+F1*(Q4*Q8-Q5*Q7)
IF (DETCR.EQ.0.0) THEN
ICRAMER=1
GO TO 999
ENDIF
X1(1)=DETS1/DETCR
X1(2)=DETS2/DETCR
X1(3)=DETS3/DETCR
ST1(J)=ST1(J)+X1(1)
ST2(J)=ST2(J)+X1(2)
ST3(J)=ST3(J)+X1(3)
999 END
c This subroutine is for solving the system of equations
SUBROUTINE MAT
INCLUDE 'PROJECT'
DO 77 I=1,NG
DO 77 J=1,NC
B2(I,J)=0.0
C(I,J)=WA(I,J)
77 C(I,J)=WA(I,J)
DO 100 I=1,1
DO 110 J=1,NC
110 B2(I,J)=C(I,J)
100 CONTINUE
M=NG-1
DO 20 K=1,M
I=K+1
DO 30 I=1,NG,1
IF (C(I,I).EQ.0.00) THEN
GO TO 99
ELSE
ENDIF
DO 40 J=K,NC
40 B2(I,J)=C(I,J)-(C(I,K)/C(K,K))*C(I,K)
30 CONTINUE
DO 41 I=1,NG
DO 42 J=1,NC
42 C(I,J)=B2(I,J)
41 CONTINUE
20 CONTINUE
DO 65 I=NG,1,-1
SUMX=0.0
DO 66 J=1+I,NG
SUM=C(I,J)*X1(J)
66 SUMX=SUMX+SUM
65 X1(I)=(1.0/C(I,I))*(C(I,NG+1)+SUMX)
99 END
c This subroutine is used to calculate the internal loads
SUBROUTINE LOAD
INCLUDE 'PROJECT'
PA1=0.0
MX=0.0
MY=0.0
DO 30 I=1,TOTAL
FRE=1.0

```

```

PA1 = PA1 + STPRP(JJ,1)*AD(0)/AB
MX = MX + Y(0)*STPRP(JJ,1)*AD(0)/DXB
MY = MY - X(0)*STPRP(JJ,1)*AD(0)/BYB
30 CONTINUE
ETB(JJ) = PA1
FDI(1) = PB-PA1
FDI(2) = MXB(JJ)*MX
FDI(3) = MYB(JJ)*MY
END
c stiffness matrix
SUBROUTINE GLOB
INCLUDE 'PROJECT'
CALL PROPTS
CALL GSUPRT
AMI = EMYT
AM2 = EMYB
IRRR = 0
DO 88 I = 1,NG
DO 88 J = 1,NC
88 WA(L,I) = 0.0
IEE = 0
CC = 0.0
CCI = 0.0
II = 1
DO 37 I = 1,INPT
PR(0) = +PR(0) + PYP(I)
MXRE(0) = MXRE(0) + MXR(I)
MYRE(0) = MYRE(0) + MYR(I)
MYP(0) = MYP(0)
PP(0) = PP(0)
Z = (I-1)*H
A0(0) = AE(0)*PBI
A1(0) = +AE(0)*Z*PBI/EL
A2(0) = (ABX*KBX*AE(0)*(Z-EL))/EL
A3(0) = AE(0)*Z*ATX*KTX/EL
A4(0) = SXE(0)*(PP(0) + PR(0) + PBI) + AE(0)*(PBI*DELY*SIN(PI*Z/EL) -
+ MABX-Z/EL*(MABX-MABX)*MXRE(0)-MXP(0))
B1(0) = +AE(0)*ABY*KBY*(EL-Z)/EL
B3(0) = +AE(0)*Z*ATY*KTY/EL
37 B4(0) = STE(0)*(PP(0) + PR(0) + PBI) + AE(0)*(MYP(0) + MYRE(0)*MABY +
+ Z/EL*(MATY + MABY)*PBI*DELY*SIN(PI*Z/EL))
BI = 2.0*ALP1(0) + A0(0)*H**2
CI = 2.0*GAM2(0) + A0(0)*H**2
WA(1,1) = 1.0
WA(2,2) = 1.0
WA(L,NC) = 0.0
WA(2,NC) = 0.0
WA(NR+1,1) = -BI
WA(NR+1,2) = -2.0*ALP2(1)
WA(NR+1,3) = 2.0*ALP1(0)
WA(NR+1,4) = 2.0*ALP2(0)
WA(NR+1,NR-1) = +AI(0)*H**2
WA(NR+1,NR+1) = -AE(0)*KBX*H**2
WA(NR+1,NR+2) = -2.0*ALP2(0)*H
WA(NR+1,NG-1) = A3(0)*H**2
WA(NR+1,NC) = A4(0)*H**2
WA(NR+2,1) = -2.0*GAMI(0)
WA(NR+2,2) = -CI
WA(NR+2,3) = 2.0*GAMI(0)
WA(NR+2,4) = -2.0*GAM2(0)
WA(NR+2,NR) = -AI(0)*H**2
WA(NR+2,NR+1) = 2.0*GAMI(0)*H
WA(NR+2,NR+2) = -(2.0*GAM2(0)*H + BI(0)*H**2)
WA(NR+2,NC) = B4(0)*H**2
I = INPT-1
KI = NR-3
BI = 2.0*ALP1(0) + A0(0)*H**2
CI = 2.0*GAM2(0) + A0(0)*H**2
WA(KI,KI-2) = ALP1(0)
WA(KI,KI-1) = ALP2(0)
WA(KI,KI) = -BI
WA(KI,KI+1) = -2.0*ALP2(0)
WA(KI,KI+2) = ALP1(0) + AI(0)*H**2
WA(KI,KI+3) = ALP2(0)
WA(KI,NR+1) = AZ(0)*H**2
WA(KI,NR+2) = ALP2(0)
WA(KI,NG-1) = A3(0)*H**2
WA(KI+1,KI-2) = GAMI(0)
WA(KI+1,KI-1) = GAM2(0)
WA(KI+1,KI) = -2.0*GAMI(0)
WA(KI+1,KI+1) = -CI
WA(KI+1,KI+2) = GAMI(0)
WA(KI+1,KI+3) = GAM2(0) + AI(0)*H**2
WA(KI+1,NR+2) = BI(0)*H**2
WA(KI+1,NG) = B3(0)*H**2
WA(KI,NC) = A4(0)*H**2
WA(KI+1,NC) = B4(0)*H**2
I = INPT
BI = 2.0*ALP1(0) + A0(0)*H**2
CI = 2.0*GAM2(0) + A0(0)*H**2
KI = NR-1
IF ( IHKX.EQ.1 ) THEN
WA(KI,KI) = (EL*KX + PBI)
WA(KI,NR+1) = +ABX*KBX
WA(KI,NG-1) = +ATX*KTX
WA(KI,NC) = +MATX + MABX
ENDIF
WA(NR,NR) = +EL*KY + PBI
WA(NR,NR+2) = +ABY*KBY
WA(NR,NG) = +ATY*KTY
WA(NR,NC) = +MATY + MABY
IF( IHKX.NE.1 ) THEN
WA(KI,NR-3) = 2.0*ALP1(0)
WA(KI,NR-2) = 2.0*ALP2(0)
WA(KI,NR-1) = GFI*EL*H**2*KX-BI
WA(KI,NR) = -2.0*ALP2(0)
WA(KI,NR+1) = -AE(0)*KBY*H**2
WA(KI,NR+3) = -2.0*ALP1(0)*H
WA(KI,NR+4) = 2.0*ALP2(0)*H

```

```

A74=H**2*(SXE(0)*(PF(0)+PR(0)+PB1)+AE(0)*PB1*DELY*SIN(P1)-
+AE(0)*(MXRE(0)+MXP(0)-AE(0)*MABX)
WA(K1,NC)=A74
ENDIF
GT=2.0*ALP1(0)+(A0(0)-A1(0))*H**2
GB=-2.0*ALP1(0)*H+A3(0)*H**2
WA(NG-1,NR-3)=-2.0*ALP1(0)
WA(NG-1,NR-2)=2.0*ALP2(0)
WA(NG-1,NR-1)=-GT
WA(NG-1,NR)=-2.0*ALP2(0)
WA(NG-1,NR+1)=-A2(0)*H**2
WA(NG-1,NG-1)=GB
WA(NG-1,NG)=2.0*ALP2(0)*H
WA(NG-1,NC)=A4(0)*H**2
WA(NG,NR-3)=2.0*GAMI(0)
WA(NG,NR-2)=2.0*GAM2(0)
WA(NG,NR-1)=-2.0*GAMI(0)
WA(NG,NR)=(2.0*GAM2(0)+H**2*(A1(0)-A0(0)))
WA(NG,NR+2)=-B1(0)*H**2
WA(NG,NG-1)=-2.0*GAMI(0)*H
WA(NG,NG)=2.0*GAM2(0)*H+B3(0)*H**2
WA(NG,NC)=B4(0)*H**2
DO 38 I=2,INPT-2
KI=P*2-1
K2=KI+1
BI=2.0*ALP1(0)+A0(0)*H**2
CI=2.0*GAM2(0)+A0(0)*H**2
WA(K1,K1-2)=ALP1(0)
WA(K1,K1-1)=ALP2(0)
WA(K1,K1)=-BI
WA(K1,K1+1)=-2.0*ALP2(0)
WA(K1,K1+2)=ALP1(0)
WA(K1,K1+3)=ALP2(0)
WA(K1,NR-1)=-A1(0)*H**2
WA(K1,NR+1)=A2(0)*H**2
WA(K1,NG-1)=A3(0)*H**2
WA(K2,K2-3)=GAMI(0)
WA(K2,K2-2)=GAM2(0)
WA(K2,K2-1)=-2.0*GAMI(0)
WA(K2,K2)=-CI
WA(K2,K2+1)=GAMI(0)
WA(K2,K2+2)=GAM2(0)
WA(K2,NR)=-A1(0)*H**2
WA(K2,NR+2)=-B1(0)*H**2
WA(K2,NG)=B3(0)*H**2
WA(K1,NC)=A4(0)*H**2
38 WA(K2,NC)=B4(0)*H**2
CALL MAT
J=1
DO 755 I=2,NG
755 WA(I,J)=0.0
DO 554 I=1,INPT+2
V(0)=XL(I)
554 U(0)=XG(I)
JS=1

```

```

DO S87 I=1,NG,2
XL(JS)=XI(0)
XG(JS)=XL(I+1)
S87 JS=JS+1
CUI(0)=STI(0)*FY/E
CUI(INPT)-STI(INPT)*FY/E
CU2(0)=-ST2(0)*2.0*FY/(E*D)
CU2(INPT)-ST2(INPT)*2.0*FY/(E*D)
CU3(0)=-ST3(0)*2.0*FY/(E*B)
CU3(INPT)-ST3(INPT)*2.0*FY/(E*B)
DO 386 I=2,INPT-1
CUX(0)=(XL(I-1)-2.0*XL(I)+XL(I+1))/H**2
CUX(I)=(XL(I)-2.0*XG(I)+2.0*XG(2)+2.0*H*XG(INPT+1))/H**2
CUY(0)=(XG(I-1)-2.0*XG(I)+XG(I+1))/H**2
CUI(0)-STI(0)*FY/E
CU2(0)-ST2(0)*2.0*FY/(E*D)
386 CU3(0)-ST3(0)*2.0*FY/(E*B)
CUX(I)=(2.0*XL(I)+2.0*XL(2)+2.0*H*XG(INPT+1))/H**2
CUY(I)=(2.0*XG(I)+2.0*XG(2)+2.0*H*XG(INPT+1))/H**2
CUX(INPT)=(2.0*XL(INPT-1)+2.0*XL(INPT)+2.0*H*XG(INPT+2))
+H**2
CUY(INPT)=(2.0*XG(INPT-1)+2.0*XG(INPT)+2.0*H
+XG(INPT+2))/H**2
I=INPT
APITT=(-E*CUP(0)*SYE(0)+E*CUY(0)*IYE(0)+E*CUX(0)*IXYE(0)-
+MYRE(0)*MYP(0))
772 CC=0.0
DO 388 I=1,INPT
CUP(I)=(E*SXE(0)*CUX(0)+E*SYE(0)*CUY(0)-PB1*PF(0)-PR(0)
+/(E*AE(0))
XM(I)=(E*CUP(I)*SXE(0)-E*CUY(I)*IXYE(0)-E*CUX(I)*IXE(0)+
+MXRE(0)+MXP(0))/MXXY
YM(I)=(E*CUP(I)*SYE(0)+E*CUY(I)*IYE(0)+E*CUX(I)*IXYE(0)-
+MYRE(0)*MYP(0))/MYYY
388 CONTINUE
DO 225 I=1,INPT
Z=H*(I-1)
XL(I)=XL(0)+DELZ*SIN(P1*Z/EL)
225 XG(I)=XG(0)+DELX*SIN(P1*Z/EL)
IC=0
DO 386 I=1,INPT+2
TEST=ABS(XL(I)-V(0))
TEST1=ABS(XG(I)-U(0))
IF (TEST.GT.CC) THEN
CC=TEST
IC=1
ENDIF
IF (TEST1.GT.CC) THEN
CC=TEST1
IC=1
ENDIF
386 EMAX=MAX(CC,TEST,TEST1)
IF (EMAX.GT.TOLG) IEE=1
42 FORMAT(3,F9.3)
991 DETB=1.0
DETU=1.0

```

```

DETI=1.0
IF ( DETE.EQ.0.0 ) THEN
DO 45 I=1,NG
45 DFI(I)=C(I)
DETD=1.0
ENDIF
DO 46 I=1,NG
46 DETB=DETB*C(I)/DFI(I)
DO 48 I=1,NR
48 DETU=DETU*C(I)/DFI(I)
IF ( ABS(XL(INPT+2)).GE.ANG ) THEN
MXT=KTX*ANG
ATX=0.0
BTX=-1.0
ELSE
ENDIF
IF ( ABS(XL(INPT+1)).GE.ANG ) THEN
MXBB=KBX*ANG
ABX=0.0
BBX=1.0
ELSE
ENDIF
IF ( ABS(XG(INPT+2)).GE.ANG ) THEN
MYT=KTY*ANG
ATY=0.0
BTY=-1.0
ELSE
ENDIF
IF ( ABS(XG(INPT+1)).GE.ANG ) THEN
MYBB=KBY*ANG
ABY=0.0
BBY=+1.0
ENDIF
999 END
c This subroutine is used to calculate the total strain
c at each element
SUBROUTINE STRAINU
INCLUDE 'PROJECT'
DO 20 I=1,TOTAL
STRN=STI(I)+STZ(I)*Y(I)-STX(I)*X(I)+STR(I)/FY
STRPRE(I,I)=STRN
IF (J1.EQ.INPT.AND.I.EQ.1) STRL=STRN
IF (J1.EQ.INPT.AND.I.EQ.4) STR2=STRN
IT(I)=1
STRY(I)=0.0
IF (NELAST.EQ.1) GO TO 21
IF (ITANG.NE.1) GO TO 22
IF (STRN.GE.1.0) THEN
IT(I)=0
STRPRE(I,I)=1.0
STRY(I)=1.0
ELSE IF (STRN.LE.-1.0) THEN
IT(I)=0
STRPRE(I,I)=-1.0
STRY(I)=-1.0
ENDIF
IF (ITANG.EQ.1) GO TO 21
STRPRE(I,I)=STRPAS(I,I)-STRU+STRN
IF (NELAST.EQ.1) GO TO 21
IF (STRPRE(I,I).GE.1.0) THEN
STRPRE(I,I)=1.0
IT(I)=0
ELSE IF (STRPRE(I,I).LE.-1.0) THEN
STRPRE(I,I)=-1.0
IT(I)=0
ENDIF
21 CONTINUE
20 CONTINUE
END
c This subroutine is used to calculate the sectional properties
SUBROUTINE GSPURT
INCLUDE 'PROJECT'
JJ=1
22 IXYE(JJ)=0.0
IXE(JJ)=0.0
IYE(JJ)=0.0
SYE(JJ)=0.0
SXE(JJ)=0.0
AE(JJ)=0.0
DO 21 I=1,TOTAL
IT(I)=1
IF (ABS(STRPRE(I,I)).GE.1.0) IT(I)=0
IF (NELAST.EQ.1) IT(I)=1
21 CONTINUE
DO 20 I=1,TOTAL
AE(IJ)=AE(IJ)+AD(I)*IT(I)*B*D/4.0
SYE(IJ)=SYE(IJ)+AD(I)*X(I)*IT(I)*B**2*D/8.0
SXE(IJ)=SXE(IJ)+AD(I)*Y(I)*IT(I)*D**3*B/8.0
IXYE(IJ)=IXYE(IJ)+IT(I)*X(I)*AD(I)*B**2*D**2/16.0
IXE(IJ)=IXE(IJ)+IT(I)*Y(I)**2*AD(I)*D**3*B/16.0
IYE(IJ)=IYE(IJ)+IT(I)*X(I)**2*AD(I)*B**3*D/16.0
3 FORMAT(14F20.4)
ALP(IJ)=(-IXE(IJ)*AE(IJ)+SXE(IJ)**2)*E
ALP2(IJ)=(-AE(IJ)*IXYE(IJ)+SXE(IJ)*SYE(IJ))*E
GAMI(IJ)=(-SXE(IJ)*SYE(IJ)+IXYE(IJ)*AE(IJ))*E
GAM2(IJ)=(-SYE(IJ)**2+IYE(IJ)*AE(IJ))*E
JI=JI+1
IF (JJ.LE.INPT) GO TO 22
999 END
c The next subroutine is used to calculate the internal
c forces due to plastic and residual stresses
SUBROUTINE PROPTS
INCLUDE 'PROJECT'
JJ=1
22 MYR(IJ)=0.0
MYP(IJ)=0.0
MXP(IJ)=0.0
MXR(IJ)=0.0
AE(IJ)=0.0

```

```

MXRE(JJ)=0.0
MYRE(JJ)=0.0
PP(JJ)=0.0
PPY(JJ)=0.0
PR(JJ)=0.0
ETB(JJ)=0.0
STPP2=0.0
STPX=0.0
STPU=0.0
STYX=0.0
STYU=0.0
STPU3=0.0
SRUY=0.0
DO 21 I=1,TOTAL
IYIT=1
IT(0)=1
STRY(0)=0.0
STRN=STI(JJ)+STZ(JJ)*Y(0)-STZ(JJ)*X(0)+STR(0)/FY
IF (ABS(STRN) .GE. 1.0 .AND. IT(JJ) .EQ. 0 ) IT(JJ)=1
IF ( STRN .GE. 1.0 ) STRY(0)=1.0
IF ( STRN .LE. -1.0 ) STRY(0)=-1.0
IF ( ABS(STRPRE(JJ)) .GE. 1.0 ) IT(0)=0
IF ( NELAST .EQ. 1 ) IT(JJ)=0
IF ( NELAST .EQ. 1 ) IT(0)=1
21 CONTINUE
DO 20 I=1,TOTAL
DDEE=0.0
KT=1
IF (ITANG .EQ. 1 ) KT=0
IF (ITANG .EQ. 1 .AND. ABS(STRPRE(JJ)) .LT. 1 ) IT(JJ)=0
STPP=0.0
STRN=STI(JJ)+STZ(JJ)*Y(0)-STZ(JJ)*X(0)+STR(0)/FY
STRU=UNL(JJ)+UNL2(JJ)*Y(0)-UNL3(JJ)*X(0)+STR(0)/FY
STRESS=(STRU-STRM)*FY
MYR(JJ)=MYR(JJ)+IT(JJ)*IT(0)*X(0)*AD(0)*STRPRE(JJ)/IVB
+*MYXY
STPP=STZ(JJ)*2.*FY/(E*B)*X(0)*B/20.*E*STI(JJ)*FY
+ -STZ(JJ)*2.*FY/(E*D)*Y(0)*D/20.*E
+ -STZ(JJ)*2.*FY/(E*B)*X(0)*B/20.*E
STYX=STYX+IT(JJ)*IT(0)*STPP*AD(0)*B*D/4.0*X(0)*B/20
STYU=STYU+IT(JJ)*IT(0)*STPX*AD(0)*B*D/4.0*Y(0)*D/20
MXR(JJ)=MXR(JJ)+IT(JJ)*IT(0)*Y(0)*AD(0)*STRPRE(JJ)/IXB*MXXY
+*KT
MYP(JJ)=MYP(JJ)+X(0)*AD(0)*(-IT(0))*STRPRE(JJ)/IVB*MYYY
MXP(JJ)=MXP(JJ)+Y(0)*AD(0)*(-IT(0))*STRPRE(JJ)/IXB*MXXY
MXRE(JJ)=MXRE(JJ)+(-IT(JJ))*AD(0)*Y(0)*IT(0)*STR(0)/
+(FY*IXB)*MXXY
MYRE(JJ)=MYRE(JJ)+(-IT(JJ))*AD(0)*X(0)*IT(0)*STR(0)/
+(FY*IVB)*MYYY
STPU=STI(JJ)*FY+IT(JJ)*IT(0)
STPU2=STZ(JJ)*2.*FY/(E*D)*Y(0)*D/20.*E+IT(JJ)*IT(0)
STPU3=STZ(JJ)*2.*FY/(E*B)*X(0)*B/20.*E+IT(JJ)*IT(0)

```

```

STPU=STPU1+STPU2+STPU3
STPP2=STPP2+STPU*AD(0)*B*D/4.0
PPY(JJ)=PPY(JJ)+IT(JJ)*IT(0)*AD(0)/AB*PY
+*STRPRE(JJ)
SRUY=SRUY+STR(0)*AD(0)*B*D/4.0*IT(0)*IT(JJ)
PP(JJ)=PP(JJ)+AD(0)*(-IT(0))*STRPRE(JJ)/AB*PY
20 PR(JJ)=PR(JJ)+(-IT(JJ))*AD(0)*STR(0)/(AB*FY)*PY*IT(0)
MYR(JJ)=(MYR(JJ)+STYX)*KT
MXR(JJ)=(MXR(JJ)+STYU)*KT
JJ=JJ+1
IF ( JJ .LE. INPT ) GO TO 22
999 END
c The next subroutine is used to print the input data
SUBROUTINE DATINP
INCLUDE 'PROJECT'
PRINT *, '##### INPT DATA #####'
PRINT *, '-----'
PRINT *, '#####'
PRINT *, 'END ROTATIONS:'
PRINT *, '#####'
PRINT *, '2. FORMAT("KTX=","E12.6," "KBX=","E12.6)
PRINT *, '3. KTY,"KBY'
PRINT *, '4. FORMAT("KTY=","E12.6," "KBY=","E12.6)
PRINT *, 'TRANSLATIONAL RESTRAINT:'
PRINT *, '#####'
PRINT *, '4. KX,KY
PRINT *, '5. FORMAT("KX=","E12.6," "KY=","E12.6)
PRINT *, '#####'
PRINT *, 'GEOMETRY PROPERTIES:'
PRINT *, '#####'
PRINT *, '#####'
IF ( B1 .EQ. 0.0 ) THEN
PRINT *, 'SECTION USED'
PRINT *, '#####'
PRINT *, '5. B,FT,D,WT
PRINT *, '6. A,IX,IY
PRINT *, '7. D=,"F6.2," "D=","F6.2," "T=","F6.2)
PRINT *, '8. A=","F6.4," "IX=","F6.4," "IY=","F6.4)
ELSE
PRINT *, 'TUBE SECTION USED'
PRINT *, '#####'
PRINT *, '7. B,D,WT
PRINT *, '8. A,IX,IY
PRINT *, '8. A=","F6.4," "IX=","F6.4," "IY=","F6.4)
ENDIF
PRINT *, '#####'
PRINT *, '10. NFW,NFH
PRINT *, '11. NWW/2,NWH
PRINT *, '12. MESH OF FLENGES=","2I3)
PRINT *, '11. MESH OF WEBS =","2I3)
PRINT *, 'TOTAL OF ELEMENTS=","TOTAL

```

```

PRINT *;
PRINT *,"MATERIAL PROPERTIES AND LENGTH;"
PRINT *,"===== "
PRINT *;
PRINT *,"FY,EI,EI
9 FORMAT('FY=','F5.2',' KSI E=','F9.2',' KSI LENGTH
+','F6.2',' IN.')"
PRINT *;
PRINT *;
C END OF INPUT DATA
C#####
IF (DXAX.EQ.1) THEN
PRINT *; DETERM. P MXT MXB DYC
+ DXT ,
ELSEIF (IYAX.EQ.1) THEN
PRINT *; DETERM. P MYT MYB DXC
+ DYT ,
ELSEIF (IXAX.EQ.2) THEN
PRINT *; DETERM. P MXT MYT XGC XGT XLC
+ XLT
ENDIF
END

```

\bar{D}	P	M_x	M_y	Δ_{yc}	Δ_{yt}	Δ_{xc}	Δ_{xt}
1	0.00E+000	1.90E-002	0.00E-000	1.44E-001	0.00E+000	1.33E-001	-4.48E-002
1	0.00E+000	3.90E-002	2.30E-002	1.35E-001	-4.28E-002	1.22E-001	-8.97E-002
1	0.00E+000	5.80E-002	4.60E-002	1.26E-001	-8.55E-002	1.11E-001	-1.34E-001
1	0.00E+000	7.80E-002	6.90E-002	1.17E-001	-1.28E-001	9.96E-002	-1.79E-001
1	0.00E+000	9.70E-002	9.20E-002	1.08E-001	-1.71E-001	8.85E-002	-2.24E-001
1	0.00E+000	1.17E-001	1.15E-001	9.88E-002	-2.14E-001	7.74E-002	-2.69E-001
1	0.00E+000	1.36E-001	1.38E-001	8.98E-002	-2.56E-001	6.63E-002	-3.14E-001
1	0.00E+000	1.56E-001	1.61E-001	8.07E-002	-2.99E-001	5.52E-002	-3.59E-001
1	0.00E+000	1.75E-001	1.84E-001	7.17E-002	-3.42E-001	4.41E-002	-4.04E-001
1	0.00E+000	1.95E-001	2.08E-001	6.27E-002	-3.85E-001	3.30E-002	-4.48E-001
1	0.00E+000	2.14E-001	2.31E-001	5.36E-002	-4.27E-001	2.19E-002	-4.93E-001
1	0.00E+000	2.34E-001	2.54E-001	4.46E-002	-4.70E-001	1.08E-002	-5.38E-001
1	0.00E+000	2.53E-001	2.77E-001	3.55E-002	-5.13E-001	-3.00E-004	-5.83E-001
1	0.00E+000	2.73E-001	3.00E-001	2.65E-002	-5.55E-001	-1.14E-002	-6.28E-001
1	0.00E+000	2.92E-001	3.23E-001	1.75E-002	-5.98E-001	-2.25E-002	-6.73E-001
1	0.00E+000	3.12E-001	3.46E-001	8.40E-003	-6.41E-001	-3.36E-002	-7.17E-001
1	0.00E+000	3.31E-001	3.69E-001	-6.00E-004	-6.84E-001	-4.47E-002	-7.62E-001
1	0.00E+000	3.51E-001	3.92E-001	-9.70E-003	-7.26E-001	-5.58E-002	-8.07E-001
1	0.00E+000	3.70E-001	4.15E-001	-1.87E-002	-7.69E-001	-6.69E-002	-8.52E-001
1	0.00E+000	3.90E-001	4.38E-001	-2.77E-002	-8.12E-001	-7.80E-002	-8.97E-001
1	0.00E+000	4.09E-001	4.61E-001	-3.68E-002	-8.55E-001	-8.91E-002	-9.42E-001
1	0.00E+000	4.29E-001	4.84E-001	-4.58E-002	-8.97E-001	-1.00E-001	-9.86E-001
1	0.00E+000	4.48E-001	5.07E-001	-5.48E-002	-9.40E-001	-1.11E-001	-1.0312
0.945	0.00E+000	4.68E-001	5.30E-001	-6.39E-002	-9.83E-001	-1.22E-001	-1.0758
0.812	0.00E+000	4.87E-001	5.53E-001	-7.29E-002	-1.0256	-1.33E-001	-1.1203
0.705	0.00E+000	5.06E-001	5.76E-001	-8.19E-002	-1.0681	-1.44E-001	-1.165

D.2 Sway Portal Frame (SPF)

```

C PROGRAM SPF ( SWAY PLANE FRAME)
C THIS PROGRAM IS INTENDED TO SOLVE A 'PORTAL' SWAY PLANE FRAME WITH
C TWO-DIMENSIONAL JOINT LOADS.
INCLUDE 'SPFINC'
IGLBCON=0
LAXIAL=0
GLDET=201.0
ISTOP=0
ISTART=1
ITERATE=1
IRERINP=1
DO 58 I=1,3
OMBX(I)=0.0
OMTX(I)=0.0
OMBY(I)=0.0
OPRI(I)=0.0
OMBX(I)=0.0
OMTX(I)=0.0
OMBY(I)=0.0
OPRI(I)=0.0
58 READ(12,*) NUM,BENDAX
444 NZ=3
IRXG=2
DO 91 NM=1,NUM
INPT=INPUT
ICONLOC=0
CALL SPFC
IF ( ICONLOC.EQ.1 ) GO TO 911
DO 893 I=1,INPT
UNL1(NM,I)=UNL1(I)
UNL2(NM,I)=UNL2(I)
UNL3(NM,I)=UNL3(I)
ST1(NM,I)=ST1(I)
ST2(NM,I)=ST2(I)
ST3(NM,I)=ST3(I)
893 CONTINUE
769 FORMAT('NM I A IX ',2B2F13)
IF ( ICONLOC.EQ.1 ) THEN
CALL ELODINC
CALL STGLOB
CALL ENDMEM
IF ( IGLBCON.GT.10 ) THEN
CALL ELODINC
IF(IGLBCON.EQ.3000 ) GO TO 999
IGLBCON=0
ENDIF
GO TO 444
ENDIF
INPUT=INPT

```

```

ISTART=2
IF ( AXFLAG(NM).NE.1 ) GO TO 943
CCCCCCCCCCCCCCCCCCCCCCCCCCCCCCCCCCCCCCCCCCCCCCCCCCCCCCCCCCCC
C THE NEXT IS TO RE-EVALUATE THE BOUNDARY CONDITIONS OF X-AXIS
C
WA(NR+1,NR+1)=WA(NR+1,NR+1)-A2(I)*H**2
WA(NR-3,NR+1)=WA(NR-3,NR+1)-A2(INPT-I)*H**2
WA(NR-1,NR+1)=WA(NR-1,NR+1)-A2(INPT)*H**2
WA(NR+1,NG-1)=WA(NR+1,NG-1)-A3(I)*H**2
WA(NR-3,NG-1)=WA(NR-3,NG-1)-A3(INPT-I)*H**2
WA(NR-1,NG-1)=WA(NR-1,NG-1)-A3(INPT)*H**2
DO 38 I=2,INPT-2
K1=I*2+1
K2=K1+1
WA(K1,NR+1)=WA(K1,NR+1)-A2(I)*H**2
WA(K1,NG-1)=WA(K1,NG-1)-A3(I)*H**2
38 WA(NR-1,NR+1)=WA(NR-1,NR+1)-AE(INPT)*KBX*H**2
WA(NR-1,NR-1)=WA(NR-1,NR-1)-AE(INPT)*EL*H**2*KX
C ***** END OF RE-EVALUATIONS OF X-AXIS *****
CCCCCCCCCCCCCCCCCCCCCCCCCCCCCCCCCCCCCCCCCCCCCCCCCCCCCCCCCCCC
C THE NEXT IS TO RE-EVALUATE THE BOUNDARY CONDITIONS OF Y-AXIS
C
IF ( AXFLAG(NM).EQ.1 ) GO TO 944
943 WA(NR+2,NR+2)=WA(NR+2,NR+2)+BI1(I)*H**2
K1=NR-3
WA(K1+1,NR+2)=WA(K1+1,NR+2)+BI1(INPT-I)*H**2
WA(NG,NR+2)=WA(NG,NR+2)+BI1(INPT)*H**2
WA(NR+2,NG)=WA(NR+2,NG)-BI3(I)*H**2
WA(K1+1,NG)=WA(K1+1,NG)-BI3(INPT-I)*H**2
WA(NG,NG)=WA(NG,NG)-BI3(INPT)*H**2
DO 318 I=2,INPT-2
K1=I*2+1
K2=K1+1
WA(K2,NR+2)=WA(K2,NR+2)+BI1(I)*H**2
WA(K2,NG)=WA(K2,NG)-BI3(I)*H**2
318 WA(NR,NR+2)=WA(NR,NR+2)-EL*KBY*H**2*AE(INPT)
WA(NR,NR)=WA(NR,NR)-AE(INPT)*KY*H**2*EL
C ***** END OF RE-EVALUATIONS OF Y-AXIS *****
944 JUJ=2
IF ( JUJ.EQ.1 ) THEN
J=NR-1
DO 332 I=1,NG
332 WA(IJ)=0.0
DO 334 I=1,NC
334 WA(IJ)=0.0
WA(IJ)=1.0
ENDIF
J=1
J1=2
DO 921 I=2,NC

```

```

WA(IJ)=0.0
92 WA(IJ)=0.0
WA(2,2)=1.0
CALL GLOAD
CALL DECOMP
CALL EVADEC
991 CONTINUE
ITERATE=2
CALL STGLOB
CALL ENDMEM
IF (IGLCON.GT.10) THEN
CALL ELOADING
IGLCON=0
GO TO 444
ENDIF
IF (ISTOP.NE.1) GO TO 444
IF (GLDET.GT.200) THEN
DO 451 I=1,NG
451 GLDETB(I)=C(I)
ENDIF
GLDET=1.0
DO 461 I=1,NG
461 GLDET=GLDET*(I)/GLDETB(I)
IGLCON=0
IAXIAL=IAXIAL+1
DETBG(IAXIAL)=GLDET
PAXIAL(IAXIAL)=PAPL
FDEBLC(IAXIAL)=X(I)
MAXIAL(IAXIAL)=MAPL
ROTATI(IAXIAL)=X(I)
PRINT 72,GLDETB(I)/FY,MAPL/MXYY,X(I),X(I)
72 FORMAT(E9.3,F14.4)
IF (LJF.GT.90.0) GO TO 9123
CALL FNONPRO
9123 CONTINUE
IF (GLDET.LT.1.0E-15) GO TO 999
IF (ISTOP.EQ.1) CALL ELOADING
IF(IGLCON.EQ.3000) GO TO 999
GO TO 444
999 CONTINUE
C
C THE NEXT SUBROUTINE IS TO EVALUATE THE DECOMPOSITION MATRICES OF
C THE BEAM-COLUMN.
END
SUBROUTINE DECOMP
INCLUDE 'SPFNC'
IK=1
NK=NR-3
NKI=NK+2
JK=1
DO 10 I=1,NK,2
II=I+1
JK=1
DO 20 J=1,NK,2
JJ=J+1
KX11(IK,JK)=WA(IJ)
KY11(IK,JK)=WA(IJ,J)
20 JK=JK+1
IK=1
DO 30 I=1,NK,1,2
JK=1
II=I+1
DO 40 J=1,NK,2
JJ=J+1
KX21(IK,JK)=V/A(IJ)
KY21(IK,JK)=V/A(IJ,J)
40 JK=JK+1
30 IK=IK+1
IK=1
DO 50 I=1,NK,2
II=I+1
JK=1
DO 60 J=1,NK,1,2
JJ=J+1
KX12(IK,JK)=WA(IJ)
KY12(IK,JK)=WA(IJ,J)
60 JK=JK+1
50 IK=IK+1
IK=1
DO 70 I=1,NK,1,2
JK=1
II=I+1
DO 80 J=1,NK,1,2
JJ=J+1
KX22(IK,JK)=WA(IJ)
KY22(IK,JK)=WA(IJ,J)
80 JK=JK+1
70 IK=IK+1
C THE NEXT STATEMENTS IS TO EVALUATE THE LOADS {FX}
C
C
C THE NEXT SUBROUTINE IS TO EVALUATE THE L*COMPOSED MATRICES
C
C
SUBROUTINE EVADEC
INCLUDE 'SPFNC'
IF (AXFLAG(NM),NE.1) GO TO 2222
C EVALUATE {KXR}
C {KXR} = {KX12} * {KX11} + {KX22}
NCC=7
M=INPT-1
NG=M
NC=NG+NCC
DO 100 I=1,M
DO 220 J=1,M
220 C(IJ)=KX11(IJ)
C(I,M+1)=KX12(I,I)

```

```

C(I,M+2)=KX12(I,2)
C(I,M+3)=KX12(I,3)
C(I,M+4)=FX1(I)
C(I,M+5)=MX1(I,1)
C(I,M+6)=MX1(I,2)
100 C(I,M+7)=MX1(I,3)
C CALL THE ROUTINE TO SOLVE FOR XM(I,J)
CALL SOLVE
C SOLVE XM(I,J) AND KX21 AND ADD KX22 TO GET KXR
DO 280 I=1,N22
DO 110 IM=1,N22
KXR(I,IM)=0.0
DO 110 J=1,M
SUM=KX21(I,J)*XM(J,IM)
110 KXR(I,IM)=KXR(I,IM)+SUM
280 CONTINUE
DO 130 I=1,N22
DO 130 J=1,N22
130 KXR(I,J)=-KXR(I,J)+KX22(I,J)
DO 320 I=1,N22
FXR(I)=0.0
DO 330 J=1,M
SUM=KX21(I,J)*XM(J,IM)
330 FXR(I)=FXR(I)+SUM
320 FXR(I)=-FXR(I)+FX2(I)
C
C NOW EVALUATE {MXR} OR {BETAX}
C {MXR} = {MX2} - [KX21] [KX11]-1 {MX1} = {BETAX} {MXA}
C ALSO REMEMBER THAT K11 AND K21 WERE SOLVED BEFORE
DO 211 I=1,N22
IN=0
DO 211 IM=5,7
JB=IM-4
BETAX(I,JB)=0.0
DO 211 J=1,M
SUM=KX21(I,J)*XM(J,IM)
211 BETAX(I,JB)=BETAX(I,JB)+SUM
DO 212 I=1,N22
DO 212 J=1,N22
212 BETAX(I,J)=-BETAX(I,J)+MX2(I,J)
C
CCCCCCCCCCCCCCCC FOR ELIMINATE ONE EQUATION CCCCCCCCCC
C
C NOW SOLVE {DEF} [KXR]=BETA * {M} + {FXR} AS
C {DEF} [KXR] [BETA]-1 = {M} + [BETA]-1 {FXR} TO GET
C {M}=[RXG] {DEF} -{SXR}
C(1,1)=BETAX(2,2)
C(1,2)=BETAX(2,3)
C(2,1)=BETAX(3,2)
C(2,2)=BETAX(3,3)
C(1,3)=KXR(2,1)
C(1,4)=KXR(2,2)
C(1,5)=KXR(2,3)
C(2,3)=KXR(3,1)
C(2,4)=KXR(3,2)

```

```

C(2,5)=KXR(3,3)
C(1,6)=FXR(2)
C(2,6)=FXR(3)
C CALL SOLVE TO GET {XM} AS 2X4, THE FIRST 3 ARE THE 2X3 [RXG] AND
C THE LAST COLUMN IS 2X1 {SXR}
NG=2
NC=6
NCC=4
CALL SOLVE
RXG(NM,1)=XM(1,2)
RXG(NM,2)=XM(1,3)
RXG(NM,3)=XM(1,1)
RXG(NM,4)=XM(2,2)
RXG(NM,5)=XM(2,3)
RXG(NM,6)=XM(2,1)
RXG(NM,7)=XM(1,4)
RXG(NM,8)=XM(2,4)
C##### Y-AXIS EVALUATIONS #####
IF ( AXFLAG(NM).EQ.1 ) GO TO 999
2222 CONTINUE
C
C EVALUATE [KYR]
C [KYR] = [KY12] * [KY11]-1 * [KY21] + [KY22]
NCC=7
M=INPT-1
NG=N.
NC=NG+NCC
DO 10 I=1,M
DO 20 J=1,M
20 C(I,J)=KY11(I,J)
C(I,M+1)=KY12(I,1)
C(I,M+2)=KY12(I,2)
C(I,M+3)=KY12(I,3)
C(I,M+4)=FY1(I)
C(I,M+5)=MY1(I,1)
C(I,M+6)=MY1(I,2)
10 C(I,M+7)=MY1(I,3)
C CALL THE ROUTINE TO SOLVE FOR XM(I,J)
CALL SOLVE
C SOLVE XM(I,J) AND KY21 AND ADD KY22 TO GET KYR
DO 28 I=1,N22
DO 11 IM=1,N22
KYR(I,IM)=0.0
DO 11 J=1,M
SUM=KY21(I,J)*XM(J,IM)
11 KYR(I,IM)=KYR(I,IM)+SUM
28 CONTINUE
DO 13 I=1,N22
DO 13 J=1,N22
13 KYR(I,J)=-KYR(I,J)+KY22(I,J)
C EVALUATE {FYR}
C {FYR} = {FY2} - [KY21] * [KY.1]-1 * {FY1}
C SOLVE KY21 AND XM(4,J) AND ADD FY2
C REMEMBER THAT K11 AND K21 WERE SOLVED BEFORE
DO 32 I=1,N22

```

```

FYR(0)=0.0
DO 33 J=1,M
SUM=KY21(J)*XM(J,A)
33 FYR(0)=FYR(0)+SUM
32 FYR(0)=-FYR(0)+FY2(0)
C
C NOW EVALUATE {MYR} OR {BETAY}
C {MYR} = {MY2} - {KY21} {KY1J}-1 {MY1} = {BETAY} {MXA}
C ALSO REMEMBER THAT K11 AND K21 WERE SOLVED BEFORE
DO 200 I=1,N22
IN=0
DO 200 IM=5,7
JB=IM-4
BETAY(IJB)=0.0
DO 200 J=1,M
SUM=KY21(J)*XM(J,IM)
200 BETAY(IJB)=BETAY(IJB)+SUM
DO 201 I=1,N22
DO 201 J=1,N22
201 BETAY(IJ)=-BETAY(IJ)+MY2(IJ)
C
CCCCCCCCCCCCCCCC FOR ELIMINATE ONE EQUATION CCCCCCCCCC
C
C NOW SOLVE {DEF} {KYR}=BETA * {M} + {FYR} AS
C {DEF} {KYR} {BETA}=1 - {M} + {BETA}+1 {FYR} TO GET
C
C(1,1)=BETAY(2,2)
C(1,2)=BETAY(2,3)
C(2,1)=BETAY(3,2)
C(2,2)=BETAY(3,3)
C(1,3)=KYR(2,1)
C(1,4)=KYR(2,2)
C(1,5)=KYR(2,3)
C(2,3)=KYR(3,1)
C(2,4)=KYR(3,2)
C(2,5)=KYR(3,3)
C(1,6)=FYR(2)
C(2,6)=FYR(3)
C
C CALL SOLVE TO GET {XM} AS 2X4, THE FIRST 3 ARE THE 2X3 {RXG} AND
C THE LAST COLUMN IS 2X1 {SXR}
NG=2
NC=5
NCC=4
CALL SOLVE
RXG(NM,1)=XM(1,2)
RXG(NM,2)=XM(1,3)
RXG(NM,3)=+XM(1,1)
RXG(NM,4)=XM(2,2)
RXG(NM,5)=XM(2,3)
RXG(NM,6)=+XM(2,1)
RXG(NM,7)=XM(1,4)*GFF1
RXG(NM,8)=XM(2,4)*GFF2
999
SUBROUTINE SOLVE
INCLUDE 'SPFNC'
END

```

```

DO 100 I=1,NG
DO 110 J=1,NC
DDD(I,J)=C(I,J)
110 B2(I,J)=C(I,J)
100 CONTINUE
M1=NG-1
DO 20 K=1,M1
H=K+1
DO 30 I=H,NG,1
IF ( C(I,I).EQ.0.00 ) THEN
GO TO 99
ELSE
ENDIF
DO 40 J=K,NC
B2(I,J)=C(I,J)-C(K,J)/C(K,K)*C(I,K)
30 CONTINUE
DO 41 I=1,NG
C(I,J)=0.0
42 C(I,J)=B2(I,J)
41 CONTINUE
20 CONTINUE
IF (.IRXG.EQ.1.) THEN
DO 666 I=1,80
DO 666 J=1,80
666 XM(I,J)=0.0
ENDIF
IF (.NCC.EQ.1.) THEN
DO 65 I=NG,1,-1
SUMX=0.0
DO 66 J=1+I,NG
SUM=C(I,J)*XI(J)
66 SUMX=SUMX+SUM
65 XI(I)=(1.0/C(I,I))*(C(L,NG+1)-SUMX)
ELSE
DO 95 I=NG,1,-1
SUMX1=0.0
SUMX2=0.0
SUMX3=0.0
SUMX4=0.0
SUMX5=0.0
SUMX6=0.0
SUMX7=0.0
DO 96 J=1+I,NG
SUM1=C(I,J)*XM(J,1)
SUM2=C(I,J)*XM(J,2)
SUM3=C(I,J)*XM(J,3)
SUM4=C(I,J)*XM(J,4)
SUM5=C(I,J)*XM(J,5)
SUM6=C(I,J)*XM(J,6)
SUM7=C(I,J)*XM(J,7)
SUMX1=SUMX1+SUM1
SUMX2=SUMX2+SUM2
SUMX3=SUMX3+SUM3
SUMX4=SUMX4+SUM4

```

```

SUMX5=SUMX5+SUM5
SUMX6=SUMX6+SUM6
96 SUMX7=SUMX7+SUM7
XM(1,1)=(1.0/C(I,1))*C(LNG+1)*SUMX1
XM(1,2)=(1.0/C(I,1))*C(LNG+2)*SUMX2
XM(1,3)=(1.0/C(I,1))*C(LNG+3)*SUMX3
XM(1,4)=(1.0/C(I,1))*C(LNG+4)*SUMX4
XM(1,5)=(1.0/C(I,1))*C(LNG+5)*SUMX5
XM(1,6)=(1.0/C(I,1))*C(LNG+6)*SUMX6
95 XM(1,7)=(1.0/C(I,1))*C(LNG+7)*SUMX7
228 CONTINUE
ENDIF
99 SUBROUTINE GLOAD
INCLUDE SFFINC
IF (AXFLAG(NM),NE.1) GO TO 2222
DO 11 I=1,INPT-1
Z=(I-1)*H
MX1(I,1)=0.0
MX1(I,2)=AE(I)*Z/EL*H**2
11 MX1(I,3)=AE(I)*Z/EL*H**2
MX2(1,1)=0.0
MX2(1,2)=1.0*H**2*AE(INPT)
MX2(1,3)=0.0
MX2(2,1)=0.0
MX2(2,2)=-1.0*AE(I)*H**2
MX2(2,3)=0.0
MX2(3,1)=0.0
MX2(3,2)=0.0
MX2(3,3)=+1.0*AE(INPT)*H**2
DO 12 I=1,INPT-1
Z=(I-1)*H
12 FX1(I)=(SXE(I)*PP(I)+PR(I)+PRI(NM))*AE(I)*PRI(NM)*DELY
+*SIN(P1Z/EL)*MXR(0)*MXP(I))*H**2
I=INPT
Z=EL
FX2(I)=(SXE(I)*PP(I)+PR(I)+PRI(NM))*AE(I)*PRI(NM)*DELY
+*SIN(P1Z/EL)*MXR(0)*MXP(I))*H**2
I=1
Z=0.0
FX3(0)=(SXE(I)*PP(I)+PR(I)+PRI(NM))*AE(I)*PRI(NM)*DELY
+*SIN(P1Z/EL)*MXR(0)*MXP(I))*H**2
I=INPT
Z=EL
FX3(0)=(SXE(I)*PP(I)+PR(I)+PRI(NM))*AE(I)*PRI(NM)*DELY
+*SIN(P1Z/EL)*MXR(0)*MXP(I))*H**2
IF ( AXFLAG(NM) .EQ. 1 ) GO TO 999
2222 DO 21 I=1,INPT-1
Z=(I-1)*H
MY1(I,1)=0.0
MY1(I,2)=AE(I)*Z/EL*H**2
21 MY1(I,3)=AE(I)*Z/EL*H**2
MY2(1,1)=0.0
MY2(1,2)=1.0*H**2*AE(INPT)
MY2(1,3)=0.0
MY2(2,1)=0.0
MY2(2,2)=-1.0*AE(I)*H**2
MY2(2,3)=0.0
MY2(3,1)=0.0
MY2(3,2)=+1.0*AE(INPT)*H**2
DO 22 I=1,INPT-1
Z=(I-1)*H
22 FY1(I)=(SXE(I)*PP(I)+PR(I)+PRI(NM))*AE(I)*PRI(NM)*DELX
+*SIN(P1Z/EL)+MYR(0)+MYP(I))*H**2
I=INPT
Z=EL
FY2(I)=(SXE(I)*PP(I)+PR(I)+PRI(NM))*AE(I)*PRI(NM)*DELX
+*SIN(P1Z/EL)+MYR(0)+MYP(I))*H**2
I=1
FY2(0)=(SXE(I)*PP(I)+PR(I)+PRI(NM))*AE(I)*PRI(NM)*DELX
+*SIN(P1Z/EL)+MYR(0)+MYP(I))*H**2
Z=0.0
FY2(0)=(SXE(I)*PP(I)+PR(I)+PRI(NM))*AE(I)*PRI(NM)*DELX
+*SIN(P1Z/EL)+MYR(0)+MYP(I))*H**2
I=INPT
Z=EL
FY2(0)=(SXE(I)*PP(I)+PR(I)+PRI(NM))*AE(I)*PRI(NM)*DELX
+*SIN(P1Z/EL)+MYR(0)+MYP(I))*H**2
999 SUBROUTINE STGLOB
INCLUDE SFFINC
IF ( IRERINP .EQ. 1 ) THEN
IRERINP=3
READ(12,'*ALPPL,ALPP2,ALPP3,NII,NIZ
READ(12,'*PAPL,MAPL
READ(12,'*KTR,RKI,RK2,RK3,RK45,RK6
READ(12,'*GFF1,GFF2,GFF3,GFF4,GFF5,GFF6
READ(12,'*LFF,FRATOP,FRATION
FPMAX=FRATOP*PY
FMMAX=FRATION*MYYY
ENDIF
IF ( HENDAX .EQ. 1 ) THEN
DO 66 I=1,20
DO 66 J=1,20
66 C(I,J)=0.0
C(1,1)=RXG(1,1)+RK1
C(1,2)=RXG(1,2)
C(1,7)=RXG(1,3)
C(1,8)=RXG(1,7)
C(2,1)=RXG(1,4)
C(2,2)=RXG(1,5)+RK23
C(2,3)=RK23
C(2,7)=RXG(1,6)
C(2,8)=RXG(1,8)+NII*MAPL
C(3,2)=RK23
C(3,3)=RXG(2,1)+RK23
C(3,4)=RXG(2,2)
C(3,8)=RXG(2,7)
C(4,3)=RXG(2,4)
C(4,4)=RXG(2,5)+RK45

```

```

C(4.5)=-RK45
C(4.8)-RXG(2.8)
C(5.4)=-RK45
C(5.5)=RXG(3.5)+RK45
C(5.6)-RXG(3.4)
C(5.7)-RXG(3.6)
C(5.8)+N12*MAPL+RXG(3.8)
C(6.5)=RXG(3.2)
C(6.6)=RXG(3.1)+RK6
C(6.7)=RXG(3.3)
C(6.8)=RXG(3.7)
C(7.1)-RXG(1.1)+RXG(1.4)
C(7.2)=RXG(1.2)+RXG(1.5)
C(7.5)=RXG(3.1)+RXG(3.4)
C(7.6)-RXG(3.2)+RXG(3.5)
C(7.7)=RXG(1.3)+RXG(1.6)+RXG(3.3)+RXG(3.6)PRI(1)-PRI(3)-KTR*EL
C(7.8)-ALPPI*PAPL*EL+RXG(1.7)+RXG(1.8)+RXG(3.7)+RXG(3.8)
ELSE
DO 61 I=1,20
DO 61 J=1,20
61 C(I,J)=0.0
C(1.1)-RXG(1.1)+RK1
C(1.2)=RXG(1.2)
C(1.7)=RXG(1.3)
C(1.8)-RXG(1.7)*GFF5
C(2.1)=RXG(1.4)
C(2.2)=RXG(1.5)+RK23
C(2.3)-RK23
C(2.7)=RXG(1.6)
C(2.8)=RXG(1.8)*GFF5+NI1*MAPL
C(3.2)-RK23
C(3.3)-RXG(2.1)+RK23
C(3.4)=RXG(2.2)
C(3.8)=RXG(2.7)
C(4.3)=RXG(2.4)
C(4.4)=RXG(2.5)+RK45
C(4.5)=-RK45
C(4.8)=RXG(2.8)
C(5.4)=-RK45
C(5.5)=RXG(3.5)+RK45
C(5.6)=RXG(3.4)
C(5.7)=RXG(3.6)
C(5.8)+N12*MAPL+RXG(3.8)*GFF6
C(6.5)=RXG(3.2)
C(6.6)=RXG(3.1)+RK6
C(6.7)=RXG(3.3)
C(6.8)=RXG(3.7)*GFF5
C(7.1)=RXG(1.1)+RXG(1.4)
C(7.2)=RXG(1.2)+RXG(1.5)
C(7.5)=RXG(3.1)+RXG(3.4)
C(7.6)=RXG(3.2)+RXG(3.5)
C(7.7)=RXG(1.3)+RXG(1.6)+RXG(3.3)+RXG(3.6)+PRI(1)+PRI(3)-KTR*EL
C(7.8)=-ALPPI*PAPL*EL+(RXG(1.7)+RXG(1.8))*GFF5+RXG(3.7)*GFF6+
+RXG(3.8)*GFF6
ENDIF

NG=7
NCC=1
NC=NG+NCC
CALL SOLVE

END

C THE NEXT SUBROUTINE IS TO EVALUATE THE END MEMBER ACTION
C
SUBROUTINE ENDMEM
INCLUDE 'SPFNC'
IF ( BENDAX .EQ. 1 ) THEN
QMBX(1)=RXG(1.1)*XI(1)+RXG(1.2)*XI(2)+RXG(1.3)*XI(7)-RXG(1.7)
QMTX(1)=RXG(1.4)*XI(1)+RXG(1.5)*XI(2)+RXG(1.6)*XI(7)-RXG(1.8)
QMBX(2)=RXG(2.1)*XI(3)+RXG(2.2)*XI(4)-RXG(2.7)
QMTX(2)=RXG(2.4)*XI(3)+RXG(2.5)*XI(4)-RXG(2.8)
QMBX(3)=RXG(3.1)*XI(5)+RXG(3.2)*XI(6)+RXG(3.3)*XI(7)-RXG(3.7)
QMTX(3)=RXG(3.4)*XI(5)+RXG(3.5)*XI(6)+RXG(3.6)*XI(7)-RXG(3.8)
ELSE
QMBX(1)=RXG(1.1)*XI(1)+RXG(1.2)*XI(2)+RXG(1.3)*XI(7)-RXG(1.7)
+*GFF3
QMTX(1)=RXG(1.4)*XI(1)+RXG(1.5)*XI(2)+RXG(1.6)*XI(7)-RXG(1.8)
+*GFF4
QMBX(2)=RXG(2.1)*XI(3)+RXG(2.2)*XI(4)-RXG(2.7)
QMTX(2)=RXG(2.4)*XI(3)+RXG(2.5)*XI(4)-RXG(2.8)
QMBX(3)=RXG(3.1)*XI(5)+RXG(3.2)*XI(6)+RXG(3.3)*XI(7)-RXG(3.7)
+*GFF4
QMTX(3)=RXG(3.4)*XI(5)+RXG(3.5)*XI(6)+RXG(3.6)*XI(7)-RXG(3.8)
+*GFF3
ENDIF
ELL(1)=EL
ELL(2)=EL
ELL(3)=EL
PRI(1)=ALPPI*PAPL+(QMBX(2)+QMTX(2))/ELL(2)
PRI(2)=-ALPPI*PAPL+(QMBX(1)+QMTX(1))/ELL(1)
IF ( BENDAX .EQ. 2 ) PRI(2)=-ALPPI*PAPL-(QMBX(1)+QMTX(1))/ELL(1)
PRI(3)=ALPPI*PAPL-(QMBX(2)+QMTX(2))/ELL(2)
ETTL=0.0
DO 66 I=1,3
TEST=ABS(QMBX(I)-QMBX(1))
TEST1=ABS(QMTX(I)-QMTX(1))
TEST2=ABS(PRI(I)-PRI(1))
66 ETTL=MAX(ETTL,TEST,TEST1,TEST2)
IGLBCON=IGLBCON+1
ISTOP=0
IF ( ETTL .LT. 0.1 ) ISTOP=1
DO 55 I=1,3
QMBX(I)=QMBX(1)
QMTX(I)=QMTX(1)
OPRI(I)=PRI(1)
C THE NEXT SUBROUTINE ARE USED TO INCREMENT THE LOADS
END
SUBROUTINE ELODING
INCLUDE 'SPFNC'
IF ( ICONLOC .EQ. 1 .OR. IGLBCON .GT. 10 ) GO TO 333
PAPL=PAPL+PAPLINC

```

```
MAPL = MAPL + MAPLINC
GO TO 999
333 PAPL = PAPL - PAPLINC
MAPL = MAPL - MAPLINC
PAPLINC = PAPLINC / 10.0
MAPLINC = MAPLINC / 10.0
PAPL = PAPL + PAPLINC
MAPL = MAPL + MAPLINC
999 CONTINUE
ETTL = 0.0
ETTL1 = ABS(PAPLINC)
ETTL2 = ABS(MAPLINC)
ETTL = MAX(ETTL1, ETTL2)
IF ( ETTL .LT. 0.01 ) IGLBCON = 3000
END
SUBROUTINE FNONPRO
INCLUDE 'SPFINC'
IF( LFF .EQ. 1 .AND. PAPL .GE. FPMAX ) THEN
MAPLINC = PAPLINC
PAPLINC = 0.0
LFF = 100
ELSE IF ( LFF .EQ. 2 .AND. PAPL .GE. FPMAX ) THEN
MAPLINC = PAPLINC
LFF = 100
ELSE IF ( LFF .EQ. 3 .AND. MAPL .GE. FMMAX ) THEN
MAPLINC = 0.0
LFF = 100
ENDIF
999 END
```

\bar{D}	P	M_x	Δ_y	θ_{x1}
1.000	0.00E+000	0.00E+000	-1.00E-006	0.00E+000
9.77E-001	2.50E-002	0.00E+000	-1.10E-003	0.00E+000
9.54E-001	5.00E-002	0.00E+000	-2.30E-003	1.00E-004
9.32E-001	7.50E-002	0.00E+000	-3.50E-003	1.00E-004
9.09E-001	1.00E-001	0.00E+000	-4.80E-003	1.00E-004
8.87E-001	1.25E-001	0.00E+000	-6.20E-003	2.00E-004
8.65E-001	1.50E-001	0.00E+000	-7.60E-003	2.00E-004
8.43E-001	1.75E-001	0.00E+000	-9.10E-003	2.00E-004
8.21E-001	2.00E-001	0.00E+000	-1.07E-002	3.00E-004
8.00E-001	2.25E-001	0.00E+000	-1.24E-002	3.00E-004
7.78E-001	2.50E-001	0.00E+000	-1.41E-002	3.00E-004
7.57E-001	2.75E-001	0.00E+000	-1.60E-002	4.00E-004
7.36E-001	3.00E-001	0.00E+000	-1.80E-002	4.00E-004
7.16E-001	3.25E-001	0.00E+000	-2.00E-002	4.00E-004
6.95E-001	3.50E-001	0.00E+000	-2.22E-002	5.00E-004
6.74E-001	3.75E-001	0.00E+000	-2.45E-002	5.00E-004
6.54E-001	4.00E-001	0.00E+000	-2.70E-002	6.00E-004
6.34E-001	4.25E-001	0.00E+000	-2.96E-002	6.00E-004
6.14E-001	4.50E-001	0.00E+000	-3.24E-002	7.00E-004
5.95E-001	4.75E-001	0.00E+000	-3.53E-002	7.00E-004
5.75E-001	5.00E-001	0.00E+000	-3.85E-002	8.00E-004
5.56E-001	5.25E-001	1.19E-002	-4.97E-002	8.00E-004
5.37E-001	5.50E-001	2.38E-002	-6.14E-002	9.00E-004
5.18E-001	5.75E-001	3.58E-002	-7.38E-002	1.00E-003
4.99E-001	6.00E-001	4.77E-002	-8.69E-002	1.00E-003
4.80E-001	6.25E-001	5.96E-002	-1.00E-001	1.10E-003
4.62E-001	6.50E-001	7.15E-002	-1.15E-001	1.20E-003
4.44E-001	6.75E-001	8.35E-002	-1.30E-001	1.30E-003
4.26E-001	7.00E-001	9.54E-002	-1.47E-001	1.40E-003
4.08E-001	7.25E-001	1.07E-001	-1.65E-001	1.50E-003
3.10E-001	7.50E-001	1.19E-001	-1.58E-001	1.40E-003
2.99E-001	7.75E-001	1.31E-001	-1.73E-001	1.50E-003
2.87E-001	8.00E-001	1.43E-001	-1.89E-001	1.60E-003
2.75E-001	8.25E-001	1.55E-001	-2.07E-001	1.60E-003
2.63E-001	8.50E-001	1.66E-001	-2.27E-001	1.70E-003
2.51E-001	8.75E-001	1.78E-001	-2.48E-001	1.80E-003
2.39E-001	9.00E-001	1.91E-001	-2.71E-001	2.00E-003
2.27E-001	9.25E-001	2.03E-001	-2.96E-001	2.10E-003
2.16E-001	9.50E-001	2.15E-001	-3.25E-001	2.30E-003
2.04E-001	9.75E-001	2.26E-001	-3.57E-001	2.50E-003

D.3 Sway Space Frame (SSF)

```

C PROGRAM SSF ( SWAY SPACE FRAME)
C THIS PROGRAM IS INTENDED TO SOLVE A SWAY SPACE FRAME
INCLUDE 'SSF3INC'
READ(12,'TLOADW,TLOAD,TLOADPZ
READ(12,'NUM,IDO,F,XXYY
133 FORMAT(4F15.4)
READ(12,'X21,X22,X23,X24,ILDST
READ(12,'P21,P22,P23,P24,DLNGFR
READ(12,'PINC21,PINC22,PINC23,PINC24
PRINT *,ILDST DLNGFR **,ILDST,DLNGFR
DO 8 I=1,NUM
8 XLAT(I)=0.0
XLAT(21)=EL-X21
XLAT(22)=X22
XLAT(23)=X23
XLAT(24)=EL-X24
DO 17 I=1,24
DO 17 J=1,8
RYG(I,J)=0.0
17 RXG(I,J)=0.0
DO 27 I=1,70
X(I)=0.0
IGLBCON=0
IAXIAL=0
GLDET=201.0
ISTTOP=0
ISTART=1
ITERATE=1
IRERINP=1
DO 58 I=1,24
QMBX(I)=0.0
QMTX(I)=0.0
QMBY(I)=0.0
QMTY(I)=0.0
58 OPRI(I)=0.0
444 NZZ=3
IRXG=2
DO 991 NM=1,NUM
INPT=INPUT
ICONLOC=0
CALL SSF3BC
IF (NM.EQ.1) WPY=PY
IF (NM.EQ.1) PRINT *,PY MY ,WPY,MYYY
IF (ICONLOC.EQ.1) GO TO 991
RFT=-99999.9
IF=1
DO 3381 ISS=1,INPT
UUI=RFT
RFT=MIN(DXE(ISS),RFT)
IF ( UUI.EQ. RFT ) THEN
IP=IP
ELSE
IP=ISS
ENDIF
3381 CONTINUE
DO 893 I=1,INPT
UNL1(NM,I)=UNL1(I)
UNL2(NM,I)=UNL2(I)
UNL3(NM,I)=UNL3(I)
ST11(NM,I)=ST1(I)
ST22(NM,I)=ST2(I)
ST33(NM,I)=ST3(I)
893 CONTINUE
769 FORMAT('NM I A IX IY',2I3,F12.3)
IF (ICONLOC.EQ.1) THEN
PRINT *,FOR ICONLOC & NM ,ICONLOC,NM
CALL ELOADING
IF(IGLBCON.EQ.300) GO TO 999
CALL STGLOB
CALL ENDMEM
IF ( IGLBCON.GT.10 ) THEN
PRINT *,FOR IGLBCON =,IGLBCON,NM
CALL ELOADING
IGLBCON=0
ENDIF
GO TO 444
ENDIF
INPUT=INPT
ISTART=2
IF ( AXFLAG(NM).EQ.2 ) GO TO 943
CCCCCCCCCCCCCCCCCCCCCCCCCCCCCCCCCCCCCCCCCCCCCCCCCCCCCCCCCCCCCCCC
C THE NEXT IS TO RE-EVALUATE THE BOUNDARY CONDITIONS OF X-AXIS
C
WA(NR+1,NR+1)=WA(NR+1,NR+1)*A2(I)*H**2
WA(NR-3,NR+1)=WA(NR-3,NR+1)*A2(INPT-I)*H**2
WA(NR-1,NR+1)=WA(NR-1,NR+1)*A2(INPT)*H**2
WA(NR+1,NG-1)=WA(NR+1,NG-1)*A3(I)*H**2
WA(NR-3,NG-1)=WA(NR-3,NG-1)*A3(INPT-I)*H**2
WA(NR-1,NG-1)=WA(NR-1,NG-1)*A3(INPT)*H**2
DO 38 I=2,INPT-2
K1=I*2-1
K2=K1+1
WA(K1,NR+1)=WA(K1,NR+1)*A2(I)*H**2
WA(K1,NG-1)=WA(K1,NG-1)*A3(I)*H**2
38 WA(NR-1,NR+1)=WA(NR-1,NR+1)*AE(INPT)*KBX*I*H**2
WA(NR-1,NG-1)=WA(NR-1,NG-1)*AE(INPT)*EL*I*H**2*KX
C *****
C END OF RE-EVALUATIONS OF X-AXIS *****
CCCCCCCCCCCCCCCCCCCCCCCCCCCCCCCCCCCCCCCCCCCCCCCCCCCCCCCCCCCCCCCC
C THE NEXT IS TO RE-EVALUATE THE BOUNDARY CONDITIONS OF Y-AXIS
C

```

```

IF ( AXFLAG(NM) .EQ. 1 ) GO TO 944
943 WA(NR+2,NR+2) = WA(NR+2,NR+2) + B11(I)*H**2
KI = NR-3
WA(KI+1,NR+2) = WA(KI+1,NR+2) + B11(INPT-1)*H**2
WA(NG,NR+2) = WA(NG,NR+2) + B11(INPT)*H**2
WA(NR+2,NG) = WA(NR+2,NG) + B3(I)*H**2
WA(KI+1,NG) = WA(KI+1,NG) + B3(INPT-1)*H**2
WA(NG,NG) = WA(NG,NG) + B3(INPT)*H**2
DO 318 I=2,INPT-2
KI = I*2-1
K2 = KI+1
WA(K2,NR+2) = WA(K2,NR+2) + B11(I)*H**2
318 WA(K2,NG) = WA(K2,NG) + B3(I)*H**2
WA(NR,NR+2) = WA(NR,NR+2) + EL*KBY*H**2 + AE(INPT)
WA(NR,NG) = WA(NR,NG) + AE(INPT)*KY*H**2 + EL
C ..... END OF RE-EVALUATIONS OF Y-AXIS .....
944 JUU = 2
IF ( JUU .EQ. 1 ) THEN
J = NR-1
DO 331 I=1,NG
332 WA(I,I) = 0.0
DO 334 I=1,NC
334 WA(I,I) = 0.0
WA(I,J) = 1.0
ENDIF
J = 1
J1 = 2
DO 92 I=2,NC
WA(I,I) = 0.0
92 WA(I,J1) = 0.0
WA(2,2) = 1.0
CALL GLOAD
CALL DECOMP
CALL EVADEC
991 CONTINUE
ITERATE = 2
CALL STGLOB
CALL ENDMEM
IF ( IGLBCON .GT. 5 ) THEN
PRINT *, 'FOR IGLBCON LATER ', IGLBCON, NM
CALL ELOADING
IGLBCON = 0
GO TO 444
ENDIF
IF ( STTOP .NE. 1 ) GO TO 444
IF ( GLDET .GT. 200 ) THEN
DO 451 I=1,NG
451 GLDETB(I) = C(I,I)
ENDIF
GLDET = 1.0
DO 461 I=1,NG
461 GLDET = GLDET * C(I,I) / GLDETB(I)
IGLBCON = 0
DETA(XIAXIAL) = GLDET
PAXIAL(IAXIAL) = PAPL
PAYEXT(IAXIAL) = P24
FDEFLX1(IAXIAL) = XI(58)
FDEFLX2(IAXIAL) = XI(60)
FDEFLX3(IAXIAL) = XI(62)
FDEFLY1(IAXIAL) = XI(57)
FDEFLY2(IAXIAL) = XI(59)
FDEFLY3(IAXIAL) = XI(61)
MAXIAL(IAXIAL) = P21
STS49(IAXIAL) = ST49
STS50(IAXIAL) = ST50
STS51(IAXIAL) = ST51
STS52(IAXIAL) = ST52
STS61(IAXIAL) = ST61
STS62(IAXIAL) = ST62
DLXX = ABS(XI(62))
DLYY = ABS(XI(61))
TANNGX = DLXX / DLNGFR
TANNGY = DLYY / DLNGFR
THXX = ATAN(TANNGX)
THYY = ATAN(TANNGY)
PRINT 7,PAPL,P21,P22,P23,P24
PRINT *, 'DEFLECTION AT SECOND AND THIRD STORY RESPECTIVELY '
PRINT *, FDEFLX1(IAXIAL), FDEFLX2(IAXIAL), FDEFLX3(IAXIAL)
7 FORMAT('PAPL P21 P22 P23 P24')
I = IAXIAL
IF ( PAPL .GT. TLOADW ) GO TO 999
IF ( P21 .GT. TLOAD ) GO TO 999
IF ( P23 .GT. TLOADP2 ) GO TO 999
IF ( LFF .GT. 90.0 ) GO TO 9123
CALL FNONPRO
9123 CONTINUE
IF ( GLDET .LT. 1.0E-20 ) GO TO 999
IF ( ISTOP .EQ. 1 ) CALL ELOADING
IF ( IGLBCON .EQ. 3000 ) GO TO 999
GO TO 444
C
C THE NEXT SUBROUTINE IS TO EVALUATE THE DECOMPOSITION MATRICES OF
C THE BEAM-COLUMN.
999 CONTINUE
IF ( XXY .EQ. 1 ) THEN
DO 527 I=1,IAXIAL
527 PRINT 72,DETA(XI),PAXIAL(I),MAXIAL(I),PAYEXT(I)
+ ,FDEFLX1(I),FDEFLX2(I),FDEFLX3(I)
ELSE IF ( XXY .EQ. 2 ) THEN
DO 528 I=1,IAXIAL
528 PRINT 72,DETA(XI),PAXIAL(I),MAXIAL(I),PAYEXT(I)
+ ,FDEFLY1(I),FDEFLY2(I),FDEFLY3(I)
ELSE
IF ( ILDST .EQ. 1 ) THEN
DO 529 I=1,IAXIAL
529 PRINT 72,DETA(XI),PAXIAL(I),MAXIAL(I),PAYEXT(I)
ELSE
PRINT *, 'FROM BEAME 49 51 FROM FRAME 49 51'
PRINT *,

```

```

DO 579 I=1,MAXIAL
PRINT 584,PAXIAL(0),MAXIAL(0),PAVENT(0),STS49(0),STS50(0)
+STSS1(0),STSS2(0)
ENDIF
579
584 FORMAT(3F6.2,4E13.3)
ENDJF
73 FORMAT(3F6.2,3F7.4,3F9.4)
72 FORMAT(5F3.6F9.4)
END
SUBROUTINE DECOMP
INCLUDE 'SFSINC'
IK=1
NK=NR3
NKL=NK+2
IK=1
DO 10 I=1,NK2
II=I+1
JK=1
DO 20 J=1,NK2
JJ=J+1
KX1(IK,JK)=WA(I,J)
KY1(IK,JK)=WA(I,J,J)
20 JK=JK+1
10 IK=IK+1
IK=1
DO 30 I=1,NK,NG-12
JK=1
II=I+1
DO 40 J=1,NK2
JJ=J+1
KX2(IK,JK)=WA(I,J)
KY2(IK,JK)=WA(I,J,J)
40 JK=JK+1
30 IK=IK+1
IK=1
DO 50 I=1,NK2
II=I+1
JK=1
DO 60 J=1,NK,NG-12
JJ=J+1
KX12(IK,JK)=WA(I,J)
KY12(IK,JK)=WA(I,J,J)
60 JK=JK+1
50 IK=IK+1
IK=1
DO 70 I=1,NK,NG-12
JK=1
II=I+1
DO 80 J=1,NK,NG-12
JJ=J+1
KX22(IK,JK)=WA(I,J)
KY22(IK,JK)=WA(I,J,J)
80 JK=JK+1
70 IK=IK+1
C THE NEXT SUBROUTINE IS TO EVALUATE THE DECOMPOSED MATRICES
C
SUBROUTINE EVADEC
INCLUDE 'SFSINC'
IF (AXELAG(NM).EQ.2) GO TO 2222
C EVALUATE [KXR]
C [KXR] = [KX12] * [KX11]-1 * [KX21] + [KX22]
NCC=7
M=INPT-1
NG=M
NC=NG+NCC
DO 100 I=1,M
DO 220 J=1,M
220 C(I,J)=KX11(I,J)
C(I,M+1)=KX12(I,1)
C(I,M+2)=KX12(I,2)
C(I,M+3)=KX12(I,3)
C(I,M+4)=FX1(I)
C(I,M+5)=MX1(I,1)
C(I,M+6)=MX1(I,2)
100 C(I,M+7)=MX1(I,3)
C CALL THE ROUTINE TO SOLVE FOR XM(I,J)
CALL SOLVE
C SOLVE XM(I,J) AND KX21 AND ADD KX22 TO GET KXR
DO 280 J=1,N22
DO 110 IM=1,N22
KXR(I,IM)=0.0
DO 110 J=1,M
SUM=KX21(I,J)*XM(I,IM)
110 KXR(I,IM)=KXR(I,IM)+SUM
280 CONTINUE
DO 130 I=1,N22
DO 130 J=1,N22
130 KXR(I,J)=-KXR(I,J)+KX22(I,J)
C EVALUATE { FXR }
C {FXR} = {FX2} - [KX21] * [KX11]-1 * {FX1}
C SOLVE KX21 AND XM(4,J) AND ADD FX2
C REMEMBER THAT K11 AND K21 WERE SOLVED BEFORE
DO 320 I=1,N22
FXR(I)=0.0
DO 330 J=1,M
SUM=KX21(I,J)*XM(J,4)
330 FXR(I)=FXR(I)+SUM
320 FXR(I)=-FXR(I)+FX2(I)
C
C NOW EVALUATE [MXR] OR [BETAX]
C {MXR} = [MX2] - [KX21] [KX11]-1 {MX1} = [BETAX] [MXA]
C ALSO REMEMBER THAT K11 AND K21 WERE SOLVED BEFORE
DO 211 I=1,N22
IN=0
DO 211 IM=5,7
JB=IM-4
BETAX(I,JB)=0.0
DO 211 J=1,M
SUM=KX21(I,J)*XM(I,IM)
211 BETAX(I,JB)=BETAX(I,JB)+SUM

```

```

DO 212 I=1,N22
DO 212 J=1,N22
212 BETAX(I,J)=-BETAX(I,J)+MX2(I,J)
C
CCCCCCCCCCCCCCCC FOR ELIMINATE ONE EQUATION CCCCCCCCCC
C
C NOW SOLVE {DEF} [KXR]=BETA * {M} + {FXR} AS
C {DEF} [KXR] [BETA]-1 = {M} + [BETA]-1 {FXR} TO GET
C {M}=[RXG] {DEF} -{SXR}
C(1,1)=BETAX(2,2)
C(1,2)=BETAX(2,3)
C(2,1)=BETAX(3,2)
C(2,2)=BETAX(3,3)
C(1,3)=KXR(2,1)
C(1,4)=KXR(2,2)
C(1,5)=KXR(2,3)
C(2,3)=KXR(3,1)
C(2,4)=KXR(3,2)
C(2,5)=KXR(3,3)
C(1,6)=FXR(2)
C(2,6)=FXR(3)
C CALL SOLVE TO GET {XM} AS 2X4, THE FIRST 3 ARE THE 2X3 [RXG] AND
C THE LAST COLUMN IS 2X1 {SXR}
NG=2
NC=6
NCC=4
CALL SOLVE
RXG(NM,1)=XM(1,2)
RXG(NM,2)=XM(1,3)
RXG(NM,3)=XM(1,1)
RXG(NM,4)=XM(2,2)
RXG(NM,5)=XM(2,3)
RXG(NM,6)=XM(2,1)
RXG(NM,7)=XM(1,4)
RXG(NM,8)=XM(2,4)
C##### Y-AXIS EVALUATIONS #####
IF ( AXFLAG(NM).EQ.1 ) GO TO 999
2222 CONTINUE
C EVALUATE [KYR]
C [KYR] = [KY12] * [KY11]-1 * [KY21] + [KY22]
NCC=7
M=INPT-1
NG=M
NC=NG+NCC
DO 10 I=1,M
DO 20 J=1,M
20 C(I,J)=KY11(I,J)
C(I,M+1)=KY12(I,1)
C(I,M+2)=KY12(I,2)
C(I,M+3)=KY12(I,3)
C(I,M+4)=FY1(I)
C(I,M+5)=MY1(I,1)
C(I,M+6)=MY1(I,2)
10 C(I,M+7)=MY1(I,3)
C CALL THE ROUTINE TO SOLVE FOR XM(I,J)

```

```

CALL SOLVE
C SOLVE XM(I,J) AND KY21 AND ADD KY22 TO GET KYR
DO 28 I=1,N22
DO 11 IM=1,N22
KYR(I,IM)=0.0
DO 11 J=1,M
SUM=KY21(I,J)*XM(I,IM)
11 KYR(I,IM)=KYR(I,IM)+SUM
28 CONTINUE
DO 13 I=1,N22
DO 13 J=1,N22
13 KYR(I,J)=-KYR(I,J)+KY22(I,J)
C EVALUATE {FYR}
C {FYR} = {FY2} - [KY21] * [KY11]-1 * {FY1}
C SOLVE KY21 AND XM(4,J) AND ADD FY2
C REMEMBER THAT K11 AND K21 WERE SOLVED BEFORE
DO 32 I=1,N22
FYR(I)=0.0
DO 33 J=1,M
SUM=KY21(I,J)*XM(I,IM)
33 FYR(I)=FYR(I)+SUM
32 FYR(I)=-FYR(I)+FY2(I)
C
C NOW EVALUATE {MYR} OR {BETAY}
C {MYR}={MY2} - [KY21] [KY11]-1 {MY1} = [BETAY] {MXA}
C ALSO REMEMBER THAT K11 AND K21 WERE SOLVED BEFORE
DO 200 I=1,N22
IN=J
DO 200 IM=5,7
JB=IM-4
BETAY(I,JB)=0.0
DO 200 J=1,M
SUM=KY21(I,J)*XM(I,IM)
200 BETAY(I,JB)=BETAY(I,JB)+SUM
DO 201 I=1,N22
DO 201 J=1,N22
201 BETAY(I,J)=-BETAY(I,J)+MY2(I,J)
C NOW SOLVE {DEF} [KYR]=BETA * {M} + {FYR} AS
C {DEF} [KYR] [BETA]-1 = {M} + [BETA]-1 {FYR} TO GET
C {M}=[RYG] {DEF} -{SYR}
C(1,1)=BETAY(2,2)
C(1,2)=BETAY(2,3)
C(2,1)=BETAY(3,2)
C(2,2)=BETAY(3,3)
C(1,3)=KYR(2,1)
C(1,4)=KYR(2,2)
C(1,5)=KYR(2,3)
C(2,3)=KYR(3,1)
C(2,4)=KYR(3,2)
C(2,5)=KYR(3,3)
C(1,6)=FYR(2)
C(2,6)=FYR(3)
C CALL SOLVE TO GET {XM} AS 2X4, THE FIRST 3 ARE THE 2X3 [RXG] AND
C THE LAST COLUMN IS 2X1 {SXR}
NG=2

```

```

NC=6
NCC=4
CALL SOLVE
RYG(NM,1)=XM(1,2)
RYG(NM,2)=XM(1,5)
RYG(NM,5)=+XM(1,1)
RYG(NM,4)=XM(2,2)
RYG(NM,5)=XM(2,3)
RYG(NM,6)=+XM(2,1)
RYG(NM,7)=XM(1,4)
RYG(NM,8)=XM(2,4)
999      END
SUBROUTINE SOLVE
INCLUDE '$SF3INC'
DO 100 I=1,NG
DO 110 J=1,NC
DD(J)=C(J)
100 CONTINUE
MI=NG-1
DO 20 K=1,MI
II=K+1
DO 30 I=II,NG,1
IF ( C(I) .EQ. 0.00 ) THEN
GO TO 99
ELSE
ENDIF
ENDIF
DO 40 J=K,NC
B2(J)=C(J)-(C(K)/C(K,K))*C(I,K)
30 CONTINUE
DO 41 I=1,NG
DO 42 J=1,NC
C(J)=0
42 C(I,J)=B2(J)
41 CONTINUE
20 CONTINUE
IF ( IHXG.EQ.1 ) THEN
DO 660 I=1,80
DO 666 J=1,80
666 XM(I,J)=0.0
ENDIF
IF ( NCC.EQ.1 ) THEN
DO 651 I=NG,1,-1
SUMX=0.0
DO 66 J=1+I,NG
SUM=C(J)*XI(I)
66 SUMX=SUMX+SUM
65 XI(I)=(1.0/C(I))*C(I,NG+1)+SUMX
ELSE
DO 95 I=NG,1,-1
SUMX1=0.0
SUMX2=0.0
SUMX3=0.0
SUMX4=0.0
SUMX5=0.0
SUMX6=0.0
SUMX7=0.0
DO 96 J=1+I,NG
SUM1=C(I,J)*XM(J,1)
SUM2=C(I,J)*XM(J,2)
SUM3=C(I,J)*XM(J,3)
SUM4=C(I,J)*XM(J,4)
SUM5=C(I,J)*XM(J,5)
SUM6=C(I,J)*XM(J,6)
SUM7=C(I,J)*XM(J,7)
SUMX1=SUMX1+SUM1
SUMX2=SUMX2+SUM2
SUMX3=SUMX3+SUM3
SUMX4=SUMX4+SUM4
SUMX5=SUMX5+SUM5
SUMX6=SUMX6+SUM6
SUMX7=SUMX7+SUM7
96 XM(I,1)=(1.0/C(I))*C(1,NG+1)+SUMX1
XM(I,2)=(1.0/C(I))*C(1,NG+2)+SUMX2
XM(I,3)=(1.0/C(I))*C(1,NG+3)+SUMX3
XM(I,4)=(1.0/C(I))*C(1,NG+4)+SUMX4
XM(I,5)=(1.0/C(I))*C(1,NG+5)+SUMX5
XM(I,6)=(1.0/C(I))*C(1,NG+6)+SUMX6
XM(I,7)=(1.0/C(I))*C(1,NG+7)+SUMX7
228 CONTINUE
228 CONTINUE
ENDIF
99      END
SUBROUTINE GLOAD
INCLUDE '$SF3INC'
IF ( AXFLAG(NM) .EQ. 2 ) GO TO 2222
DO 11 I=1,INPT-1
Z=(I-1)*H
MX1(I,1)=0.0
MX1(I,2)=AE(I)*(Z-EL)/EL*H**2
11  MX1(I,3)=AE(I)*Z/EL*H**2
MX2(I,1)=0.0
MX2(I,2)=1.0*H**2*AE(INPT)
MX2(I,2)=0.0
MX2(I,1)=0.0
MX2(2,2)=-1.0*AE(1)*H**2
MX2(2,3)=0.0
MX2(3,1)=0.0
MX2(3,2)=0.0
MX2(3,3)=+1.0*AE(INPT)*H**2
DO 12 I=1,INPT-1
Z=(I-1)*H
12  FX(I)=(SXE(I)*(PP(I)+PR(I)+PRI(NM))+AE(I)*(PRI(NM)*DELY
+*SIN(PI*Z/EL)*MXRE(0)-MXE(I)))**H**2
I=INPT
Z=EL
FX2(1)=(SXE(I)*(PP(I)+PR(I)+PRI(NM))+AE(I)*(PRI(NM)*DELY
+*SIN(PI*Z/EL)*MXRE(0)-MXE(I)))**H**2
I=1
Z=0.0
FX2(2)=(SXE(I)*(PP(I)+PR(I)+PRI(NM))+AE(I)*(PRI(NM)*DELY

```

```

+*SIN(P1*Z/EL)*MXRE(0)-MXP(0)))*H**2
1=INPT
Z=EL
FX(3)=(SXE(0)*(PP(0)+PR(0)+PRI(NM))+AE(0)*(PRI(NM))*DELY
+*SIN(P1*Z/EL)*MXRE(0)-MXP(0)))*H**2
C
C***** Y-AXIS EVALUATION *****
IF (AXFLAG(NM) EQ. 1.) GO TO 999
222 DO 21 I=1,INPT-1
Z=(I-1)*H
MY(1,1)=0.0
MY(1,2)=AE(0)*(Z-EL)/EL*H**2
21 MY(1,3)=AE(0)*Z/EL*H**2
MY2(1,1)=0.0
MY2(1,3)=1.0*H**2*AE(INPT)
MY2(1,2)=0.0
MY2(2,1)=0.0
MY2(2,2)=-1.0*AE(1)*H**2
MY2(2,3)=0.0
MY2(3,1)=0.0
MY2(3,3)=+1.0*AE(INPT)*H**2
DO 22 I=1,INPT-1
Z=(I-1)*H
FY(1)=-S(YE(0)*(PP(0)+PR(0)+PRI(NM))+AE(0)*(PRI(NM))*DELY
+*SIN(P1*Z/EL)*MYRE(0)+MYP(1)))*H**2
1=INPT
Z=EL
FY2(1)=-S(YE(0)*(PP(0)+PR(0)+PRI(NM))+AE(0)*(PRI(NM))*DELY
+*SIN(P1*Z/EL)*MYRE(0)+MYP(1)))*H**2
1=1
Z=0.0
FY2(2)=-S(YE(0)*(PP(0)+PR(0)+PRI(NM))+AE(0)*(PRI(NM))*DELY
+*SIN(P1*Z/EL)*MYRE(0)+MYP(1)))*H**2
1=INPT
Z=EL
FY2(3)=-S(YE(0)*(PP(0)+PR(0)+PRI(NM))+AE(0)*(PRI(NM))*DELY
+*SIN(P1*Z/EL)*MYRE(0)+MYP(1)))*H**2
999
SUBROUTINE STGLOB
END
INCLUDE 'SSF3INC'
IF (IRERINP EQ. 1.) THEN
IRERINP=24
READ(12,'JALFPX1,ALFPY1,ALFPX2,ALFPY2,ALFPX3,ALFPY3
READ(12,'JALEX2,ALEY2
READ(12,'JALPZ5,ALFPZ6,ALFPZ7,ALFPZ8
READ(12,'JALFPZ9,ALFPZ10,ALFPZ11,ALFPZ12
READ(12,'JALFPZ13,ALFPZ14,ALFPZ15,ALFPZ16,ALFPZ17,ALFPZ18,ALFPZ19,ALFPZ20
READ(12,'JALFPZ21,ALFPZ22,ALFPZ23,ALFPZ24,ALFPZ25,ALFPZ26,ALFPZ27,ALFPZ28
READ(12,'JALFPZ29,ALFPZ30,ALFPZ31,ALFPZ32
PRINT *, 'PAPL MAPL PEXTX,PEXTY
PRINT *, 'APPLIED PAPL ,PAPL
READ(12,'JNX5,NX6,NX7,NX8
READ(12,'JNY5,NY6,NY7,NY8
READ(12,'JNX17,NX18,NX19,NX20
READ(12,'JNY17,NY18,NY19,NY20
READ(12,'JNX29,NX30,NX31,NX32
READ(12,'JNY29,NY30,NY31,NY32
READ(12,'JTRX1,KTRY1
READ(12,'JTRX2,KTRY2
READ(12,'JTRX3,KTRY3
READ(12,'JXX1,KX2,KX3,KX4
READ(12,'JXY1,KY2,KY3,KY4
READ(12,'JXX5,KX6,KX7,KX8
READ(12,'JXY5,KY6,KY7,KY8
READ(12,'JXX17,KX18,KX19,KX20
READ(12,'JXY17,KY18,KY19,KY20
READ(12,'JXX29,KX30,KX31,KX32
READ(12,'JXY29,KY30,KY31,KY32
READ(12,'JPAFLNC,MAPFLNC,PEXINC,PEYINC
READ(12,'JGFF1,GFF2,GFF3,GFF4,GFF5,PMODIF
READ(12,'JLPR,FRATOP,FRATION,FXEXT,FYEXT,P2IMAX
CALL CROOK
P2IMAX=P2IMAX*WPY
FPMAX=FRATOP*WPY
FMMAX=FRATION*MYTY
PEXMAX=FXEXT*WPY
PEYMAX=FYEXT*WPY
ENDIF
7 FORMAT(' INPUT ',5E12,3)
DO 66 J=1,70
66 C(J)=0.0
ELL(1)=EL
ELL(2)=EL
ELL(3)=EL
ELL(4)=EL
ELL(5)=EL
ELL(6)=EL
ELL(7)=EL
ELL(8)=EL
ELL(9)=EL
ELL(10)=EL
ELL(11)=EL
ELL(12)=EL
ELL(13)=EL
ELL(14)=EL
ELL(15)=EL
ELL(16)=EL
ELL(17)=EL
ELL(18)=EL
ELL(19)=EL
ELL(20)=EL
ELL(21)=EL
ELL(22)=EL
ELL(23)=EL
ELL(24)=EL
FM21B=+(P21*X21)**2*(ELL(21)-X21)/ELL(21)**2*GFF1
FM21T=-(P21*(ELL(21)-X21)**2*X21)/ELL(21)**2*GFF4
FM22B=+(P22*X22**2*(ELL(22)-X22)**2)/ELL(22)**2*GFF1
FM22T=-(P22*(ELL(22)-X22)*X22**2)/ELL(22)**2*GFF4
PRINT *, 'RRRRRRR ,FM22B,FM22T

```

FMZB3 = + (P23*X23*(ELI(23)*X23)**2)/ELI(23)**2*GFF2
 FMZT1 = -(P23*(ELI(23)*X23)*X23**2)/ELI(23)**2*GFF2
 FMZB18 = + (P24*X24**2*(ELI(24)*X24)**2)/ELI(24)**2*GFF2
 FMZT1 = -(P24*(ELI(24)*X24)**2*X24)/ELI(24)**2*GFF2
 C(1,1) = RXG(1,1)+KY1
 C(1,9) = RXG(1,2)
 C(1,57) = RXG(1,5)
 C(1,63) = RXG(1,7)
 C(2,2) = RYG(1,1)+KY1
 C(2,10) = RYG(1,2)
 C(2,58) = RYG(1,5)
 C(2,63) = RYG(1,7)
 C(3,3) = RXG(2,1)+KX2
 C(3,11) = RXG(2,2)
 C(3,57) = RXG(2,3)
 C(3,63) = RXG(2,7)
 C(4,4) = RYG(2,1)+KY2
 C(4,12) = RYG(2,2)
 C(4,58) = RYG(2,3)
 C(4,63) = RYG(2,7)
 C(5,5) = RXG(3,1)+KX3
 C(5,13) = RXG(3,2)
 C(5,57) = RXG(3,3)
 C(5,63) = RXG(3,7)
 C(6,6) = RYG(3,1)+KY3
 C(6,14) = RYG(3,2)
 C(6,58) = RYG(3,3)
 C(6,63) = RYG(3,7)
 C(7,7) = RXG(4,1)+KX4
 C(7,15) = RXG(4,2)
 C(7,57) = RXG(4,3)
 C(7,63) = RXG(4,7)
 C(8,8) = RYG(4,1)+KY4
 C(8,16) = RYG(4,2)
 C(8,58) = RYG(4,3)
 C(8,63) = RYG(4,7)
 C(9,1) = RXG(4,4)
 C(9,9) = RXG(4,5)+RXG(9,1)+KX5
 C(9,23) = KX5
 C(9,25) = RXG(9,2)
 C(9,57) = RXG(1,6),RXG(9,3)
 C(9,59) = RXG(9,3)
 C(9,63) = NX8*MAPL+RXG(1,8)+RXG(9,7)
 C(10,2) = RYG(1,4)
 C(10,10) = RYG(1,5)+KY5+RYG(9,1)
 C(10,17) = KY5
 C(10,26) = RYG(9,2)
 C(10,58) = RYG(1,6),RYG(9,3)
 C(10,60) = RYG(9,3)
 C(10,63) = NY5*MAPL+RYG(1,8)+RYG(9,7)
 C(11,3) = RXG(2,4)
 C(11,11) = RXG(2,5)+KX6+RXG(10,1)
 C(11,19) = KX6
 C(11,27) = RXG(10,2)
 C(11,57) = RXG(2,6),RXG(10,3)

C(11,59) = RXG(10,3)
 C(11,63) = NX6*MAPL+RXG(2,8)+RXG(10,7)
 C(12,4) = RYG(2,4)
 C(12,12) = RYG(2,5)+KY6+RYG(10,1)
 C(12,18) = KY6
 C(12,28) = RYG(10,2)
 C(12,58) = RYG(2,6),RYG(10,3)
 C(12,60) = RYG(10,3)
 C(12,63) = NY6*MAPL+RYG(2,8)+RYG(10,7)
 C(13,5) = RXG(9,4)
 C(13,13) = RXG(3,5)+KX7+RXG(11,1)
 C(13,20) = KX7
 C(13,29) = RXG(11,2)
 C(13,57) = RXG(3,6),RXG(11,3)
 C(13,59) = RXG(11,3)
 C(13,63) = NX7*MAPL+RXG(3,8)+RXG(11,7)
 C(14,6) = RYG(3,4)
 C(14,14) = RYG(3,5)+KY7+RYG(11,1)
 C(14,22) = KY7
 C(14,50) = RYG(11,2)
 C(14,58) = RYG(3,6),RYG(11,3)
 C(14,60) = RYG(11,3)
 C(14,63) = NY7*MAPL+RYG(3,8),RYG(11,7)
 C(15,7) = RXG(4,4)
 C(15,15) = RXG(4,5)+KX8+RXG(12,1)
 C(15,24) = KX8
 C(15,31) = RXG(12,2)
 C(15,57) = RXG(4,6),RXG(12,3)
 C(15,59) = RXG(12,3)
 C(15,63) = NX8*MAPL+RXG(4,8)+RXG(12,7)
 C(16,8) = RYG(4,4)
 C(16,16) = RYG(4,5)+KY8+RYG(12,1)
 C(16,21) = KY8
 C(16,32) = RYG(12,2)
 C(16,58) = RYG(4,6),RYG(12,3)
 C(16,60) = RYG(12,3)
 C(16,63) = NY8*MAPL+RYG(4,8)+RYG(12,7)
 C(17,10) = KY5
 C(17,17) = RXG(5,1)+KY5
 C(17,18) = RXG(5,2)
 C(17,63) = RXG(5,7)
 C(18,12) = KY6
 C(18,17) = RXG(5,4)
 C(18,18) = RXG(5,5)+KY6
 C(18,63) = RXG(5,8)
 C(19,11) = KX6
 C(19,19) = RXG(6,1)+KX6
 C(19,20) = RXG(6,2)
 C(19,27) = RXG(5,7)
 C(20,13) = KX7
 C(20,19) = RXG(6,4)
 C(20,20) = RXG(6,5)+KX7
 C(20,63) = RXG(5,8)
 C(21,16) = KY8
 C(21,21) = RXG(7,1)+KY8

C(21,22) = RXG(7,2)
 C(21,65) = RXG(7,7)
 C(22,14) = -KY7
 C(22,21) = RXG(7,4)
 C(22,22) = RXG(7,5) + XY7
 C(22,65) = RXG(7,8)
 C(23,9) = -KX5
 C(23,23) = RXG(8,1) + KX5
 C(23,24) = RXG(8,2)
 C(23,65) = RXG(8,7)
 C(24,15) = -KX8
 C(24,23) = RXG(8,4)
 C(24,24) = RXG(8,5) + KX8
 C(24,63) = RXG(8,8)
 C(25,9) = RXG(9,4)
 C(25,23) = RXG(9,5) + RXG(17,1) + KX17
 C(25,59) = -KX17
 C(25,41) = RXG(17,2)
 C(25,57) = -RXG(9,6)
 C(25,59) = RXG(9,6) + RXG(17,3)
 C(25,61) = RXG(17,3)
 C(25,63) = RXG(9,8) + RXG(17,7) + NX17*MAPL
 C(26,10) = RYG(9,4)
 C(26,26) = RYG(9,5) + RYG(17,1) + KY17
 C(26,33) = -KY17
 C(26,42) = RYG(17,2)
 C(26,58) = -RYG(9,6)
 C(26,60) = RYG(9,6) + RYG(17,3)
 C(26,62) = RYG(17,3)
 C(26,63) = RYG(9,8) + RYG(17,7) + NY17*MAPL
 C(27,11) = RXG(10,4)
 C(27,27) = RXG(18,1) + RXG(10,5) + KX18
 C(27,35) = -KX18
 C(27,43) = -RXG(18,2)
 C(27,57) = -RXG(10,6)
 C(27,59) = RXG(10,6) + RXG(18,3)
 C(27,61) = RXG(18,3)
 C(27,63) = RXG(10,8) + RXG(18,7) + NX18*MAPL
 C(28,12) = RYG(10,4)
 C(28,28) = RYG(10,5) + RYG(18,1) + KY18
 C(28,34) = -KY18
 C(28,44) = RYG(18,2)
 C(28,58) = -RYG(10,6)
 C(28,60) = RYG(10,6) + RYG(18,3)
 C(28,63) = RYG(18,3)
 C(28,65) = RYG(10,8) + RYG(18,7) + NY18*MAPL
 C(29,13) = RXG(11,4)
 C(29,29) = RXG(11,5) + RXG(19,1) + KX19
 C(29,36) = -KX19
 C(29,45) = RXG(19,2)
 C(29,57) = -RXG(11,6)
 C(29,59) = -RXG(19,3) + RXG(11,6)
 C(29,61) = RXG(19,3)
 C(29,63) = RXG(11,8) + RXG(19,7) + NX19*MAPL
 C(30,4) = RYG(11,4)

C(30,30) = RYG(11,5) + RYG(19,1) + KY19
 C(30,38) = -KY19
 C(30,46) = RYG(19,2)
 C(30,58) = -RYG(11,6)
 C(30,60) = RYG(11,6) + RYG(19,3)
 C(30,62) = RYG(19,3)
 C(30,63) = RYG(11,8) + RYG(19,7) + NY19*MAPL
 C(31,15) = RXG(12,4)
 C(31,31) = RXG(12,5) + RXG(20,1) + KX20
 C(31,40) = -KX20
 C(31,47) = RXG(20,2)
 C(31,57) = -RXG(12,6)
 C(31,59) = RXG(12,6) + RXG(20,3)
 C(31,61) = RXG(20,3)
 C(31,63) = RXG(12,9) + RXG(20,7) + NX20*MAPL
 C(32,16) = RYG(12,4)
 C(32,32) = RYG(12,5) + RYG(20,1) + KY20
 C(32,37) = -KY20
 C(32,40) = RYG(20,2)
 C(32,58) = -RYG(12,6)
 C(32,60) = RYG(12,6) + RYG(20,3)
 C(32,62) = RYG(20,3)
 C(32,63) = RYG(12,9) + RYG(20,7) + NY20*MAPL
 C(33,26) = -KY17
 C(33,33) = RXG(13,1) + KY17
 C(33,54) = RXG(13,2)
 C(33,63) = RXG(13,7)
 C(34,28) = -KY18
 C(34,33) = RXG(13,4)
 C(34,34) = RXG(13,5) + KY18
 C(34,63) = RXG(13,8)
 C(35,27) = -KX18
 C(35,35) = RXG(14,1) + KX18
 C(35,36) = RXG(14,2)
 C(35,63) = RXG(14,7)
 C(36,29) = -KX19
 C(36,35) = RXG(14,4)
 C(36,36) = RXG(14,5) + KX19
 C(36,63) = RXG(14,8)
 C(37,32) = -KY20
 C(37,37) = RXG(15,1) + KY20
 C(37,38) = RXG(15,2)
 C(37,63) = RXG(15,7)
 C(38,30) = -KY19
 C(38,37) = RXG(15,4)
 C(38,38) = RXG(15,5) + KY19
 C(38,63) = RXG(15,8)
 C(39,25) = -KX17
 C(39,39) = RXG(16,1) + KX17
 C(39,40) = RXG(16,2)
 C(39,63) = RXG(16,7)
 C(40,31) = -KX20
 C(40,39) = RXG(16,4)
 C(40,40) = RXG(16,5) + KX20
 C(40,63) = RXG(16,8)

C(41.25) = RXG(17.4)
C(41.41) = RXG(17.5) + KCX29
C(41.50) = -KCX29
C(41.59) = -RXG(17.6)
C(41.61) = RXG(17.6)
C(41.63) = RXG(17.8) + NX29*MAPL
C(42.26) = RYG(17.4)
C(42.42) = RYG(17.5) + KY29
C(42.49) = -KY29
C(42.60) = -RYG(17.6)
C(42.62) = RYG(17.6)
C(42.63) = RYG(17.8) + NY29*MAPL + FM21B*GFFS
C(43.27) = RXG(18.4)
C(43.43) = RXG(18.5) + KCX30
C(43.51) = -KCX30
C(43.59) = -RXG(18.6)
C(43.61) = RXG(18.6)
C(43.63) = RXG(18.8) + NX30*MAPL + FM22B*GFFS
C(44.28) = RYG(18.4)
C(44.44) = RYG(18.5) + KY30
C(44.50) = -KY30
C(44.60) = -RYG(18.6)
C(44.62) = RYG(18.6)
C(44.63) = RYG(18.8) + NY30*MAPL + FM21T*GFFS
C(45.29) = RXG(19.4)
C(45.45) = RXG(19.5) + KCX31
C(45.52) = -KCX31
C(45.59) = -RXG(19.6)
C(45.61) = RXG(19.6)
C(45.63) = RXG(19.8) + NX31*MAPL + FM22T*GFFS
C(46.30) = RYG(19.4)
C(46.46) = RYG(19.5) + KY31
C(46.54) = -KY31
C(46.60) = -RYG(19.6)
C(46.62) = RYG(19.6)
C(46.63) = RYG(19.8) + NY31*MAPL
C(47.21) = RXG(20.4)
C(47.47) = RXG(20.5) + KCX32
C(47.50) = -KCX32
C(47.59) = -RXG(20.6)
C(47.61) = RXG(20.6)
C(47.63) = RXG(20.8) + NX32*MAPL
C(48.32) = RYG(20.4)
C(48.48) = RYG(20.5) + KY32
C(48.53) = -KY32
C(48.60) = -RYG(20.6)
C(48.62) = RYG(20.6)
C(48.63) = RYG(20.8) + NY32*MAPL
C(49.42) = -KY29
C(49.49) = RXG(21.1) + KY29
C(49.50) = RXG(21.2)
C(49.63) = RXG(21.7) - FM21B
C(50.44) = -KY30
C(50.49) = RXG(21.4)
C(50.50) = RXG(21.5) + KY30

C(50.63) = RXG(21.8) - FM21T
C(51.49) = -KCX30
C(51.51) = RXG(22.1) + KCX30
C(51.52) = RXG(22.2)
C(51.63) = RXG(22.7) - FM22B
C(52.45) = -KCX31
C(52.51) = RXG(22.4)
C(52.52) = RXG(22.5) + KCX31
C(52.63) = RXG(22.8) - FM22T
C(53.48) = -KY32
C(53.53) = RXG(23.1) + KY32
C(53.54) = RXG(23.2)
C(53.63) = RXG(23.7) - FM22B
C(54.46) = -KY31
C(54.53) = RXG(23.4)
C(54.54) = RXG(23.5) + KY31
C(54.63) = RXG(23.8) - FM22T
C(55.41) = -KCX29
C(55.55) = RXG(24.1) + KCX29
C(55.56) = RXG(24.2)
C(55.63) = RXG(24.7) - FM22B
C(56.47) = -KCX32
C(56.55) = RXG(24.4)
C(56.56) = RXG(24.5) + KCX32
C(56.63) = RXG(24.8) - FM22T
C(57.1) = RXG(1.1) + RXG(1.4)
C(57.3) = RXG(2.1) + RXG(2.4)
C(57.5) = RXG(3.1) + RXG(3.4)
C(57.7) = RXG(4.1) + RXG(4.4)
C(57.9) = RXG(1.2) + RXG(1.5)
C(57.11) = RXG(2.2) + RXG(2.5)
C(57.13) = RXG(3.2) + RXG(3.5)
C(57.15) = RXG(4.2) + RXG(4.5)
C(57.17) = RXG(1.3) + RXG(1.6) + RXG(2.3) + RXG(3.3) + RXG(3.6)
+ + RXG(4.3) + RXG(4.6) - PRI(1) - PRI(2) - PRI(3) - PRI(4) + KTRV1*EL
ELC = EL
C(57.59) = + KTRV2*EL
C(57.61) = + KTRV3*EL
C(57.63) = 2*(ALPPY1 + ALPPY2 + ALPPY3)
+ RXG(1.8) + RXG(2.7) + RXG(2.8) + RXG(3.7) + RXG(3.8) + RXG(4.7) + RXG(4.8)
+ + 2.0*ALEY2*PEXTY*EL
C(58.2) = RYG(1.1) + RYG(1.4)
C(58.4) = RYG(2.1) + RYG(2.4)
C(58.6) = RYG(3.1) + RYG(3.4)
C(58.8) = RYG(4.1) + RYG(4.4)
C(58.10) = RYG(1.2) + RYG(1.5)
C(58.12) = RYG(2.2) + RYG(2.5)
C(58.14) = RYG(3.2) + RYG(3.5)
C(58.16) = RYG(4.2) + RYG(4.5)
C(58.58) = RYG(1.3) + RYG(1.6) + RYG(2.3) + RYG(2.6) + RYG(3.3) + RYG(3.6)
+ + RYG(4.3) + RYG(4.6) + PRI(1) + PRI(2) + PRI(3) + PRI(4) - KTRX1*EL
C(58.60) = -KTRX2*EL
C(58.62) = -KTRX3*EL
C(58.63) = -2.0*(ALPPX1 + ALPPX2)*PAPL*ELC

```

+ RXG(17.8)+RXG(18.7)
+ +RXG(18.8)+RXG(19.7)+RXG(19.8)+RXG(20.7)+RXG(20.8)
C(62.26) =RYG(17.1)+RYG(17.4)
C(62.28) =RYG(18.1)+RYG(18.4)
C(62.30) =RYG(19.1)+RYG(19.4)
C(62.32) =RYG(20.1)+RYG(20.4)
C(62.42) =RYG(17.2)+RYG(17.5)
C(62.44) =RYG(18.2)+RYG(18.5)
C(62.46) =RYG(19.2)+RYG(19.5)
C(62.48) =RYG(20.2)+RYG(20.5)
C(62.60) =PRI(17)+PRI(18)+PRI(19)+PRI(20)+RYG(17.3)+RYG(17.6)
+RYG(18.3)+RYG(18.6)+RYG(19.3)+RYG(19.6)+RYG(20.3)+RYG(20.6)
C(62.62) =PRI(17)+PRI(18)+PRI(19)+RYG(17.3)+RYG(17.6)+
+RYG(18.3)+RYG(18.6)+RYG(19.3)+RYG(19.6)+RYG(20.3)+RYG(20.6)
+KTRX3*EL
C(62.63) =-2*ALPPX3*PAPL*EL+RYG(17.7)
+ +RYG(17.8)
+ +RYG(18.7)+RYG(18.8)+RYG(19.7)+RYG(19.8)+RYG(20.7)+RYG(20.8)
NG =IDOF
NCC =1
NC =NG+NC
IF ( IDOF.EQ.26 ) THEN
PRINT *, IDOF PFFFFFF, IDOF
DO 46 I =1,24
C(I, IDOF-1) =C(I, 157)
C(I, IDOF) =C(I, 158)
46 C(I, NC) =C(I, 63)
DO 38 I =1,24
J =IDOF-1
K =IDOF
C(I, J) =C(I, 57, I)
C(K, I) =C(I, 58, I)
38 C(25, 25) =C(57, 57)
C(26, 25) =C(58, 57)
C(26, 26) =C(58, 58)
C(I, 27) =C(57, 63)
C(K, 27) =C(58, 63)
ELSE IF ( IDOF.EQ.44 ) THEN
PRINT *, IDOF PFFFFFF, IDOF
DO 47 I =1,40
C(I, IDOF-3) =C(I, 157)
C(I, IDOF-2) =C(I, 158)
C(I, IDOF-1) =C(I, 159)
C(I, IDOF) =C(I, 60)
47 C(I, NC) =C(I, 63)
C*VDIR: PREFER VECTOR ON
DO 39 I =1,40
C(41, I) =C(57, I)
C(42, I) =C(58, I)
C(43, I) =C(59, I)
39 C(44, I) =C(60, I)
C(41, 41) =C(57, 57)
C(41, 42) =C(57, 58)
C(41, 43) =C(57, 59)

```

```

+ -2.0*ALPPX3*PAPL*ELC
+ +RYG(1.7)+RYG(1.8)+RYG(2.7)+
+RYG(2.8)+RYG(3.7)+RYG(3.8)+RYG(4.7)+RYG(4.8)
+ -2.0*ALEY2*PEXTX*EL
C(59.9) =RXG(9.1)+RXG(9.4)
C(59.11) =RXG(10.1)+RXG(10.4)
C(59.13) =RXG(11.1)+RXG(11.4)
C(59.15) =RXG(12.1)+RXG(12.4)
C(59.25) =RXG(9.2)+RXG(9.5)
C(59.27) =RXG(10.2)+RXG(10.5)
C(59.29) =RXG(11.2)+RXG(11.5)
C(59.31) =RXG(12.2)+RXG(12.5)
C(59.57) = +RYG(9)+PRI(10)+PRI(11)+PRI(12)+RXG(9.3)+RXG(9.6)
+RXG(10.3)+RXG(10.6)+RXG(11.3)+RXG(11.6)+RXG(12.3)+RXG(12.6)
C(59.59) = -PRI(9)+PRI(10)+PRI(11)+PRI(12)+RXG(9.3)+RXG(9.6)+
+RXG(10.3)+RXG(10.6)+RXG(11.3)+RXG(11.6)+RXG(12.3)+RXG(12.6)
+ +KTRY2*EL
C(59.61) =KTRY3*EL
C(59.63) =-2*(ALPFY2+ALPPY3)*PAPL*EL
+ +RXG(9.7)+RXG(9.8)
+ +RXG(10.7)+RXG(10.8)+RXG(11.7)+RXG(11.8)+RXG(12.7)+RXG(12.8)
+ +2.0*ALEY2*PEXTX*EL
C(60.10) =RYG(9.1)+RYG(9.4)
C(60.12) =RYG(10.1)+RYG(10.4)
C(60.14) =RYG(11.1)+RYG(11.4)
C(60.16) =RYG(12.1)+RYG(12.4)
C(60.26) =RYG(9.2)+RYG(9.5)
C(60.28) =RYG(10.2)+RYG(10.5)
C(60.30) =RYG(11.2)+RYG(11.5)
C(60.32) =RYG(12.2)+RYG(12.5)
C(60.58) = -PRI(9)+PRI(10)+PRI(11)+PRI(12)+RYG(9.3)+RYG(9.6)+
+RYG(10.3)+RYG(10.6)+RYG(11.3)+RYG(11.6)+RYG(12.3)+RYG(12.6)
C(60.60) = PRI(9)+PRI(10)+PRI(11)+PRI(12)+RYG(9.3)+RYG(9.6)+
+RYG(10.3)+RYG(10.6)+RYG(11.3)+RYG(11.6)+RYG(12.3)+RYG(12.6)
+KTRX2*EL
C(60.62) =-KTRX3*EL
C(60.63) =-2.0*(ALPPX2)*PAPL*EL
+ -2.0*ALPPX3*PAPL*EL
+ +RYG(9.7)+RYG(9.8)+RYG(10.7)+RYG(10.8)
+ +RYG(11.7)+RYG(11.8)+RYG(12.7)+RYG(12.8)
+ -2.0*ALEY2*PEXTX*EL
C(61.25) =RXG(17.1)+RXG(17.4)
C(61.25) =RXG(18.1)+RXG(18.4)
C(61.29) =RXG(19.1)+RXG(19.4)
C(61.31) =RXG(20.1)+RXG(20.4)
C(61.41) =RXG(17.2)+RXG(17.5)
C(61.43) =RXG(18.2)+RXG(18.5)
C(61.45) =RXG(19.2)+RXG(19.5)
C(61.47) =RXG(20.2)+RXG(20.5)
C(61.59) = PRI(17)+PRI(18)+PRI(19)+PRI(20)+RXG(17.3)+RXG(17.6)+
+RXG(18.3)+RXG(18.6)+RXG(19.3)+RXG(19.6)+RXG(20.3)+RXG(20.6)
C(61.61) = -PRI(17)+PRI(18)+PRI(19)+PRI(20)+RXG(17.3)+RXG(17.6)+
+RXG(18.3)+RXG(18.6)+RXG(19.3)+RXG(19.6)+RXG(20.3)+RXG(20.6)
+ +KTRY3*EL
C(61.63) =-2*ALPPY3*PAPL*EL+RYG(17.7)+

```



```

VR21R = P21 + VR21L
VRZL = (OMBX(2) + QMTX(2) + P22*(ELL(2)-XZ2))/ELL(2)
VRZR = VRZL - P22
VRZL = (OMBX(23) + OMTX(23) + P23*(ELL(23)-XZ3))/ELL(23)
VRZR = P23 + VRZL
VRZL = (OMBX(24) + OMTX(24) + P24*XZ4)/ELL(24)
VRZR = P24 + VRZL
PRI(17) = ALPPZ30*PAPL + VRZL
PRI(18) = ALPPZ30*PAPL + VRZL - VRZ1R
PRI(19) = ALPPZ31*PAPL - VRZ1R - VRZ3R
CMY18 = (CMY(18) + OMBY(18))/ELL(18)*0.5 - QMTY(18)
EST = CMY18*0.5/(2000*0.97)
ST61 = (BST - PRI(19)/(1.27*E))*100.0
ST62 = (BST - PRI(18)/(1.27*E))*100.0
PRINT *, STRAIN INSIDE FRAME ,
PRINT *, ST49,ST51
PRI(20) = ALPPZ32*PAPL - VRZ4R + VRZ3L
PRI(21) = ALPPX3*PAPL - VRX17
PRI(22) = + ALPPY3*PAPL - VRX18
PRI(23) = - ALPPX3*PAPL - VRX20
PRI(24) = + ALPPY3*PAPL - VRX17
PRI(25) = - VRX9 + VRX17 - ALPPZ17*PAPL + VR13 + VR16
PRI(13) = - VRX9 + VRX17 - ALPPZ2*PAPL - ALEX2*PEXTX
PRI(16) = - ALPPY2*PAPL + VRX17 - VRX9 + ALEY2*PEXTY
PRI(14) = - ALPPY2*PAPL + VRX17 + VRX9 + ALEY2*PEXTY
PRI(10) = PRI(19) + ALPPZ18*PAPL + VR14 - VR13
PRI(15) = - VRX11 - VRX19
PRI(11) = ALPPZ19*PAPL + PRI(19) - VR14 - VR15
PRI(12) = - ALPPZ20*PAPL + PRI(20) + VR15 - VR16
PRI(9) = - ALPPX1*PAPL - VRX1 + VRX9
PRI(1) = + ALPPZ5*PAPL + PRI(9) + VR5 + VR8
PRI(8) = ALPPY1*PAPL + VRX9 - VRX1
PRI(2) = - ALPPZ6*PAPL + PRI(10) + VR6 - VR5
PRI(6) = ALPPY1*PAPL + VRX10 - VRX2
PRI(7) = VRX3 - VRX11
PRI(3) = ALPPZ7*PAPL + PRI(11) - VR6 - VR7
PRI(4) = ALPPZ8*PAPL + PRI(12) + VR7 - VR8
ETTL = 0.0
DO 66 I = 1,NUM
TEST = ABS(OMBX(I) - OMBX(I))
TEST1 = ABS(QMTX(I) - OMTX(I))
TEST2 = ABS(OMBY(I) - OMBY(I))
TEST3 = ABS(OMTY(I) - OMTY(I))
TEST4 = ABS(PRI(I) - OPRI(I))
66 ETTL = MAX(ETTL,TEST,TEST1,TEST2,TEST3,TEST4)
IGLBCON = IGLBCON + 1
ISTOP = 0
IF ( ETTL .LT. 0.01 ) ISTOP = 1
DO 55 I = 1,NUM
OMTX(I) = OMTX(I)
OMBX(I) = OMBX(I)
OMTY(I) = OMTY(I)
OMBY(I) = OMBY(I)
55 OPRI(I) = PRI(I)
END

```

```

OMBX(19) = RXG(19,1)*X1(29) + RXG(19,2)*X1(45) + RXG(19,3)*X1(61)
+ X1(159) - RXG(19,7)
OMTX(19) = RXG(19,4)*X1(29) + RXG(19,5)*X1(45) + RXG(19,6)*X1(61)
+ X1(159) - RXG(19,8)
OMBX(20) = RXG(20,1)*X1(31) + RXG(20,2)*X1(47) + RXG(20,3)*X1(61)
+ X1(159) - RXG(20,7)
OMTX(20) = RXG(20,4)*X1(31) + RXG(20,5)*X1(47) + RXG(20,6)*X1(61)
+ X1(159) - RXG(20,8)
OMBY(17) = RYG(17,1)*X1(26) + RYG(17,2)*X1(42) + RYG(17,3)*X1(62)
+ X1(160) - RYG(17,7)
OMTY(17) = RYG(17,4)*X1(26) + RYG(17,5)*X1(42) + RYG(17,6)*X1(62)
+ X1(160) - RYG(17,8)
OMBY(18) = RYG(18,1)*X1(28) + RYG(18,2)*X1(44) + RYG(18,3)*X1(62)
+ X1(160) - RYG(18,7)
OMTY(18) = RYG(18,4)*X1(28) + RYG(18,5)*X1(44) + RYG(18,6)*X1(62)
+ X1(160) - RYG(18,8)
OMBY(19) = RYG(19,1)*X1(30) + RYG(19,2)*X1(46) + RYG(19,3)*X1(62)
+ X1(160) - RYG(19,7)
OMTY(19) = RYG(19,4)*X1(30) + RYG(19,5)*X1(46) + RYG(19,6)*X1(62)
+ X1(160) - RYG(19,8)
OMBY(20) = RYG(20,1)*X1(32) + RYG(20,2)*X1(48) + RYG(20,3)*X1(62)
+ X1(160) - RYG(20,7)
OMTY(20) = RYG(20,4)*X1(32) + RYG(20,5)*X1(48) + RYG(20,6)*X1(62)
+ X1(160) - RYG(20,8)
OMBX(21) = RXG(21,1)*X1(49) + RXG(21,2)*X1(50) - RXG(21,7) + FM21B
OMTX(21) = RXG(21,4)*X1(49) + RXG(21,5)*X1(50) - RXG(21,6) + FM21T
OMBX(22) = RXG(22,1)*X1(51) + RXG(22,2)*X1(52) - RXG(22,7) + FM22B
OMTX(22) = RXG(22,4)*X1(51) + RXG(22,5)*X1(52) - RXG(22,6) + FM22T
PRINT *, FROM OM22 , OMBX(22), OMTX(22)
OMBX(23) = RXG(23,1)*X1(53) + RXG(23,2)*X1(54) - RXG(23,7) + FM23B
OMTX(23) = RXG(23,4)*X1(53) + RXG(23,5)*X1(54) - RXG(23,6) + FM23T
OMBX(24) = RXG(24,1)*X1(55) + RXG(24,2)*X1(56) - RXG(24,7) + FM24B
OMTX(24) = RXG(24,4)*X1(55) + RXG(24,5)*X1(56) - RXG(24,6) + FM24T
VRX1 = (OMBY(1) + OMTY(1))/ELL(1)
VRX1 = (OMBX(1) + OMTX(1))/ELL(1)
VRX2 = (OMBY(2) + OMTY(2))/ELL(2)
VRX2 = (OMBX(2) + OMTX(2))/ELL(2)
VRX3 = (OMBY(3) + OMTY(3))/ELL(3)
VRX3 = (OMBX(3) + OMTX(3))/ELL(3)
VR5 = (OMBY(5) + OMTY(5))/ELL(5)
VR5 = (OMBX(5) + OMTX(5))/ELL(5)
VR6 = (OMBY(6) + OMTY(6))/ELL(6)
VR6 = (OMBX(6) + OMTX(6))/ELL(6)
VR7 = (OMBY(7) + OMTY(7))/ELL(7)
VR7 = (OMBX(7) + OMTX(7))/ELL(7)
VR8 = (OMBY(8) + OMTY(8))/ELL(8)
VR8 = (OMBX(8) + OMTX(8))/ELL(8)
VRX9 = (OMBY(9) + OMTY(9))/ELL(9)
VRX9 = (OMBX(9) + OMTX(9))/ELL(9)
VRX10 = (OMBY(10) + OMTY(10))/ELL(10)
VRX10 = (OMBX(10) + OMTX(10))/ELL(10)
VRX11 = (OMBY(11) + OMTY(11))/ELL(11)
VRX11 = (OMBX(11) + OMTX(11))/ELL(11)
VR13 = (OMBY(13) + OMTY(13))/ELL(13)
VR13 = (OMBX(13) + OMTX(13))/ELL(13)
VR14 = (OMBY(14) + OMTY(14))/ELL(14)
VR14 = (OMBX(14) + OMTX(14))/ELL(14)
VR15 = (OMBY(15) + OMTY(15))/ELL(15)
VR15 = (OMBX(15) + OMTX(15))/ELL(15)
VR16 = (OMBY(16) + OMTY(16))/ELL(16)
VR16 = (OMBX(16) + OMTX(16))/ELL(16)
VRX17 = (OMBY(17) + OMTY(17))/ELL(17)
VRX17 = (OMBX(17) + OMTX(17))/ELL(17)
VRX18 = (OMBY(18) + OMTY(18))/ELL(18)
VRX18 = (OMBX(18) + OMTX(18))/ELL(18)
VRX19 = (OMBY(19) + OMTY(19))/ELL(19)
VRX19 = (OMBX(19) + OMTX(19))/ELL(19)
VRX20 = (OMBY(20) + OMTY(20))/ELL(20)
VRX20 = (OMBX(20) + OMTX(20))/ELL(20)
VRZ1L = (OMBX(21) + OMTX(21) + P21*XZ1)/ELL(21)

```

```

SUBROUTINE ELODINC
INCLUDE 'SSF3INC'
IF ( ICONLOC .EQ. 1 .OR. IGLBCON .GT. 10 ) GO TO 333
PAPL = PAPL + PAPLINC
MAPL = MAPL + MAPLINC
PEXTX = PEXTX + PEXINC
PEXTY = PEXTY + PEYINC
P21 = P21 + PINC21
P22 = P22 + PINC22
P23 = P23 + PINC23
P24 = P24 + PINC24
GO TO 999
333 PAPL = PAPL - PAPLINC
MAPL = MAPL - MAPLINC
PEXTX = PEXTX - PEXINC
PEXTY = PEXTY - PEYINC
P21 = P21 - PINC21
P22 = P22 - PINC22
P23 = P23 - PINC23
P24 = P24 - PINC24
PAPLINC = PAPLINC / 10.0
MAPLINC = MAPLINC / 10.0
PEXINC = PEXINC / 10.0
PEYINC = PEYINC / 10.0
PINC21 = PINC21 / 10.0
PINC22 = PINC22 / 10.0
PINC23 = PINC23 / 10.0
PINC24 = PINC24 / 10.0
PAPL = PAPL + PAPLINC
MAPL = MAPL + MAPLINC
PEXTX = PEXTX + PEXINC
PEXTY = PEXTY + PEYINC
P21 = P21 + PINC21
P22 = P22 + PINC22
P23 = P23 + PINC23
P24 = P24 + PINC24
999 CONTINUE
ETTL = 0.0
ETTL1 = ABS(PAPLINC)
ETTL2 = ABS(MAPLINC)
ETTL3 = ABS(PEXINC)
ETTL4 = ABS(PEYINC)
ETTL = MAX(PAPLINC, MAPLINC, PINC21, PINC22, PINC23, PINC24)
IF ( ETTL .LT. 0.01 ) IGLBCON = 3009
END
SUBROUTINE FNONPRO
INCLUDE 'SSF3INC'
IF ( LPF .EQ. 1 .AND. PAPL .GE. FPMAX ) THEN
MAPLINC = PAPLINC
PAPLINC = 0.0
LPF = 100
ELSE IF ( LPF .EQ. 2 .AND. PAPL .GE. FPMAX ) THEN
MAPLINC = PAPLINC
LPF = 100
ELSE IF ( LPF .EQ. 3 .AND. MAPL .GE. FMMAX ) THEN

```

```

MAPLINC = 0.0
LPF = 100
ELSE IF ( LPF .EQ. 4 .AND. MAPL .GE. FMMAX ) THEN
PAPLINC = MAPLINC
MAPLINC = 0.0
LPF = 100
ELSE IF ( LPF .EQ. 5 .AND. PEXTY .GE. PEYMAX ) THEN
PEXINC = PEYINC
PEYINC = 0.0
LPF = 6
ELSE IF ( LPF .EQ. 6 .AND. PAPL .GE. 2.0 ) THEN
PEXINC = 0.0
ALPPZ30 = 1
ALPPZ32 = 1
LPF = 100
ENDIF
IF ( LPF .EQ. 7 .AND. PAPL .GE. FPMAX ) THEN
P21 = PAPLINC
P22 = PAPLINC
PINC21 = P21 * PMODIF
PINC22 = P21 * PMODIF
PAPLINC = 0.0
ALPPX3 = 1.0 / PAPL
ALPPY3 = 1.0 / PAPL
LPF = 8
KTRX1 = EMKX1
KTRX2 = ENKX2
KTRX3 = EMKX3
KTRY1 = EMKY1
KTRY2 = EMKY2
KTRY3 = EMKY3
ENDIF
IF ( LPF .EQ. 8 .AND. P21 .GE. P21MAX ) THEN
P23 = PINC21
P24 = PINC21
PINC23 = PINC21
PINC24 = PINC21
PINC21 = 0.0
PINC22 = 0.0
LPF = 9
P21MAX = 19.4
ENDIF
IF ( LPF .EQ. 9 .AND. P23 .GE. P21MAX ) THEN
P21 = P21 + PINC23
P22 = P22 + PINC23
PINC21 = PINC23
PINC22 = PINC24
PINC23 = 0.0
PINC24 = 0.0
LPF = 10
P21MAX = 20.4
ENDIF
IF ( LPF .EQ. 10 .AND. P21 .GE. P21MAX ) THEN
P23 = P23 + PINC21
P24 = P24 + PINC21

```

ENDIF
END

```

PINC23 = PINC21
PINC24 = PINC22
PINC21 = 0.0
PINC22 = 0.0
LFF = 100
ENDIF
999 END
SUBROUTINE CROOK
INCLUDE 'SSF3INC'
LC1 = ((INPT+1)/2+1)/2
LC2 = (INPT+1)/2
LC3 = LC1+LC2+1
READ(12,') ICROOK
DO 11=1,NUM
1 READ(12,')K,XLC(1),XLC(1,LC1),XLC(1,LC2),XLC(1,LC3),XLC(1,INPT)
3 READ(12,')K,XGC(1),XGC(1,LC1),XGC(1,LC2),XGC(1,LC3),XGC(1,INPT)
READ(12,')EMKX1,EMKY1
READ(12,')EMKX2,EMKY2
READ(12,')EMKX3,EMKY3
DO 5 I=1,NUM
Z=0.0
DO 6 J=1,INPT
Z=(J-1)*H
GLG1 = (Z*(Z-0.5*EL)*(Z-0.75*EL)/(Z-EL))/
+(0.25*EL*(0.25*EL-0.5*EL)*(0.25*EL-0.75*EL)/(0.25*EL-EL))
GLG2 = (Z*(Z-0.25*EL)*(Z-0.75*EL)/(Z-EL))/
+(0.5*EL*(0.5*EL-0.25*EL)*(0.5*EL-0.75*EL)/(0.5*EL-EL))
GLG3 = (Z*(Z-0.25*EL)*(Z-0.5*EL)/(Z-EL))/
+(0.75*EL*(0.75*EL-0.25*EL)*(0.75*EL-0.5*EL)/(0.75*EL-EL))
GLG4 = (Z*(Z-0.25*EL)*(Z-0.5*EL)/(Z-0.75*EL))/
+(EL*(EL-0.25*EL)*(EL-0.5*EL)/(EL-0.75*EL))
XL(I,J) = GLG1*XLC(1,LC1) + GLG2*XLC(1,LC2) + GLG3*XLC(1,LC3)
++ GLG4*XLC(1,INPT)
XG(I,J) = GLG1*XGC(1,LC1) + GLG2*XGC(1,LC2) + GLG3*XGC(1,LC3)
++ GLG4*XGC(1,INPT)
XLC(I,J) = XL(I,J)
XGC(I,J) = XG(I,J)
XLT(I,J) = XL(I,J)
XGT(I,J) = XG(I,J)
V(I) = XL(I,J)
U(I) = XG(I,J)
6 continue
5 IF ( ICROOK.EQ. 0 ) THEN
DO 9 I=1,NUM
DO 9 J=1,INPT
XL(I,J) = 0.0
XG(I,J) = 0.0
XLC(I,J) = 0.0
XGC(I,J) = 0.0
XLT(I,J) = 0.0
XGT(I,J) = 0.0
9 U(I) = XG(I,J)

```

\bar{D}	P	M_x	Δ_y	Δ_x
.100E+01	0.000	0.000	0.000	0.000
.926E+00	0.044	0.000	0.001	0.001
.857E+00	0.088	0.000	0.002	0.002
.791E+00	0.131	0.000	0.004	0.004
.729E+00	0.175	0.000	0.005	0.005
.671E+00	0.219	0.000	0.006	0.006
.616E+00	0.263	0.000	0.008	0.008
.564E+00	0.306	0.000	0.009	0.009
.516E+00	0.350	0.000	0.011	0.011
.471E+00	0.394	0.000	0.013	0.013
.428E+00	0.438	0.000	0.015	0.015
.389E+00	0.481	0.000	0.017	0.017
.352E+00	0.525	0.000	0.019	0.019
.317E+00	0.569	0.000	0.022	0.022
.285E+00	0.613	0.000	0.024	0.024
.256E+00	0.656	0.000	0.027	0.027
.228E+00	0.700	0.000	0.031	0.031
.203E+00	0.744	0.021	0.014	0.055
.201E+00	0.748	0.023	0.012	0.058
.198E+00	0.753	0.025	0.010	0.060
.196E+00	0.757	0.027	0.008	0.063
.194E+00	0.761	0.029	0.006	0.065
.191E+00	0.766	0.031	0.005	0.068
.189E+00	0.770	0.033	0.003	0.071
.187E+00	0.775	0.035	0.001	0.073
.184E+00	0.779	0.038	-0.001	0.076
.182E+00	0.783	0.040	-0.003	0.079
.179E+00	0.788	0.042	-0.005	0.082
.180E+00	0.788	0.042	-0.005	0.081
.179E+00	0.789	0.042	-0.005	0.082
.179E+00	0.789	0.042	-0.006	0.082
.179E+00	0.789	0.043	-0.006	0.082
.179E+00	0.790	0.043	-0.006	0.082
.179E+00	0.790	0.043	-0.006	0.083
.178E+00	0.791	0.043	-0.006	0.083
.178E+00	0.791	0.043	-0.007	0.083
.178E+00	0.792	0.044	-0.007	0.083
.178E+00	0.792	0.044	-0.007	0.084
.178E+00	0.792	0.044	-0.007	0.084
.178E+00	0.792	0.044	-0.007	0.084

VITA

Name: Saleh Ali Eidan
Born: April 7, 1956
Place of birth: Buraydah, Saudi Arabia
Permanent Address: P. O. Box 9338
Riyadh-11413, Saudi Arabia

The author was born to Ali Abdullah Eidan and Muneera Ibrahim Al-Rubaishi, and grew up in the city of Buraydah, Saudi Arabia. He completed his early education up to the high school in Saudi Arabia. He received B. S. and M. S. in Civil Engineering from the California State University at Sacramento in January, 1981, and July, 1983, respectively. He then worked for the government of Saudi Arabia as a structural engineer in the Ministry of Post, Telegram, and Telephone from July, 1983 to October, 1984. In October, 1984, he joined the King Abdulaziz City for Science and Technology as a "Researcher A" and worked as a projects coordinator for KACST development office. In August, 1987, he joined Old Dominion University to pursue a Ph.D. degree program in Civil Engineering. He is married to his lovely wife Adeeba Eidan and they have four daughters, Rolla, Rana, Raneem, and Raniah.